Technische Universität München
TUM School of Life Sciences

Protein Modification and Interaction Partners of the Small GTPase RACB in the Barley-Powdery Mildew Pathosystem

Lukas Sebastian Weiß

Vollständiger Abdruck der von der TUM School of Life Sciences der Technischen Universität München zur Erlangung des akademischen Grades eines

Doktors der Naturwissenschaften (Dr. rer. nat.)

genehmigten Dissertation.

Vorsitz:	Prof. Dr. J. Philipp Benz
Prüfer der Dissertation:	1. Prof. Dr. Ralph Hückelhoven
	2. Prof. Dr. Brigitte Poppenberger-Sieberer

Die Dissertation wurde am 15.09.2022 bei der Technischen Universität München eingereicht und durch die TUM School of Life Sciences am 22.12.2022 angenommen.

Summary

Every year, crop production worldwide suffers from heavy economic yield losses due to plant infection by pathogens. To tackle this problem, considerable efforts are being made to understand the relationship between plants and pathogens. For instance, the barley-powdery pathosystem is used to investigate the molecular principles behind disease susceptibility. In this particular system, the barley Rho-of-plant GTPase RACB has been identified as a susceptibility factor that supports the invasion of barley by the powdery mildew fungus *Blumeria graminis* f.sp. *hordei* (*Bgh*). Unlike other susceptibility genes, however, RACB is not a negative regulator of plant immunity. Instead, it is hypothesized that RACB-signaling is hijacked by *Bgh* to facilitate infection. Since the exact molecular mechanisms behind RACB-mediated susceptibility are still unclear, this work investigated on the one hand the possible regulation of RACB via posttranslational modifications and on the other hand novel RACB-interaction partners to pinpoint susceptibility-associated cellular pathways. Activated RACB was found to be ubiquitinated at K167, an amino acid that is involved in regulating RACB's protein stability. Mutational exchange of this residue does not affect RACB's downstream signaling processes, but ubiquitination of this site is hypothesized to do so. Conservation of this residue in other RACB-like Rho proteins of plants and animals suggests that the regulatory mechanisms could be maintained across kingdoms. Additionally, three novel interaction partners of RACB established a link to the plant's anionic phospholipid-signaling pathway. The corresponding candidate plant interactors Phospholipase C 6-like (PLC) and Phosphoinositide phosphosphatase (PIP) function in resistance against *Bgh*, whereas the putative *Bgh* effector protein 9o9 directly targets activated RACB and increases the susceptibility of barley towards infection when overexpressed in barley epidermal cells. The candidate interactors and RACB itself were further found to bind overlapping anionic phospholipid species *in vitro*, suggesting convergent signaling processes. It was also shown that markers for four anionic phospholipid species displayed an altered subcellular localisation during *Bgh* attack, indicating a potential involvement of those lipids in the barley-*Bgh*-interaction. In summary, this work provided novel insights into the RACB-mediated susceptibility signaling in barley and identified plant anionic phospholipids as a potential virulence target of *Bgh*.

Zusammenfassung

Ein großer Teil der jährlichen Ernteausfälle der Pflanzenproduktion ist auf die Infektion mit Pflanzenpathogenen zurückzuführen. Um dieses Problem anzugehen, werden Studien durchgeführt, die die Beziehung zwischen Pflanze und Erreger besser verstehen wollen. Ein Beispiel hierfür ist das Gerste-Mehltau-Pathosystem, in dem man die molekularen Grundlagen von Krankheitsanfälligkeit untersucht. In diesem System wurde die Rho-of-plant GTPase RACB als pflanzlicher Anfälligkeitsfaktor identifiziert, der die Infektion von Gerste durch den Echten Mehltaupilz *Blumeria graminis* f.sp. *hordei* (*Bgh*) begünstigt. Im Gegensatz zu anderen Anfälligkeitsfaktoren inhibiert RACB nicht die Pflanzenabwehr, sondern wird wahrscheinlich von *Bgh* ausgenutzt, um Gerste zu infizieren. Die zugrundeliegende molekularen Mechanismen sind aber noch nicht vollständig geklärt. Daher hat sich diese Arbeit einerseits mit der Regulation von RACB durch posttranslationale Modifikationen beschäftigt und andererseits neue Interaktionspartner von RACB aufgedeckt, mit dem Ziel die zellulären Signalwege zu identifizieren, die mit Anfälligkeit zusammenhängen. Eine Ubiquitinierung von RACB wurde am Rest der Aminosäure K167 nachgewiesen, was die Proteinstabilität beeinflusst. Eine Mutation dieses Lysins beeinflusst die Signaltransduktion von RACB nicht, jedoch wird diskutiert, dass Ubiquitinierung selbst hier einen Einfluss haben kann. Da K167 in anderen RACB-ähnlichen Rho Proteinen aus Pflanzen und Tieren konserviert ist, deutet dies weit verbreitete regulatorische Funktionen an. Weiterhin wurden drei neue mögliche Interaktionspartner für RACB entdeckt, die eine Verbindung zu pflanzlichen anionischen Phospholipiden herstellen. Im Gerste-Mehltau-Pathosystem spielen die entdeckten Phospholipase PLC und die Phosphoinositid-Phosphatase PIP eine Rolle in der Resistenz. Im Gegensatz dazu bindet das *Bgh*-Effektorprotein 9o9 direkt an aktiviertes RACB und beeinflusst nach Überexpression in der Gerstenepidermis die Anfälligkeit von Gerste zugunsten des Pilzes. Auch sind überlappende Signalprozesse denkbar, da die drei Interaktoren und RACB *in vitro* zum Teil an die gleichen anionischen Phospholipide binden. Außerdem wurde bei Markerproteinen für vier pflanzliche anionische Phospholipidspezies ein verändertes subzelluläres Muster während der Mehltauinfektion festgestellt, was auf eine Rolle der Lipide im Gerste-Mehltau-Pathosystem hindeutet. Insgesamt liefert diese Arbeit neue Erkenntnisse über die Signalwege des Anfälligkeitsfaktors RACB und deckt pflanzliche anionische Phospholipide als mögliches Ziel der Virulenzfunktionen von *Bgh* auf.

Abbreviations and Acronyms

°C	Degrees Celsius
µg	Microgram
µL	Microliter
µM	Micromolar
µm	Micrometer
9o9	Nine out of nine
A. thaliana	*Arabidopsis thaliana*
A. tumefaciens	*Agrobacterium tumefaciens*
AA	Amino acid
AB	Agrobacterium buffer
AGC	Protein family containing PKA, PKG and PKC members
AGC (MS)	Automatic gain control
AGT	Appressorial germ tube
AKT	Stock A Strain k AKR mouse thymoma
ANOVA	Analysis of variance
AP	Alkalic phosphatase
Arf	ADP-ribosylation factor
ARO	ARMADILLO-REPEAT ONLY
At	*Arabidopsis thaliana*
ATP	Adenosine triphosphate
Avr	Avirulence gene
BAK1	Brassinosteroid insensitive 1-associated kinase 1
BaRTD	Barley reference transcript database
BCIP	5-bromo-4-chloro-3-indolyl phosphate di-sodium salt
Bgh	*Blumeria graminis* f.sp. *hordei*
Bgt	*Blumeria graminis* f.sp. *tritici*
β-Tub2	β-Tubulin 2
CA	Constitutively active
CC	Coiled-coil
CD	Conserved domain
Cdc42	Cell division control protein 42 homolog
cDNA	Complementary DNA
CEBiP	CHITIN OLIGOSACCHARIDE ELICITOR-BINDING PROTEIN
CEP	Candidate effector protein
CERK1	CHITIN ELICITOR RECEPTOR KINASE 1
CFP	Cyan fluorescent protein
Ch	*Colletotrichum higginsianum*
cIRF	Calculated internal response factor
CLSM	Confocal laser scanning microscopy
cm	centimeter
CNL	CC-NB-LRR receptor
CoIP	Co-immunoprecipitation
CRIB	Cdc42/Rac-interactive binding domain
CSEP	Candidate secreted effector protein
Ct	Cycle threshold
cv.	Cultivar
CWA	Cell wall apposition
d	day
D6PK	D6 protein kinase
DAG	Diacylglycerol
DAMP	Damage-associated molecular pattern
ddH_2O	Double-distilled water
DEPC	Di-ethyl dicarbonate
DGK	Diacylglycerol kinase
DMSO	Dimethyl sulfoxide
DN	Dominant negative
DNA	Deoxyribonucleic acid
dOCRL	Drosophila melanogaster OCRL protein
dpa	Days post anthesis
dpi	Days post infection
DTT	Dithiothreitol
E. coli	*Escherichia coli*
Ec	*Erysiphe cichoracearum*
EDTA	Ethylenediaminetetraacetic acid
eGFP	Enhanced GFP
EHM	Extra-haustorial matrix
EIHM	Extra-invasive hyphal membrane
EKA	Effector homologous to AvrK1 and AvrA10
ER	Endoplasmic reticulum
ETI	Effector-triggered immunity
ETS	Effector-triggered susceptibility
FAB1	FORMATION OF APLOID AND BINUCLEATE CELLS 1
FAPP	Four-Phosphate Adapter Protein
FBXL19	F-box/LRR protein 19
Fig.	Figure
flg22	A 22 amino acid peptide of bacterial flagellin
FLS2	FLAGELLIN-SENSING 2
fmol	Femtomolar
FRET	Förster-resonance energy transfer
FRET-FLIM	FRET fluorescence lifetime imaging microscopy
f.sp.	*Forma specialis*
g (force)	Gravitational force
g (weight)	Gram
GAP	GTPase activating protein
GAPDH	Glyceraldehyde-3-phosphate dehydrogenase
GDI	Guanine nucleotide dissociation inhibitor
GDP	Guanosine diphosphate
GEF	Guanine nucleotide exchange factor
GFP	Green fluorescent protein
Go	*Golovinomyces orontii*
G-protein	Guanine nucleotide-binding protein

GST	Glutathione *S*-transferase	**mM**	Millimolar
GTP	Guanosine triphosphate	**MS**	Mass spectrometry
GUS	β-glucoronidase	***Ms***	*Medicago sativa*
h	Hour	**MVB/LE**	Multi-vesicular bodies/late endosomes
HA	Hemagglutinin		
Hpa	*Hyaloperonospora arabidopsidis*	**n**	Number of observations
hpi	Hours post infection	***N. benthamiana***	*Nicotiana benthamiana*
HPLC	High-performance liquid chromatography	**n.d.**	Not determined
		n.s.	Not significant
HR	Hypersensitive response	**NA/n.a.**	Not available
HRP	Horseradish peroxidase	**NB**	Nucleotide-binding
Hv	*Hordeum vulgare*	**NBT**	Nitro blue tetrazolium chloride
HVR	Hypervariable region	**ng**	Nanogram
HyD	Hybrid detector	**NLR**	NB-LRR receptor
Hz	Hertz	**nm**	Nanometer
I	Input fraction	**ns**	Nanosecond
ICRs	Interactors of Constitutive Active ROPs	***Nt***	*Nicotiana tabacum*
		oD$_{600}$	Optical density at 600 nm
IMAC	Immobilized metal affinity chromatography	**OEX**	Overexpression
		Os	*Oryza sativa*
inHg	Inches of mercury	***Os*GH1**	GRAIN NUMBER AND PLANT HEIGHT 1
InsP$_3$	Inositol-1,4,5-trisphosphate		
IP	Immunoprecipitation	**pa**	Post anthesis
IPTG	Isopropyl β-D-1-thio-galactopyranoside	**PA**	Phosphatidic acid
		pad4	PHYTOALEXIN DEFICIENT 4
ISR	Induced systemic resistance	**PaTox**	*Photorhabdus asymbiotica* protein toxin
kb	Kilobase		
kDa	Kilo Dalton	**PBR**	Polybasic region
kg	Kilogram	**PBS-T**	Phosphate-buffered saline with Tween20
L	Liter		
LACT	Lactadherin	**PC**	Phosphatidylcholine
LC	Liquid chromatography	**PCR**	Polymerase chain reaction
LINE	Long-interspersed element	**PE**	Phosphatidylethanolamine
LORE	Lipooligosaccharide-specific reduced elicitation	**PEG**	Polyethylene glycol
		pen2	PENETRATION 2
LRR	Leucine-rich repeat	**PH**	Pleckstrin-homology
LYK5	LysM-CONTAINING RECEPTOR-LIKE KINASE 5	**PI**	Phosphatidylinositol
		PI3P	Phosphatidylinositol-3-phosphate
m	Meter		
M	Molar	**PI4P**	Phosphatidylinositol-4-phosphate
m/z	Mass per charge ratio		
MAGAP1	MICROTUBULE-ASSOCIATED ROP-GTPASE ACTIVATING PROTEIN 1	**PI5P**	Phosphatidylinositol-5-phosphate
		PI(3,4)P$_2$	Phosphatidylinositol-3,4-bisphosphate
MAMP	Microbe-associated molecular pattern	**PI(3,5)P$_2$**	Phosphatidylinositol-3,5-bisphosphate
MAPK	MAP-kinase		
MBP	Maltose-binding protein	**PI(4,5)P$_2$**	Phosphatidylinositol-4,5-bisphosphate
Mbp	Megabasepairs		
meGFP	Monomeric enhanced GFP	**PI(3,4,5)P$_3$**	Phosphatidylinositol-3,4,5-trisphosphate
MES	2-(N-morpholino)ethanesulfonic acid	**PIP**	Phosphoinositide phosphatase
		PIP5K	Phosphoinositide-4-phosphate 5-kinase
mg	Milligram		
MHz	Megahertz		
min	Minute	**PLC**	Phospholipase C
mL	Milliliter	**PM**	Plasma membrane
ML1N	Mucolipin 1	**pmol**	Picomol
MLO	Mildew resistance locus O	**PMSF**	Phenylmethylsulfonyl fluoride
MLU	Martin-Luther University	**PMT**	Photomultiplier tube
mm	Millimeter	**PNK**	Poly-nucleotide kinase

PRM	Parallel reaction monitoring
PRONE	Plant-specific ROP nucleotide exchanger
PRR	Pattern-recognition receptor
PS	Phosphatidylserine
psi	Pounds per square inch
PTI	Pattern-triggered immunity
PTM	Posttranslational modification
PVDF	Polyvinylidene difluoride
qRT-PCR	Quantitative reverse-transcription PCR
Rab	Ras-like proteins in brain
Rac	Ras-related C3 botulinum toxin substrate
Ran	Ras-like nuclear
Ras	Rat sarcoma
RBK1	ROP binding protein kinase 1
RBOHD	Respiratory burst oxidase homolog D
REN	ROP enhancer
R-gene	Resistance-gene
Rho	Ras homologous
RhoBTB	Rho-related BTB domain containing protein
RIC	ROP-interactive and CRIB-motif containing protein
RIN4	RPM1-INTERACTING PROTEIN 4
RIP	ROP Interactive Partner
RLCK	Receptor-like cytoplasmic kinase
RLK	Receptor-like kinase
RLP	Receptor-like protein
RNA	Ribonucleic acid
RNAi	RNA interference
RNAseq	RNA sequencing
Rnd	Round
ROI	Region of interest
ROP	Rho-of-plant protein
ROPIP1	ROP-INTERACTIVE PEPTIDE 1
ROS	Reactive oxygen species
s	Second
S	Supplemental
SAC	Suppressor of actin
sag101	SENESCENCE-ASSOCIATED GENE 101
SAR	Systemic acquired resistance
SCF	SKP1-cullin1-F-box protein complex
SCN1	SUPERCENTIPEDE 1
SD	Standard-defined medium
SDS	Sodium dodecyl sulfate
SDS-PAGE	SDS polyacrylamide gel-electrophoresis
***S*-gene**	Susceptibility gene
SKP1L	S-phase kinase 1-associated protein-like
SP	Signal peptide
SUC2	β-fructofuranosidase SUC2
TBS	Tris-buffered saline
TCSPC	Time-correlated single photon counting
TE	Tris-EDTA
TGN/EE	Trans-Golgi network/early endosomes
TIM	Triosephosphate isomerase
TIR	Toll-interleukin 1 receptor
TNL	TIR-NB-LRR receptor
TPM	Transcripts per million
TRIS	Tris(hydroxymethyl)amino-methane
TUM	Technical University of Munich
U	Unit
U (IP)	Unbound fraction
UBC2	Ubiquitin-conjugating enzyme 2
W	Wash fraction
v/v	Volume per volume
w/v	Weight per volume
WT	Wildtype
Zm	*Zea mays*

Contents

List of Figures

List of Tables

Publications

Several findings of this dissertation have been published in:

Weiß, L., Gaelings, L., Reiner, T., Mergner, J., Kuster, B., Fehér, A., Hensel, G., Gahrtz, M., Kumlehn, J., Engelhardt, S., and Hückelhoven, R. 2022. Posttranslational Modification of the RHO of Plants Protein RACB by Phosphorylation and Cross-Kingdom Conserved Ubiquitination. *PLOS ONE*, 17(3):1–30

1 Introduction

1.1 Motivation

The population of our planet was projected to reach 10 billion people between the years 2050 and 2060, according to the United Nations (United Nations and Social Affairs, 2019). To feed future generations, more food has to be produced on the same amount of arable land that is available today. For this reason, crops need to produce more yield than they currently do. While breeding of high-yielding crop varieties aims to tackle this problem, farmers and food industries are also facing additional challenges. Due to climate change, the average global temperature is expected to increase by up to four degrees until the end of this century (IPCC, 2014). This will result in heat waves and extended drought periods, which will negatively impact crop yield as well. On top, more unpredictable yield losses will be caused by plant pathogens that are capable of causing devastating epidemics (Dangl et al., 2013). In extreme cases, they can wipe out whole fields within the course of days (Goellner et al., 2010). Already today, our agriculture is facing many of these challenges. To alleviate some of the pressure that is generated by the global food deficit and to keep plant pathogens in check, many strategies are employed to improve plant health and food production. The main strategies include pesticide treatments and field management practices, such as ploughing and crop rotation, as well as the use of disease-resistant crop cultivars (Dodds and Rathjen, 2010; Dangl et al., 2013; Engelhardt et al., 2018). Especially breeding of the latter profits greatly from fundamental research, which is why considerable efforts are being made to understand the plant immune system and plant-pathogen-relationships.
Particularly how and why plants are susceptible towards diseases is little understood. Using a plant protein involved in the establishment of the powdery mildew disease on barley, I wanted to deepen our knowledge about the molecular mechanisms underlying disease susceptibility.

1.2 Plant immunity

In contrast to animals, plants lack specialized mobile immune cells and an adaptive immune system (Jones and Dangl, 2006; Boller and Felix, 2009; Spoel and Dong, 2012). Instead, they rely on pre-determined genetic factors and a multilayered immune response to defend themselves against attackers. The first line of defense consists of preformed physical and chemical barriers, such as the plant cell wall, leaf cuticle and antimicrobial compounds (Nürnberger and Lipka, 2005; Malinovsky et al., 2014). If these barriers are overcome, plants respond with a two-tiered immune response composed of pattern-triggered immunity (PTI) and effector-triggered immunity (ETI) (Jones and Dangl, 2006; Ngou et al., 2022). Initially, PTI and ETI were described to be strictly divided, with ETI being successive to PTI (Jones and Dangl, 2006). This was long discussed to be an oversimplification, due to for example partially overlapping signaling pathways (Thomma et al., 2011; Peng et al., 2018). Recently, several studies confirmed this by showing that PTI- and ETI-signaling processes are co-dependent and can potentiate each other, which results in stronger defense responses (Ngou et al., 2021; Yuan et al., 2021; Ngou et al., 2022). Nonetheless, for the sake of simplicity, PTI and ETI will be introduced separately in the paragraphs below.

In PTI, plants use pattern recognition receptors (PRRs) to perceive pathogenic microbes, which live in the extracellular space between plant cells (called the apoplast) (Zebell and Dong, 2015). So far, all characterized PRRs are cell surface localized, but they can be divided into two classes: receptor-like kinases (RLKs) and kinase domain-lacking transmembrane receptor-like proteins (RLPs) (Dodds and Rathjen, 2010; Macho and Zipfel, 2014). PRRs are able to recognize elicitors, small molecules that can induce defense responses in plants (Dodds and Rathjen, 2010; Boutrot and Zipfel, 2017). PRRs either identify whole classes of microbes via their molecular signatures (termed microbe-associated molecular patterns, MAMPs) or plant molecules derived from damage (damage-associated molecular patterns, DAMPs) (Boller and Felix, 2009; Boutrot and Zipfel, 2017; Tanaka and Heil, 2021). MAMPs are not present in the host and therefore give plants the ability of non-self recognition. PRRs and MAMPs are widely conserved among both plants and microbes, and several pairs have been described in the past. Perhaps the most prominent example for any PRR-MAMP pair is the bacterial elicitor flg22, a 22 amino acid-long peptide of bacterial flagella, which is perceived by the RLK FLAGELLIN-SENSING 2 (FLS2) and its co-receptor Brassinosteroid insensitive 1-associated kinase 1 (BAK1) in *Arabidopsis thaliana* (Gómez-Gómez and Boller, 2000; Chinchilla et al., 2007). For fungi, it was shown that chitin can be recognized by the RLP CHITIN OLIGOSACCHARIDE ELICITOR-BINDING PROTEIN (CEBiP) and its co-receptor CHITIN ELICITOR RECEPTOR KINASE 1 (CERK1) in rice (Kaku et al., 2006; Shimizu et al., 2010)

and the RLK LysM-CONTAINING RECEPTOR-LIKE KINASE 5 (LYK5) and CERK1 in *Arabidopsis* (Cao et al., 2014). In general, MAMP perception and signal transduction are cooperative processes that involve many different proteins, but in the end all lead to activation of hallmark PTI responses (Boller and Felix, 2009; Yu et al., 2017). Among the earliest reactions are influx of Ca^{2+}-ions, reactive-oxygen species (ROS) production by Respiratory burst oxidase homolog D (RBOHD), alkalinization of the apoplast and Mitogen-activated protein kinase (MAPK)-activation (Felix et al., 1999; Nürnberger et al., 2004; Nühse et al., 2007; Yu et al., 2017; Bi et al., 2018). These are followed by ethylene production and defense gene activation and later by callose deposition at the cell periphery and growth inhibition, which is likely a result of the plant redirecting resources from growth to immunity-related processes (Chinchilla et al., 2007; Boller and Felix, 2009; Luna et al., 2011; Albert et al., 2015).
To overcome plant immunity and subdue the host, pathogens employ so-called effectors that bypass or suppress plant defense responses (Jones and Dangl, 2006; Ngou et al., 2022). These effectors are often under strong selective pressure and are therefore highly diverse in sequence and molecular function (Dodds and Rathjen, 2010; Spoel and Dong, 2012; Asai and Shirasu, 2015). However, effectors share certain characteristic features: some effectors are apoplastic, but most of them are secreted into host cells via specialized delivery machineries, which differ for each kingdom. Bacteria use the type III secretion system, fungi and oomycetes translocate effectors through haustoria and aphids and nematodes deliver them via stylets during feeding (Gheysen and Mitchum, 2011; Bozkurt et al., 2012; Rodriguez and Bos, 2013; Petre and Kamoun, 2014; Macho and Zipfel, 2015). Once inside the host cell, effectors interact with plant targets, altering their activity or stability in the process (Dangl et al., 2013; Doyle et al., 2013). This suppresses or modifies immune responses to a point, where pathogens can successfully proliferate in their host (Dangl et al., 2013). Thus, this process is referred to as effector-triggered susceptibility (ETS) (Jones and Dangl, 2006; Ngou et al., 2022).
Recognition of these pathogenic effectors by the plant is hence called effector-triggered immunity, which is race-specific and originates from dominantly inherited resistance (R-) genes (Jones and Dangl, 2006; Pavan et al., 2010; Ngou et al., 2022). In general, ETI results in renewed and stronger immune responses, as well as a localized programmed cell death called hypersensitive response (HR) (Jones and Dangl, 2006; Dodds and Rathjen, 2010; Zebell and Dong, 2015; Cui et al., 2015). Effector perception is achieved via intracellular nucleotide-binding (NB) leucine-rich repeat (LRR) receptors (NB-LRRs or NLRs), which can be divided into two classes based on their N-terminal domain. This can be either a Toll-interleukin 1 receptor (TIR) domain (TNLs) or a coiled-coil (CC) domain (CNLs). Additionally, two archetypes of NLRs exist: sensor and helper NLRs. Sensor NLRs recognize pathogen interference

in the host, while helper NLRs are required for full activation of immune responses (Tamborski and Krasileva, 2020). NLRs are the fastest evolving genes in plants, likely due to the high selective pressure to recognize adapted pathogens (Cui et al., 2015). In order to avoid constitutive defense responses and spontaneous cell death, NLR activation is highly controlled via autoinhibition (Cui et al., 2015). This is alleviated, when the NLR directly or indirectly recognizes an effector. Direct recognition means that the NLR itself binds an effector protein, which consecutively activates ETI (Dodds and Rathjen, 2010). Indirect perception follows the "guard hypothesis" (Jones and Dangl, 2006), in which an effector does not bind the NLR, but a different target in the host. This target is called the "guardee", as its presence or modification is monitored by an NLR (Jones and Dangl, 2006). Manipulation of the guardee by an effector is beneficial for the pathogen, for example by hampering activation or transduction of PTI responses (Macho et al., 2014). However, this manipulation of the guardee creates a "pathogen-induced modified self" that is recognized by the NLR, which abolishes autoinhibition and triggers ETI (Spoel and Dong, 2012). The guard hypothesis was also extended by the "decoy model" (van der Hoorn and Kamoun, 2008), in which selected plant proteins mimic the structural fold of an actual effector target. These decoys would be preferably recognized and modified by effectors, leading to NLR activation. Recognized effectors are called avirulence factors (in short: Avrs), because their presence provokes strong defense responses in the plant and therefore leads to avirulence of the pathogen.
In summary, plants and pathogens are under high selective pressure at all times (Jones and Dangl, 2006). In order to stay virulent, pathogens have to either create new effectors, or lose or diversify recognized Avrs to avoid or suppress ETI. In turn, plants need to acquire new NLR specificities to keep up with pathogen evolution. This cycle of plant-pathogen co-evolution can be extended endlessly, which is why it was called an "evolutionary arms race" (Jones and Dangl, 2006).
Activation of plant immunity can also trigger so-called induced resistance in distal, uninfected parts of the plant in order to prepare these tissues for oncoming invasion. The induced resistance after pathogen attack is called systemic acquired resistance (SAR), which can be initiated after PTI or ETI (Mishina and Zeier, 2007; Spoel and Dong, 2012). The SAR signal is generated locally in infected leaves and transported through the vasculature towards uninfected systemic tissues, where it leads to priming of immune responses (Vernooij et al., 1994; Nandi et al., 2004; Park et al., 2007; Jung et al., 2009; Chanda et al., 2011; Spoel and Dong, 2012). Ultimately, SAR is highly effective at limiting growth of a broad range of pathogens (Spoel and Dong, 2012). Another form of induced resistance exists, which is called induced systemic resistance (ISR). ISR is facilitated through beneficial microbes, such as plant-growth promoting bacteria and fungi in the plant's rhizosphere (Pieterse et al., 2014). Similar to SAR,

ISR leaves the plant in a primed state, where it is able to respond quicker and stronger to pathogen attacks in distal tissues. In either case, the primed state is usually maintained throughout the whole life of the plant and can be even passed down to future generations (Mauch-Mani et al., 2017).

1.3 Susceptibility factors

Apart from trying to overcome or bypass plant immunity, pathogens can also benefit from host processes that facilitate their establishment. Plant genes involved in such processes are dominantly inherited and called susceptibility factors or susceptibility genes (*S*-genes), because mutation or loss of these *S*-genes results in more resistant plants (Eckardt, 2002; van Schie and Takken, 2014). Hence, *S*-gene-associated resistance is recessively inherited, which stands in contrast to the dominantly inherited R-genes (Pavan et al., 2010). From a plant's perspective, *S*-genes are usually indispensable for growth and developmental processes, but from a pathogen's point of view, they can be sorted into the following functional categories (van Schie and Takken, 2014; Engelhardt et al., 2018): susceptibility factors can be important for host compatibility, either early during host recognition and entry or later for sustained accommodation of the pathogen. Alternatively, *S*-genes can be negative regulators of plant immune signaling by for example suppressing PTI or ETI. Pathogens can hijack susceptibility factors of any category in order to establish themselves in the plant, which is why *S*-genes can even be guarded by R-genes (van Schie and Takken, 2014; Engelhardt et al., 2018).

The example of RPM1-INTERACTING PROTEIN 4 (RIN4) in the *Arabidopsis thaliana-Pseudomonas syringae* pathosystem nicely illustrates the complex nature of susceptibility factors and their role in plant immunity. Functionally, RIN4 is a negative regulator of plant immune responses and important for stomata re-opening after pathogen invasion or drought stress (Mackey et al., 2002; Kim et al., 2005b; Liu et al., 2009a; Kaundal et al., 2017). This marks it as an ideal target for bacterial effector proteins, because the only way of entry for bacteria is often through natural openings such as stomata (Liu et al., 2009a). Hence, bacteria try to exploit RIN4 function to enter the host. To date, RIN4 was found to be targeted by at least six effector proteins from different *Pseudomonas syringae* pathovars, which degrade or modify RIN4 in order to keep stomata open and suppress immunity (Mackey et al., 2002; Axtell and Staskawicz, 2003; Day et al., 2005; Kim et al., 2005a; Wilton et al., 2010; Afzal et al., 2011; Liu et al., 2011; Choi et al., 2021). Plants however cannot simply lose RIN4 by ways of selection, because it appears to be an important regulator of stomata re-opening after drought stress and pathogen attack (van Schie and Takken, 2014; Kaundal et al., 2017). Instead, *Arabidopsis* guards RIN4 by two different R-proteins, which recognize effector-induced modification or degradation of

RIN4 (Mackey et al., 2002; Axtell and Staskawicz, 2003; Day et al., 2005; Liu et al., 2011; Choi et al., 2021).
Susceptibility factors have been successfully used in breeding of resistant crops. One of the oldest characterized *S*-genes, *Mildew resistance locus O* (*MLO*), was originally described in the 1940s (Jørgensen, 1992), but *mlo*-plants were already collected during expeditions to Ethiopia in the 1930s, where it may have been selected for by highland farmers (Piffanelli et al., 2004). *mlo*-mediated resistance against powdery mildew fungi was described to be durable and non-race specific, and ever since its first use in spring barley during the 1980s has not been overcome in the field (Jørgensen, 1992; Kusch and Panstruga, 2017). While it could be recently demonstrated that MLO-proteins are active Ca^{2+}-channels that are involved in plant fertilization (Gao et al., 2022), the molecular mechanism behind *mlo*-mediated resistance is not fully clear yet, despite several years of extensive studies (Kusch and Panstruga, 2017). In the barley-*Bgh*-pathosystem (see Section 1.4), an *mlo*-knockout results in pre-penetration resistance, meaning *Bgh* spores fail at penetrating barley epidermal cells, which leads to fungal growth arrest and no infection (Jørgensen and Mortensen, 1977). The cell wall appositions (CWAs) that are built by the plant right at the penetration site as a means of defense are larger and more numerous in an *mlo* genotype and were shown to contain callose (Skou, 1982; Skou et al., 1984; Stolzenburg et al., 1984). Moreover, defense-related compounds and transcripts are overproduced in *mlo*-plants and mesophyll cells below attacked epidermal cells can even undergo an HR-like response. In summary, parts of the *mlo*-mediated resistance against powdery mildew fungi resembles more the response to a non-host pathogen than an adapted pathogen (Kusch and Panstruga, 2017).
Resistance mediated by an *mlo*-knockout also illustrates the price that using a susceptibility factor for breeding of resistant plants can have on plant physiology. Since *S*-genes are often essential in physiological processes of the plant, their knockout can result in various pleiotropic effects (Engelhardt et al., 2018). For instance, *mlo*-mutants spontaneously develop CWAs in absence of pathogens or other stresses and show early leaf senescence, which might cause problems for cultivation of *mlo*-plants in the field (Wolter et al., 1993; Peterhansel et al., 1997; Piffanelli et al., 2002; Makepeace et al., 2007). Additionally, a knockout of *MLO*-genes highlights the "ambivalence" of susceptibility factors in disease resistance (Jarosch et al., 1999). While *mlo*-plants are virtually resistant against any kind of powdery mildew fungus, they show higher susceptibility towards the non-biotrophic pathogens *Magnaporthe grisea* and *Bipolaris sorokiniana* (Jarosch et al., 1999; Kumar et al., 2001). Nonetheless, *mlo* exemplifies that *S*-genes can be an invaluable tool for breeding of resistant plants.
Apart from *RIN4* and *MLO*, several other susceptibility factors have been described to date, one of them being another barley protein called RACB, which will be

introduced in Section 1.6.

1.4 The barley-powdery mildew pathosystem

To study plant immunity and plant-pathogen interactions, so-called plant-pathosystems are widely used. Their main advantages are that both plant and pathogen can be cultivated under laboratory conditions and either one or preferably both organisms can be genetically modified. One paradigm example for such a pathosystem is the powdery mildew disease on barley, which has been extensively used to study the cell biology of plant-microbe interactions (Hückelhoven and Panstruga, 2011). Cultivated barley (*Hordeum vulgare* L. subspecies *vulgare*, in short: *Hv*) is the world's fourth most important cereal, after maize, rice and wheat. While as a crop it is mainly used for the production of animal feed and high-quality malt, it is also a well-recognized model organism for genetic and developmental biology research (Langridge, 2018). Barley can be genetically modified transiently through for example particle bombardment (Hensgens et al., 1993), but also transgenic plants can be generated through *Agrobacterium tumefaciens*-mediated transformation of embryos (Hensel et al., 2009). The causal agent for the powdery mildew disease on barley is the obligate biotrophic fungus *Blumeria graminis* DC. *forma specialis* (f.sp.) *hordei* (Marchal; abbreviated as *Bgh*), which belongs to the order of Erysiphales in the Ascomycota phylum. Powdery mildew fungi in general infect a wide range of economically important plants, such as cereals, fruits and ornamental plants and can cause significant economic losses (Glawe, 2008; Oerke, 2006). These fungi are extremely specialized pathogens with a high degree of host adaptation. *Bgh* for instance can only infect barley, but not other closely related crops such as rye or oat. However, it was shown that *formae speciales* of *Blumeria graminis* crop isolates can infect wild grasses as well, suggesting that these might be temporary hosts between seasons and serve as a source of fresh inoculum in the new crop vegetation period (Eshed and Wahl, 1970, 1975; Troch et al., 2014). The main characteristic disease symptom for powdery mildew fungi is the appearance of white-to-yellow pustules on aerial plant organs, such as leaves or fruits (see Fig. 1.1 A, Glawe (2008)). These pustules contain asexual fungal spores (known as conidia), which are dispersed by wind. Concerning *Blumeria graminis*, conidia are most probably the main source of infection in the field, as genome comparisons of four field isolates revealed mostly clonal or near-clonal reproduction (Wicker et al., 2013; Jankovics et al., 2015). The other means of infection comes in form of ascospores, which are produced in sexual fruiting bodies called chasmothecia. It was long believed that mainly ascospores initiate the infection cycle of *Blumeria graminis* in the field (Agrios, 2005), but a more recent study proposed that this is not the case. Instead, chasmothecia could be formed as oversummering structures when environmental conditions are unfavorable

(Jankovics et al., 2015). Hence, the asexual life cycle, which is also most studied in this pathosystem, will be described below.
The asexual infection cycle starts, when a *Bgh* spore lands on the surface of a barley leaf (see Fig. 1.1 B). Immediately after landing, the spore begins to secrete lytic enzymes to attach to the leaf surface (Carver et al., 1999; Wright et al., 2002). Within the first hour, the spore germinates and forms the primary germ tube (Kunoh, 2002), which is unique for *Blumeria graminis*, as other powdery mildew fungi do not produce this structure (Glawe, 2008). The primary germ tube proceeds to penetrate the cuticle and is believed to soak up water and electrolytes from the leaf (Edwards, 2002). After 4-8 hours post infection (hpi), the *Bgh* spore forms a secondary germ tube, which differentiates into a hook-shaped attack structure called the appressorium (or appressorial germ tube, AGT) (Zhang et al. (2005) and personal observations). Within the next two hours, the AGT builds a penetration peg and tries to penetrate the plant cell wall using cell wall-softening lytic enzymes and mechanical force generated by turgor pressure (Green et al., 2002; Zhang et al., 2005). Directly below the penetration peg, the plant deposits modified cell wall material in a dome-shaped structure called the papilla (or cell wall apposition), which is believed to serve as a mechanical and chemical barrier against the attack (Hückelhoven, 2005). However, if the infection is successful, the penetration peg extends, invaginates the host cell and forms a haustorium at 12-18 hpi (Glawe, 2008). The haustorium is fully developed at 48 hpi and believed to serve as an organ for nutrient uptake and effector delivery (Zhang et al., 2005; O'Connell and Panstruga, 2006; Giraldo and Valent, 2013). Furthermore, the haustorium is surrounded by the extrahaustorial matrix and the so-called extrahaustorial membrane (EHM), which extends from the host plasma membrane (PM) but is different in its composition (Koh et al., 2005; Glawe, 2008). Currently, the EHM in the barley-powdery mildew pathosystem is believed to be similar to the membrane of the endoplasmatic reticulum (ER) (Kwaaitaal et al., 2017). Following 24 hpi, secondary hyphae will emerge from the AGT, which can also attack other epidermal cells via appressoria (Zhang et al., 2005). Repeated branching and elongation of these secondary hyphae then form a circular powdery mildew colony, which can be seen by eye 5-8 days post infection (dpi) (Glawe, 2008). Finally, these hyphae will build conidiophores that reach maturity at 6 dpi and can disperse new conidia via wind (Moriura et al., 2006).
This brief life cycle and easy propagation of spores makes *Bgh* a suitable model pathogen to work with, even though *Bgh* could not be genetically modified to date. Nonetheless, the genome of *Bgh* has been fully sequenced and, with roughly 120 Mbp in size, was found to be considerably larger than that of most other Ascomycetes (Spanu et al., 2010). This genome size expansion could be attributed to extensive retrotransposon proliferation, as 64 % of the genome consist of transposable elements.

At the same time, the genome of *Bgh* showed severe losses of genes associated with primary and secondary metabolism, transporters and plant cell wall degradation enzymes. It was hypothesized that these gene losses are one of the main factors responsible for the obligate biotrophic lifestyle of *Bgh*. The genome was also mined for putative effector candidates, which revealed 491 candidate secreted effector proteins (CSEPs) (Pedersen et al., 2012) and over 1350 effectors homologous to *AvrK1* and *AvrA10* (EKAs) (Spanu et al., 2010; Amselem et al., 2015). CSEPs contain an N-terminal signal peptide, lack transmembrane domains and have no similar proteins outside of the mildew pathogens (Spanu et al., 2010). CSEPs can be grouped into two major families: one family harbors proteins, which are 100-150 amino acids in length and highly expressed in haustoria, while the other family contains 300-400 amino acid long proteins with lower levels of expression (Pedersen et al., 2012). In turn, EKAs originated from truncations of the ORF1 protein of class I long-interspersed element (LINE) retrotransposons and were initially described to lack N-terminal signal sequences (Ridout et al., 2006; Amselem et al., 2015). However, recent literature puts doubt on the nature of the name-giving member *AvrA10*, because an independent CSEP was observed to have AvrA10 function (Saur et al., 2019). Still, members of both CSEPs and EKAs have been shown to contribute to *Bgh* virulence (Ridout et al., 2006; Pliego et al., 2013).

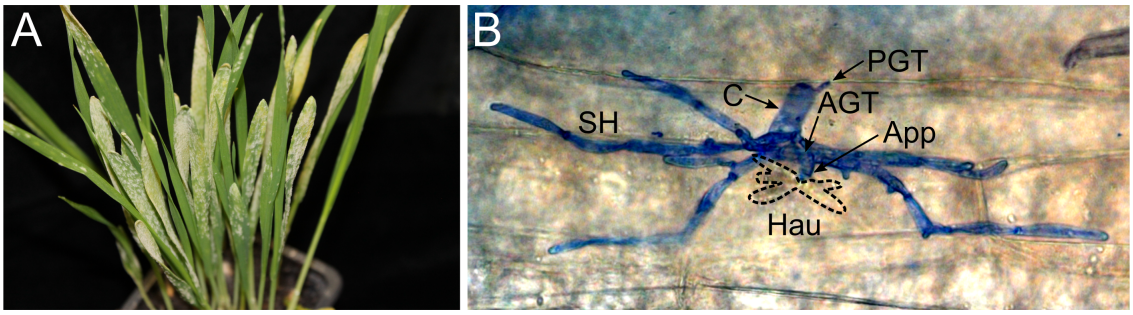

Figure 1.1: The powdery mildew disease on barley.
The barley powdery mildew fungus *Blumeria graminis* f.sp. *hordei* (*Bgh*) causes white pustules as disease symptoms on barley leaves (**A**). The asexual life cycle of *Bgh* (**B**) begins, when a conidium (C) lands on the leaf surface. After formation of a primary germ tube (PGT), *Bgh* forms a secondary appressorial germ tube (AGT) that differentiates into an attack structure termed appressorium (App). If the appressorium is successful in penetrating the plant cell wall, *Bgh* invaginates the host cytoplasm and establishes a feeding structure called the haustorium (Hau, dashed lines). Afterwards, *Bgh* forms secondary hyphae (SH) on the leaf surface to further colonize the barley leaf. For (**A**), images were taken 7 days post *Bgh*-infection. For (**B**), leaves were fixed and destained at 48 hours post *Bgh*-infection and fungal structures were stained with ink before analysis via light microscopy.

1.5 Rho-of-plant proteins

Rho-of-plant proteins belong to the guanine nucleotide-binding (G-) proteins, which are master regulators of cellular signaling processes (Gu et al., 2004). They are named after a family of small monomeric G-proteins in mammals, which are organized in one superfamily: the rat sarcoma (Ras) superfamily contains the name-giving Ras family itself, as well as the ADP-ribosylation factor (Arf), Ras-like proteins in brain (Rab), Ras-like nuclear (Ran) and Ras homologous (Rho) families (Wennerberg et al., 2005). The Rho family is further subdivided into cell division control protein 42 homolog (Cdc42)-like, Ras-related C3 botulinum toxin substrate (Rac)-like, Rho-like, Rho-related BTB domain containing (RhoBTB) and Round (Rnd) subfamilies (Lawson and Ridley, 2018). Plants possess members of the Arf, Rab and Ran families, but only one member of the Rho-subfamily: the Rho-of-plant proteins (ROPs) (Yang, 2002). Historically, ROPs were also called Racs, because they are more similar in their sequence to metazoan Rac proteins than Rho proteins (Winge et al., 2000). ROPs can be further divided into type I and type II ROPs, depending on their exon-intron structure and C-terminal motives for lipid modification (Winge et al., 2000). Several ROPs have been identified in different plant species: *Arabidopsis thaliana* (*At*) contains eleven members, while rice (*Oryza sativa*, *Os*) has seven and barley has six (Winge et al., 2000; Schultheiss et al., 2003; Miki et al., 2005).
Structurally, ROPs have a catalytic G-domain at the N-terminus and a hypervariable region (HVR) at the C-terminus (Berken and Wittinghofer, 2008; Yalovsky, 2015). The G-domain consists of the G-box motives G1-G5 and a Rho-specific insert region (also called the insert helix αi) (Berken and Wittinghofer, 2008). The G-box motives are responsible for interactor- and nucleotide-binding, as well as GTP hydrolysis and Mg^{2+}-complexation, while the insert helix is thought to be important for interaction with other proteins (Berken and Wittinghofer, 2008). Specifically the G2 and G3 boxes are also known as the Switch I and Switch II regions, because they change conformation depending on the bound nucleotide, which enables interactor binding (Feiguelman et al., 2018). Conveniently, several point mutations of conserved G-box residues lock ROPs in a particular activity state: mutation of a glycine in G1 or glutamine in G3 creates a constitutively activated (CA) mutant, which is incapable of GTP-hydrolysis and therefore remains bound to GTP indefinitely (Berken and Wittinghofer, 2008). Mutation of a threonine in G1 or aspartic acid in G4 creates dominant negative (DN) mutants, which have a lower affinity for any nucleotide and associate stronger with the ROP-activating guanine nucleotide exchange factors (GEFs) (Berken and Wittinghofer, 2008). These DN mutants can outcompete intrinsic ROPs for GEF-binding, which effectively inhibits ROP-activation in a cell and causes the dominant negative effect on signaling (Berken and Wittinghofer, 2008). The C-terminal HVR is responsible for the subcellular localization of ROPs,

because it contains a sequence motif for posttranslational lipid modifications and a polybasic region (PBR), which is enriched in arginines and lysines (Yalovsky, 2015). Interestingly, ROPs can undergo different kinds of lipid modifications: type I ROPs contain a CaaX-box (cysteine - 2x aliphatic amino acids - any amino acid), in which the cysteine can be prenylated (Yalovsky, 2015; Sorek et al., 2017). Some type I ROPs possess an additional *S*-acylation motif in their G5-domain and were experimentally shown to be palmitoylated (Berken and Wittinghofer, 2008; Sorek et al., 2017). In contrast, type II ROPs lack the CaaX-box and instead own a GC-CG-box (glycine - cysteine - 5/6x aliphatic amino acids - cysteine - glycine) for constitutive *S*-acylation (Lavy et al., 2002; Lavy and Yalovsky, 2006). These lipidations together with the positively charged PBR were shown to be necessary for ROP membrane association and lipid interaction (Lavy and Yalovsky, 2006; Sorek et al., 2009; Platre et al., 2019).

In literature, ROPs are often called molecular switches, because they cycle between an inactive, guanosine diphosphate (GDP)-bound "Off"-state and a signaling-active, guanosine triphosphate (GTP)-bound "On"-state (see Fig. 1.2, Berken (2006); Berken and Wittinghofer (2008)). The aforementioned GEFs hereby facilitate the GDP-to-GTP exchange (Berken et al., 2005). Two different classes of ROPGEFs exist in plants: the PRONE-GEFs, named after their plant-specific ROP nucleotide exchanger (PRONE) domain (Berken et al., 2005) and GEFs distantly related to animal RhoGEFs (Basu et al., 2008; Yamaguchi et al., 2012). Members of both classes were shown to stimulate the nucleotide exchange in ROPs (Berken et al., 2005; Basu et al., 2008; Yamaguchi et al., 2012). Once a ROP becomes GTP-bound, it changes its conformation, which enables association with downstream interactors possessing specialized domains (Feiguelman et al., 2018). ROP-interactive and CRIB-motif containing proteins (RICs) target activated ROPs via their Cdc42/Rac-interactive binding (CRIB) domain (Wu et al., 2000; Engelhardt et al., 2021), while ROP Interactive Partners (RIPs, also called Interactors of Constitutive Active ROPs (ICRs)) bind ROPs via their QWRKAA motif (Lavy et al., 2007; Li et al., 2008; McCollum et al., 2020). Other proteins without these motives can also associate with ROPs, but RICs and RIPs/ICRs are the best characterized ROP interactors to date. Activated ROPs are also targeted by another class of regulatory proteins: GTPase activating proteins (GAPs) terminate ROP signaling by stimulating a ROP's catalytic activity to hydrolyze GTP (Wu et al., 2000). The mechanism of assisting ROPs in GTP-hydrolysis appears to be conserved between GAPs of plants and animals (Berken and Wittinghofer, 2008): GAPs possess a conserved arginine that reaches into the nucleotide binding pocket of Rho-like proteins and stabilizes the transition state of the cleaved γ-phosphate (Bos et al., 2007). Two GAP families were found in plants: CRIB-GAPs (also called RopGAPs) and pleckstrin-homology (PH-)

GAPs (or ROP enhancer GAPs, RENGAPs) (Wu et al., 2000; Hwang et al., 2008; Feiguelman et al., 2018). While CRIB-GAPs are believed to bind activated ROPs directly via their CRIB domain (Wu et al., 2000; Klahre and Kost, 2006; Feiguelman et al., 2018), PH-GAPs were suggested to rely on the help of scaffolding proteins that preferentially associate with GTP-bound ROPs and thereby bridge the ROP-GAP interaction (Hwang et al., 2008; Kulich et al., 2020). Apart from GEFs and GAPs, other ROP-regulatory proteins include guanosine nucleotide dissociation inhibitors (GDIs) (Bischoff et al., 2000). These GDIs can interact with GDP-bound ROPs and sequester them in the cytosol to keep them from signaling (Boulter and Garcia-Mata, 2010). Plant GDIs structurally resemble animal RhoGDIs and were found to control precise ROP-localization and -recycling in cells (Bischoff et al., 2000; Klahre et al., 2006; Hwang et al., 2010; Sun et al., 2015). Interestingly, GDIs possess a binding pocket for prenylated Rho-like proteins, meaning they likely target only type I ROPs *in planta* (Dransart et al., 2005; Berken and Wittinghofer, 2008; Feiguelman et al., 2018).

Besides their canonical regulation, Rho-like proteins can also be influenced via posttranslational modifications (PTMs). While plenty of data is available for PTMs of mammalian Rho-like proteins (Abdrabou and Wang, 2018), data regarding ROPs is quite limited. Until now, phosphomimetic mutations of a conserved serine in *At*ROP4 and *Medicago sativa* (*Ms*) *Ms*ROP6 were described to inhibit ROPGEF binding and reduce association with a downstream signaling kinase (Fodor-Dunai et al., 2011). Furthermore, *in vitro* phosphorylation of *At*ROP4 and *At*ROP6 by a receptor-like cytoplasmic kinase (RLCK) has been shown and potential implications of this PTM for auxin-mediated cell expansion have been suggested (Enders et al., 2017). Apart from these results, however, no functional data for the PTMs of ROPs is available.

As mentioned earlier, G-proteins are master regulators of cellular processes (Gu et al., 2004). Conclusively, it was shown that ROPs orchestrate several processes in plant development and immunity. For instance, it was demonstrated that ROPs organize structure and dynamics of the cytoskeleton. In *Arabidopsis*, it was shown that the GEF *At*SPK1, type I ROPs and downstream ROP interactors mediate nucleation and branching of the actin cytoskeleton, which is essential for polar growth processes such as trichome branching (Basu et al., 2008). Other ROP interactors, RICs, were instead shown to govern microtubule-related processes. *At*RIC1 for example can activate a subunit of the microtubule-severing protein katanin, which promotes ordering of cortical microtubules in *Arabidopsis* pavement cells (Lin et al., 2013). Several *At*ROPs were shown to regulate *At*RIC1 during this process, with partially opposing functions (Fu et al., 2005, 2009; Lin et al., 2013).

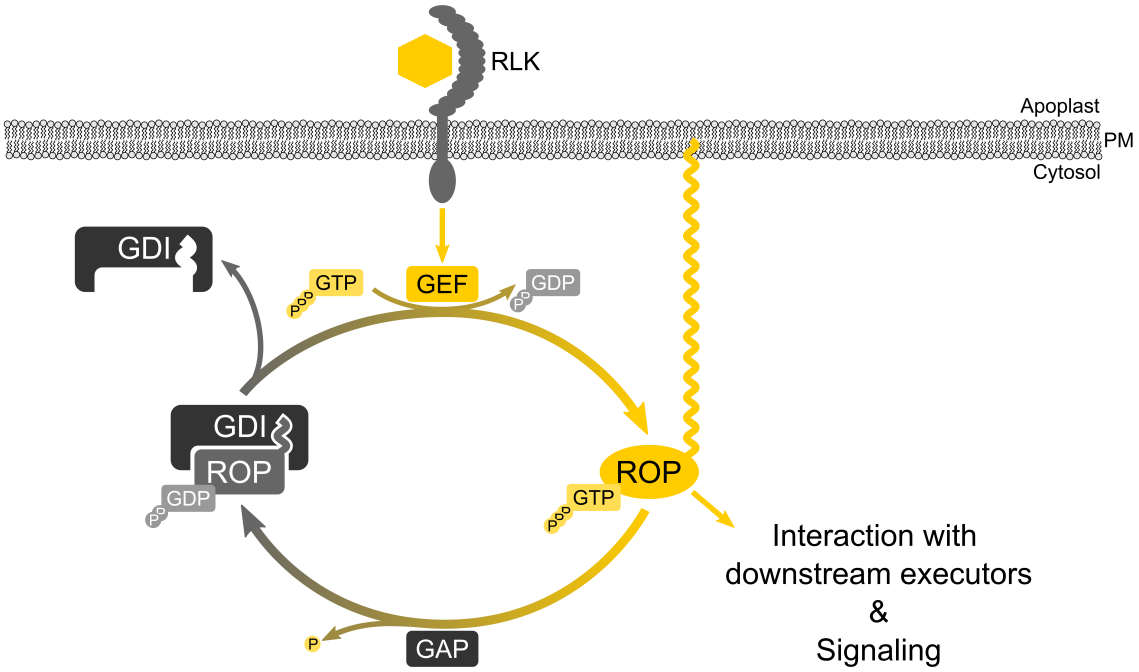

Figure 1.2: The ROP activity cycle.
The activity state of Rho-of-plant proteins (ROPs) regarding their downstream signaling capacity depends on the bound nucleotide. Guanosine diphosphate (GDP)-bound ROPs are inactive, whereas guanosine triphosphate (GTP)-bound ROPs represent the activated form. A nucleotide exchange from GDP to GTP is stimulated by guanosine nucleotide exchange factors (GEFs), which can become activated by receptor-like kinases (RLKs) after signal (yellow hexagon) perception. Binding to GTP causes a conformational shift in ROPs and leads to their plasma membrane-association via lipidations. In this state, ROPs are signaling-active and can interact with downstream executors. GTP-bound ROPs can be inactivated via GTPase activating proteins (GAPs) that stimulate the weak intrinsic GTPase activity of ROPs, leading to GTP-hydrolysis and release of a phosphate group. The GTP-to-GDP conversion reverts the conformational shift and enables guanosine nucleotide dissociation inhibitors (GDIs) to bind GDP-bound ROPs. GDIs also mask the lipidation of ROPs and thereby sequester them in the cytosol. In a new activation cycle, GDIs become displaced during ROP-activation.

Controlling polar growth processes seems to be one of the main functions of ROPs. The highly polar process of pollen tube outgrowth for instance is heavily influenced by the activity of *At*ROP1, *At*ROP5 and *Nicotiana tabacum* (*Nt*) *Nt*RAC5, and interference in their signaling capacities results in severe growth phenotypes in *Nicotiana tabacum* (Kost et al., 1999; Gu et al., 2005; Klahre et al., 2006). All three ROPs localize to the tip region of pollen tubes, and for *At*ROP1 it was shown that its localization at the tip is maintained by the activity of the GAPs RopGAP1 and REN4 (Hwang et al., 2010; Li et al., 2018). Furthermore, a close connection between ROPs and phosphoinositides in this system was also highlighted (Kost et al., 1999; Fratini et al., 2021), which will be introduced in Section 1.7.
Similarly, root hair outgrowth in *Arabidopsis thaliana* is mediated by *At*ROP2, *At*ROP4 and *At*ROP6 (Molendijk et al., 2001; Jones et al., 2002; Denninger et al.,

2019). In this case, ROPs are again the main mediators of root hair growth, but the positioning of the root hair initiation site depends on the GDI SUPERCENTIPEDE1 (SCN1) and the PRONE-GEF *At*GEF3 (Carol et al., 2005; Denninger et al., 2019). While SCN1 restricts ROP signaling to one spot in the initiation site, *At*GEF3 recruits ROPs to the future tip and likely activates them in the process (Carol et al., 2005; Denninger et al., 2019). After root hair initiation, *At*GEF4 takes over and maintains ROP activity throughout root hair extension (Denninger et al., 2019). Interestingly, while the two GEFs maintain ROP activity in the root hair tip, the PH-GAP REN1 becomes localized to the region behind the tip by the scaffold proteins ARMADILLO REPEAT ONLY 2, 3 and 4 (ARO2-4) (Kulich et al., 2020). Since the AROs were shown to preferentially bind GTP-loaded *At*ROPs, it was speculated that the AROs mediate the ROP-GAP interaction by recruiting REN1 to domains of activated *At*ROPs (Kulich et al., 2020). In summary, these particular GEF and GAP localization patterns ensure that ROP signaling processes are spatially confined in the root hair tip and directed root hair outgrowth is possible. Moreover, this exemplifies how ROP-regulators can work in concert to orchestrate activation and deactivation of master regulators of cellular signaling processes (Smokvarska et al., 2021).

Furthermore, a particular rice ROP nicely illustrates the *de facto* involvement of ROPs in immunity-related processes. *Os*RAC1 is a positive regulator of plant immunity and was shown to be involved in both PTI and ETI (Engelhardt et al., 2020). In PTI, chitin perception by the *Os*CEBiP-*Os*CERK1 complex leads to phosphorylation and thereby activation of *Os*RacGEF1, which subsequently triggers GTP-loading in *Os*RAC1 (Shimizu et al., 2010; Akamatsu et al., 2013). Activated *Os*RAC1 then directly interacts with the rice homolog of RBOHD and stimulates its activity, which leads to ROS production (Wong et al., 2007). Additionally, it was shown that activation of *Os*RAC1 during PTI causes MAPK-cascade activation, transcription of defense genes and other immune responses (Kawano et al., 2014). During ETI, *Os*RAC1 becomes activated by the non-PRONE-GEF *Os*SPK1 (Wang et al., 2018). Activated *Os*RAC1 was shown to be required for immune responses and downstream signaling conferred by the two resistance genes Piα and Pit, which trigger HR and ROS production after effector perception (Chen et al., 2010; Kawano et al., 2010; Wang et al., 2018).

1.6 The barley ROP RACB

While some ROPs are involved in pathogen resistance, others can act as susceptibility factors. One example is the barley type I ROP RACB, which is required for full susceptibility towards *Bgh*-infection (Schultheiss et al., 2002, 2003; Hoefle et al., 2011; Scheler et al., 2016). In unchallenged barley plants, RACB is a mediator of cell

polarity and this function was elucidated in stable transgenic barley plants, in which RACB-signaling was either partially inhibited or constitutively enhanced. In different plant lines, inhibition was achieved by silencing *RACB* expression with a double-stranded RNA interference (RNAi) construct (Hoefle et al., 2011; Scheler et al., 2016), while over-activation of the RACB pathway was caused by an overexpression of the constitutively activated form of RACB (RACB-CA), which carries a G15V mutation in its G1-box (Pathuri et al., 2008). Both plant lines display several developmental defects, which could be attributed to disrupted cell polarity signaling: *RACB*-RNAi plants grow shorter, have no root hairs and show defects in the asymmetric cell division events giving rise to stomata subsidiary cells (Hoefle et al., 2011; Scheler et al., 2016). In turn, RACB-CA-overexpressing plants have larger, irregularly shaped leaf epidermal cells and produce shorter and swollen root hairs (Pathuri et al., 2008). RACBs role in susceptibility towards *Bgh* was demonstrated in both transiently and stably transformed plants. Overexpression of RACB-CA caused higher penetration frequency of *Bgh* in barley epidermal cells, whereas *RACB*-silencing resulted in higher resistance towards *Bgh*-attacks (Schultheiss et al., 2002, 2003; Pathuri et al., 2008; Hoefle et al., 2011). Interestingly, RACB can only induce susceptibility when it is activated and targeted to the plasma membrane. A mislocalized RACB-CA truncation lacking the C-terminal prenylation motif "CSIL" for instance was not able to increase susceptibility to *Bgh*. In turn, neither overexpression of wildtype RACB (RACB-WT) nor dominant negative RACB (RACB-DN, carrying a T20N mutation in the G1-box) had an effect on the infection outcome (Schultheiss et al., 2003). RACB also appears to be required for full susceptibility of barley towards *Bgh*, because *RACB*-RNAi plants showed less pustules and fungal haustoria were smaller in size (Hoefle et al., 2011). How RACB acts mechanistically in barley susceptibility towards *Bgh*, however, is not fully clear yet. Focusing of the actin cytoskeleton towards the fungal attack site, which is important for resistance, was less frequently observed when RACB-CA was overexpressed and more frequent when *RACB* was silenced (Opalski et al., 2005). RACBs influence on the actin cytoskeleton in this case was only quantitative, not qualitative. Moreover, RACB is not a negative regulator of plant immunity, because chitin- and flg22-triggered ROS production, MAPK-cascade activation and defense gene expression are mostly normal in both RACB-CA overexpressing plants and *RACB*-RNAi plants (Scheler et al., 2016). Instead, it was proposed that RACBs role as a susceptibility factor stems from its involvement in cell polarity signaling. In the "inverted tip growth" hypothesis, the inward growth of the haustorium during fungal invasion was compared to pollen tube and root hair growth, which are processes organized by ROPs (Schultheiss et al., 2003; Scheler et al., 2016). Accordingly, RACBs usual function in root hair formation would benefit *Bgh* during attempted haustorium establishment (Scheler

et al., 2016). Some evidence for this hypothesis was already collected, because *RACB*-RNAi plants, which have no root hairs, also harbor less haustoria and plants overexpressing RACB-CA show isotropic root hair growth and are more frequently penetrated (Pathuri et al., 2008; Hoefle et al., 2011; Scheler et al., 2016). Which exact pathways are involved in the "inverted tip growth" has not been shown yet and needs further analysis.

ROP-activity regulating proteins have also been investigated in the barley-*Bgh*-pathosystem. For instance, barley PRONE-GEF 14 (*Hv*GEF14) interacts with RACB-WT, RACB-CA and another RACB variant that is characterised by its low nucleotide affinity (RACB-D121N, carrying a D121N mutation in its G4 domain; Cool et al. (1999); Trutzenberg et al. (2022)). *Hv*GEF14 is further able to activate RACB-WT *in vivo* and acts in susceptibility, since overexpression of *Hv*GEF14 caused higher penetration by *Bgh* and RNAi against *HvGEF14* showed a trend of increased resistance (Trutzenberg et al., 2022). In contrast, the MICROTUBULE-ASSOCIATED ROP-GTPASE ACTIVATING PROTEIN 1 (MAGAP1) was shown to act in resistance against powdery mildew infection (Hoefle et al., 2011). MAGAP1 binds to activated RACB in yeast and *in planta*, and re-localizes from cortical microtubules to the plasma membrane during RACB-interaction in barley epidermal cells. Functionally, MAGAP1 assists in focusing the microtubules towards the fungal attack site and this, as well as its role in *Bgh*-resistance, relies on its catalytic arginine residue (Hoefle et al., 2011). Several downstream interaction partners of RACB have been identified. Among the canonical ROP interactors, two barley RICs, RIC157 and RIC171, and one RIP/ICR, RIPb, have been characterized in their interaction with RACB to date (Schultheiss et al. (2008); McCollum et al. (2020) and non-peer-reviewed Engelhardt et al. (2021)). All three preferentially interact with RACB-CA, and in case of RIC157 and RIC171, RACB-binding is mediated by the CRIB domain, while RIPb relies on its QWRKAA motif (Schultheiss et al. (2008); McCollum et al. (2020) and Dr. Stefan Engelhardt, TUM, personal communication). *In planta*, their interaction with RACB takes place at the plasma membrane and, strikingly, both RICs and RIPb accumulate at the haustorial neck region during infection, where they co-localize with RACB-CA (Schultheiss et al., 2008; McCollum et al., 2020; Engelhardt et al., 2021). Additionally, all three proteins are involved in susceptibility, since their overexpression leads to increased fungal penetration (Schultheiss et al., 2008; McCollum et al., 2020; Engelhardt et al., 2021) Mechanistically, the RICs and RIPb were suggested to be scaffolding proteins that mediate binding between RACB and so far unknown downstream proteins (Schultheiss et al., 2008; McCollum et al., 2020; Engelhardt et al., 2021).

Until now, one non-canonical interaction partner of RACB has been found. Barley ROP binding protein kinase 1 (RBK1) is recruited by RACB-CA to the PM in

barley epidermal cells (Huesmann et al., 2012). While being a weak auto-active kinase, RBK1s kinase activity against a generic substrate *in vitro* is stimulated by the presence of RACB-CA (Huesmann et al., 2012). In contrast to the other RACB downstream interaction partners, RBK1 works as a resistance factor during *Bgh* infection (Huesmann et al., 2012). This was attributed to RBK1s function in regulating microtubule stability, as *RBK1*-silencing via RNAi caused increased microtubule fragmentation (Huesmann et al., 2012). RBK1 itself interacts with S-phase kinase 1-associated protein-like (SKP1L), which is also involved in resistance against *Bgh* (Reiner et al., 2015). SKP1L was predicted to be part of an SKP1-cullin 1-F-box (SCF)–E3 ubiquitin ligase complex that belongs to the plant's ubiquitination machinery (Hua and Vierstra, 2011; Reiner et al., 2015). Even though no direct interaction between RACB and SKP1L could be detected, silencing of *SKP1L*, *RBK1* or pharmacological inhibition of the proteasome increased protein stability of RACB-CA (Reiner et al., 2015). Hence, it was suggested that RBK1 and SKP1L act in a negative feedback loop towards RACB-CA, which would explain their opposite phenotypes in the barley-*Bgh*-interaction (Reiner et al., 2015). The current working hypothesis follows a model from the mammalian system, in which a human (*Homo sapiens*, *Hs*) RACB-homolog is first phosphorylated by a kinase and then recognized by an SCF-complex for polyubiquitination and degradation (Zhao et al., 2013). Accordingly, RACB-CA would interact with RBK1 and becomes phosphorylated in the process, which could trigger recognition by an SCF-complex containing SKP1L (Reiner et al., 2015). This would lead to polyubiquitination of RACB-CA and ultimately to its degradation in the proteasome (Reiner et al., 2015).
Finally, *Bgh* targets RACB-signaling directly via a secreted, retrotransposon-encoded effector protein called ROP-INTERACTIVE PEPTIDE 1 (ROPIP1) (Nottensteiner et al., 2018). ROPIP1 was demonstrated to interact with RACB-WT and RACB-CA and to modulate barley susceptibility in favor of *Bgh*. When co-expressed with MAGAP1, ROPIP1 decorates cortical microtubules and can even recruit RACB-CA in the process (Nottensteiner et al., 2018). The microtubules are apparently a virulence target of the effector protein, as overexpression of ROPIP1 lead to increased microtubule fragmentation (Nottensteiner et al., 2018). In conclusion, this underlines that RACB-CA and barley susceptibility towards powdery mildew infection are tightly connected. However, more studies are needed to entangle the particular pathways that are involved.

1.7 Anionic phospholipid-signaling in plants

Membranes surround all eukaryotic cells and their intracellular organelles to create environments, in which specialized chemical reactions can occur (Noack and Jaillais, 2020). Since multiple organelles exist within cells, they have to gain some form of

identity to be distinguished from one another. This is facilitated through varying membrane compositions: different bi-layer-forming lipid species and membrane-associated proteins contribute to membrane identity (Noack and Jaillais, 2020). With the exception of thylakoid membranes in chloroplasts, all membranes consist of three main lipid classes: glycerophospholipids (often referred to as phospholipids), sphingolipids and steroles (Gerth et al., 2016), with the ratio between them varying greatly between plant species (Furt et al., 2010). The different lipid species can be described according to their biochemical parameters: phospholipids for instance are not only classified by abundance or saturation of their fatty acid chains. They can also carry different headgroups that give them additional attributes, which influence for example charge and shape (Colin and Jaillais, 2020). In general though, highly abundant lipids are called structural lipids, because their main task is to generate a hydrophobic barrier that separates adjacent milieus (Furt et al., 2010; Colin and Jaillais, 2020). In contrast, low abundant lipid species are referred to as signaling lipids, since they often have regulatory functions and a fast turn-over (Furt et al., 2010; Colin and Jaillais, 2020). One prominent example for the latter are phospholipids carrying a negative charge (called anionic phospholipids), which make up less than 1 % of total lipids in *A. thaliana* leaves (Colin and Jaillais, 2020).
Anionic phospholipids are produced from diacylglycerol (DAG). Even though length and saturation of the fatty acid chains in DAG molecules can vary, anionic phospholipids are exclusively named after their modified headgroups (Pokotylo et al., 2018). The simplest anionic phospholipid is phosphatidic acid (PA), which is a phosphorylated DAG molecule (Pokotylo et al., 2018). Phosphatidylserine (PS) can be generated either through headgroup exchanges from phosphatidylcholine (PC) or phosphatidylethanolamine (PE) with L-serine or through addition of L-serine onto phosphorylated DAG via phosphatidylserine synthases (Manoharan et al., 2000). Esterification of DAG with D-*myo*-inositol creates uncharged phosphatidylinositol (PI), which is the precursor of phosphoinositides (Gerth et al., 2016). The hydroxy-groups at positions three, four and five of the inositol-headgroup of PI can be phosphorylated by special kinases, giving rise to phosphatidylinositol-3-phosphate (PI3P), phosphatidylinositol-4-phosphate (PI4P) and phosphatidylinositol-5-phosphate (PI5P) (Gerth et al., 2016). Subsequent phosphorylation of the monophosphates creates phosphatidylinositol-3,4-bisphosphate (PI(3,4)P_2), phosphatidylinositol-3,5-bisphosphate (PI(3,5)P_2), phosphatidylinositol-4,5-bisphosphate (PI(4,5)P_2) and ultimately phosphatidylinositol-3,4,5-trisphosphate (PI(3,4,5)P_3) (Gerth et al., 2016). The presence of all seven phosphoinositides was demonstrated in animals, but not in plants (Heilmann, 2016). PI(3,4)P_2 and PI(3,4,5)P_3 are missing, because plants lack the kinases that generate PI(3,4)P_2 and PI(3,4,5)P_3 from PI3P and PI(4,5)P_2, respectively (Mueller-Roeber and Pical, 2002).

Phosphoinositides can also be degraded via specialized enzymes. Phosphatases dephosphorylate single positions, which essentially converts a phosphoinositide into a different species or back into phosphatidylinositol (Zhong and Ye, 2003; Gerth et al., 2016). Lipases instead cleave phosphoinositides at the phosphate bridging DAG and the phosphorylated inositol headgroup, which results in formation of DAG and soluble inositol polyphosphates (Mueller-Roeber and Pical, 2002).
Studying anionic phospholipids *in vivo* is difficult, because their abundance cannot be controlled directly and they cannot be directly tagged with for example fluorescent proteins. Instead, knock-out and overexpression mutants of their synthesis and break-down genes, as well as pharmacological inhibitors have been used to elucidate their signaling processes (Novakova et al., 2014; Hirano et al., 2016; Qin et al., 2020). Their subcellular localization has been revealed using so-called genetically-encoded biomarkers. These are fusion constructs of a fluorescent protein and a lipid-binding domain specific for a particular lipid species (Simon et al., 2014; Hirano et al., 2017). Recently, the addition of an engineered enzyme that inducibly and specifically depletes only one phosphoinositide species has brought a new tool into the field, which should help future studies (Doumane et al., 2021).
Using all these approaches, and incorporating data form the animal field, it was proposed that it could actually be the phosphoinositides that give organelles their identity through the generation of a "lipid code" (Kutateladze, 2010; Dubois and Jaillais, 2021). However, this is currently under debate, because phosphoinositides for instance are not as organelle-specific as initially believed (Wang et al., 2019; Dubois and Jaillais, 2021). Apart from potentially generating this lipid code, each anionic phospholipid has its own distinct localization and task. Overall, they were shown to be highly stress-responsive and appear to regulate cellular trafficking processes, such as endo- and exocytosis, as well as polar growth (Van Leeuwen et al., 2007; Gerth et al., 2016; Noack and Jaillais, 2017; Qin et al., 2020). Table 1.1 summarizes data, which was mostly gathered in unstressed *Arabidopsis* root cells (as reviewed by Noack and Jaillais (2020)) and outlines the subcellular localization and most important functions for each anionic phospholipid.
As mentioned in Section 1.5, the signaling processes of ROPs and anionic phospholipids have already been linked. During the preparation of this thesis, several groups have studied the interplay and co-dependence of ROPs and anionic phospholipids (Hirano et al., 2018; Platre et al., 2019; Fratini et al., 2021). Additionally, some ROP-regulating proteins, such as GAPs, were also shown to bind phosphoinositides (Kulich et al., 2020). Previous and recent findings about the connection of ROP- and anionic phospholipid-signaling will be discussed in detail in Section 3.4.

Table 1.1: Summary of the anionic phospholipid signaling pathways in plants. The subcellular localization and main functions for each anionic phospholipid species are listed together with their source publications. PM: plasma membrane; MVB/LE: multivesicular bodies/late endosomes; TGN/EE: trans-golgi network/early endosomes; NA: not available; *: for PI5P, no data is available in plants.

Lipid	Localization	Function	References
PA	PM (uniform and flank region of pollen tubes and root hairs)	precursor for phospholipids, second messenger during (a)biotic stress responses	Potocký et al. (2014); Platre et al. (2018); Pokotylo et al. (2018)
PI3P	autophagosomes, tonoplast, MVB/LE	maintenance of vacuolar morphology and fusion	Vermeer et al. (2006); Novakova et al. (2014); Simon et al. (2014)
PI4P	PM, TGN/EE	generation of the PM's electrostatic field	Simon et al. (2014, 2016); Platre et al. (2018); Lin et al. (2019)
PI5P*	unknown	unknown	NA
$PI(3,5)P_2$	PM (shank region in root hairs), MVB/LE	association of endosomes with microtubules, maturation of late endosomes, cell wall hardening of root hairs	Hirano et al. (2015, 2016, 2017, 2018)
$PI(4,5)P_2$	PM (uniform and apex region of pollen tubes and root hairs)	regulation of polar tip growth via actin-stabilization and clathrin-mediated endocytosis	Kost et al. (1999); Zhao et al. (2010); Ischebeck et al. (2011); Simon et al. (2014); Fratini et al. (2021)
PS	PM (uniform and nanodomains), TGN/EE	generation of the PM's electrostatic field, auxin-induced relocalization of ROPs into PM nanodomains	Platre et al. (2018, 2019)

1.8 Objectives

Several open question remain about how the RACB-signaling pathway influences susceptibility in the barley-*Bgh*-pathosystem. In previous studies, it was shown that RACB can be non-canonically regulated by RBK1, SKP1L and the proteasome, which presumably act together in a negative feedback loop towards the G-protein. Since RBK1 is an active kinase *in vitro* and interacts with RACB *in planta*, and SKP1L is suggested to be part of the plant's ubiquitination machinery, it was speculated that RACB is targeted for phosphorylation and ubiquitination *in vivo*. Therefore, one main goal of this dissertation was to investigate, if RACB is really targeted by these posttranslational modifications *in planta*. If this was the case, I wanted to use point mutations to analyse the influence of these PTMs on RACB-signaling processes. With these experiments, I wanted to shed some light on how plant Rho-like proteins

can be regulated by PTMs, since there is very little information on this topic available at the moment.
Secondly, as it is not yet known how RACB causes susceptibility mechanistically, my other goal was to find novel RACB interaction partners to pinpoint the cellular pathways that are targeted by the ROP. To achieve this, I have used untargeted co-immunoprecipitation experiments followed by mass spectrometry (supported by Dr. Julia Mergner, TUM) to identify candidate proteins. From the list of candidates I chose three proteins to verify their interaction with RACB and investigated their role in the barley-*Bgh*-pathosystem. Since these novel interaction partners were predicted to be involved with the anionic phospholipid-signaling pathway, I further aimed to elucidate their lipid-binding specificity.

2 Results

2.1 Characterization of stable transgenic barley lines

Investigating posttranslational modifications of RACB *in planta* and finding novel RACB-interacting proteins required large amounts of purified protein. Hence, stable transgenic barley plants overexpressing tagged signaling-active RACB-CA were used for these experiments. Cloning of constructs and generation of transgenic plants was achieved by Dr. Tina Reiner (TUM), Dr. Götz Hensel (IPK Gatersleben) and Dr. Jochen Kumlehn (IPK Gatersleben) before this thesis was started. In these plants, RACB-CA protein was overexpressed under the control of the maize *Polyubiquitin 1* promoter and contained either an N-terminal enhanced GFP (eGFP)-tag or a triple HA (3xHA)-tag. Apart from tagged full-length RACB-CA, also plant lines expressing a truncated RACB-CA variant were generated: these mutants were called RACB-CA-ΔCSIL, as the C-terminal prenylation motif CSIL was missing in RACB-CA (Schultheiss et al., 2003). Finally, plants expressing only the eGFP-tag or 3xHA-tag were created as controls. Since no homozygous plants could be obtained in multiple rounds of propagation during the preparation of this dissertation, all plants had to be selected for transgene presence before use (see Section 4.2).
Firstly, it had to be verified that the RACB-CA fusion proteins are properly expressed in the transgenic plants. This could be confirmed via Western blots targeting the eGFP- or 3xHA-tag (see Fig. 2.1 A, Weiß et al. (2022)). Presence of tagged full-length or truncated RACB-CA as well as free eGFP could be observed in the first leaves of transgenic barley plants. Only the 3xHA-tag alone was never detected in any Western blots. Since downstream experiments required large amounts of purified proteins, it was checked if the fusion proteins can be purified via immunoprecipitation (IP). Using the first leaves of transgenic barley as sample material, it could be shown that eGFP- and 3xHA-tagged proteins can be successfully enriched via αGFP- and αHA-IPs (see Fig. 2.1 A, Weiß et al. (2022)).
Next, it had to be verified that the tagged RACB-CA fusion proteins are functional and show no affected behaviour due to the tags. As a starting point, the subcellular localization of full-length and truncated RACB-CA was investigated in first leaves of the eGFP-tagged plant lines via confocal laser scanning microscopy (CLSM) (see Fig. 2.1 B). Previous transient experiments have shown that GFP-tagged full-length RACB-CA localizes to the plasma membrane, while the RACB-CA-ΔCSIL mutant is mislocalized to the cytosol and nucleus (Schultheiss et al., 2003). Conclusively, in transgenic plants, full-length eGFP-RACB-CA localized to the PM and showed almost no cytoplasmic background, whereas both the eGFP-tag alone and the eGFP-RACB-CA-ΔCSIL mutant were present in the cytosol and nucleus of barley epidermal cells.

Secondly, the susceptibility of the transgenic plants towards *Bgh* invasion was checked (see Fig. 2.1 C, Weiß et al. (2022)), since RACB is a susceptibility factor in this interaction (Schultheiss et al., 2002). Only plants overexpressing tagged full-length RACB-CA were more susceptible towards *Bgh* penetration, while the efficiency of *Bgh* penetration was unchanged in tagged RACB-CA-ΔCSIL-expressing plants when compared to the respective control. In summary, the transgenic plants behaved in accordance to previously described findings and allow the purification of functional protein, which makes them suitable for further experiments.

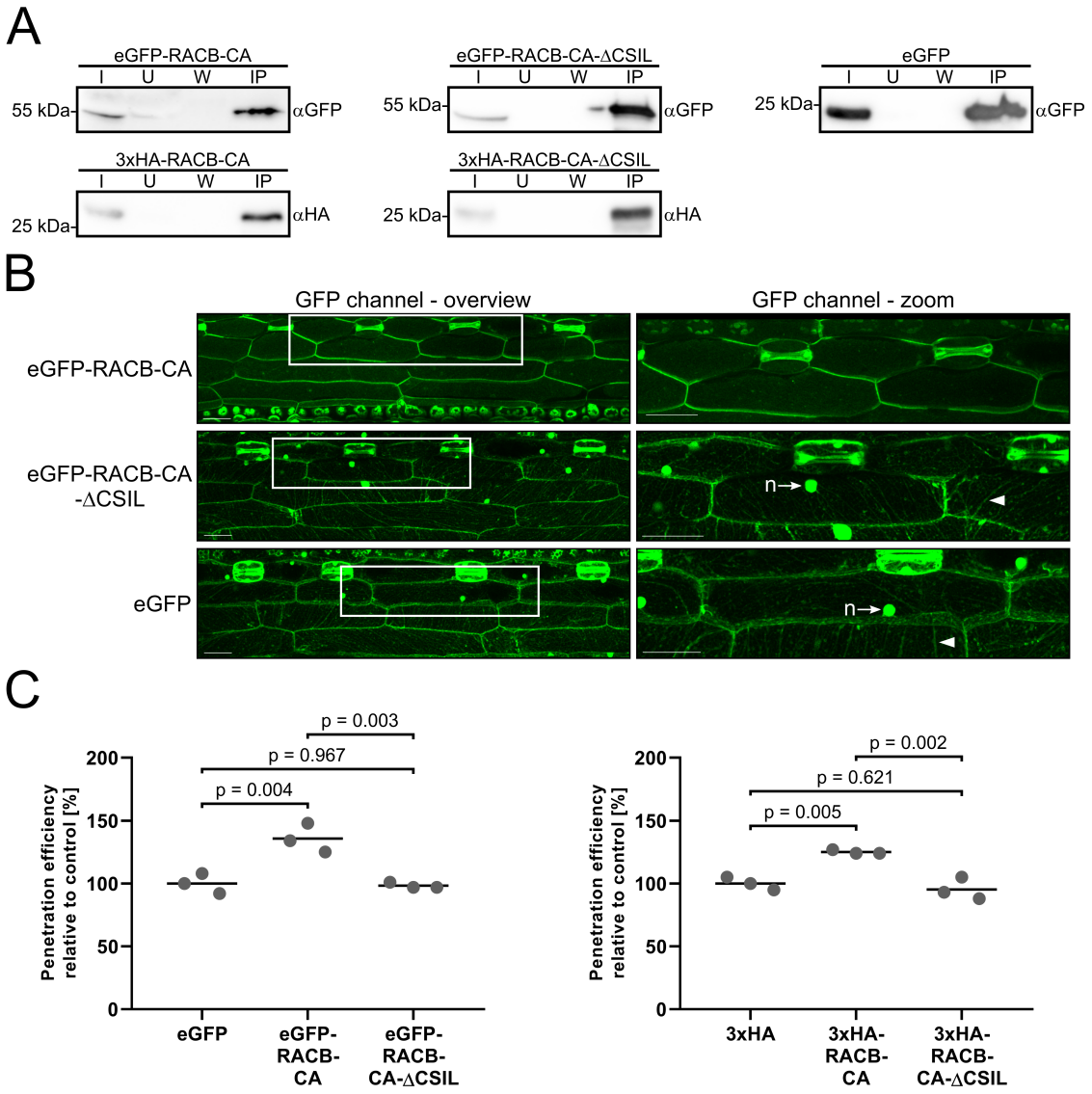

Figure 2.1: Transgenic barley lines express functional tagged RACB-CA protein. (**A**) Tagged RACB-CA(-ΔCSIL) proteins are stably expressed in the first leaves of transgenic barley plants and can be enriched via immunoprecipitation (IP). eGFP- and 3xHA-fusion proteins were detected by αGFP- and αHA-Western blotting. IP fractions: Input (I), Unbound (U), Wash (W) and eluate after IP (IP). Expected protein sizes: eGFP-RACB-CA: 49 kilo Dalton (kDa), eGFP-RACB-CA-ΔCSIL: 49 kDa, eGFP: 28 kDa, 3xHA-RACB-CA: 25 kDa, 3xHA-RACB-CA-ΔCSIL: 25 kDa. (**B**) Confocal laser scanning microscopy showed that eGFP-RACB-CA localizes to the plasma membrane in epidermal cells of transgenic barley plants, while eGFP-RACB-CA-ΔCSIL and free eGFP instead localize to the cytosol and nucleus. Selected nuclei (n, arrows) and prominent cytoplasmic strands (arrowheads) are highlighted. Zoom is a re-scanned 2x magnification of the overview image (white rectangles). Scale bar: 50 µM. Images are maximum intensity projections of at least 29 Z-steps of 2 µm increments. Image brightness was uniformly enhanced post-scanning for better visibility. (**C**) Overexpression of tagged RACB-CA causes increased penetration of *Bgh* into leaf epidermal cells of transgenic plants. Tagged RACB-CA-ΔCSIL and the tag-only controls show comparable levels of susceptibility. Graphs show susceptibility relative to the respective tag-only control. Three leaves of one plant line per construct were tested. Data points correspond to individual leaves. The crossbar displays averaged relative susceptibility. Statistics were assessed by a One-way ANOVA with Tukey's HSD. Data for the 3xHA-tagged lines in (**A**) and (**C**) were modified from Fig. 3 of Weiß et al. (2022).

2.2 Posttranslational modification of RACB

2.2.1 RACB-CA is not detectably phosphorylated *in vivo*

Previous experiments have shown that RACB-CA interacts with the protein kinase RBK1 *in planta* and can stimulate its kinase activity *in vitro* (Huesmann et al., 2012). Further *in vitro* kinase assays resulted in the identification of *in vitro* phosphorylation sites for RACB-CA via mass spectrometry (experiments were performed by Dr. Tina Reiner (TUM), Dr. Julia Mergner (TUM) and Prof. Dr. Attila Fehér (BRC Szeged); Weiß et al. (2022)). Taken together, this suggests that RACB-CA could be also phosphorylated by RBK1 *in vivo*. Several experiments were conducted to investigate this, but ultimately no *in vivo* RACB-CA phosphorylation site could be identified. All attempts were fully described in Weiß et al. (2022), but will be briefly outlined here (for a schematic overview, please see Fig. S1).
In the first experiment, mesophyll protoplasts were isolated from 3xHA-RACB-CA transgenic plants and treated with the proteasome inhibitor MG132, because it was initially hypothesized that phosphorylated RACB-CA might be recognized by the plant's ubiquitination machinery and targeted for degradation (see Section 1.6, Reiner et al. (2015)). Following protein extraction, αHA-IP and tryptic digest, phosphorylated peptides were enriched via immobilized metal affinity chromatography (IMAC) and identified via mass spectrometry (MS). No phosphorylated RACB-CA peptides could be recovered. In a second attempt, GFP-tagged RBK1 was co-overexpressed in transgenic 3xHA-RACB-CA-expressing protoplasts before MG132 treatment to stimulate potential RACB-CA phosphorylation. Subsequently, αHA-IP or IMAC were selectively performed before tryptic digest and MS to increase chance of phosphorylated RACB-CA peptide recovery. This also yielded no *in vivo* phosphorylation sites for RACB-CA. Finally, GFP-RBK1 was again co-overexpressed in 3xHA-RACB-CA-expressing protoplasts before MG132 treatment. After protein extraction, the αHA-IP was skipped and IMAC was directly performed after tryptic digest. The samples were then further fractionated according to their hydrophobicity, which was shown to increase recovery rate of low-abundant peptides (Dr. Julia Mergner, TUM, personal communication). Again, no RACB-CA phosphorylation sites could be identified with this approach.

2.2.2 RACB-CA is ubiquitinated at K167 *in vivo*

Earlier studies have demonstrated a negative influence of RBK1, SKP1L and the proteasome on RACB-CA protein abundance (Reiner et al., 2015). Conclusively, it was suggested that RACB-CA might become ubiquitinated *in vivo*. To investigate this, the drug MG132 was used to inhibit the proteasome in a leaf-floating assay conducted with transgenic 3xHA-RACB-CA-overexpressing barley plants. Following

αHA-IP, 3xHA-RACB-CA and higher molecular weight bands could be observed in an αHA-Western blot (see Fig. 2.2 A, Weiß et al. (2022)). Repetition of this experiment with a DMSO control has shown that this laddering pattern is indeed independent of MG132 and can be observed naturally (see Fig. S2, Weiß et al. (2022)). Research on other proteins had demonstrated before that this band pattern can be an indicator for protein ubiquitination (Göhre et al., 2008; Lu et al., 2011). Hence, the first experiment was repeated and subjected to mass spectrometry to identify any potential ubiquitination sites in 3xHA-RACB-CA. A global mass spectrometry measurement and subsequent parallel reaction monitoring (PRM) approach revealed that 3xHA-RACB-CA is ubiquitinated at K167 (see Fig. 2.2 B, Weiß et al. (2022)). Evidence for this was provided by 3xHA-RACB-CA peptides carrying a mass shift equal to two glycine residues, which typically remain at the ubiquitinated lysine after ubiquitin is cleaved off by trypsin during sample preparation (Peng et al., 2003). Sequence comparison of all ROPs from barley, rice and *Arabidopsis* revealed that RACB-K167 is fully conserved (see Fig. S3, Weiß et al. (2022)). Further bioinformatic analyses revealed that K167 appears to be part of the binding interfaces for PRONE-GEFs and CRIB-domain containing proteins in RACB (see Fig. S4, Weiß et al. (2022)), which suggests regulatory functions of K167-ubiquitination.

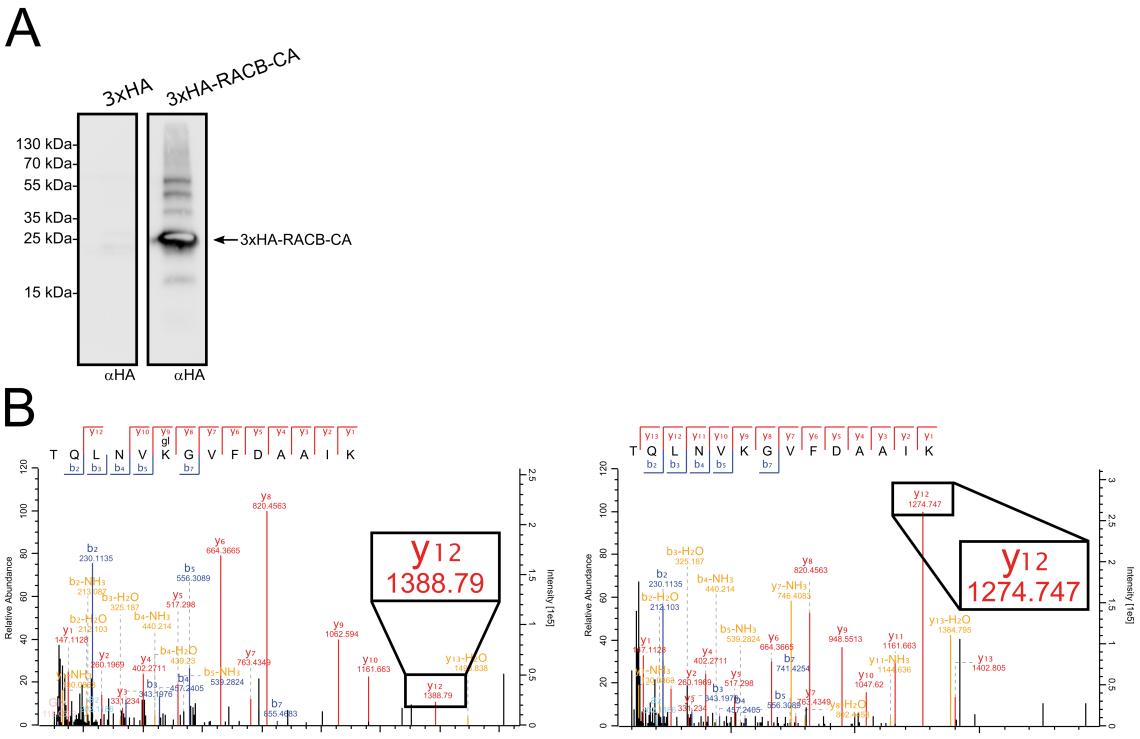

Figure 2.2: RACB-CA is ubiquitinated *in vivo*.
(**A**) Bands corresponding to 3xHA-RACB-CA and higher molecular weight derivatives were observed by αHA-Western blotting after αHA-IP of leaf material overexpressing 3xHA-RACB-CA, which was floated on a solution containing MG132. (**B**) Spectra from the PRM mass spectrometry experiment, in which RACB-K167 was identified as a ubiquitin acceptor site. Samples were generated as described in (**A**). Spectra of modified peptides (left) and corresponding unmodified peptides (right) are shown. The box depicts one example: peptide "y12" was identified with two different masses. This difference equals the mass of two glycine molecules, which characteristically remain after tryptic digest of ubiquitinated proteins (Peng et al., 2003). Calculation: $y12_{modified}$ - $y12_{unmodified}$ = 1388.79 m/z - 1274.747 m/z = 114.04 m/z = 2 * glycine (57.02 m/z). This figure was adapted from Fig. 4 of Weiß et al. (2022). All mass spectrometry experiments were performed by Dr. Julia Mergner (TUM).

2.2.3 RACB-K167 regulates protein stability

Identification of RACB-K167 as a ubiquitination site raised the question if this residue plays a role in regulating protein stability. To analyse this, wildtype, constitutively active and dominant negative (T20N) RACB point mutants were generated, in which K167 was exchanged with an arginine (termed RACB-K167R, Weiß et al. (2022)). Arginine was chosen as it shares biochemical properties with lysine, but cannot be ubiquitinated. To be able to measure a difference in protein abundance between regular and K167R RACB forms, monomeric enhanced GFP (meGFP) was fused to the N-terminus of the different RACB proteins. This allowed indirect quantification of protein abundance via GFP-fluorescence intensity measurements using CLSM of transiently transformed barley epidermal cells expressing the fusion proteins. To correct for variations in signal strength between different transformed cells, free

mCherry was co-expressed as a control in all experiments. For every measured cell, a GFP-to-mCherry ratio was calculated, which could be used for the comparison of abundance between regular meGFP-RACB-WT/CA/DN and their corresponding K167R mutants (see Fig. 2.3, Weiß et al. (2022)). This revealed higher fluorescence levels of meGFP-RACB-CA-K167R and meGFP-RACB-DN-K167R compared to their unmutated versions. In contrast, both regular meGFP-RACB-WT and its K167R mutant showed comparable levels of fluorescence.

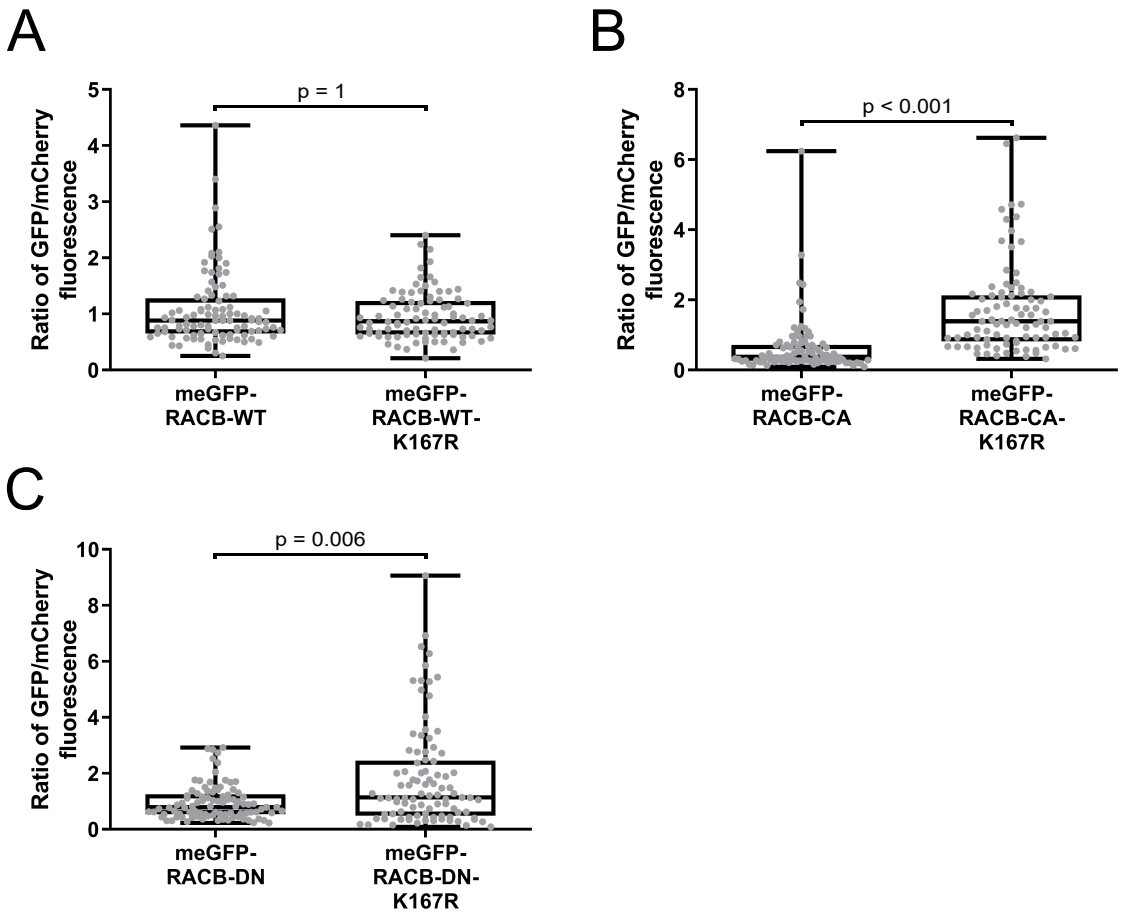

Figure 2.3: Quantification of meGFP-RACB(-K167R) fluorescence levels. Fluorescence intensities of meGFP-RACB-WT (**A**), -CA (**B**) and -DN (**C**) were compared against those of their K167R mutants in transiently transformed barley epidermal cells. Free mCherry was co-expressed in all cells as a normalizer and used for the calculation of a GFP-to-mCherry ratio, which served as the basis for abundance comparisons. meGFP-RACB-CA-K167R and meGFP-RACB-DN-K167R showed higher levels of fluorescence compared to their regular versions, while the K167R mutation in meGFP-RACB-WT had no effect. Mean pixel fluorescence intensities for both fluorophores were measured by CLSM. Each datapoint corresponds to the calculated GFP-to-mCherry ratio of one transformed cell. Laser and detector settings were different between RACB-activity forms, but kept constant for each set. Data was collected over three independent biological replicates. Statistical significances were determined by Wilcoxon rank-sum tests with continuity correction. Data for this figure was taken from Fig. 6 of Weiß et al. (2022).

To make sure that the RACB-K167R mutants are functional, signaling-competent proteins, two control experiments were conducted: since RACB-CA is the signaling-active form, it was tested if RACB-CA-K167R was able to i) promote barley's susceptibility to *Bgh* and ii) recruit downstream interactors to the plasma membrane similar to previous observations for regular RACB-CA (Schultheiss et al., 2003, 2008). For the first experiment, untagged RACB-CA or RACB-CA-K167R were transiently overexpressed in barley epidermal cells and the penetration efficiency of *Bgh* into these cells was scored (see Fig. 2.4 A, Weiß et al. (2022)). Overexpression of RACB-CA resulted in a 39 % higher susceptibility relative to the empty vector control, while RACB-CA-K167R increased penetration frequency by 35 %. In conclusion, both forms of RACB showed a similar trend of increasing susceptibility towards infection, which is in agreement with previous findings (Schultheiss et al., 2003).
To test the ability of RACB-CA-K167R to interact with downstream proteins, a recruitment assay with the known RACB-interaction partner RIC171 was performed (Schultheiss et al., 2008). In this experiment, the subcellular localization patterns of meGFP-RACB-CA(-K167R) and mCherry-RIC171 were analysed by CLSM in transiently transformed barley epidermal cells (see Fig. 2.4 B, Weiß et al. (2022)). Free CFP was co-expressed as a marker for cytosolic and nuclear localization. When overexpressed together with free GFP, mCherry-RIC171 localized to the cytosol and nucleus. However, in presence of meGFP-RACB-CA or meGFP-RACB-CA-K167R, mCherry-RIC171 was strongly recruited from the cytosol to the plasma membrane, where also fluorescence of the GFP-tagged RACB proteins could be observed. This demonstrated that RACB-CA-K167R is able to recruit mCherry-RIC171 exactly like regular RACB-CA. In summary, both the *Bgh*-susceptibility analysis and the recruitment assay have shown that RACB-CA-K167R proteins are functional.

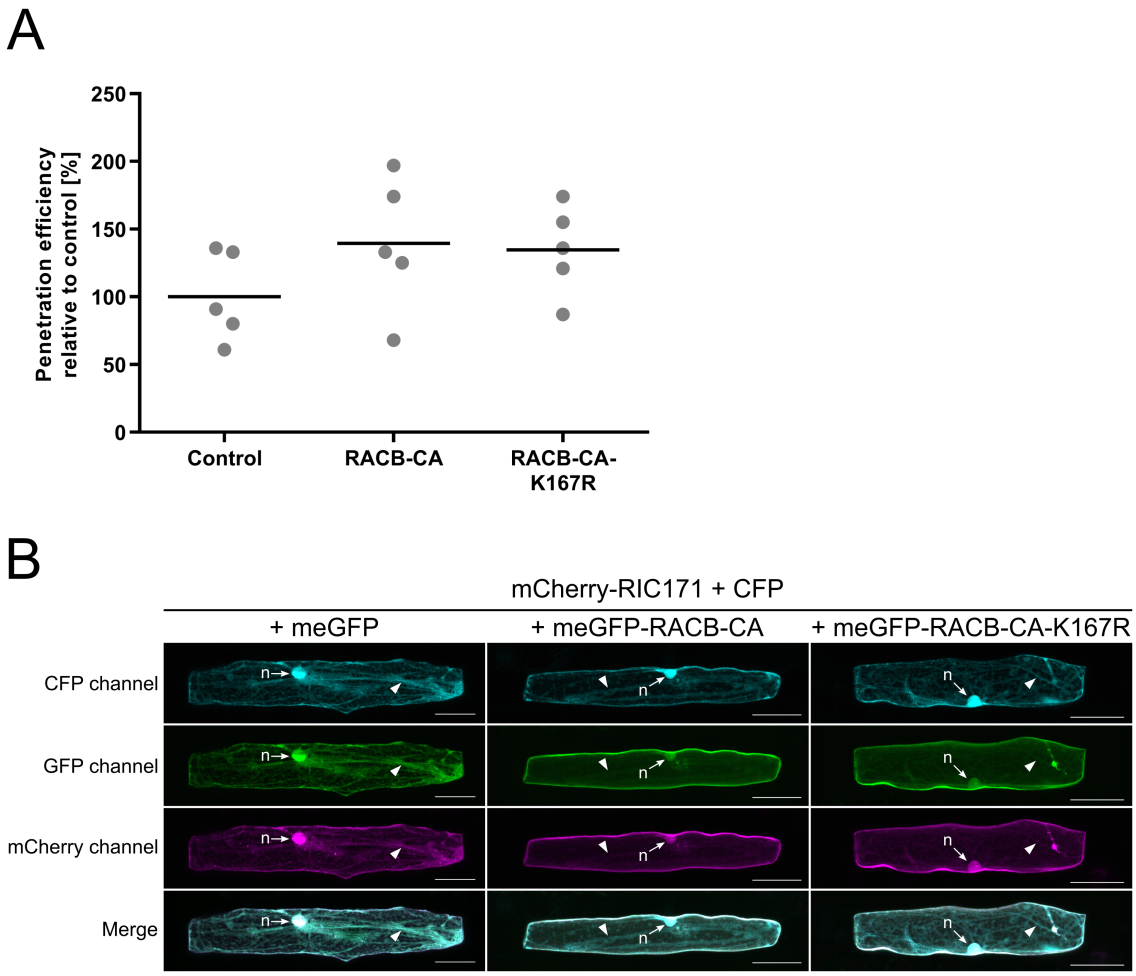

Figure 2.4: RACB-CA-K167R increases barley susceptibility to *Bgh* and recruits mCherry-RIC171.
(**A**) Barley epidermal cells show a trend of increased susceptibility towards *Bgh*-invasion after transient overexpression of RACB-CA or RACB-CA-K167R. The empty expression vector was used as control. Only transformed cells were used for analysis. Each datapoint represents the penetration efficiency of a single experiment relative to the averaged empty vector control. Crossbars display the average susceptibility over five independent biological replicates. Statistical analysis was performed via a One-way ANOVA with Tukey's HSD and found to be not significant. (**B**) Both meGFP-RACB-CA and meGFP-RACB-CA-K167R recruit mCherry-RIC171 from the cytosol to the plasma membrane. Free meGFP was expressed as a non-recruiting control, in which mCherry-RIC171 could be found in the cytoplasm (arrowheads: cytosolic strands) and nucleus (n, arrows). Free CFP was used as a marker for cytosolic and nuclear localization. Images were acquired in transiently transformed barley epidermal cells via CLSM and display maximum intensity projections of at least 11 XY-optical sections captured in 2 µm Z-steps. Images are representatives of three independent biological experiments, in which 15 cells per combination were imaged each. Scale bar: 50 µm. Image brightness was uniformly enhanced post-scanning for better visibility. This figure was modified from Fig. 7 of Weiß et al. (2022).

2.3 Identification of novel RACB-CA interaction partners

RACB's function in barley susceptibility towards *Bgh* cannot be fully explained at the moment. To gain insight into the cellular processes regulated by this ROP, I wanted to identify unknown RACB-interacting proteins to pinpoint associated cellular pathways. To achieve this, an untargeted co-immunoprecipitation (CoIP) screen followed up by liquid chromatography (LC)-tandem MS/MS identification of candidate proteins was conducted (see Fig. 2.5 A). For this screening, leaves of transgenic plants overexpressing eGFP-RACB-CA, eGFP-RACB-CA-ΔCSIL or free eGFP were either mock-treated or infected with *Bgh*. At 24 hpi, epidermal peels of mock-treated or infected leaves were collected, since *Bgh* only infects the epidermal cell layer of barley (Zhang et al., 2005). These epidermal peels were then used as sample material for the enrichment of eGFP-tagged proteins and their putative interactors via αGFP-IP. Precipitated proteins were subsequently identified by LC-MS/MS (performed by Dr. Julia Mergner, TUM), which resulted in recovery of 1399 proteins of plant and fungal origin. To sort out unspecific hits, identified proteins were filtered according to their statistically significant enrichment in eGFP-RACB-CA samples. Comparison of *Bgh*-infected samples of full-length eGFP-RACB-CA and free eGFP revealed 24 proteins that were significantly enriched in eGFP-RACB-CA (see Table S1). Under mock conditions, 17 peptides were significantly more abundant in eGFP-RACB-CA compared to free eGFP (see Table S2). In the infected samples, one *Bgh* protein stood out, as it was highly enriched in all 9 biological replicates of eGFP-RACB-CA and eGFP-RACB-CA-ΔCSIL and annotated as a putative *Bgh* effector protein (see Fig. 2.5 B). This protein received the working title "9o9" (for "nine out of nine" replicates) and was selected for further characterisation. From the plant side, two candidate interaction partners were chosen after comparing the filtered dataset with literature. During mock conditions, a phosphoinositide phospholipase C 6-like protein (termed "PLC") associated reproducibly with eGFP-RACB-CA, while after inoculation, a phosphoinositide phosphatase (called "PIP") was found to be enriched in eGFP-RACB-CA samples (see Fig. 2.5 B). ROP-signaling and phosphoinositide-associated proteins have been linked before (see Section 1.7 and Chapter 3), which is why PLC and PIP were selected for further studies.

A

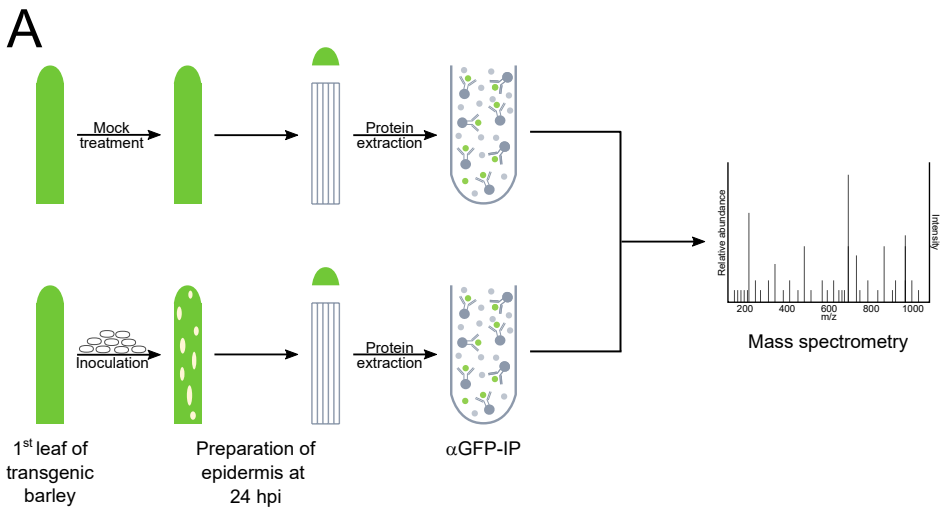

B

			eGFP-RACB-CA vs eGFP + *Bgh*		eGFP-RACB-CA vs eGFP Mock	
Name	**Gene identifier**	**Annotation**	**Enrichment factor**	***t*-test**	**Enrichment factor**	***t*-test**
9o9	BLGH_00506	Putative effector protein	64.45	p = 0.007	not found	n.d.
PLC	HORVU2Hr1G013730.2	Phosphoinositide phospholipase C 6	1.19	n.s.	1.44	p = 0.007
PIP	HORVU4Hr1G077220.4	Phosphoinositide phosphatase family protein	exclusive	p < 0.001	1.61	n.s.

Figure 2.5: Discovery of 9o9, PLC and PIP as novel RACB-CA interaction partners.
(**A**) Schematic overview of the workflow resulting in identification of 9o9, PLC and PIP as putative RACB-CA interaction partners. Transgenic barley plants overexpressing eGFP-RACB-CA, eGFP-RACB-CA-ΔCSIL and free eGFP were either mock-treated or infected with *Bgh*-spores. After preparation of epidermal peels at 24 hpi, eGFP-tagged proteins and associated putative interactors were enriched and purified via αGFP-IP. Pulled-down proteins were identified via mass spectrometry. (**B**) 9o9, PLC and PIP were found as putative RACB-CA interactors in the screening described in (**A**). Gene identifiers and annotation were taken from the barley proteome Morex V2 published in Mascher et al. (2017) or the *Bgh* DH14 proteome available on UniProt (ID: UP000015441, Spanu et al. (2010)), respectively. The enrichment factor shows the fold-increase in peptide abundance in mock-treated or infected samples of eGFP-RACB-CA compared to the corresponding eGFP samples. Significant differences in peptide abundance between the aforementioned samples were calculated by a Student's *t*-test against a p-value of 0.05. "exclusive" means that the protein was only found in eGFP-RACB-CA(-ΔCSIL) samples and not in the free eGFP control; "not found" states that the protein was not detected in eGFP-RACB-CA samples. n.s.: not significant; n.d.: not determined. Mass spectrometry was performed by Dr. Julia Mergner (TUM).

2.4 Bioinformatic analysis of 9o9, PLC and PIP

2.4.1 Annotation of functional domains

9o9, PLC and PIP have been identified as candidate RACB-CA interaction partners. To gain some information about these proteins, several bioinformatic analyses were performed. First, it was checked if they possess any conserved domains or predicted molecular functions using UniProt (The UniProt Consortium, 2020) or the NCBI conserved domain (CD)-search tool (Lu et al., 2020). For 9o9, no conserved domains or putative functions could be predicted with both tools. It appears to be a completely unknown protein. For PLC, the NCBI CD-search algorithm identified a phosphoinositide phospholipase C (PI-PLC)-domain in amino acids 121-463 (identifier: cd08599, see Fig. S5 A) and a lipid-binding C2-domain (identifier: cd00275) in amino acids 480-610. The PLC domain is split into the two subdomains PI-PLC-X and PI-PLC-Y (identifiers: PF00387 and PF00388, residues 124-266 and 347-463), which cooperate to form a triosephosphate isomerase (TIM)-barrel structure that hydrolyzes PI(4,5)P_2 to DAG and inositol-1,4,5-trisphosphate ($InsP_3$) in a Ca^{2+}-dependent manner (Rhee and Choi, 1992; Essen et al., 1997). The barley PLC isoform described here contains all functionally required amino acids, which consist of the two catalytic histidines H137 and H183, residues for Ca^{2+}-binding (N138, E167, D169, E217) and other active site amino acids (S264, K266, S377, R404, Y406) (Essen et al., 1996, 1997; Williams, 1999; Jezyk et al., 2006). The C2-domain participates in Ca^{2+}-binding, but is also necessary for membrane association of PLCs (Rizo and Südhof, 1998). For PIP, a suppressor of actin (SAC)-like phosphoinositide phosphatase domain was predicted between residues 149-514 by UniProt (PIP's UniProt ID: A0A287PS01_HORVV, see Fig. S5 B). This domain is known to dephosphorylate PI3P, PI4P and PI(3,5)P_2 using the conserved C-X(any)$_5$-R-(T/S) motif (Liu et al., 2009b). Barley PIP possesses the full catalytic site at residues ^{453}C-IDCLD-R-T^{460}, but is predicted by UniProt to specifically dephosphorylate only PI(3,5)P_2.

Identification of these conserved domains also predicted the putative subcellular localization for PLC and PIP. Accordingly, PLC should be present at the plasma membrane due to its C2-domain, while PIP could be localized to the endomembrane system because of its homology to plant SACs (see Section 2.4.2, Mao and Tan (2021)). Since 9o9 appears to be a protein of yet uncharacterized features, prediction of its subcellular localization is not feasible and should instead be elucidated experimentally. What can be done, however, is investigate if 9o9 possesses a canonical signal peptide for secretion, similar to many other effectors from *Bgh* (Spanu et al., 2010; Pedersen et al., 2012). One of the most renowned signal peptide prediction tools, SignalP (Version 6.0, Teufel et al. (2022)) did not detect a canonical signal

sequence in 9o9 (see Fig. S6 A). Interestingly, generation of a putative protein model of 9o9 via Alphafold (Version 2.1.0, Jumper et al. (2021)) predicted that its very N-terminus is part of a structural motif containing four β-sheets (see Fig. S6 B). This could indicate that the N-terminal amino acids are indeed part of the protein structure and not a signal peptide. To test if 9o9 possesses a functional N-terminal signal peptide, a secretion assay in yeast was conducted (Krijger et al., 2008). For this, a yeast strain was used, which cannot hydrolyze sucrose in the medium, since it doesn't contain a secreted invertase. This yeast therefore starves on media in which sucrose is the only sugar source. To complement this sucrose auxotrophy, the invertase gene *SUC2* can be reintroduced into this strain. To make use of this in a secretion assay, the signal peptide for secretion was deleted in *SUC2*. When another protein possessing a functional signal peptide is now fused in frame to the N-terminus of SUC2 proteins, their fusion constructs become secreted and yeast can grow on sucrose-containing media. In this case, full-length 9o9, a potential signal peptide of 9o9 (SP^{9o9}, amino acids 1-21) or a signal peptide mutant (9o9-Δ15, lacking amino acids 2-15) were fused to SUC2 and introduced into yeast strain Y02321 (see Fig. S6 C). The signal peptide of the *Arabidopsis* RLK *LORE* (SP^{LORE}, AT1G61380) was either used alone or additionally fused to full-length 9o9 to generate two positive controls. The functionality of SP^{LORE} has been confirmed in different experiments (Julian Maroschek, TUM, personal communication). The secretion assay showed that only yeast expressing SP^{LORE}-SUC2 could grown on selective media, but none of the other constructs. All constructs including an empty vector control expressing non-secreted SUC2 grew on non-selective medium containing glucose. In summary, this experiment could not prove that 9o9 possesses a canonical signal peptide.

2.4.2 Identification of homologous proteins

Next, it was checked if 9o9, PLC and PIP are part of putative gene families in *Bgh* or barley. Therefore, BLASTP searches with their amino acid sequences as queries were conducted against the current reference proteomes of *Bgh* (race DH14, Spanu et al. (2010)) and barley (*cv.* Morex (V3), Mascher (2021)). Identified homologous sequences were used for the generation of maximum-likelihood trees, in which the phylogenetic relationship between the query and its homologs can be seen. BLASTP searches with 9o9 revealed nine homologous proteins in *Bgh*, of which only one appeared to be part of the same clade (see Fig. S7 A). Interestingly, several closely related proteins belong to the CSEPs of *Bgh*. PLC has eleven homologs in barley, which can be grouped into two clades (see Fig. S7 B). Inside its clade, PLC has no directly related protein. For PIP, eight homologous proteins could be found in barley, of which three form a subfamily with PIP (see Fig. S7 C).
To identify homologs of PLC and PIP in other species, BLASTP searches against

the proteomes of *Arabidopsis* (Araport11, Cheng et al. (2017)) and rice (IRGSP 1.0, Kawahara et al. (2013)) were performed. As before, maximum-likelihood trees were built to highlight particularly related homologs. The BLASTP searches for PLC identified that it is closely related to the *At*PLC family in *Arabidopsis*, which contains nine members (see Fig. S8 A, Tasma et al. (2008)). BLASTP predicted the closest homolog to be *At*PLC2, but in the maximum-likelihood tree barley PLC showed a higher similarity to *At*PLC3 and *At*PLC5. Similarly, the rice homologs of barley PLC were also from the PLC family (see Fig. S8 B). Among its four rice family members (Singh et al., 2013), *Os*PLC1 displayed the highest similarity to barley PLC in both analyses and could therefore be considered as its ortholog.
In turn, PIP is highly similar to SAC proteins in *Arabidopsis* (see Fig. S9 A). Compared to the nine known *At*SACs (Zhong and Ye, 2003), barley PIP appeared to be most related to *At*SAC1 and *At*SAC3 in maximum-likelihood analyses or *At*SAC2 in BLASTP searches. In rice, PIP displayed close homology to uncharacterized proteins annotated as SACs and Synaptojanins (see Fig. S9 B). Both tools predicted barley PIP to be a direct homolog of Os03t0182400-01, which is currently an uncharacterized protein.

2.4.3 Expression patterns of *PLC* and *PIP*

Lastly, the gene expression patterns of *PLC* and *PIP* in different tissues and developmental stages of barley was checked. Using a public dataset from an RNAseq experiment, the gene expression of *PLC* and *PIP* could be analysed in sixteen different samples and tissues from barley *cv.* Morex (Mascher et al., 2017; Rapazote-Flores et al., 2019). *PLC* showed strong expression in etiolated seedlings and tillers, and moderate expression in the leaf epidermis and rachis (see Fig. S10 A). In the other twelve tissues, expression of *PLC* was low.
PIP was highly expressed in lemmata and moderately expressed in etiolated seedlings, lodicules, paleae, leaf epidermises and senescing leaves (see Fig. S10 B). In the other tissues, *PIP* was not or only weakly expressed.

2.5 Characterization of 9o9, PLC and PIP

The bioinformatic analyses from the previous section could only provide some initial information about 9o9, PLC and PIP. To gather more functional data for these proteins, several experiments were performed, which will be described in the following section. For instance, the involvement of the three proteins in the barley-*Bgh*-pathosystem, as well as their putative interaction with RACB have been investigated.

2.5.1 Gene expression analysis during *Bgh*-invasion

A gene expression database had indicated that *PLC* and *PIP* are expressed in the epidermal cell layer of barley leaves. Since the epidermis is colonized by *Bgh* (Zhang et al., 2005) and both proteins potentially interact with RACB, a susceptibility factor in the barley-*Bgh*-pathosystem (Schultheiss et al., 2003), it was checked if *PLC* and *PIP* are differentially expressed in this tissue during *Bgh*-attack. Furthermore, an expression profile for *9o9* during the early stages of invasion was generated.
To analyse the expression of the three genes, wildtype barley plants (*cv.* Golden Promise) were infected with conidia of *Bgh* and sampled at 8, 12 and 24 hours post infection (hpi). Mock-treated plants were used as controls for each timepoint. Additionally, fully untreated leaves were used as a reference and called -1 hpi, since they were grown together with the other plants, but sampled 1 hour before infection. At each timepoint, epidermal peels were produced and used for quantitative reverse-transcription polymerase chain reaction (qRT-PCR). For profiling of *9o9*, only the infected leaves were considered and complemented by a sample consisting of only *Bgh*-spores. Fold changes in *9o9*, *PLC* and *PIP* expression were analysed by the $2^{-\Delta\Delta Ct}$-method from Livak and Schmittgen (2001), in which *PLC* and *PIP* were normalized to the barley reference genes *glyceraldehyde-3-phosphate dehydrogenase* (*GAPDH*) and *ubiquitin-conjugating enzyme 2* (*UBC2*), while *9o9* was normalized to *Bghβ-tubulin 2* (*β-TUB2*) (Sherwood and Somerville, 1990; Rapacz et al., 2012; Schnepf et al., 2018).
qRT-PCR showed that transcript of *9o9* was already present in spores (see Fig. 2.6 A). During infection, *9o9* expression increased steadily up to a maximum of an average 116-fold at 24 hpi compared to spores. In contrast, neither transcripts of *PLC* nor *PIP* changed significantly in abundance during the course of this experiment, with one exception (see Fig. 2.6 B, C): when normalized to *UBC2*, *PLC* expression increased 1.2-fold in the infected samples at 12 hpi. However, as this increase is small and was not observed when normalization was performed with the reference gene *GAPDH*, I conclude that this increase is not biologically relevant.

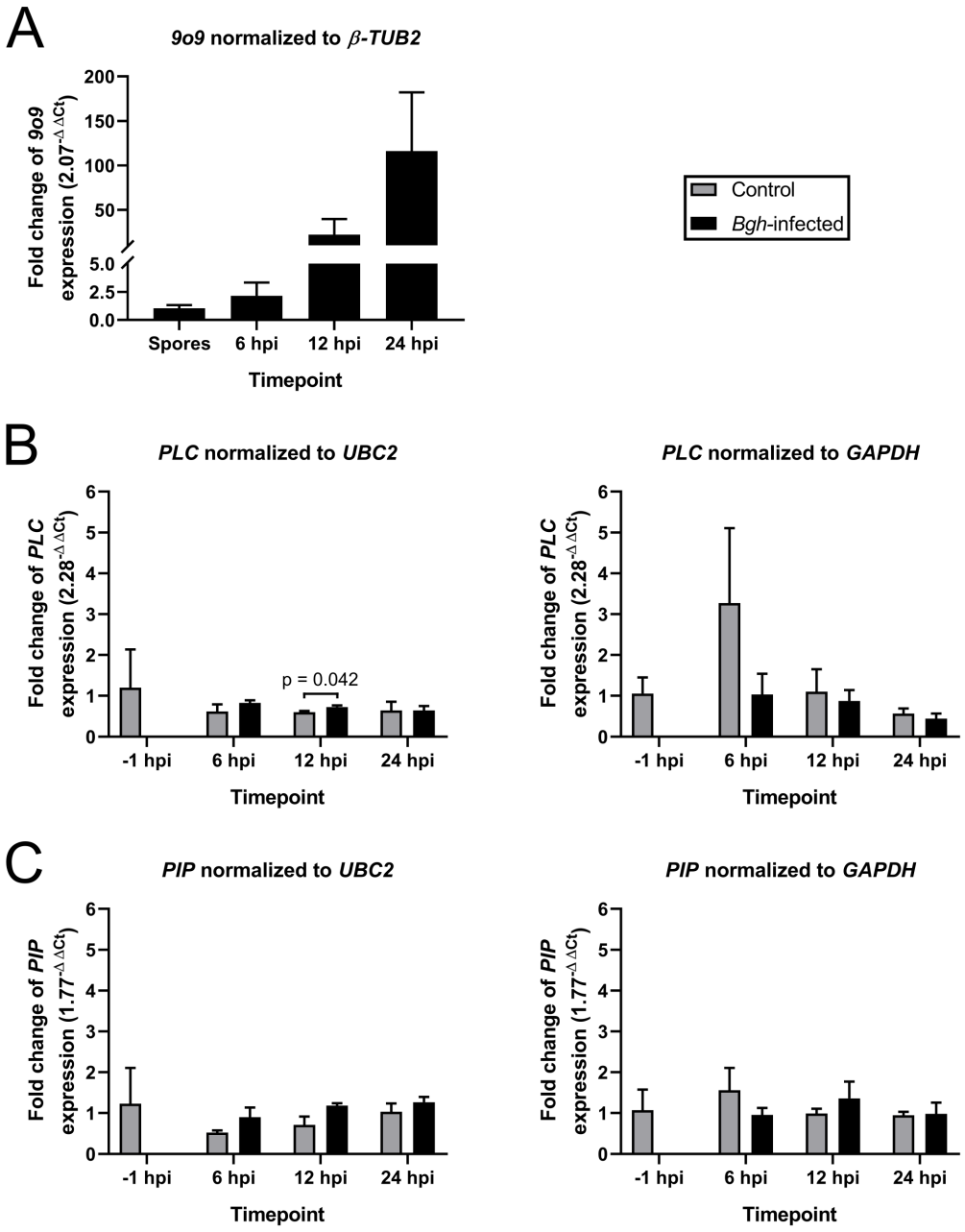

Figure 2.6: Gene expression analysis of *9o9*, *PLC* and *PIP* during *Bgh*-attack. Gene expression patterns of *9o9* (**A**), *PLC* (**B**) and *PIP* (**C**) were monitored during the early stages of *Bgh*-infection. Transcript of *9o9* was already present in spores, but increased during *Bgh*-invasion. Gene expression of *PLC* and *PIP* did not change significantly when *Bgh* colonized leaves, with one exception (indicated by the p-value). Grey bars indicate mock treated samples, black bars show *Bgh*-spores or infected samples at the respective timepoint. -1 hpi means that the sample was harvested one hour before the infection experiment began. Gene expression was measured as fold-changes according to the $2^{-\Delta\Delta Ct}$-method from Livak and Schmittgen (2001). *UBC2* and *GAPDH* were chosen as reference-genes for barley, and *β-TUB2* as housekeeping gene for *Bgh* (Sherwood and Somerville, 1990; Rapacz et al., 2012; Schnepf et al., 2018). All bars show the average fold-change with standard deviation over three independent biological replicates. Significant differences were only assessed for barley genes; multiple *t*-tests against an α of 0.05 with Holm-Sidak correction for multiple testing were performed and p-values were indicated when significant.

2.5.2 Involvement of 9o9, PLC and PIP in the barley-*Bgh*-interaction

To investigate a potential role of 9o9, PLC and PIP in the barley-*Bgh*-interaction, *Bgh*-penetration assays were performed. Hereby, 9o9, PLC or PIP were either transiently overexpressed under the cauliflower mosaic virus 35S promoter or silenced via RNA interference (RNAi) in barley epidermal cells before *Bgh*-infection. Transient transformation was achieved via particle bombardment of detached barley leaves and susceptibility to *Bgh* was evaluated at 48 hpi. Transformed cells could be identified via co-expression of the transformation marker β-glucoronidase plus (GUS+) (Schweizer et al., 1999; Vickers et al., 2003). The susceptibility towards *Bgh*-infection between different samples could be compared by analysing the penetration efficiency of *Bgh* into transformed barley epidermal cells. This penetration efficiency represents the ratio of successful *Bgh*-attacks that lead to establishment of haustoria inside host cells compared to the sum of all successful and unsuccessful penetration attempts. Conclusively, a higher penetration efficiency of *Bgh* could be classified as higher susceptibility and vice versa.
Overexpression of 9o9 increased the susceptibility towards *Bgh*-colonization by 36 % compared to the empty vector control, while RNAi against *9o9* had no effect on the infection outcome (see Fig. 2.7 A, B). Conversely, overexpression of neither PLC nor PIP changed the susceptibility of barley towards *Bgh*-invasion (see Fig. 2.7 C). Instead, RNAi-mediated silencing resulted in an elevated penetration frequency of *Bgh* of 36 % for *PLC*-RNAi or 67 % for *PIP*-RNAi compared to their empty vector controls (see Fig. 2.7 D).
In summary, these experiments suggested that 9o9 has the potential of supporting the virulence of *Bgh*, whereas both PLC and PIP appear to work in the plant's resistance against *Bgh*-infection.

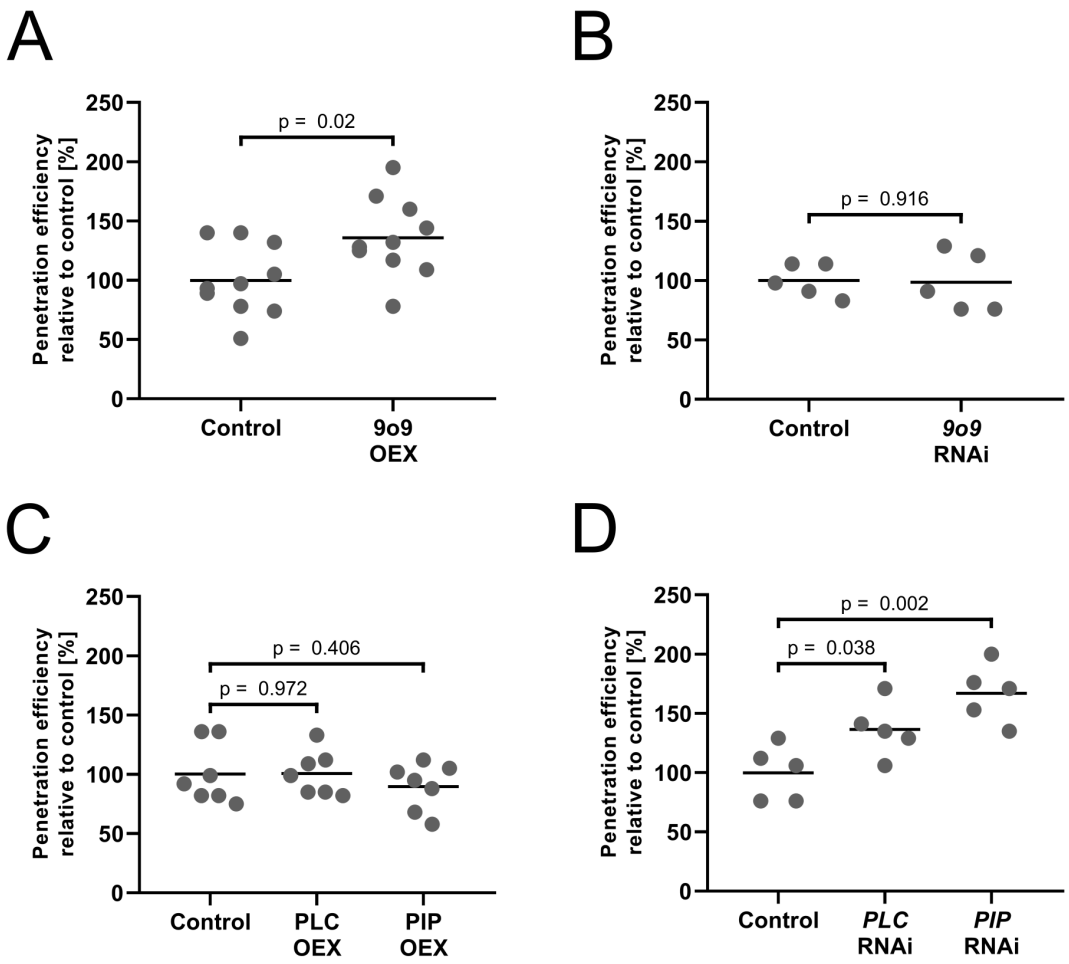

Figure 2.7: Effects of overexpression and silencing of 9o9, PLC and PIP on barley susceptibility towards *Bgh*.
The penetration efficiency of *Bgh* into barley epidermal cells was analysed after transient overexpression (**A**, **C**) or RNAi-mediated silencing (**B**, **D**) of 9o9, PLC and PIP. Overexpression of 9o9 or silencing of *PLC* and *PIP* increased the rate of *Bgh* colonization, whereas silencing of *9o9* or overexpression of PLC and PIP had no effect. The respective empty vectors were used as controls. Specificity of the RNAi-silencing constructs was confirmed using the si-Fi RNAi-off-target prediction tool (Lück et al., 2019). Only transformed cells were considered for evaluation. Each datapoint represents the *Bgh* penetration efficiency of a single experiment relative to its averaged empty vector control. Crossbars display the average susceptibility over ten (**A**), five (**B**, **D**) and seven (**C**) independent biological replicates. Significant differences in *Bgh*-penetration efficiency between an overexpression or silencing construct compared to its respective empty vector control were determined by two-tailed Student's *t*-tests. OEX: Overexpression.

2.5.3 Subcellular localization of 9o9, PLC and PIP *in planta*

To further characterize 9o9, PLC and PIP, their subcellular localization was investigated *in planta*. First, all three proteins were tagged either N- or C-terminally with mCherry and expressed in barley epidermal cells via particle bombardment. The fusion constructs of all three proteins were localized to the cytosol and nucleus (see Fig. S11), which in case of PLC and PIP did not match the predicted subcellular localization patterns (see Section 2.4.1). Since also the fluorescence intensity levels of all constructs were quite low, it was investigated if fluorophore-tagged proteins are stable in barley. Therefore, GFP-tagged 9o9, PLC and PIP were expressed in barley protoplasts and protein stability was analysed via αGFP-Western blotting (see Fig. S12). This revealed that neither GFP-tagged 9o9, PLC nor PIP are stably expressed in barley. Hence, the subcellular localization of the three proteins was investigated in *Nicotiana benthamiana*, since in this system the expression of stable fusion proteins could be confirmed via Western blots (see Section 2.5.4).
For subcellular localisation experiments, *N. benthamiana* leaves were transiently transformed with *Agrobacterium tumefaciens* to express mCherry-fusion proteins of 9o9, PLC and PIP (see Fig. 2.8). Free GFP was co-expressed in all samples to serve as a marker for cytosolic and nuclear fluorescence. In *N. benthamiana*, mCherry-tagged 9o9 was also localized to the cytosol. N-terminally tagged mCherry-9o9 was excluded from the nucleoplasm, while C-terminally tagged 9o9-mCherry could be detected inside the nucleus. N-terminally tagged mCherry-PLC could be detected at the cell periphery, but showed a strong nuclear and weak cytosolic fluorescence as well. Interestingly, C-terminally tagged PLC-mCherry displayed an almost exclusive localization at the cell periphery, with hardly any fluorescence visible in the cytosol or nucleoplasm. mCherry-tagged PIP showed only low levels of fluorescence, but could be observed mainly in the cytosol. Lastly, free mCherry mirrored the cytoplasmic and nuclear localization of the GFP-marker.
Co-expression of GFP-tagged RACB-CA, such as during FRET-FLIM experiments (see Section 2.5.4), did not have an impact on the subcellular localization of any of the three proteins and also GFP-RACB-CA was not differently localized in presence of 9o9, PLC or PIP (see Fig. S13).

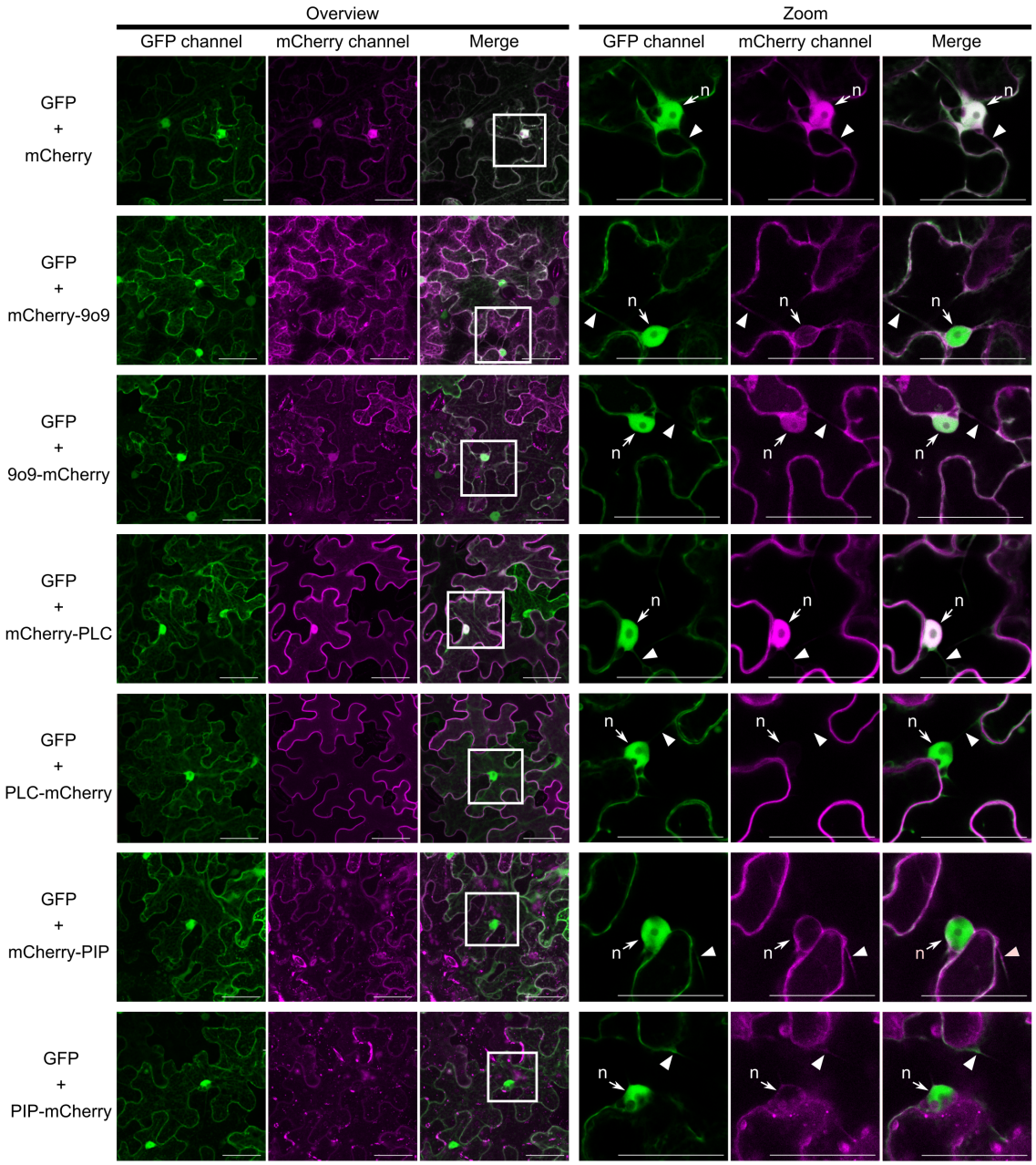

Figure 2.8: Subcellular localization of 9o9, PLC and PIP in *N. benthamiana*. The subcellular localization of the three proteins was investigated by CLSM of *A. tumefaciens*-transformed *N. benthamiana* leaves expressing free GFP and mCherry-fusion proteins. mCherry-tagged 9o9 was present mainly in the cytoplasm. N-terminally tagged mCherry-9o9 was excluded from nuclei, whereas C-terminally tagged 9o9-mCherry was also observed in the nucleoplasm. mCherry-tagged PLC showed localization at the cell periphery, which was stronger for C-terminally tagged PLC-mCherry, as N-terminally tagged mCherry-PLC displayed a higher cytoplasmic and nuclear background. mCherry-tagged PIP could be observed in the cytoplasm, but showed no nuclear fluorescence. Free GFP and mCherry served as markers for cytoplasmic and nuclear fluorescence. Arrowheads point to cytoplasmic strands. Arrows highlight nuclei (n). Overview images show maximum intensity projections of Z-stacks comprised of at least 11 XY-optical sections captured in 1.5 µm Z-steps. The white rectangle in the merge channel shows the area that was re-scanned for the magnified images, which display single slices of Z-stacks captured in 0.5 µm steps. Scale bar: 50 µm. Image brightness was uniformly enhanced post-imaging for better visibility.

2.5.4 Interaction studies between RACB and 9o9, PLC and PIP

PLC, PIP and 9o9 were identified as candidate interaction partners of RACB in an untargeted CoIP-screening (see Section 2.3). To verify their interaction with RACB *in planta*, two different experiments were conducted in *N. benthamiana*. This model plant was again used instead of barley, as the three candidates and RACB showed stable expression of fusion constructs there (see below and Section 2.5.3), which makes this system suitable for interaction studies.
First, I tried to confirm the interaction of 9o9, PLC and PIP with RACB in a targeted CoIP assay. Hereby, one protein is enriched and purified via immunoprecipitation, whereas the putative interactor is only retained during purification, when it can bind to the bait protein. To perform this experiment and enable protein detection via Western blotting, a GFP-tag was fused to the N-terminus of RACB-WT, -CA or -DN, while a 3xHA-tag was linked either to the N- or C-termini of 9o9, PLC and PIP. Free GFP was used as a unspecific-binding control. Enrichment and purification were conducted with an αGFP-trap, which targets GFP-tagged proteins. In all experiments, GFP-tagged RACB-WT and RACB-CA, as well as free GFP were well expressed and could be enriched via αGPF-IP (see Fig. 2.9). Only GFP-RACB-DN could not be detected in any sample, but this has also been observed by others (Dr. Stefan Engelhardt, TUM, personal communication). For 9o9, it could be shown that it was initially co-expressed with the three forms of RACB and free GFP, but it only co-precipitated with GFP-RACB-CA (see Fig. 2.9 A, B). This interaction was independent of the terminal fusion side of the tag on 9o9. PLC was also co-expressed with the GFP-tagged proteins in all samples, but did not show an interaction with any form of GFP-RACB (see Fig. 2.9 C). For PIP, no presence of its HA-tagged fusion proteins could be detected, irrespective of the terminal fusion side of the tag (see Fig. 2.9 D).

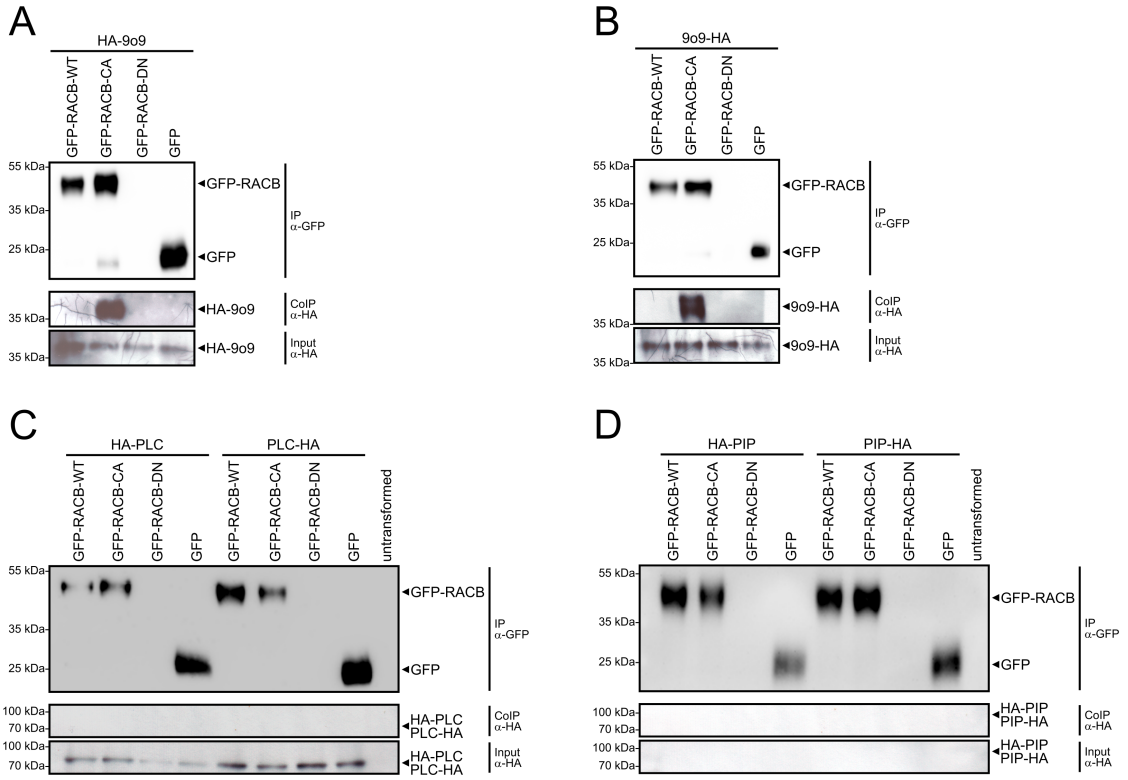

Figure 2.9: HA-tagged 9o9 interacts with GFP-RACB-CA in CoIPs from *N. benthamiana*.
Western blots showing the results of CoIP experiments from *A. tumefaciens*-transformed *N. benthamiana* plants. GFP-tagged RACB-WT, RACB-CA and free GFP could be enriched via αGFP immunoprecipitation from *N. benthamiana* leaves. GFP-RACB-DN could not be detected in any sample. N-terminally (**A**) and C-terminally (**B**) HA-tagged 9o9 were initially expressed in all samples, but could only co-precipitate with GFP-RACB-CA. HA-tagged PLC (**C**) was also co-expressed with all GFP-tagged proteins in input samples, but showed no retainment after IP. HA-tagged PIP (**D**) was not expressed in *N. benthamiana* leaves. These results could be confirmed in three independent biological replicates. Input: total protein extracts. Untransformed: non-transformed *N. benthamiana* samples serving as unspecific-binding controls for αGFP- and αHA-antibodies.

Next, a Förster resonance energy transfer fluorescence lifetime imaging microscopy (FRET-FLIM) experiment was conducted in *N. benthamiana* to further investigate protein-protein interaction. For this, monomeric enhanced GFP (meGFP)-tagged RACB-CA was used as the FRET-donor, while 9o9, PIP and PLC, as well as negative and positive controls, were fused to mCherry, which can act as a GFP-FRET-acceptor. Measuring the lifetime of GFP-donor molecules serves as a proxy to investigate direct protein-binding between two candidates, as energy is conferred via FRET from GFP to mCherry during protein-protein interaction, which in turn lowers the GFP-lifetime of the donor. All FRET-FLIM measurements were conducted at the cell periphery of directly adjacent GFP- and mCherry-expressing abaxial *N. benthamiana* epidermal cells. The analysis was performed especially in areas where cytoplasmic strands were absent, to make sure that any detected interaction took place at likely plasma

membrane-associated locations. When expressed alone, meGFP-RACB-CA exhibited a GFP-lifetime of roughly 2.7 ns in all experiments (see Fig. 2.10). In presence of the RACB-unrelated negative control glutathione *S*-transferase (GST)-mCherry, the GFP-lifetime of the donor did not change. However, when the positive control CRIB46-mCherry was co-expressed, the lifetime of meGFP-RACB-CA decreased significantly to an average of roughly 2.6 ns or 2.45 ns, depending on the experiment. CRIB46 comprises the CRIB-domain and surrounding amino acids of the known RACB interactor RIC171, for which it could already be shown that the CRIB46 peptide is sufficient for the interaction with RACB-CA (Schultheiss et al., 2008). In case of 9o9, co-expression of the N-terminally tagged mCherry fusion protein showed a clear lifetime decrease in meGFP-RACB-CA to an average 2.6 ns, which was comparable to that of the positive control (see Fig. 2.10 A). Combination of meGFP-RACB-CA with C-terminally tagged 9o9-mCherry lead to a less strong, but significant GFP-lifetime decrease to 2.66 ns. For PLC, only co-expression of C-terminally tagged PLC-mCherry lead to a significant lifetime reduction to 2.64 ns in meGFP-RACB-CA, whereas N-terminally tagged mCherry-PLC had no effect on donor lifetime (see Fig. 2.10 B, C). Lastly, presence of N-terminally tagged mCherry-PIP significantly lowered the GFP-lifetime to 2.65 ns, but co-expression of C-terminally tagged PIP-mCherry did not change GFP-lifetime (see Fig. 2.10 B, C). In summary, 9o9 appears to be able to directly interact with RACB-CA *in planta*, whereas this is less clear, but indicated for PLC and PIP.

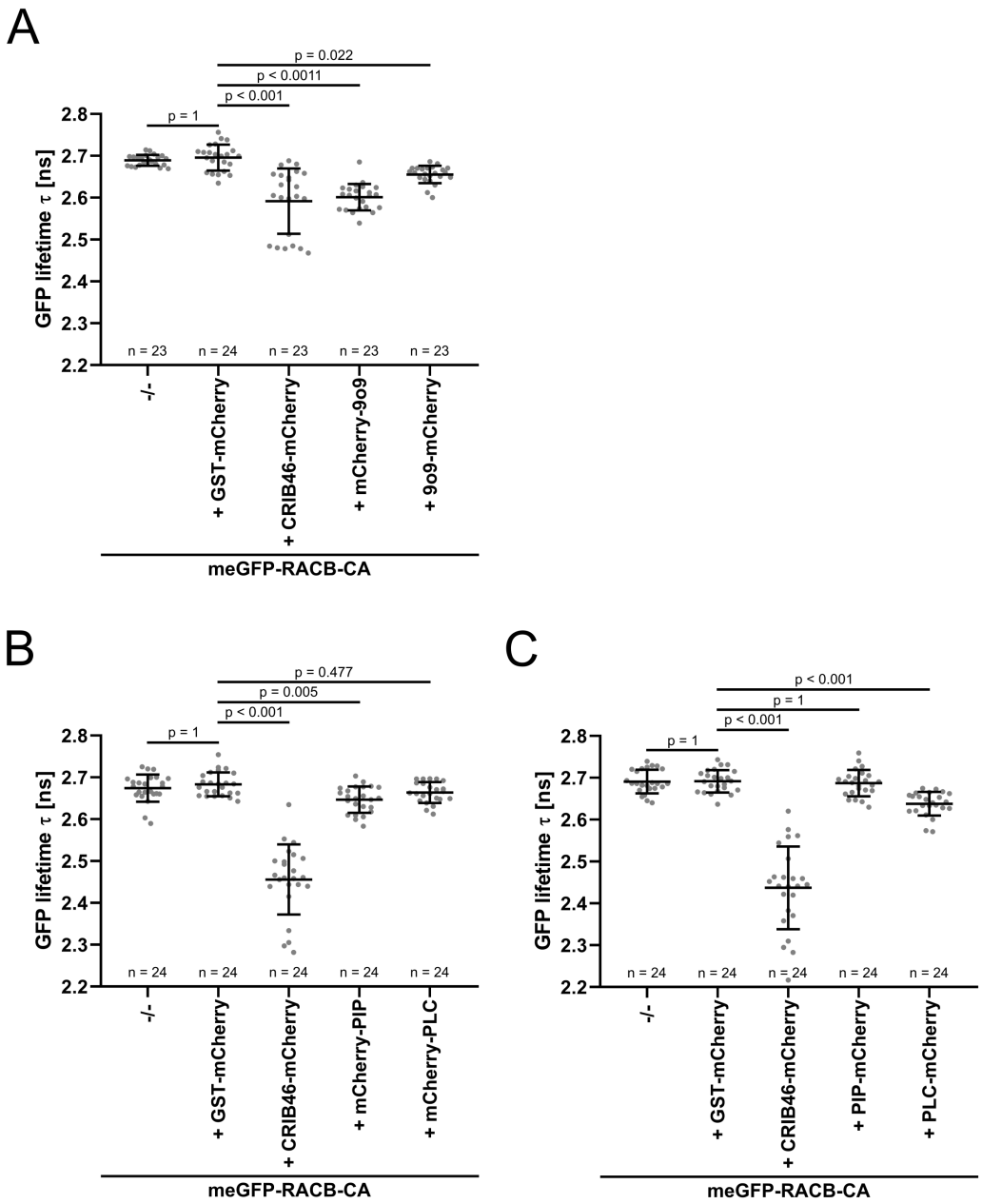

Figure 2.10: GFP-RACB-CA interacts with mCherry-tagged 9o9, PLC or PIP in FRET-FLIM experiments in *N. benthamiana*.
A FRET-FLIM experiment in *A. tumefaciens*-transformed *N. benthamiana* was conducted to investigate the ability of RACB-CA to interact with 9o9 (**A**), PLC or PIP (**B**: N-terminal mCherry fusions; **C**: C-terminal mCherry fusions). The GFP-donor lifetime of meGFP-RACB-CA did not change in presence of the negative control GST-mCherry, but was clearly decreased when the positive control CRIB46-mCherry was co-expressed. Both N- and C-terminally mCherry-tagged 9o9 lowered the GFP-lifetime of meGFP-RACB-CA. Only N-terminally tagged PIP or C-terminally tagged PLC decreased the GFP-lifetime of the donor. -/-: FRET-donor-only control. The lifetime of GFP (τ) was measured in nanoseconds (ns). Single cell measurements were collected over three biological replicates and the number of observations (n) are shown below each column. The crossbar depicts the average lifetime, while the whiskers show standard deviation. Statistical differences were assessed by Wilcoxon-Rank-Sum tests with Bonferroni correction for multiple testing. Selected p-values are shown; all p-values can be seen in Fig. S14.

2.5.5 Lipid-binding assays

PLC and PIP were predicted to interact with phosphoinositides and show enzymatic activity against particular phospholipid species (see Section 2.4.1). To identify which phospholipids they can target, I collaborated with the working group of Prof. Dr. Ingo Heilmann from the Martin-Luther-University of Halle that specializes in lipid-binding proteins. RACB-WT was carried along in all experiments that were performed, because during the preparation of this dissertation it was shown that the wildtype form of the RACB-homologous ROP *At*ROP6 could also bind to phospholipids (Platre et al., 2019). Since the other two putative RACB-interaction partners were predicted to be phospholipid-associated proteins, I decided to test if 9o9 could interact with phospholipids as well.

To study lipid-binding, the proteins first had to be heterologously expressed in *E. coli*. To enable subsequent purification steps, RACB-WT was fused to GST, while PLC, PIP and 9o9 were fused to a maltose-binding protein (MBP). A novel RACB mutant was also included in these assays, because it was demonstrated that the phospholipid-binding capacity of *At*ROP6 relied on its C-terminal polybasic stretch consisting of lysines and arginines (Platre et al., 2019). Mutation of these lysines and arginines to neutral glutamines completely abolished lipid-binding of *At*ROP6 (Platre et al., 2019). Conclusively, the corresponding five lysines K184-K188 in RACB's polybasic region were exchanged with five glutamines (5Q) and this mutant of RACB was termed RACB-5Q. After expression in *E. coli*, proteins of interest were enriched and purified by affinity chromatography targeting the GST- or MBP-tag. Only MBP-9o9 could not be purified, as it repeatedly precipitated in the insoluble fraction before purification. Hence, a total protein extract from MBP-9o9-expressing *E. coli* had to be used for further experiments.

Lipid-binding specificity was determined by incubating membranes with different pre-spotted lipids with the purified proteins. Protein-lipid-interaction would enable the protein to remain attached to the membrane during washing steps, after which it could be detected via tag-specific antibodies. In these experiments, the unconjugated MBP- and GST-tags were used as non-lipid-binding controls, while GST-*At*ROP6 was used as a lipid-binding positive control. These lipid-binding assays revealed that GST-RACB-WT could weakly bind to PI3P, PI4P and PI5P and strongly to PS, whereas the GST-RACB-5Q mutant showed no detectable lipid-binding (see Fig. 2.11). In comparison, the positive control GST-*At*ROP6 also associated with PI3P, PI4P, PI5P and PS, but could further bind to PI(3,4)P_2, PI(3,5)P_2, PI(4,5)P_2, PI(3,4,5)P_3 and PA. Interestingly, all three putative RACB interactors also exhibited lipid-binding capacities: 9o9, PLC and PIP could all bind to PI3P, PI4P and PI5P. In addition, PIP and 9o9 could further associate with PS, but 9o9 could also interact with PI(3,4)P_2, PI(3,5)P_2, PI(4,5)P_2, PI(3,4,5)P_3 and PA. Neither unconjugated

GST nor MBP alone showed any capacity of lipid-binding.
In conclusion, RACB and its putative interaction partners displayed overlapping patterns of lipid-binding capacities, and in case of RACB, this could be directly attributed to its C-terminal polybasic stretch.

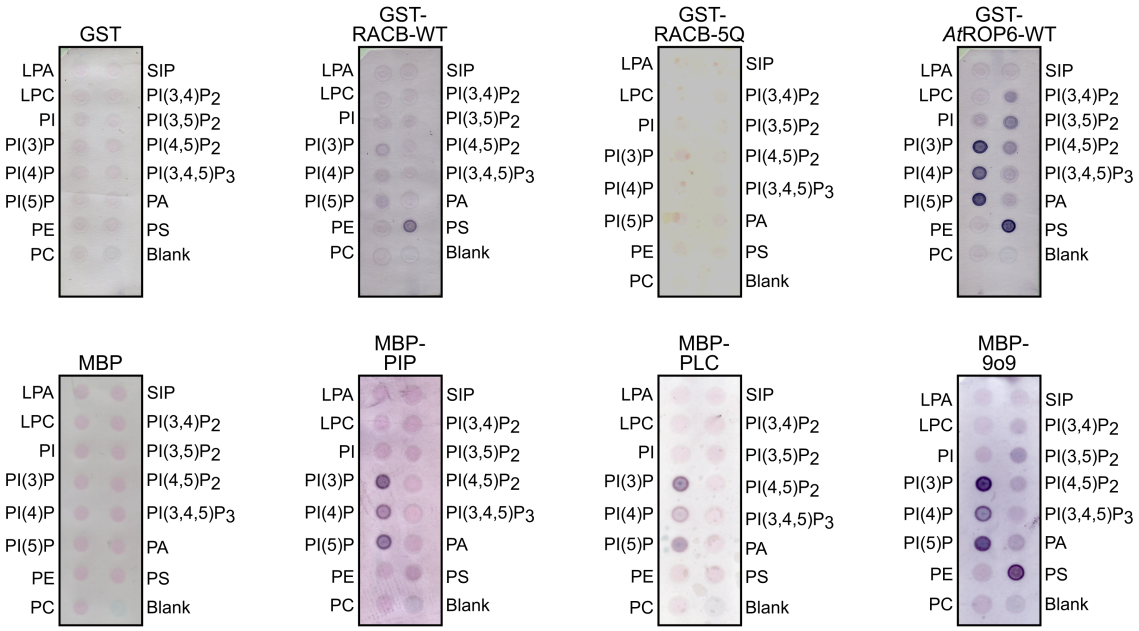

Figure 2.11: Interaction of RACB, 9o9, PLC and PIP with phospholipids *in vitro*.
Recombinant GST-tagged RACB-WT, RACB-5Q and *At*ROP6, as well as MBP-tagged 9o9, PLC and PIP were expressed in and purified from *E. coli*. Only for MBP-9o9 a non-purified total protein extract from *E. coli* had to be used, as MBP-9o9 had always precipitated in the insoluble fraction during purification. Protein-lipid interaction was determined by incubating lipid-spotted membranes with the recombinant proteins and detecting the GST- or MBP-tags via antibodies. Unconjugated GST and MBP were used as non-lipid-binding controls. All fusion proteins could interact with PI3P, PI4P and PI5P, except for the GST-RACB-5Q mutant, which did not interact with any lipid. All fusion proteins except MBP-PLC further bound PS. GST-*At*ROP6 and MBP-9o9 also associated with $PI(3,4)P_2$, $PI(3,5)P_2$, $PI(4,5)P_2$, $PI(3,4,5)P_3$ and PA. LPA: lysophosphatidic acid; LPC: lysophosphatidylcholine; SIP: sphingosine 1-phosphate; blank: no lipid spotted. All other phospholipid abbreviations can be found in Section 1.7. These experiments were performed in collaboration with Dr. Mareike Heilmann (MLU Halle).

2.6 Anionic phospholipid-localization in barley

Since RACB and its three putative interaction partners displayed lipid-binding capacities *in vitro*, I wanted to gain a deeper understanding about anionic phospholipids in barley. The following lipid species were investigated in this dissertation: PI4P was chosen, since it showed a distinct localization during powdery mildew attack in *Arabidopsis* (Qin et al., 2020), whereas $PI(3,5)P_2$, $PI(4,5)P_2$ and PS were studied, as they had been linked to ROP-signaling already (Kost et al., 1999; Hirano et al.,

2018; Platre et al., 2019; Qin et al., 2020; Fratini et al., 2021).

2.6.1 Subcellular localization of PI4P, PI(3,5)P_2, PI(4,5)P_2 and PS in barley

The four different anionic phospholipids were all visualized by published genetically-encoded biomarkers, which are protein domains shown to specifically interact with distinct lipid species *in vivo* (Simon et al., 2014; Hirano et al., 2017). PI4P was detected with a GFP-tagged double pleckstrin homology domain of the human Four-Phosphate Adapter Protein (GFP-2xPH^{FAPP1}, Simon et al. (2014)), while PI(3,5)P_2 could be imaged with an mCitrine-tagged tandem repeat of the lipid-binding domain of mammalian Mucolipin 1 (mCitrine-2xML1N, Hirano et al. (2017)). PI(4,5)P_2 was visualized with a GFP-tagged double PH-domain of rat PLCδ1 (GFP-2xPH^{PLC}, Simon et al. (2014)) and PS was observed via a GFP-tagged C2-domain of bovine Lactadherin (GFP-C2^{LACT}, Platre et al. (2018)). All biomarkers were visualized by CLSM of transiently transformed barley epidermal cells and, in case of *Bgh* infection, were imaged at 16 hpi.

Fluorescence of the PI4P-marker was observed exclusively at the PM in untreated leaves and did not shift localization in non-attacked cells after inoculation with *Bgh* (see Fig. 2.12). In attacked non-penetrated cells fluorescence could also be observed inside the papilla. However, emission wavelength analysis via λ-scanning could show that this is mainly auto-fluorescence coming from the deposited cell wall material at the attack site and not a specific GFP-signal. In penetrated cells harboring a haustorium, the marker for PI4P was excluded from the EHM and could be observed at the haustorial neck region in a ring-like structure in addition to its regular PM localization. In this case, λ-scanning could prove that this is a true GFP-signal and not auto-fluorescence.

The marker for PI(3,5)P_2 was also localized to the PM, but it showed a strong cytoplasmic and nuclear background (see Fig. 2.13). In some cells, mCitrine-2xML1N could also be seen in small vesicular structures that seemingly resembled endosomes (see Fig. 2.13 B). During *Bgh* attack, the PI(3,5)P_2-marker was recruited to the papilla in non-penetrated cells. In cells harboring haustoria, however, this could not be observed. λ-scanning could show that fluorescence at the papilla originated mainly from mCitrine-2xML1N and not from auto-fluorescence.

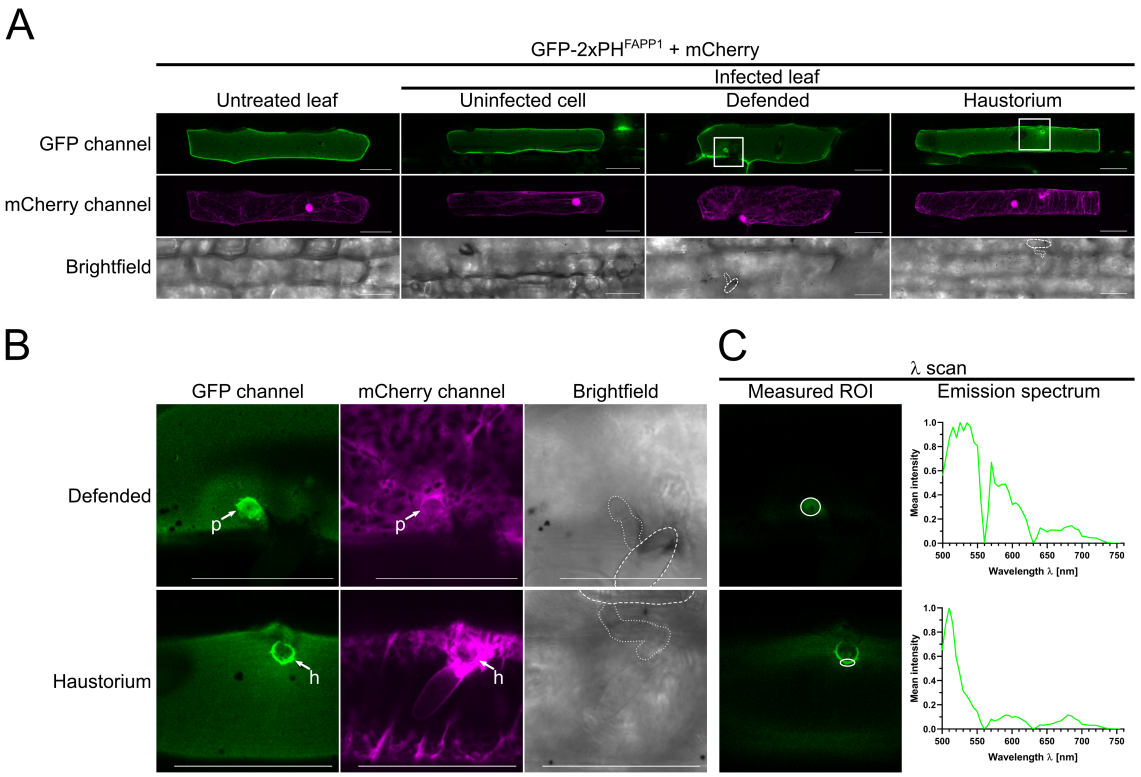

Figure 2.12: Subcellular localisation of PI4P in barley during *Bgh*-attack. The PI4P marker GFP-2xPH^{FAPP1} was expressed in barley epidermal cells via particle bombardment and observed via CLSM. Free mCherry was co-expressed as a marker for nuclear and cytoplasmic fluorescence. (**A**) Overview images showing presence of PI4P at the PM in untreated leaves, but also in uninfected, attacked and penetrated cells at 16 hpi. The white rectangle highlights the area that was re-scanned with a higher magnification (**B**). In attacked, but non-penetrated cells (defended), green fluorescence could also be observed inside the papilla (p). In penetrated cells (haustorium), fluorescence from GFP-2xPH^{FAPP1} was also visible in a ring-like structure around the haustorial neck (h). Emission wavelength analysis via λ-scanning (**C**) showed that only fluorescence in the ring-like structure clearly resembled a typical GFP-emission spectrum with a peak around 510 nm (Tsien, 1998), whereas the signal from inside the papilla looked different and as such is most likely auto-fluorescence. λ-scanning was performed by selecting the plane from (**B**) that showed strongest fluorescence levels and analysing emission in 5 nm steps after excitation with a 488 nm laser. Fluorescence emission was analysed in the highlighted region of interest (ROI, white circles). All images except λ-scans and brightfield pictures show maximum intensity projections of Z-stacks containing at least 16 (overview) or 4 (zoom) XY-optical sections captured in 1.5 µm Z-steps. Scale bar: 50 µm. Image brightness was uniformly enhanced post-scanning for better visibility. Brightfield images are single XY-optical sections, in which spores are outlined with dashed lines and secondary germ tubes are shown with dotted lines.

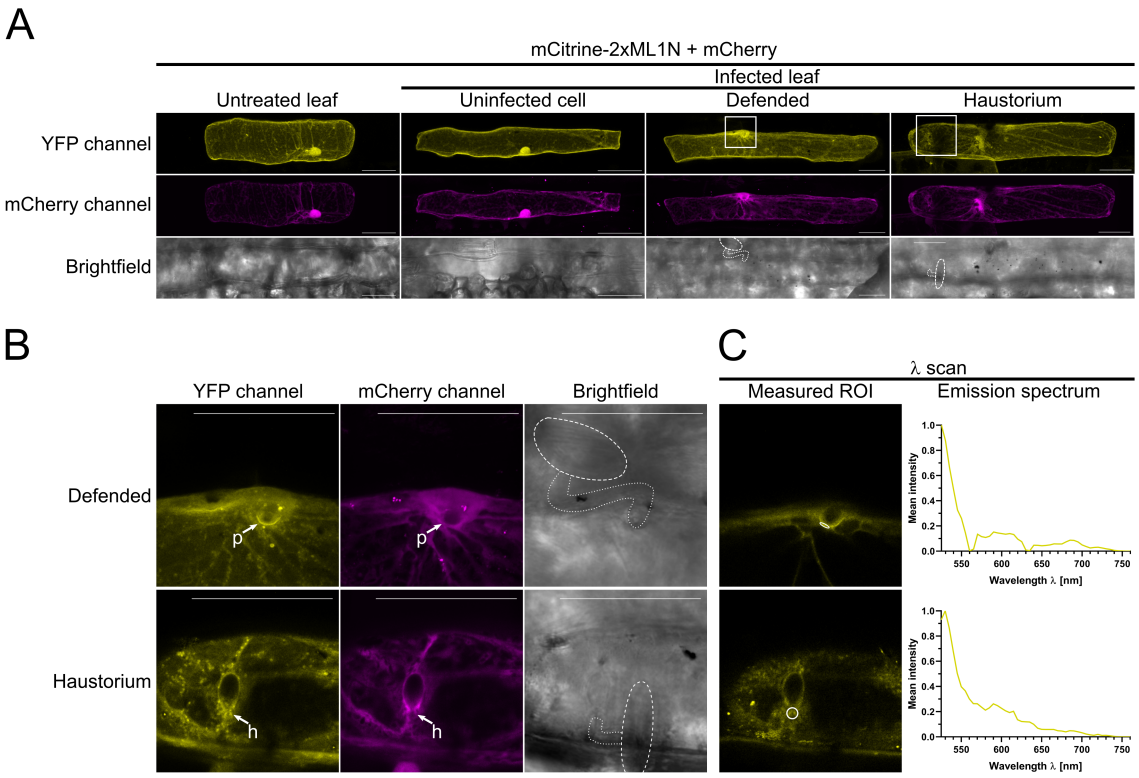

Figure 2.13: Subcellular localisation of PI(3,5)P_2 in barley during *Bgh*-attack. The PI(3,5)P_2 marker mCitrine-2xML1N was expressed in barley epidermal cells via particle bombardment and observed via CLSM. Free mCherry was co-expressed as a marker for nuclear and cytoplasmic fluorescence. (**A**) Overview images showing PI(3,5)P_2-marker fluorescence at the periphery, but also inside the cytosol and nucleus at 16 h post *Bgh*-infection. (**B**) Zoomed-in images of non-penetrated (defended) and penetrated (haustorium) cells. The white rectangles in (**A**) outline the areas that were re-scanned with a higher magnification. Fluorescence from mCitrine-2xML1N accumulated strongly around the papilla (p), but not noticeably at haustorial entry points (h). (**C**) λ-scans showing that fluorescence signals inside the papilla or at haustorial entry points originated mainly from mCitrine-2xML1N and not from auto-fluorescence, since the detected emission spectrum matched that of YFP (Lybarger et al., 1998). The white circles highlight the regions of interest (ROIs) that were measured. λ-scans were collected in the planes from (**B**) that showed highest fluorescence levels. Emission spectra were analysed in 5 nm steps after excitation with a 514 nm laser source. All images except λ-scans and brightfield pictures show maximum intensity projections of Z-stacks containing at least 18 (overview) or 6 (zoom) XY-optical sections captured in 1.5 µm Z-steps. Scale bar: 50 µm. Image brightness was uniformly enhanced post-scanning for better visibility. Brightfield images are single XY-optical sections, in which spores are outlined with dashed lines and secondary germ tubes are shown with dotted lines.

Fluorescence of the PI(4,5)P_2-marker was visible at the PM with a weak cytosolic and nuclear background in untreated leaves and non-attacked cells (see Fig. 2.14 A, B). In attacked cells, however, this became harder to gauge, as auto-fluorescence was overshadowing the weak fluorescence of GFP-2xPH^{PLC}. This auto-fluorescence appeared to be stronger in the images of GFP-2xPH^{PLC} (see Fig. 2.14 C) when compared to the other biomarkers, likely because higher laser excitation and detector gain settings had to be used to image GFP-2xPH^{PLC} due to its low fluorescence levels. Hence, a non-penetrated, non-transformed cell was scanned with the same settings to visualize the auto-fluorescence emission spectrum (see Fig. 2.14 B, C). Irrespective of the auto-fluorescence, PI(4,5)P_2-marker fluorescence appeared to be more cytosolic and nuclear in attacked transformed cells. Additionally, fluorescence levels of GFP-2xPH^{PLC} seemed to be higher in penetrated cells harboring a haustorium. To clarify this, the fluorescence intensities of the PI(4,5)P_2-marker were compared between uninfected, non-penetrated and haustorium-harboring cells using quantitative imaging at 16 h after *Bgh* infection. In this case, 2xPH^{PLC} was fused to mCherry, while free GFP was used as a normalizer for variations in fluorescence signal strength between different transformed cells. This experiment showed that in cells containing a haustorium the fluorescence levels of mCherry-2xPH^{PLC} were indeed higher when compared to uninfected or non-penetrated cells, while its intensity levels were comparable between uninfected and non-penetrated cells (see Fig. 2.15).
Finally, the marker for PS was targeted mainly to the PM, but could be additionally observed in small speckles in most cells (see Fig. 2.16). GFP-C2^{LACT} further exhibited weak fluorescence in the cytoplasm, but was excluded from the nucleus. In infected leaves, the PS-marker retained its PM-localization, but showed a slightly stronger cytoplasmic background in attacked cells. Interestingly, in successfully infected cells, GFP-C2^{LACT} could be further observed in the rim region of penetrated papillae. As before, λ-scanning could confirm that this is a true GFP-signal and not auto-fluorescence.
In summary, all four investigated anionic phospholipid species displayed an altered behaviour during *Bgh* invasion, which could indicate their involvement in the barley-*Bgh*-interaction.

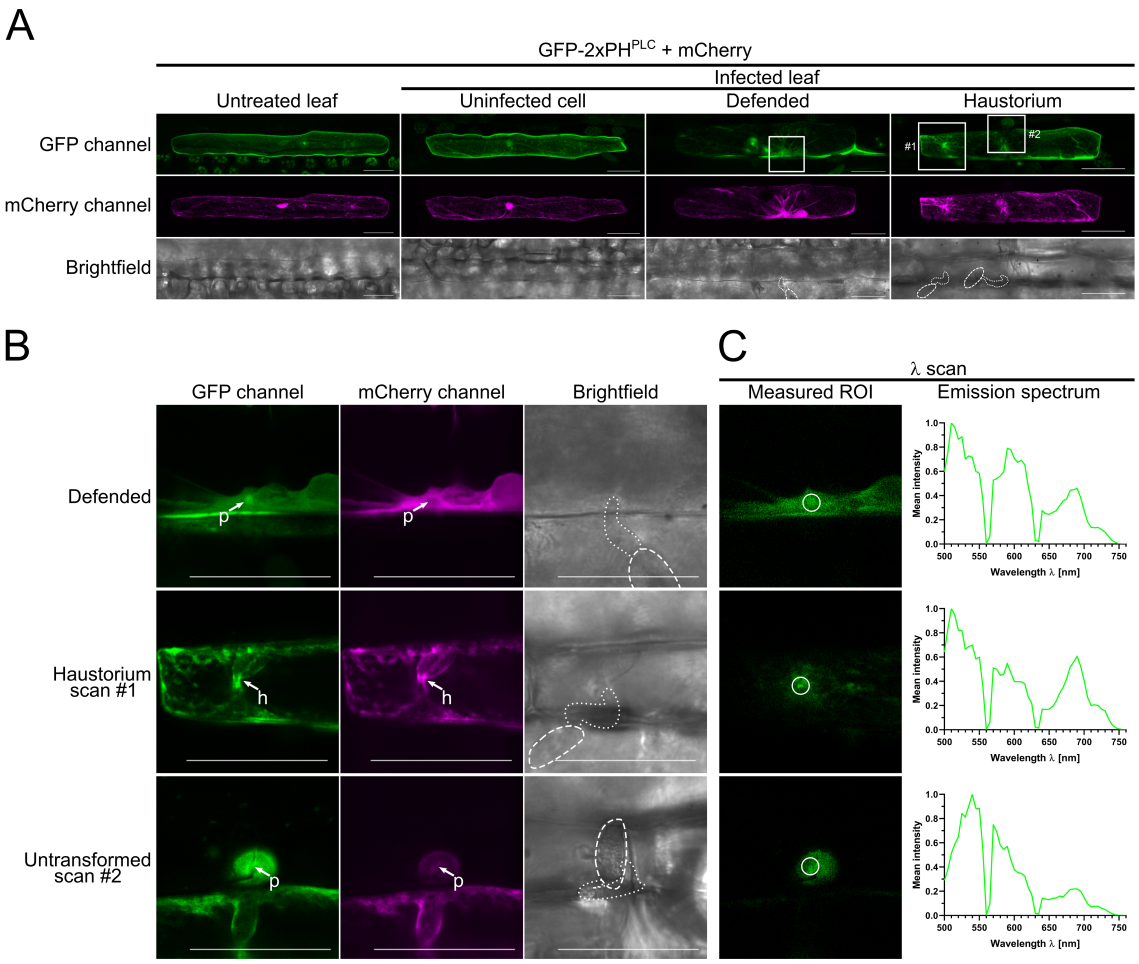

Figure 2.14: Subcellular localisation of PI(4,5)P_2 in barley during *Bgh*-attack. PI(4,5)P_2 was visualized in barley epidermal cells via CLSM after transient expression of the GFP-2xPH^{PLC} biomarker. Free mCherry was co-expressed as a marker for nuclear and cytoplasmic fluorescence. (**A**) Overview images of transformed cells from uninfected leaves or non-attacked, non-penetrated (defended) or penetrated (haustorium) cells at 16 h after *Bgh* infection. (**B**) Higher magnification of the areas shown in (**A**). Unsuccessful penetration events (p) and haustorial entry points (h) are highlighted with arrows. In untreated leaves or uninfected cells, PI(4,5)P_2-marker fluorescence could be mainly observed at the PM and weakly in the cytosol and nucleus. In attacked cells, GFP-2xPH^{PLC} displayed a more cytoplasmic and nuclear localisation, but this was more difficult to evaluate, as auto-fluorescence was overshadowing the weak fluorescence of the marker. λ-scanning (**C**) confirmed a large presence of non-GFP-signals in attacked cells in measured regions-of-interest (ROIs, white circles). A non-penetrated, non-transformed cell (scan #2) was scanned to observe the auto-fluorescence emission spectrum. λ-scanning was performed by selecting the plane from (**B**) that showed strongest fluorescence levels and analysing emission in 5 nm steps after excitation with a 488 nm laser source. All images except λ-scans and brightfield pictures show maximum intensity projections of Z-stacks containing at least 17 (overview) or 8 (zoom) XY-optical sections captured in 1.5 µm Z-steps. Scale bar: 50 µm. Image brightness was uniformly enhanced post-scanning for better visibility. Brightfield images are single XY-optical sections, in which spores are outlined with dashed lines and secondary germ tubes are shown with dotted lines.

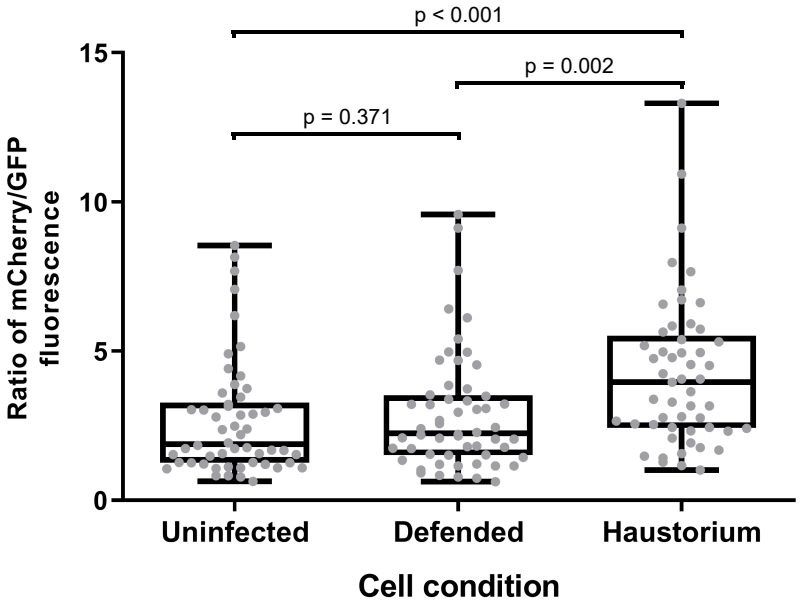

Figure 2.15: Quantification of mCherry-2xPH^{PLC} fluorescence levels during *Bgh* attack.
The fluorescence intensity levels of the PI(4,5)P_2-marker mCherry-2xPH^{PLC} were measured in transiently transformed barley epidermal cells at 16 h after *Bgh* infection. Free GFP was co-expressed as a normalizer for between-cells variation in fluorescence levels. CLSM was used to determine the mean pixel intensities for both fluorophores in each measured cell. Each datapoint represents the calculated mCherry-to-GFP ratio of an individual cell, which allowed the comparison of fluorescence intensities of the PI(4,5)P_2-marker between uninfected, non-penetrated ("defended") and penetrated ("haustorium") cells. In cells harboring a haustorium, higher fluorescence of mCherry-2xPH^{PLC} could be observed. Single cell measurements were collected over three independent biological replicates, in which laser and detector settings were kept identical throughout. Significant differences between conditions were determined by a Wilcoxon rank-sum test with continuity correction.

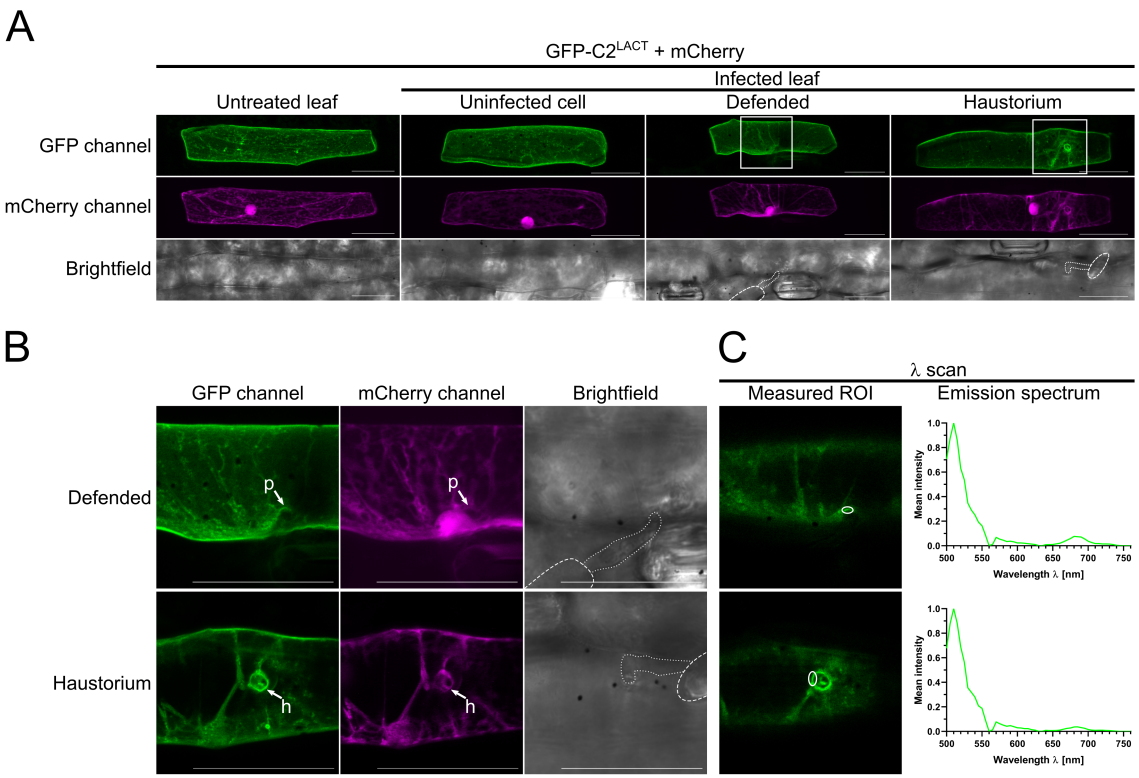

Figure 2.16: Subcellular localisation of PS in barley during *Bgh*-attack.
The subcellular localization of PS in barley epidermal cells was investigated via CLSM after transient expression of the GFP-C2^{LACT} biomarker. Free mCherry was co-expressed as a marker for nuclear and cytoplasmic fluorescence. (**A**) shows overview images, from which the area marked by the white rectangle was re-scanned with a higher magnification in (**B**). In all cells, GFP-C2^{LACT} was localized to the PM and showed only weak fluorescence in the cytosol. Additionally, the PS-marker could be observed in small speckles in most cells. In attacked cells, the cytoplasmic fluorescence of GFP-C2^{LACT} was more prominent and the PS-marker could be further observed in the rim region of penetrated papillae at 16 hpi. (**C**) λ-scanning was performed to analyse the signal from unsuccessful penetration events (p) and haustorial entry sites (h) in the magnified images. In both cases, a clear peak at 510 nm could be observed, which is characteristic for GFP-fluorescence (Tsien, 1998). The white circles show the region of interest (ROI) that was measured. All images except λ-scans and brightfield pictures show maximum intensity projections of Z-stacks containing at least 17 (overview) or 12 (zoom) XY-optical sections captured in 1.5 µm Z-steps. Scale bar: 50 µm. Image brightness was uniformly enhanced post-scanning for better visibility. Brightfield images are single XY-optical sections, in which spores are outlined with dashed lines and secondary germ tubes are shown with dotted lines.

2.6.2 Manipulation of PI(4,5)P_2-levels in barley via dOCRL

Apart from being involved with ROP signaling, PI(4,5)P_2 has been shown to be a susceptibility factor in the plant-powdery mildew interaction (Qin et al., 2020). More precisely, a knockout of the kinases that produce PI(4,5)P_2 was responsible for a vastly increased resistance of *Arabidopsis thaliana* towards penetration by *Erysiphe cichoracearum*. Since a gene knock-out is technically challenging in barley, I used an enzyme that degrades PI(4,5)P_2 in order to lower the levels PI(4,5)P_2 in barley cells. The enzyme *Drosophila melanogaster* inositol polyphosphate 5-phosphatase OCRL protein (dOCRL) was shown in *Arabidopsis* to specifically degrade PI(4,5)P_2 (Doumane et al., 2021). For full functionality, dOCRL contains an N-terminal myristoylation and palmitoylation (MAP) motif followed by an mCherry-tag, which targets the enzyme to the PM and simultaneously enables detection via its mCherry-tag (Doumane et al., 2021). To verify its functionality in barley, MAP-mCherry-dOCRL was co-expressed with the PI(4,5)P_2-marker GFP-2xPH^{PLC} in barley epidermal cells via particle bombardment. MAP-2xmCherry and the enzymatically-dead MAP-mCherry-dOCRL^{dead} mutant were used as non-lipid-degrading negative controls (Doumane et al., 2021). Free mCherry had to be included as a transformation marker, since the fluorescence levels of GFP-2xPH^{PLC} and the MAP-mCherry-tagged proteins were too low to otherwise find transformed cells. In this experiment, the PI(4,5)P_2-marker displayed PM localization with weak cytoplasmic and nuclear background in cells co-expressing MAP-mCherry or MAP-mCherry-dOCRL^{dead} (see Fig. 2.17). In presence of functional MAP-mCherry-dOCRL, however, fluorescence of GFP-2xPH^{PLC} was exclusively found in the cytosol and surrounding the nucleus. This indicated a successful degradation of PI(4,5)P_2 via dOCRL, as in absence of PI(4,5)P_2, its marker GFP-2xPH^{PLC} was shown to be released from the PM into the cytosol (Doumane et al., 2021). In conclusion, dOCRL appears to be functional in barley and could be a valuable tool for further studies involving PI(4,5)P_2 and its role in susceptibility towards *Bgh*.

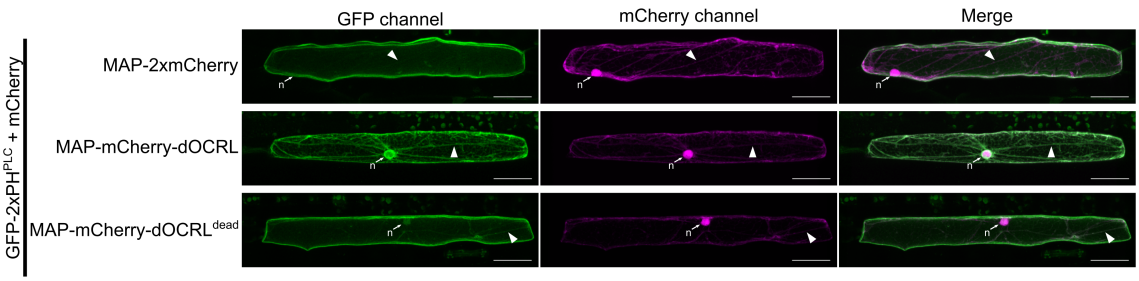

Figure 2.17: Co-expression of dOCRL removes the PI(4,5)P_2-marker from the plasma membrane.
The PI(4,5)P_2-marker GFP-2xPH^{PLC} was co-expressed in barley epidermal cells with MAP-2xmCherry, MAP-mCherry-dOCRL or MAP-mCherry-dOCRL^{dead} via particle bombardment. Free mCherry was included in all samples as a transformation marker to identify transformed cells and shows exclusively cytosolic (arrowheads: cytosolic strands) and nuclear (n, arrows) fluorescence. Signal from GFP-2xPH^{PLC} was visible mainly at the PM and weakly in the cytosol and nucleus when MAP-2xmCherry or MAP-mCherry-dOCRL^{dead} were co-expressed. In presence of MAP-mCherry-dOCRL, fluorescence from GFP-2xPH^{PLC} shifted from the PM to the cytosol and around the nucleus. All cells were imaged by CLSM. Images show maximum intensity projections of Z-stacks containing a minimum of 20 XY-optical sections captured in 1.5 µm Z-steps. Scale bar: 50 µm. Image brightness was uniformly enhanced post-scanning for better visibility. These results could be reproduced in three independent biological experiments.

3 Discussion

The barley ROP GTPase RACB acts in polar cell development, but it has also been classified as a susceptibility factor in the barley-*Bgh* interaction (Schultheiss et al., 2002, 2003; Hoefle et al., 2011; Scheler et al., 2016). Although several RACB-regulating proteins and downstream interaction partners have already been identified (Schultheiss et al., 2008; Hoefle et al., 2011; McCollum et al., 2020; Engelhardt et al., 2021; Trutzenberg et al., 2022), it is still mostly unclear by which mechanism RACB mediates susceptibility and how it can be regulated apart from the canonical GDP/GTP-cycling. The data presented in this work provide evidence for RACB-regulation through ubiquitination at K167, which governs protein stability (Weiß et al., 2022). Additionally, novel RACB-CA interaction partners of plant and fungal origin established a link to anionic phospholipid signaling processes *in planta*, which have been shown to be involved in other plant-pathogen interactions (Shimada et al., 2019; Qin et al., 2020).

3.1 Posttranslational modifications of RACB

Since small monomeric G-proteins are master regulators of cellular signaling processes, their activity has to be tightly controlled. On one hand, their activation and deactivation via GEFs and GAPs is often spatio-temporally restricted (Denninger et al., 2019; Kulich et al., 2020). On the other hand, Rho-like proteins are targeted by posttranslational modifications, which can also influence Rho protein activity (Abdrabou and Wang, 2018). In animals, the RACB-homolog Rac1 for instance is both modified by phosphorylation and ubiquitination. Phosphorylation of Y64, S71 or T108 via different kinases was shown to have inhibitory effects on Rac1 activity, either by interfering with its activation and GTP-loading or through targeting it for degradation (Kwon et al., 2000; Chang et al., 2011; Tong et al., 2013; Zhao et al., 2013). Similarly, ubiquitination was found to affect the output of Rac1-signaling, as modification of K147 or K166 mark Rac1 for proteasomal degradation and thereby inhibit its function in cell polarity signaling and motility (Torrino et al., 2011; Oberoi et al., 2012; Castillo-Lluva et al., 2013; Zhao et al., 2013). Interestingly, not only host proteins partake in non-canonical regulation of Rho-like proteins. Effector proteins from pathogens were also found to bind and modify Rhos (Aktories, 2011). For instance, the human pathogen *Photorhabdus asymbiotica* employs the effector protein *P. asymbiotica* protein toxin (PaTox), which glycosylates human Rac1 and other members of the Rho-family at Y32 (Jank et al., 2013). Glycosylation prevents activation of Rhos and blocks interaction with downstream proteins, which effectively inhibits signaling and leads to cytotoxicity. Another example is the cytotoxic necrotizing factor-1 (Cnf1) from *Escherichia coli*, which deamidates RhoA at Q63. This

fully blocks the GTPase activity of RhoA, causing it to become locked in the active state (Schmidt et al., 1997). In comparison, data for posttranslational modifications of plant Rho-like proteins is limited and mainly restricted to lipidation (Yalovsky, 2015) or *in vitro* studies (see Section 1.5). Regarding other PTMs, only *in vivo* phosphorylation of *At*ROP10 and *At*ROP11 could be shown, but no experiments investigating their function have been conducted yet (Mergner et al., 2020). To deepen our knowledge on this topic, this work explored potential PTMs of the barley ROP RACB. As RACB was found to physically associate with the protein kinase RBK1 and stimulate its kinase activity *in vitro* (Huesmann et al., 2012), it was proposed that this might lead to phosphorylation during protein-protein interaction *in vivo* (Huesmann et al., 2012; Reiner et al., 2015). Additional indications for potential *in vivo* phosphorylation of RACB were provided by *in vitro* kinase assays conducted with RACB-CA and RBK1. These experiments identified five *in vitro* phosphorylation sites in RACB-CA, of which three were speculated to be suitable targets for phosphorylation *in vivo* (Weiß et al., 2022). Furthermore, since both RBK1 and its interaction partner SKP1L, a putative subunit of an E3 ubiquitin ligase complex, were shown to negatively regulate RACB protein abundance in a proteasome dependent manner, it was hypothesized that RACB is targeted for ubiquitination (Reiner et al., 2015). Using stable transgenic barley plants overexpressing tagged signaling-active RACB-CA, potential posttranslational modifications of RACB could be investigated. First, it was checked if RACB is phosphorylated *in vivo*. However, even though RBK1 was co-overexpressed and progressively elaborate techniques and workflows were used, no phosphorylation site could be identified in RACB-CA (Weiß et al., 2022). One reason for this could be that the conditions under which RACB becomes phosporylated were not met. For instance, RBK1 might not be the kinase that phosphorylates RACB *in vivo*, since it belongs to a different class of kinases than those which phosphorylate animal Rhos. RBK1 is a member of RLCK class VI_A (Jurca et al., 2008; Huesmann et al., 2012; Reiner et al., 2014), while the kinase that phosphorylates for example mammalian Rac1, AKT, belongs to the AGC family (Rademacher and Offringa, 2012). Phosphorylation of RACB by an AGC kinase appears possible, because it was shown that ROPs and AGC kinases cooperate during polar cell development in *Arabidopsis* (Stanislas et al., 2015). In this case the AGC kinase D6PK coordinates root hair formation and outgrowth together with *At*ROP2 and *At*ROP6, which are RACB-like type I ROPs. Although Stanislas et al. (2015) did not investigate phosphorylation of *At*ROP2/6 by D6PK in their study, it remains a possibility.

Regarding ubiquitination, 3xHA-tagged RACB-CA and higher molecular weight derivatives were evidenced on a Western blot after enrichment of RACB via immunoprecipitation (see Fig. 2.2). Since the appearance of these RACB derivatives

resembled a model ubiquitination pattern as observed for example for the plant PRR FLS2 (Göhre et al., 2008; Lu et al., 2011), a potential ubiquitination of these higher molecular weight RACB forms was investigated via mass spectrometry. This revealed RACB-K167 as a ubiquitin acceptor site, and experiments employing a non-ubiquitinatable RACB-K167R mutant demonstrated that this residue is involved in regulating protein stability. Interestingly, only signaling-active RACB-CA and dominant negative RACB-DN became more stable through the K167R mutation, but the abundance of RACB-WT-K167R remained unchanged (see Fig. 2.3). On one hand, this could mean that ubiquitination is a slow process that occurs when RACB remains in either its active or inactive conformation for too long. This would explain the observed phenotypes, as RACB-CA and RACB-DN are locked in either state and eventually become ubiquitinated, but RACB-WT can still cycle between states and would thus be unaffected. On the other hand, efficient deubiquitination could only be available for regulated RACB-WT(-K167R), but not its activity mutants.
The downstream-signaling ability of RACB appears to be independent of the presence of K167. Both RACB-CA and RACB-CA-K167R were able to induce super-susceptibility towards *Bgh*-infection upon overexpression in barley (see Fig. 2.4 A). Consequently, the abundance of overexpressed RACB-CA alone seems not to be limiting factor for its role in susceptibility, as GFP-tagged RACB-CA-K167R accumulates to higher levels than its regular RACB-CA form (see Fig. 2.3 B). Instead, *Bgh* might profit from other elements, such as RACB's signaling processes in general. The downstream signaling capacities of RACB also appear not to be hampered by the K167R mutation, because both GFP-tagged RACB-CA and RACB-CA-K167R were able to recruit RIC171 to the plasma membrane (see Fig. 2.4 B). RIC171 is a known interaction partner of RACB, which is recruited to the cell periphery in presence of signaling-active RACB (Schultheiss et al., 2008). In conclusion, presence or absence of the biochemical properties of K167 might not influence RACB's signaling processes, but its role as a ubiquitin-acceptor site likely does, because it is part of the binding interfaces of both PRONE-GEFs and CRIB-domain containing proteins (see Fig. S4). This suggests that binding of either proteins would mask the ubiquitination site, thus preventing RACB from becoming degraded. In case of inactive GDP-bound RACB, only those RACB proteins that are not bound by GEFs would be targeted for ubiquitination, hence providing a disposal mechanism for surplus inactive RACB proteins. As for activated GTP-bound RACB, interaction with a CRIB-domain containing protein would lead to higher stability of GTP-RACB, which would ensure its role in crucial signaling processes. After that, unbound GTP-RACB molecules could be targeted by either GAPs or ubiquitination to terminate their signaling capacities. In contrast, ubiquitination of RACB at K167 could have the exact opposite effects. Addition of one or more ubiquitin molecules to RACB-K167 would sterically block

interaction with GEFs or CRIB-proteins, leading to inhibition of RACB-signaling.
In a previous study, Reiner et al. (2015) proposed a mechanism by which RACB could be targeted by PTMs. This hypothesis was based on data from mammalian Rac1, which becomes phosphorylated at S71 by the AGC kinase AKT (Kwon et al., 2000). Phosphorylation of Rac1 leads to recognition by the SCF^{FBXL19}-E3 ubiquitin ligase complex, which polyubiquitinates Rac1 at K166 and targets it for proteasomal degradation (Zhao et al., 2013). Correspondingly, Reiner et al. (2015) speculated that RACB-CA would interact with RBK1 and becomes phosphorylated in the process. This would lead to recognition by an SCF-complex harboring the RBK1-interactor SKP1L, which then polyubiquitinates RACB-CA and targets it for degradation. This hypothesis is now partially supported by data from this work. Although no phosphorylation site for RACB could be identified, regulation of RACB via ubiquitination could be shown. The ubiquitination site in RACB at K167 corresponds to Rac1-K166, and both sites govern protein stability (Zhao et al., 2013; Weiß et al., 2022). The presence of this lysine in all ROPs from barley, rice and *Arabidopsis* (see Fig. S3) further suggests that the stability regulating mechanisms discussed here are conserved across kingdoms.
Regarding other PTMs, data from this dissertation also support the hypothesis that lipidation is essential for the signaling capacity of ROPs (Sorek et al., 2011; Yalovsky, 2015). In the transgenic barley lines used in this work, a correlation between barley susceptibility towards *Bgh* and the subcellular localization of RACB-CA could be observed (see Fig. 2.1). In the eGFP-tagged RACB-CA-expressing lines, super-susceptibility towards *Bgh*-infection was only detected in plants in which overexpressed full-length RACB-CA was localized to the plasma membrane. In contrast, plants overexpressing the eGFP-RACB-CA-ΔCSIL mutant showed levels of susceptibility towards *Bgh* similar to eGFP-overexpressing plants, but also a mislocalization of eGFP-RACB-CA-ΔCSIL to the cytosol and nucleus. Correspondingly, the susceptibility of the 3xHA-tagged RACB-CA-expressing lines towards *Bgh*-infection was only increased, when full-length RACB-CA was overexpressed (Weiß et al., 2022). These findings are corroborated by data from previous transient experiments, in which only full-length RACB-CA localized to the plasma membrane and increased susceptibility towards *Bgh*, whereas the RACB-CA-ΔCSIL mutant did not (Schultheiss et al., 2003). The mislocalization of the RACB-CA-ΔCSIL mutants can be attributed to the deletion of the CaaX prenylation motif, which is mainly responsible for the membrane association of type I ROPs (Berken and Wittinghofer, 2008; Sorek et al., 2017). Mechanistically, it is possible that the RACB-CA-ΔCSIL mutants are compromised in the interaction with their signal-transducing downstream proteins, as this usually takes place at the plasma membrane (Schultheiss et al., 2008; Hoefle et al., 2011; McCollum et al., 2020). Alternatively, the mislocalized RACB-

CA-ΔCSIL mutants might deplete their interactors from the plasma membrane and recruit them to the cytosol, which inhibits their signaling processes. In either case, the prenylation-mediated localization of RACB at the plasma membrane appears to be as important for its role in susceptibility towards *Bgh* as its activation status.

3.2 9o9 is a *Bgh* effector protein targeting activated RACB

To gain insight into how RACB could be mechanistically connected to barley susceptibility towards *Bgh*-infection, I screened the *Bgh*-infected epidermis of transgenic barley plants overexpressing eGFP-tagged RACB-CA for novel interaction partners. This way, 9o9 was identified as a candidate interactor of activated RACB (see Fig. 2.5). The data gathered in this work point towards 9o9 being a true effector protein of *Bgh*, for the following reasons: first, homologs of 9o9 belong to the CSEP-family (see Fig. S7 A), which represents the best validated and second largest family of effector proteins in *Bgh* (Spanu et al., 2010; Amselem et al., 2015).
Second, overexpression of 9o9 in barley causes increased susceptibility towards *Bgh*-infection. Another protein from *Bgh*, for which an effector function could be determined, corroborates this. When overexpressed in barley, the *Bgh*-effector ROP-interactive peptide 1 (ROPIP1) also increased susceptibility towards invasion (Nottensteiner et al., 2018). In turn, silencing of 9o9 via cross-kingdom RNAi had no effect on the infection outcome, but this can be explained by the fact that 9o9 transcript was already found in spores (see Fig. 2.6). Hence, by the time that host-induced gene silencing would become effective, 9o9 protein was likely already formed and sufficient for infection. In general, however, cross-kingdom RNAi can be effective against effectors from *Bgh*, as for instance host-induced silencing of the *Bgh* effector candidates 1011 and 1054 resulted in a strongly reduced penetration efficiency of *Bgh* into barley epidermal cells (Pliego et al., 2013).
Third, 9o9's transcript abundance is upregulated drastically during infection, which matches the expression pattern of other effector proteins (Hacquard et al., 2013). Timecourse RNAseq experiments in *Bgh*-susceptible *Arabidopsis pen2 pad4 sag101* triple mutants revealed that other *Bgh* effector proteins from the CSEP-family are transcribed in waves (Hacquard et al., 2013). CSEP-transcriptional patterns peaked at either host cell entry at 12 hpi or haustorium differentiation at 24 hpi. Since 9o9's expression levels also increased during infection and were highest at 24 hpi (see Fig. 2.6), this could infer a potential role for 9o9 in haustorium development as well.
Fourth, when expressed in *N. benthamiana*, 9o9 could directly associate with activated RACB-CA (see Fig. 2.9, 2.10). For an effector protein this would make sense, as targeting a susceptibility factor could enable infection. Indeed, this mechanism has been shown in various cases (Engelhardt et al., 2018): as mentioned in Section 1.3, *Arabidopsis* RIN4, a negative regulator of plant immunity, is targeted by at least

six different effector proteins, which modify or degrade RIN4 to facilitate infection (Mackey et al., 2002; Axtell and Staskawicz, 2003; Day et al., 2005; Kim et al., 2005a; Wilton et al., 2010; Afzal et al., 2011; Liu et al., 2011; Choi et al., 2021). Another example is a homolog of barley MLO in *Arabidopsis*. *At*MLO2 is targeted by HopZ2, an effector protein from the bacterium *Pseudomonas syringae* (Lewis et al., 2012). Presence of *At*MLO2 and its interaction with HopZ2 were shown to be essential for the virulence function of HopZ2 (Lewis et al., 2012). Additionally, 9o9 targeting a small monomeric G-protein could also be a viable virulence strategy. In animals, this case has been documented extensively, as several RACB-like Rho proteins are targeted by a multitude of bacterial effectors (Aktories, 2011). For instance, the RACB-homologous protein Rac1 is first activated by the *Salmonella typhimurium* effector protein SopE, which possesses a GEF-like function (Hardt et al., 1998). GTP-bound Rac1 then reorganizes the actin cytoskeleton and promotes membrane ruffling, which leads to internalization of the bacterium (Hardt et al., 1998). Once inside the host cell, *Salmonella typhimurium* secretes a different effector protein, SptP (Fu and Galán, 1999). SptP outcompetes SopE in Rac1-binding and shuts down Rho-signaling through its GAP-activity, which reverses the effect on the actin cytoskeleton and thereby likely promotes host cell survival (Fu and Galán, 1999). Since 9o9 was found to bind only activated RACB-CA *in planta*, an activating GEF-like function appears unlikely. However, this cannot be fully ruled out, because barley *Hv*GEF14 has been shown to possess the ability to both activate RACB-WT and still interact with RACB-CA *in planta* (Trutzenberg et al., 2022). I would also argue against an inhibitory function for 9o9, since the current hypothesis about RACB-mediated susceptibility involves *Bgh* co-opting the signaling processes of activated RACB (Hückelhoven et al., 2013). Therefore, I would suggest that in binding RACB, 9o9 either keeps the ROP or its signaling processes active, but this remains to be seen in the future.

There are also some other open questions left. For example, the mechanism by which 9o9 is transported into the plant cell is not clear yet. Unlike the CSEPs, which are characterized by their N-terminal signal sequences for secretion (Spanu et al., 2010), no signal peptide could be identified in 9o9. Neither computational tools could predict a signal sequence in 9o9 nor could its secretion be evidenced experimentally (see Fig. S6). Protein modelling via Alphafold further predicted that the N-terminus of 9o9 is part of the protein structure, which argues against the N-terminus being a signal peptide. Instead, it has to be assumed that 9o9 is secreted in a non-conventional way. This is not uncommon, as for example the candidate effector proteins (CEPs) from *Blumeria graminis* f.sp. *tritici* (*Bgt*) are believed to act inside host cells without possessing an N-terminal secretion signal (Wicker et al., 2013). This is also supported by data for the *Bgh* effector ROPIP1, which lacks a

canonical N-terminal signal peptide but could still be detected in the host cytoplasm of *Bgh*-infected barley epidermal cells using immunogold-labeling and transmission electron microscopy (Nottensteiner et al., 2018).
Furthermore, the mode-of-action for 9o9 is still unknown. It is tempting to speculate that 9o9 targets the plant's anionic phospholipid-signaling pathway as a virulence target, since 9o9 was shown to bind several phospholipid species *in vitro* (see Fig. 2.11). Proteins usually bind lipids through dedicated domains or polybasic stretches (Dowler et al., 2000; Simon et al., 2014; Platre et al., 2019). In 9o9, however, lipid-binding has to be mediated through a novel motif, as 9o9 is not predicted to possess any known lipid-binding domains or polybasic stretches in its amino acid sequence. Nonetheless, binding the plant's anionic phospholipids could achieve a series of things. For one, this might be the way for 9o9 to meet activated RACB in the cell. As shown through evidence from the transgenic lines and previous studies, RACB has to be plasma membrane localized to act as a susceptibility factor (Schultheiss et al., 2003; Weiß et al., 2022). When membrane-targeted, activated RACB likely associates with anionic phospholipids, similar to what has been demonstrated for a ROP from *Arabidopsis*. To become signaling-competent, GTP-bound *At*ROP6 needs to undergo a re-localization into phosphatidylserine (PS)-containing membrane nanodomains (Platre et al., 2019). While not shown for RACB yet, a similar mechanism appears plausible, because it can also bind to PS *in vitro*. Since 9o9 associates with similar anionic phospholipids species as RACB and *At*ROP6 *in vitro* (see Fig. 2.11), this could enable 9o9 to identify and interact with active ROP-signaling hubs in plant cells. This also opens up the question whether 9o9 only targets RACB or whether it can also associate with other barley ROPs. Interactors of ROPs are usually not restricted to only one ROP-protein and can bind several family members. Barley RIC171 for example is able to interact with four out of six barley ROPs (Schultheiss et al., 2008), whereas barley RBK1 can interact with both barley RACB and and the type II ROP GTPase RAC1 (Huesmann et al., 2012). In any case, interaction between 9o9 and RACB or multiple ROPs requires a to-date uncharacterized binding domain, since no canonical binding-interface could be identified in 9o9.
Another reason why 9o9 binds anionic phospholipids might be because they themselves are its virulence target. Other pathogen effector proteins were found to associate with phospholipids as part of their virulence function. For example, the *Legionella pneumophila* effector SidF converts the PI(3,4)P_2- and PI(3,4,5)P_3-containing host phagosomes into PI4P-outlined *Legionella*-containing vacuoles, where the bacterium proliferates (Hsu et al., 2012). Deletion of *SidF* inhibits this conversion and causes other *Legionella* effectors to be mislocalized, as they need to bind PI4P (Hsu et al., 2012). It was also speculated that the SidF-mediated dephosphorylation of PI(3,4)P_2 and PI(3,4,5)P_3 is part of its survival strategy, because the host can

transform these phospholipids into PI3P, which serves as a signal for lysosome-fusion and degradation of vacuolar contents (Vergne et al., 2003; Flannagan et al., 2009; Hsu et al., 2012). Correspondingly, 9o9 could associate with plant phospholipids for two possible reasons: 9o9 could be an active, unknown enzyme that influences the plant anionic phospholipid constitution to fit the needs of *Bgh*, potentially during development of the extrahaustorial membrane. The gene expression analysis seems to suggest a role for 9o9 in this process, because 9o9 expression levels peaked at 24 hpi (see Fig. 2.6), the stage at which haustorium differentiation takes place (Hacquard et al., 2013). Interestingly, the EHM surrounding the haustorium was shown to be composed of different phospholipids than the plant plasma membrane, even though they are in continuum (Kwaaitaal et al., 2017). Thus, an enzymatic activity of 9o9 could possibly modify the plant's anionic phospholipid composition at the plasma membrane so that the identity of the EHM can be established and the haustorium can grow into the infected cell using the host's machinery (Kwaaitaal et al., 2017). Alternatively, 9o9 could only adopt the fold of a phospholipid-metabolizing enzyme, but be enzymatically inactive. This could potentially allow 9o9 to outcompete plant enzymes, which would normally alter the plant's phospholipid composition towards signaling processes that lead to disease resistance. In summary, both mechanisms would effectively influence the plant's anionic phospholipid pathway in favor of *Bgh*, so that the fungus can better infect its host.
Lastly, 9o9 is not the first *Bgh*-effector targeting activated RACB. ROPIP1 was shown before to increase barley susceptibility in favor of *Bgh* and interact with activated RACB (Nottensteiner et al., 2018). Inside the host cell, ROPIP1 induces fragmentation of the plant's microtubules, a process that has been associated with increased penetration (Huesmann et al., 2012; Nottensteiner et al., 2018). In summary, *Bgh* converges on RACB-mediated susceptibility signaling by employing two effector proteins that target the ROP directly. One effector destabilizes the plant's cytoskeleton (Nottensteiner et al., 2018), whereas the other might influence the plant's anionic phospholipids in a way that the fungus can efficiently establish its haustorium.

3.3 PLC and PIP are resistance factors in the barley-*Bgh*-pathosystem

Apart from 9o9, two plant proteins were also identified as novel candidate interactors of RACB-CA. PLC and PIP co-precipitated with RACB-CA in untreated and *Bgh*-infected barley samples, respectively (see Fig. 2.5). Bioinformatic analysis suggested PLC to be a PI(4,5)P_2-hydrolyzing phospholipase C, while PIP could be suppressor of actin (SAC)-class PI(3,5)P_2-dephosphorylating phosphatase, since both proteins possess the corresponding catalytic sites (see Section 2.4.1 and Fig. S5). This is also

supported by their homologous proteins in rice and *Arabidopsis*, which both come from the PLC- or SAC-families (see Figs. S8, S9). The closest homolog, and perhaps ortholog, of barley PLC in rice is *Os*PLC1, whereas in *Arabidopsis* no clear ortholog could be determined (see Fig. S8). Regarding PIP, phylogenetic analysis classified it as a clade I SAC-like protein, since it is most closely related to other members of this clade, namely *At*SAC1-5 (see Fig. S9). Apart from this, no more information could be collected for PIP, because no clear ortholog could be found in *Arabidopsis*, and the rice orthologous protein, Os03t0182400-01, is currently uncharacterized. The predicted subcellular localization patterns of PLC and PIP could be partially confirmed. Initially, it was attempted to localize them in barley. However, these experiments were not conclusive, because fusion proteins for both PLC and PIP were not stable (see Fig. S12). Hence, their subcellular localization was investigated in *N. benthamiana*. PLC was reproducibly found at the plasma membrane, with the C-terminally mCherry-tagged PLC displaying an almost exclusive localization there (see Fig. 2.8). This fits to the bioinformatic data, because PLC contains a C-terminal C2-domain that should mediate its PM-localization (Rizo and Südhof, 1998). On the other hand, PIP was predicted to be localized to the endomembrane system or vacuole, due to its homology to plant SACs (see Fig. S9, Mao and Tan (2021)). This could not be confirmed, as PIP was mostly visible in the cytosol in *N. benthamiana* (see Fig. 2.8). However, it is possible that PIP was mislocalized because it was not expressed in its native environment in barley. The heterologous expression system in *N. benthamiana* could lack certain factors that would normally enable PIP's targeted localization in barley. One example for such a factor might be the presence of interaction partners that recruit PIP to its destination, where it exerts its putative catalytic activity. This could follow a mechanism similar to that of yeast Sac1p, which requires interaction with Vps74 for its localized activity inside the Golgi apparatus (Cai et al., 2014). Correspondingly, if *N. benthamiana* would lack the interactors that recruit PIP to the endomembrane compartment or vacuole, it would be mislocalized.

Since PLC and PIP were co-precipitated with the barley susceptibility factor RACB in the interactor screening, their role in the barley-*Bgh*-pathosystem was investigated. First, their gene expression profiles during the early stages of *Bgh*-infection were generated. Both genes were expressed in the epidermal cell layer of barley (see Fig. 2.6), which fits both to an RNAseq experiment from barley *cv.* Morex (see Fig. S10, Mascher et al. (2017); Rapazote-Flores et al. (2019)) and to the fact that PLC and PIP protein could be identified in the mass spectrometry experiment. During the first 24 h of *Bgh*-invasion, however, no change in *PLC* or *PIP* transcript levels could be observed. Nonetheless, this does not rule out the possibility that they could be involved in the barley-*Bgh*-interaction. Similar results have also been observed for

other susceptibility-inducing interaction partners of RACB (McCollum, 2021) and *RACB* itself, which undergoes only minor transcriptional changes during invasion (Schultheiss et al., 2002). Indeed, both PLC and PIP appear to work in resistance towards *Bgh*-infection, because the susceptibility of barley towards *Bgh*-penetration was strongly increased, when *PLC* and *PIP* were silenced (see Fig. 2.7). In wildtype plants, resistance against powdery mildew infection could depend on the putative catalytic activities of PLC and PIP. The enzymatic activity of both proteins could lead to changes in the phospholipid composition inside a plant cell, which could act as a cue for resistance signaling. While unknown for PIP-like proteins, this has been indicated for members of the PLC-family (Abd-El-Haliem et al., 2016). Hydrolysis of PI(4,5)P_2 via PLC would generate the second messengers InsP_3 and DAG (Gerth et al., 2016), of which the latter has been shown to be indirectly involved in mediating plant defense responses. After production, DAG for instance is phosphorylated by diacylglycerol kinases (DGKs) to become PA, another second messenger that engages in highly branched signaling processes (Pokotylo et al., 2018). In biotic stress scenarios, PA was shown to recruit interaction partners that mediate ROS burst, MAPK-activation and other defense-related processes (Anthony et al., 2004; Rentel et al., 2004; Testerink et al., 2004). Correspondingly, the catalytic activity of barley PLC or PIP could be needed for defense against powdery mildew attack. When *PLC* or *PIP* are silenced, production of the second messenger molecules would be attenuated, leading to insufficient resistance-signaling and hence increased *Bgh*-penetration.

Their function in resistance also puts PLC and PIP into an interesting position, since canonical RACB-interactors are usually associated with susceptibility. The putative scaffolding proteins RIC157, RIC171 and RIPb preferentially bind to activated RACB-CA and increase susceptibility towards *Bgh*-infection when overexpressed (Schultheiss et al., 2008; McCollum et al., 2020; Engelhardt et al., 2021). Conversely, RACB-interacting proteins that work in resistance were instead found to antagonize RACB's signaling processes. MAGAP1 for instance is suggested to inhibit RACB-signaling through its GTPase-activating function and promotes resistance by focusing the microtubule cytoskeleton towards fungal attack sites (Hoefle et al., 2011). Moreover, RBK1 and SKP1L are negatively regulating RACB's protein stability, which likely attenuates its signaling capacity in a cell (Reiner et al., 2015). Concerning PLC and PIP, this could suggest that they either influence RACB's signaling activity directly, or they could oppose RACB-associated signaling processes indirectly through their own predicted catalytic activities. Currently, the latter seems more likely, because although they were initially identified as candidate interaction partners for RACB, a direct protein-protein interaction could not be fully confirmed yet. While C-terminally mCherry-tagged PLC showed some interaction with RACB-CA in a FRET-FLIM

assay in *N. benthamiana* (see Fig. 2.10), CoIP experiments in the same system could not corroborate this (see Fig. 2.9). As for PIP, interaction studies with RACB were difficult, because of PIP's low expression levels. No PIP protein could be detected in CoIP assays and FRET-FLIM only showed a minimal, but statistically significant interaction with RACB-CA (see Figs. 2.9, 2.10). However, it is possible that PLC and PIP converge with RACB-mediated signaling processes at anionic phospholipids *in planta*, because the three proteins share the ability to bind PI3P, PI4P and PI5P *in vitro* (see Fig. 2.11). PIP and RACB could further meet at PS, since they both bind this lipid *in vitro*. When binding the same anionic phospholipids *in planta*, RACB, PLC and PIP could enact opposing signaling processes. For instance, RACB could be recruited by particular phospholipid species which are associated with susceptibility, whereas PLC and PIP aim to degrade the same lipids to enforce resistance (please see Section 3.5 for an elaboration of this hypothesis).
In summary, this would be the first evidence of PLCs and SACs working in concert with ROPs. In animals, an interaction between Rho-like proteins and PLCs has already been shown. It was demonstrated that Rac1 directly interacts with the phospholipases PLC-β2 and PLC-γ1, and this interaction leads to activation of their signaling processes (Jezyk et al., 2006; Rao et al., 2008; Li et al., 2009). In plants however, no such data is available yet. So far, plant PLC enzymes were demonstrated to be involved in a variety of signaling processes. In abiotic stress scenarios, the overexpression of PLC proteins increased tolerance towards drought and salt stress in tobacco, maize and rape seed (Wang et al., 2008; Georges et al., 2009; Tripathy et al., 2012). Additionally, expression of PLC proteins in pea plants was upregulated during heat stress and PLC activity was increased during heat treatment (Liu et al., 2006). In biotic stress, silencing of tomato PLC6 led to increased colonization of tomato plants by the fungi *Cladosporium fulvum* and *Verticillium dahliae*, but also by the bacterium *Pseudomonas syringae* (Vossen et al., 2010). Furthermore, the gene expression of *OsPLC1* was enhanced in presence of SAR-stimulating chemical and biological signals, and it was therefore suggested that *Os*PLC1 could play a role in disease resistance (Song and Goodman, 2002). In conclusion, these studies suggest that a function of barley PLC in resistance towards powdery mildew infection appears plausible. Regarding SACs, clade I members of this family, to which also barley PIP belongs to, were so far only shown to be involved in maintaining vacuolar morphology (Novakova et al., 2014). Indeed, all characterized SACs to date were exclusively studied with regard to endomembrane trafficking and organelle morphology (Mao and Tan, 2021). Thus, PIP's function in resistance towards powdery mildew infection could contribute novel insights into the involvement of SACs in biotic stress responses.

3.4 The role of anionic phospholipids in ROP-signaling and the barley-*Bgh* interaction

RACB and its three novel candidate interaction partners were found to bind different anionic phospholipid species *in vitro* (see Fig. 2.11). This suggests that they could also associate *in vivo* and their signaling processes could be connected. During the preparation of this thesis, several links between the signaling processes of ROPs and anionic phospholipids were established by other groups. For instance, PI(3,5)P_2 mediates hardening of the root hair shank region in *Arabidopsis*, and this was shown to also involve activity of the type II ROP *At*ROP10 (Hirano et al., 2018). In particular, it was demonstrated that both the kinase generating PI(3,5)P_2, FORMATION OF APLOID AND BINUCLEATE CELLS 1 (FAB1), and *At*ROP10 localize to the shank region of the PM in root hairs. Their localization is co-dependent, because if one signaling process is perturbed, the other protein is mislocalized and wavy root hairs with defects in cell wall hardening are formed (Hirano et al., 2018).
PI(4,5)P_2 was shown to localize to the PM of the subapical region of *Nicotiana tabacum* (*Nt*) pollen tubes, a domain that is also inhabited by RACB-like type I ROPs (Kost et al., 1999; Fratini et al., 2021). In the subapical region, PI(4,5)P_2 displays two distinct localization patterns: diffusely distributed or packed into nanodomains, which are generated by the PI(4,5)P_2-producing kinase *A. thaliana* phosphoinositide-4-phosphate 5-kinase 2 (*At*PIP5K2) (Fratini et al., 2021). The ROP *Nt*RAC5 is also found in these nanodomains, where it organizes the actin cytoskeleton (Kost et al., 1999; Fratini et al., 2021). Mechanistically, it was suggested that PI(4,5)P_2 itself could act as a displacement factor for ROP GDIs, because of the following reasons: ROPs organize pollen tube growth via regulation of the actin cytoskeleton (Kost et al., 1999; Fratini et al., 2021). Disturbing ROP signaling causes two phenotypes: over-activation results in depolarized growth (observed as tip-swelling or "ballooning"), which can be seen after overexpression of activated ROPs (Kost et al., 1999; Fratini et al., 2021). Inhibition instead causes stunted growth, for instance through introduction of signaling-incapable DN-ROPs or inhibitors of ROP-activation, such as GDIs (Kost et al., 1999; Klahre et al., 2006). Since overproduction of PI(4,5)P_2 through overexpression of *At*PIP5K2 was shown to mimic the depolarized growth phenotype and the actin cytoskeleton was stabilized in a ROP-like manner, it was assumed that PI(4,5)P_2 leads to activation of endogenous ROP-signaling, for example through alleviating inhibition by GDIs (Ischebeck et al., 2011; Fratini et al., 2021). This hypothesis was tested in a titration experiment, in which increasing concentrations of *Nt*RhoGDI2 were shown to gradually rescue the tip-swelling phenotype back to wildtype-like conditions (Ischebeck et al., 2011; Fratini et al., 2021). Although tested indirectly, it is thus currently assumed that PI(4,5)P_2 can act as a GDI displacement factor *in planta* (Fratini et al., 2021).

ROPs further mediate root hair formation and outgrowth in a PI(4,5)P_2-dependent manner (Jones et al., 2002; Kusano et al., 2008; Stanislas et al., 2015). In *Arabidopsis* root hairs, PI(4,5)P_2 was localized to the apical region, which also contains *At*ROP2 (Jones et al., 2002; Hirano et al., 2018). During the early stages of root hair outgrowth, *At*ROP2 and *At*ROP6 are indirectly recruited to the root hair initiation site by the PI(4,5)P_2-producing kinase *At*PIP5K3 and other proteins (Stanislas et al., 2015). Loss of *pip5k3* causes shorter root hairs, similar to activity-mutants of *At*ROP2, which display depolarized tip-growth or stunting phenotypes in a comparable fashion to what is observed in pollen tubes (Jones et al., 2002; Kusano et al., 2008).
Lastly, PS was found to be essential for ROP-signaling during root gravitropism (Platre et al., 2019). Upon auxin perception, *At*ROP6 usually shifts its localization at the PM from a uniform distribution into PS-containing nanodomains, in which it becomes immobilized and signaling-active (Platre et al., 2019). In absence of PS, these nanoclusters are not formed and the plant displays no gravitropic response even after auxin-stimulus (Platre et al., 2019). This is also the case when PS is present, but *At*ROP6 cannot associate with it due to a mutated polybasic region (PBR), which highlights that the interaction of ROPs with anionic phospholipids is crucial for their signaling processes (Platre et al., 2019).
In addition to ROPs themselves, some of their regulating proteins were also shown to bind phospholipids. The polybasic region of ARMADILLO REPEAT ONLY (ARO) proteins in *Arabidopsis* mediates their phospholipid-binding and targets AROs to the plasma membrane (Kulich et al., 2020). The PBR was further demonstrated to be essential in preventing an ectopic spread of *At*ROP2-signaling in root hair growth. This is likely achieved by targeting AROs to the subapical region of growing root hairs, where they facilitate the interaction between ROPs and RENGAPs (Kulich et al., 2020).
Strikingly, an involvement of anionic phospholipids in several plant-pathogen interactions has also been shown. During the infection of *Arabidopsis thaliana* with the hemi-biotrophic fungus *Colletotrichum higginsianum* (*Ch*), an enrichment of PI(4,5)P_2 at the biotrophic extra-invasive hyphal membrane (EIHM) was observed (Shimada et al., 2019). Interestingly, the PI(4,5)P_2-producing enzyme *At*PIP5K3 was also localized to the EIHM and classified as a susceptibility factor, because its overexpression resulted in an increased invasion rate of *Ch* (Shimada et al., 2019).
When the oomycete *Hyaloperonospora arabidopsidis* (*Hpa*) colonized *Arabidopsis*, signals for PI4P could be observed at the haustorial neck region, but were excluded from the EHM (Shimada et al., 2019). In turn, PI(4,5)P_2 was again visible inside the EHM (Shimada et al., 2019).
During infection of *Arabidopsis* with the powdery mildew fungus *Golovinomyces orontii* (*Go*), PI(4,5)P_2 became localized to the EHM, but was not enriched in

abundance (Shimada et al., 2019). This is slightly different compared to when another powdery mildew fungus, *Erysiphe cichoracearum* (*Ec*), infects *Arabidopsis*. There, PI(4,5)P_2 was not only recruited to the EHM, but also increased in abundance (Qin et al., 2020). Additionally, two PI(4,5)P_2-producing enzymes, *At*PIP5K1 and *At*PIP5K2, were again demonstrated to be susceptibility factors, since their knock-out made *Arabidopsis* drastically more resistant towards powdery mildew infection (Qin et al., 2020). In this pathosystem, PI4P could also be found at the haustorial neck region, but was again excluded from the EHM (Qin et al., 2020).
Due to the overlapping signaling pathways of ROPs and anionic phospholipids and the involvement of the latter in various plant-pathogen interactions, I attempted to localize several anionic phospholipid species in the barley-*Bgh* pathosystem. In uninfected conditions, the subcellular localization patterns of the markers for PI4P, PI(3,5)P_2, PI(4,5)P_2 and PS matched the previously published data, even though their biosensors were mostly characterized in *Arabidopsis* roots (Simon et al., 2014; Hirano et al., 2018; Platre et al., 2018). PI4P, PI(4,5)P_2 and PS were all found at the plasma membrane, which is in agreement with published results (see Figs. 2.12, 2.14, 2.16; Simon et al. (2014); Platre et al. (2018)). Only the marker for PI(3,5)P_2 displayed a strong cytoplasmic and nuclear background next to its localization at the plasma membrane and endosome-like structures (see Fig. 2.13), but whether this is something unusual cannot be said, as mCitrine-2xML1N has not been investigated in leaf tissue so far (Hirano et al., 2017, 2018).
During the early stages of *Bgh* infection at 16 hpi, all four anionic phospholipid species displayed an altered behaviour. PI4P could be observed at the haustorial neck region, but was excluded from the EHM (see Fig. 2.12). This could be a general pattern, because a similar localization was observed in the interaction of *Arabidopsis* with *Hpa* or *Ec* (Shimada et al., 2019; Qin et al., 2020). PI(4,5)P_2 shifted from its localization at the plasma membrane to a more cytosolic and nuclear presence, but in penetrated cells the overall signal of 2xPH^{PLC} became stronger (see Figs. 2.14, 2.15). This marks PI(4,5)P_2 as a highly pathogen-responsive lipid, considering that it was also strongly enriched at the haustorial interfaces of *Ec* and *Ch* in *Arabidopsis* (Shimada et al., 2019; Qin et al., 2020). This could also reflect on the need of several pathogens for a presence of PI(4,5)P_2, since the producing enzymes were classified as susceptibility factors (Shimada et al., 2019; Qin et al., 2020). Thus, several pathogens could stimulate the production of PI(4,5)P_2 to facilitate infection. The other two anionic phospholipids have not yet been characterized in plants with regard to pathogen infection. In the barley *Bgh*-pathosystem, PI(3,5)P_2 was found to be seemingly enriched at the papilla of non-penetrated cells, but this could not be seen in cells harboring a haustorium (see Fig. 2.13). In turn, PS displayed a clear localization at the haustorial neck region in penetrated cells, while also showing a more prominent

cytoplasmic background (see Fig. 2.16). The fact that all four anionic phospholipids displayed distinct subcellular localization patterns during *Bgh*-infection suggests that they could be involved in the barley-powdery mildew pathosystem. In analogy to their roles in pollen tube and root hair development (Stanislas et al., 2015; Hirano et al., 2018; Fratini et al., 2021), they could act as signaling molecules and recruiters for proteins, which mediate susceptibility- or resistance-associated signaling processes. When strictly separating the different species, PI(4,5)P_2 could be a prime susceptibility factor, due to its pathogen-dependent increase in abundance and enrichment at fungal feeding structures in other plants than barley (Shimada et al., 2019; Qin et al., 2020). It is also highly likely that PI(4,5)P_2-mediated susceptibility involves ROP-signaling, since a very strong relationship between ROPs and this lipid have already been established (Kost et al., 1999; Stanislas et al., 2015; Fratini et al., 2021). In particular, *At*PIP5K3, which produces PI(4,5)P_2 in the root hair initiation site and indirectly recruits *At*ROP2, is a susceptibility factor in the *Arabidopsis-Ch* interaction (Stanislas et al., 2015; Shimada et al., 2019). Correspondingly, in the barley-*Bgh* pathosystem an *At*PIP5K3-homolog could produce PI(4,5)P_2, which recruits ROPs such as the susceptibility factor RACB, and the signaling processes of the latter could then enable fungal infection. In contrast, PI(3,5)P_2 could be involved in the plant's resistance, since it is only recruited to papillae in cells that successfully defended an attack. When the fungus penetrates, it could potentially disperse PI(3,5)P_2 and its signaling processes, which subdues the host cell and facilitates infection. In turn, PI4P and PS could again be involved in susceptibility, since their shared localization at the haustorial neck region strongly resembles that of the susceptibility factor RACB and its canonical interactors RIC157, RIC171 and RIPb during *Bgh*-invasion (Schultheiss et al., 2008; McCollum et al., 2020; Engelhardt et al., 2021). Hence, PI4P and PS could recruit RACB and its interactors to the fungal attack site, which establishes the link to barley susceptibility (please see Section 3.5 for a deeper explanation of the potential interplay between ROPs and anionic phospholipids in the barley-*Bgh* pathosystem).

The next step would be to test the importance of the different anionic phospholipids species for the susceptiblity of barley towards *Bgh*-infection. Unfortunately, a knockout of one or several synthesis enzymes is harder to do in barley than it is in for example *Arabidopsis*, because the generation of transgenic barley lines is a long and complex process (Hensel et al., 2009). To address this issue, I investigated the possibility to deplete particular phospholipid species via specific enzymes in a transient assay. Since the presence of PI(4,5)P_2 was shown to be a susceptibility factor in plant-powdery mildew interaction (Qin et al., 2020), I focused on the PI(4,5)P_2-depleting enzyme dOCRL in pilot experiments (Doumane et al., 2021). Transient overexpression of dOCRL in barley epidermal cells completely abolished

the plasma membrane localization of PI(4,5)P_2 (see Fig. 2.17), which indicates an efficient depletion of this lipid and therefore proper function of dOCRL in barley (Doumane et al., 2021). Conclusively, a susceptibility assay in which dOCRL is expressed before *Bgh*-infection could shed light on the importance of this phosphoinositide for the barley-*Bgh*-pathosystem, similar to what has been obtained for the PI(4,5)P_2-synthesis knock-out plants in *Arabidopsis* (Shimada et al., 2019; Qin et al., 2020).
Apart from dOCRL, however, only one other *in planta* phosphoinositide-degrading enzyme exists to date (Simon et al., 2016). If more enzymes with unique abilities against every phospholipid-species are discovered or created in the future, this would open up the possibility to perform comprehensive studies about the importance of anionic phospholipids in different plant-pathosystem that are not as easily genetically tractable as model plants.

3.5 Concluding remarks: *Bgh* benefits from the plant's anionic phospholipid-signaling pathway and RACB to enter the host

Taken together, the data presented in this work suggest a likely involvement of anionic phospholipid-signaling in the barley-*Bgh* interaction. The four tested species all reacted in polarized manner during *Bgh*-attack. In other scenarios, such as pollen tube or root hair growth, their polarization was found to be a cue for the recruitment of proteins that mediate these processes (Kost et al., 1999; Hirano et al., 2018; Fratini et al., 2021). This could also be the case in the barley-*Bgh*-pathosystem. While PI(3,5)P_2 could act in resistance signaling, PI4P, PI(4,5)P_2 and PS could be involved in susceptibility (see Section 3.4). Particularly PI4P and PS could recruit known susceptibility factors, such as RACB and its scaffolding proteins RIC157, RIC171 and RIPb, because they all display the same localization at the haustorial neck region in infected cells (Schultheiss et al., 2008; McCollum et al., 2020; Engelhardt et al., 2021). This interaction between anionic phospholipids and proteins from the RACB-signaling pathway is likely facilitated through sequence motifs containing several positively charged amino acids. For instance, RACB was found to require its polybasic region for phospholipid-interaction *in vitro* (see Fig. 2.11). While lipid-binding was not shown yet experimentally for the RICs and RIPb, these proteins also contain polybasic stretches and they are also membrane-targeted by themselves or in presence of activated RACB (Schultheiss et al., 2008; McCollum et al., 2020; Engelhardt et al., 2021). Conclusively, polarization of PI4P or PS could provide the signal for RACB, RIC157, RIC171 and RIPb to localize towards the fungal attack site. There, signaling processes from the RACB-pathway could enable fungal

invasion. *Bgh* might also enforce this by using two effector proteins that target RACB directly. While ROPIP1 could cripple the plant's defenses by destabilizing the host microtubule cytoskeleton via RACB (Nottensteiner et al., 2018), 9o9 likely targets the plant anionic phospholipid pathway. Although 9o9's virulence mechanism is not known yet, its clear association with the same phospholipid species as ROPs and its ability to bind only activated RACB indicate its involvement in both processes. For example, 9o9 could either modify the plant's phospholipid-pathway to match the needs of *Bgh* or, alternatively, the polarized anionic phospholipids could provide a platform for 9o9 to find active RACB-signaling hubs (see Section 3.2).
In contrast, a higher resistance against *Bgh*-invasion comes from either shutting down RACB-signaling or by potentially depleting susceptibility-associated phospholipids. The former is facilitated through MAGAP1, which likely deactivates RACB through its GAP function, or RBK1 and SKP1L, which are involved in the proteasomal degradation of RACB (Hoefle et al., 2011; Huesmann et al., 2012; Reiner et al., 2015). The latter could be achieved via the enzymatic activities of PLC and PIP, since *Bgh* could invade barley more frequently when they were silenced. Although their substrate specificities are not known yet, both PLC and PIP could degrade the plant phospholipids that benefit *Bgh*-invasion, which would result in a higher resistance against infection. A likely target would be PI4P, due to its speculated function in susceptibility and association with the RACB-pathway. Although PLC and PIP are predicted to hydrolyze either $PI(4,5)P_2$ and $PI(3,5)P_2$, the possibility that they degrade PI4P exists, since both proteins were found to bind this lipid *in vitro*. During *Bgh*-infection, a depletion of PI4P could lead to either insufficient targeting of the RACB-pathway towards fungal entry sites or attenuated association of 9o9 with activated RACB. An interference of PLC and PIP in both processes could thus decrease fungal penetration success. Even though I also speculated that PS potentially has similar functions as PI4P in susceptibility, it is not a suitable substrate for PLC and PIP, since degradation of PS involves decarboxylases and deacylases, instead of phospholipases and phosphatases (Lenoir et al., 2021).
The link between RACB-signaling and anionic phospholipids also extends the inverted-tip growth hypothesis from Schultheiss et al. (2003). Initially, it was suggested that invagination of the host plasma membrane by *Bgh* and inward growth of the haustorium resemble an inverted form of pollen tube or root hair outgrowth (Schultheiss et al., 2003). Since at that time ROPs were discussed to be the main regulators of these polar growth processes (Kost et al., 1999; Jones et al., 2002), it was speculated that the inverted-tip growth is also mostly orchestrated by ROPs such as RACB (Schultheiss et al., 2003). However, I assume that not only ROP-signaling mediates the inverted tip-growth of *Bgh*. Data from recent studies and this work also suggest a heavy involvement of plant anionic phospholipids, which were

shown to govern both powdery mildew susceptibility and polarized ROP-signaling (Qin et al., 2020; Fratini et al., 2021). Apart from PI4P and PS, I suspect that particularly PI(4,5)P_2 could be involved in the colonization of barley by *Bgh*, for the following reasons: i) several kinases that produce PI(4,5)P_2 are susceptibility factors in biotic interactions (Shimada et al., 2019; Qin et al., 2020); ii) PI(4,5)P_2 is present at plant-fungal interfaces and enriched in colonized cells (see Fig. 2.15; Shimada et al. (2019); Qin et al. (2020)); iii) in both pollen tube and root hair growth, PI(4,5)P_2 is considered to be a main recruiter and activator of ROPs inside the growing tip (Kost et al., 1999; Stanislas et al., 2015; Hirano et al., 2018; Fratini et al., 2021); iv) overproduction of PI(4,5)P_2 by *At*PIP5K6 causes pollen tube branching, a process resulting from excessive plasma membrane invaginations (Zhao et al., 2010). Conclusively, an increased presence of PI(4,5)P_2 at the plant-fungal interface could lead to plasma membrane invaginations and recruitment/activation of ROPs, which then stimulate polar growth processes that facilitate inward growth of the haustorium.

Finally, I'd like to point out that, to my knowledge, my thesis shows for the first time a connection between ROP-signaling and anionic phospholipids in plants interacting with filamentous microbes. Furthermore, it proposes a potential mechanism by which a haustorium-shaping organism could exploit host anionic phospholipids for colonization. Therefore, this thesis represents a basic concept for future studies, which could aim to further unravel the involvement of anionic phospholipid rearrangements in plant susceptibility.

4 Experimental Procedures

4.1 Plant and fungal growth conditions

Wildtype barley (*Hordeum vulgare* L. subspecies *vulgare*) plants cultivar Golden Promise or stable transgenic barley lines were sown on soil (CL-ED73, Einheitserdewerke Werkverband e.V., Sinntal-Altengronau, Germany) and grown in a climate chamber (Conviron, Winnipeg, Canada) providing the following conditions: a 16 h light/ 8 h dark cycle, a photon flux of 150 µM s^{-1} m^{-2}, a temperature of 18 °C and a relative humidity of 65 %.
The barley powdery mildew fungus *Blumeria graminis* f.sp. *hordei* race A6 (*Bgh*) was propagated on wildtype barley plants growing under the same conditions. *Bgh*-infected barley leaves at roughly 7 dpi served as inoculum for infection experiments.
Wildtype *Nicotiana benthamiana* plants were sown on a mix of 5 parts soil and 1 part vermiculite (1/3 mm, Raiffeisen Gartenbau, Köln, Germany), stratified for more than 2 d at 4 °C and grown under long day conditions (16 h light at 23 °C, 8 h dark at 21 °C, a photon flux of 150 µM s^{-1} m^{-2} and 55 % relative humidity).

4.2 Generation of transgenic barley lines

The plasmids for the generation of the transgenic barley lines used in this dissertation were created by Dr. Tina Reiner (TUM, see Table S3). The transgenic plant lines were generated by the labs of Dr. Jochen Kumlehn and Dr. Götz Hensel (both IPK Gatersleben). Both methods were described in Weiß et al. (2022) for the HA-tagged lines. The GFP-tagged lines were created with the same methods.
I received seeds of generation T_1, which were still segregating. Hence, all plants had to be selected for transgene presence before use. Only Hygromycin B-resistant plants (see Weiß et al. (2022)) or plants showing GFP-fluorescence were considered for experiments. I also propagated two lines per construct in the greenhouse. For each of the following lines, ten transgenic T_1 plants and one azygous plant were chosen for propagation:

Table 4.1: Propagated transgenic barley lines.

Construct	Lines
eGFP-RACB-CA	BG654 E02 & E12
eGFP-RACB-CA-ΔCSIL	BG655 E01 & E10
eGFP	BG656 E01 & E06
3xHA-RACB-CA	BG657 E03 & E04
3xHA-RACB-CA-ΔCSIL	BG658 E04 & E09
3xHA	BG659 E02 & E03

All lines could be successfully propagated, but no homozygous lines could be obtained and the offspring remained segregating in generation T_2. Therefore, the descendants had to be screened for transgene presence as described above or in Weiß et al. (2022) before they were used in experiments.

4.3 RNA extraction

Routine RNA extraction was performed by collecting four primary leaves of wildtype barley plants, freezing them in liquid N_2 and homogenizing them with a mortar and pestle. 1 g of ground plant material was transferred into a 2 mL tube and 1 mL TRIzol (Thermo Fisher Scientific, Waltham USA) was added. Following thorough vortexing, cell debris was pelleted via centrifugation at 12000 g for 10 min at 4 °C, after which the supernatant was transferred into a new tube. 200 µL of chloroform were added and the tube was inverted for 15 s before the sample was incubated at room temperature for 10 min. Subsequently, the sample was centrifuged at 12000 g for 15 min at 4 °C, after which the supernatant was again transferred into a new tube. 500 µL of 2-propanol were added, followed by another 10 min incubation step at room temperature. Afterwards, the sample was centrifuged at 12000 g for 10 min at 4 °C and the supernatant was removed. The pellet was washed once with 1 mL of 70 % ethanol and spun down again at 7500 g for 5 min at 4 °C, before it was left to dry. Finally, 30 µL of di-ethyl dicarbonate (DEPC)-treated ddH_2O were added to solubilize the RNA in the pellet. This solution was incubated at 60 °C for 10 min in order to increase reconstitution efficiency. RNA quality was checked using a spectrophotometer (Nanodrop ND-1000, PEQLAB Biotechnologie, Erlangen, Germany) and 2 % agarose gelelectrophoresis with 0.5 µg/mL ethidium bromide (Roth, Karlsruhe, Germany).
For the initial cloning of *Bgh9o9*, *Bgh*-infected primary barley leaves (48 hpi) were used as source material for RNA extraction.
RNA extraction for gene expression analysis via qRT-PCR followed a different protocol (see Section 4.9).

4.4 cDNA synthesis

To obtain cDNA for molecular cloning purposes, the QuantiTect Reverse Transcription Kit (QIAGEN, Hilden, Germany) was used. First strand cDNA was synthesized from 2 µg of RNA according to the manufacturer's instructions.
cDNA synthesis for gene expression analysis via qRT-PCR utilized a different kit (see Section 4.9).

4.5 Polymerase chain reaction

To amplify genes and plasmids for molecular cloning procedures, polymerase chain reactions (PCRs) were carried out. All PCRs used the Phusion High-Fidelity polymerase (Thermo Fisher Scientific, Waltham, USA) running a Touchdown-protocol (see Tables 4.2 and 4.3). The duration of the amplification step was adjusted individually for each gene. Plasmids or cDNA were used as PCR templates. PCR amplicons were analysed via gel electrophoresis on 0.8 % agarose gels containing 0.5 µg/mL ethidium bromide (Roth, Karlsruhe, Germany). Expected products were extracted with the NucleoSpin Gel and PCR Clean-up kit (Macherey Nagel, Düren, Germany) following the manufacturer's instructions.

Table 4.2: PCR mix for 1 reaction.

Volume	Component
32.5 µL	ddH_2O
10 µL	5x Phusion buffer HF/GC
2.5 µL	Primer forward (10 pmol/µL)
2.5 µL	Primer reverse (10 pmol/µL)
1 µL	dNTPs (10 mM)
1 µL	DNA template (5 ng/µL)
0.5 µL	Phusion HF polymerase (2 U/µL)

Table 4.3: Touchdown PCR program.

Cycles	Time	Temperature
1x	1 min	98 °C
	10 s	98 °C
	10 s	70 °C (-0.5 °C/cycle)
40x	30 s/kb	72 °C
	10 s	98°C
	10 s	50 °C
5x	30 s/kb	72 °C
1x	10 min	72 °C

4.6 Transformation of *Escherichia coli*

For the propagation of plasmids, *Escherichia coli* (*E. coli*) strain DH5α (genotype F^-φ80*lac*ZΔM15 Δ(*lac*ZYA-*arg*F)U169 *rec*A1 *end*A1 *hsd*R17(r_K^-, m_K^+) *pho*A *sup*E44 λ^- *thi*-1 *gyr*A96 *rel*A1; Thermo Fisher Scientific, Waltham, USA) was used. 50 µL of chemically competent DH5α cells were thawed on ice and combined with 5 µL insert-plasmid ligation reactions (see Section 4.8). After incubation on ice for

30 min, cells were heat-shocked at 42 °C for 1 min, followed by a 1 min regeneration on ice. 1 mL of liquid LB-medium was added to the cells and the solution was incubated for 1 h at 37 °C with constant shaking. Afterwards, the cells were pelleted in a centrifuge running at 11000 g for 1 min. Most of the supernatant (around 950 µL) was removed and the cells were resuspended in the remaining medium. Cells were plated on LB-agar plates supplied with selective antibiotics and incubated overnight at 37 °C. For the selection of pGY1-, pIPKTA30N-, pGEX-6P-1-, pMAL-c5X- and pSmash-plasmids 100 mg/mL Ampicillin was used, whereas pIPKTA38- and pGWB-plasmids were selected on 50 mg/mL Kanamycin and pDONR223-plasmids were selected on 50 mg/mL Streptomycin or Spectinomycin.

Table 4.4: LB-medium.
Antibiotics were added post-sterilization; *: only included in solid media.

Amount	Component
1 % (w/v)	Peptone
1 % (w/v)	NaCl
0.5 % (w/v)	Yeast extract
2 % (w/v)	Agar*

4.7 Plasmid extraction and purification

Following selection on LB-agar plates containing antibiotics, several growing *E. coli* clones were singled-out and used for the inoculation of 2 mL liquid LB-medium supplied with the respective antibiotics. After incubation at 37 °C overnight in a shaker, plasmids were extracted with the NucleoSpin Plasmid Kit (Macherey-Nagel, Düren, Germany) according to the manufacturer's instructions. To check for the correct insertion of genes-of-interest into plasmids of choice, plasmids were first analysed with a diagnostic digest (see Table 4.5) followed by 0.8 % agarose gel electrophoresis with 0.5 µg/mL ethidium bromide (Roth, Karlsruhe, Germany). Restriction enzymes were chosen, which enabled the detection of plasmids with correctly inserted genes-of-interest. Plasmids displaying correct digestion-patterns were further subjected to Sanger sequencing (Eurofins Genomics, Ebersberg, Germany) to verify their sequence integrity.

Table 4.5: Diagnostic digest.
Reactions were incubated for at least 1 h before gel electrophoresis. For each restriction enzyme, incubation temperatures were set as specified by the manufacturer (Thermo Fisher Scientific, Waltham, USA).

Volume	Component
3 µL	Plasmid DNA
1 µL	10x Restriction enzyme buffer
1 U	Restriction enzyme
add up to 10 µL	ddH_20

For the large-scale preparation of already verified plasmids (i.e. for biolistic transformation of barley), 100 mL LB overnight cultures were used for plasmid extraction with the NucleoBond Xtra Midi/Maxi Kit (Macherey-Nagel, Düren, Germany).

4.8 Molecular cloning

To enable protein expression in different organisms, all genes had to be inserted into fitting expression vectors containing organism-specific expression cassettes and tags. To achieve this, three common cloning techniques were used in this dissertation: classical restriction enzyme-mediated cloning, the Gateway^{TM}-system (Invitrogen, Waltham, USA) and GoldenGate-based techniques (Engler et al., 2008).
In classical cloning, a gene-of-interest was amplified via PCR using gene-specific primers carrying overhangs for restriction enzyme sites. Following PCR product purification, the gene-of-interest and destination plasmid were first digested with the respective restriction enzymes (see Table 4.6; all enzymes were from Thermo Fisher Scientific, Waltham, USA) and then fused with a T4 DNA Ligase (Thermo Fischer Scientific, Waltham, USA) in a subsequent ligation reaction (see Table 4.7).

Table 4.6: Preparative digest.
Reactions were incubated for 4 h. Incubation temperatures were set according to the manufacturer's instructions for each enzyme (Thermo Fisher Scientific, Waltham, USA).

Amount	Component
2 µg / 1 µg	Vector / Insert
5 µL	10x Restriction enzyme buffer
10 U	Restriction enzyme
add up to 50 µL	ddH_2O

Table 4.7: Regular T4 DNA ligation.
Reactions were incubated for 1 h at room temperature. Molar ratio refers to the concentration of insert to vector; in this case, 3x the concentration of insert compared to vector was used.

Amount	Component
50 ng	Pre-digested vector
3:1 molar ratio	Pre-digested insert
2 µL	10x T4 DNA ligase buffer
1 µL	T4 DNA Ligase (5 U/µL)
add up to 20 µL	ddH_2O

In the Gateway^{TM}-system, genes were first amplified via PCR using gene-specific primers with attB-attachment-site overhangs. Followingly, the PCR products were ligated into the entry vector pDONR223 via Gateway^{TM} BP Clonase^{TM} II reactions (see Table 4.8; Invitrogen, Waltham, USA). Verified pDONR223-entry clones were shuffled into different destination vectors via Gateway^{TM} LR Clonase^{TM} II reactions (see Table 4.9; Invitrogen, Waltham, USA).

Table 4.8: BP reaction.
Reactions were incubated for at least 1 h at 25 °C.

Amount	Component
50 fmol	Entry vector pDONR223
150 fmol	Insert with attB-sites
add up to 5 µL	TE buffer pH 8
+2 µL	BP Clonase^{TM} II Mix

Table 4.9: LR reaction.
Reactions were incubated for at least 1 h at 25 °C.

Amount	Component
50 ng	Destination vector
50 ng	Entry vector with insert of choice
add up to 5 µL	TE buffer pH 8
+2 µL	LR Clonase^{TM} II Mix

For GoldenGate-based cloning, genes-of-interest were amplified via PCR using gene-specific primers with Esp3I-overhangs carrying variable restriction sites. This was necessary, as restriction sites were chosen individually to enable directional cloning. Inserts and destination plasmids were included in a one step restriction-ligation reaction which combined everything according to the chosen restriction sites (see

Tables 4.10 and 4.11, Engler et al. (2008)).

Table 4.10: Restriction-Ligation reaction.
All enzymes were from Thermo Fisher Scientific, Waltham, USA.

Amount	Component
50 ng	Per insert / vector
5 µL	10x Tango buffer
5 µL	10 mM DTT
5 µL	10 mM ATP
1 µL	Esp3I (10 U/µL)
0.5 µL	T4 DNA ligase (5 U/µL)
add up to 50 µL	ddH_2O

Table 4.11: Restriction-Ligation cycling.

Cycles	Time	Temperature
	5 min	37 °C
50x	2 min	16 °C
1x	60 min	16 °C
1x	20 min	80 °C

Coding sequences of *9o9* and *PIP* were amplified from cDNA from *Bgh*-infected and non-infected barley leaves, respectively. Full-length *PLC* could not be cloned from cDNA; its coding sequence was instead synthesized with a *Zea mays* codon-optimized nucleotide sequence and attB1 and attB2 Gateway-attachment sites by Twist Bioscience (San Franscisco, USA). Hence, all constructs containing the synthesized *PLC* sequence carry the suffix: _Zm (for *Zea mays*).
Generation of the FRET-FLIM constructs from this dissertation used a combination of GoldenGate and Gateway approaches. Fluorescent proteins containing a 10x glycine-linker and genes-of-interest were first amplified separately via PCR to carry an Esp3I-restriction site at one terminus and a Gateway attB-attachment site at the other. Followingly, the fluorescent protein with the 10x glycines was linked to the gene-of-interest in a GoldenGate reaction before it was used in Gateway BP cloning. The chimera of SP^{LORE}-9o9 used in the yeast secretion assay was cloned in a similar fashion, only combining a preceding GoldenGate-ligation with subsequent classical cloning into pSmash via EcoRI and NotI.
To create proteins carrying single amino acid mutations, a site-directed mutagenesis protocol based on the QuikChange Multi Site-Directed Mutagenesis Kit (Agilent, Santa Clara, USA) was used. In this case, verified plasmids containing the to-be-mutated gene were used as templates in PCR reactions using primers with desired

nucleotide exchanges. After PCR, the parental DNA was digested by adding 1 µL of DpnI (Thermo Fisher Scientific, Waltham, USA) and incubating the mixture at 37 °C for 1 h before proceeding with transformation of *E. coli* strain DH5α.
The RACB-5Q mutant was generated by a combination of PCR and blunt-end ligation. First, the whole pGEX-RACB-WT plasmid was amplified in a PCR with primers exchanging the five lysines in RACB to five glutamines. The PCR product was analysed and prepared as described in Section 4.5. Since the amplicon was still linearized, it was first phosphorylated in a poly-nucleotide kinase (PNK) reaction with buffer A (see Table 4.12; Thermo Fisher Scientific, Waltham, USA) before a circularizing blunt-end ligation with a T4 DNA ligase (see Table 4.13; Thermo Fisher Scientific, Waltham, USA) was carried out.

Table 4.12: PNK reaction.
Reactions were incubated for 20 min at 37 °C before termination at 75 °C for 10 min.

Volume	Component
15 µL	PCR product
2 µL	10x PNK buffer A
2 µL	10 mM ATP
1 µL	PNK (10 U/µL)

Table 4.13: Blunt-end ligation.
Reactions were incubated for 4 h at 22 °C.

Volume	Component
10 µL	ddH_2O
5 µL	Phosphorylated PCR-product
2 µL	10x T4 DNA Ligation buffer
2 µL	50 % PEG4000
1 µL	T4 DNA Ligase (5 U/µL)

All PCRs were conducted as described in Section 4.5 with primers from Table S4. After each ligation reaction, *E. coli* strain DH5α were transformed with the newly ligated plasmids as detailed in Section 4.6. Verification of desired plasmids was achieved via diagnostic restriction digests and Sanger sequencing as written in Section 4.7.
Table S3 summarizes the plasmids that were generated in this dissertation and outlines by which technique they were created. If a plasmid was not created by me, I have stated the original source.

4.9 Quantitative reverse-transcription polymerase chain reaction

To measure gene expression of *9o9*, *PLC* and *PIP*, a quantitative reverse-transcription polymerase chain reaction (qRT-PCR) experiment was performed. For one biological replicate, 7 pots containing 20 seeds of wildtype barley cultivar Golden Promise were grown in a climate chamber (see Section 4.1). One week after sowing, 3 pots were infected with 100-130 spores/mm^2 of *Bgh* race A6 and placed in a different growth chamber operating under the same conditions to avoid contamination. At 6, 12, and 24 hpi, the abaxial epidermis was peeled off from all plants in one pot and collected in a 2 mL tube cooled in liquid N_2. Each tube contained 2 glass beads of 4 mm diameter for subsequent sample homogenization. Uninfected plants were collected in the same manner at the respective timepoints and served as non-infected controls. One hour before the infection timecourse experiment was started, epidermal peels from the last pot were harvested to be used as a fully untreated control. Accordingly, this sample was called -1 hpi. Fungal spores were collected by placing single infected leaves from *Bgh* propagation (see Section 4.1, roughly 7 dpi) in a 15 mL tube and shaking vigorously until all spores had fallen off the leaves. This was repeated until all spores from 20 infected leaves were collected. Spores sticking to the sides of the tube were washed down using 1 mL ddH_2O supplied with 0.05 % Tween20 and gentle inversion of the tube. Afterwards, the spore solution was transferred into a 2 mL tube and briefly centrifuged for 10 s at 6000 g to remove the liquid. Then, 2 glass beads of 4 mm diameter and 100 mg glass beads of 0.1 mm diameter were added to the tube. After harvesting, all samples were frozen in liquid N_2 and stored at -80 °C until homogenization. Three biological replicates were collected in this fashion.
All samples were homogenized in a bead mill (TissueLyser II, QIAGEN, Hilden, Germany), which ran twice for 1 min at 30 Hz with a cooling step in liquid N_2 in between. Subsequently, 1 mL of TRIzol (Thermo Fisher Scientific, Waltham USA) was added and the samples were mixed by vortexing. For RNA extraction, the Direct-zol RNA Mini Prep Kit (R2052, Zymo Research Europe, Freiburg, Germany) was used and the manufacturer's instructions including the on-column DNAse treatment were followed. RNA quality was analysed via 2 % agarose gelelectrophoresis with 0.5 µg/mL ethidium bromide (Roth, Karlsruhe, Germany) and measurement with a spectrophotometer (Nanodrop ND-1000, PEQLAB Biotechnologie, Erlangen, Germany).
cDNA was synthesized with the RevertAid RT Kit (Thermo Fisher Scientific, Waltham, USA) as recommended by the manufacturer. 500 ng of RNA was used as template and the optional boiling step for GC-rich templates was performed as advised by the manual. After synthesis, cDNA was stored at -20 °C until use.
qRT-PCR was carried out in an AriaMx Real-time PCR System (Agilent, Santa

Clara, USA) using the Takyon^{TM} Low ROX SYBR 2x MasterMix dTTP Blue Kit (Kaneka Eurogentec S.A., Seraing, Belgium). For one reaction, 10 ng of cDNA and 300 nM of each forward and reverse primer were used (see Tables 4.14 and 4.15).

Table 4.14: qRT-PCR mix for 1 well.

Volume	Component
5 µL	Takyon^{TM} Low ROX SYBR 2x MasterMix dTTP Blue
3.4 µL	Nuclease-free ddH_2O
1 µL	cDNA (10 ng/µL)
0.3 µL	Forward primer (10 pmol/µL)
0.3 µL	Reverse primer (10 pmol/µL)

Table 4.15: qRT-PCR cycling.

Cycles	Time	Temperature	Description
1x	3 min	95 °C	Hot start
	5 s	95 °C	qRT-PCR cycling
	20 s	60 °C	
40x	20 s	72 °C	
	30 s	95 °C	Start of melt curve analysis
	30 s	65 °C	Ramp-up: 0.5 °C
1x	30 s	95 °C	End of melt curve analysis

For each gene, all timepoints and samples were measured in triplicate on the same plate to avoid inter-run variances. After each run, outliers were identified according to differences in melt curves or discrepancies between technical replicates and excluded from analysis. The cycle threshold (Ct) values of each valid measurement were exported as ΔRn, which included automatic software-based correction steps from the Agilent AriaMx software V1.8 (Agilent, Santa Clara, USA).
For each primer pair used in this experiment, a primer test was conducted prior to gene expression measurements. First, samples were pooled according to treatment. Either plant-only samples (lacking the spore sample) or *Bgh*-containing samples (lacking the uninfected leaves samples) were combined. These two pools were diluted from 10 ng/µL cDNA to 0.01 ng/µL cDNA in 1/10 dilution steps. All primer pairs targeting barley genes were tested on the dilution curve made from plant-only samples, while the primer pairs for *Bgh* genes were tested on the diluted *Bgh*-containing cDNA pool. The efficiency for each primer pair was calculated directly by the Agilent AriaMx V1.8 software. Since all primer pairs except the one targeting *Bghβ-Tub2* showed an efficiency deviating from 100 % amplification rate, their corrected values had to be used for gene expression analysis (see below). Gene specificity of each primer pair could be confirmed via Sanger sequencing (Genewiz Europe, Leipzig,

Germany) of PCR amplicons.
Gene expression data for *9o9*, *PLC* and *PIP* was calculated in Microsoft Excel 2016 (Microsoft, Redmond, USA) according to the $2^{-\Delta\Delta Ct}$-method from Livak and Schmittgen (2001) with experimentally-determined primer efficiencies. Graphs were created in GraphPad Prism V8.0 (GraphPad Software, San Diego, USA). Statistical analysis was performed in GraphPad Prism V8.0 (GraphPad Software, San Diego, USA) on $\log_{10}$-transformed $2^{-\Delta\Delta Ct}$-values using a multiple *t*-test with Holm-Sidak correction for multiple testing against an α of 0.05. All primers can be found in Table S4. Gene identifiers for the measured genes can be seen in Table S5. For barley, the housekeeping genes *glyceraldehyde-3-phosphate dehydrogenase* (*GAPDH*) and *ubiquitin-conjugating enzyme 2* (*UBC2*) were used, while *β-tubulin 2* (*β-TUB2*) was used for *Bgh* (Sherwood and Somerville, 1990; Rapacz et al., 2012; Schnepf et al., 2018).

4.10 Yeast secretion assay

The yeast secretion assay performed in this dissertation followed the protocol from Krijger et al. (2008) with some adaptations. Chemically competent yeast (*Saccharomyces cerevisiae*) cells of strain Y02321 (BY4741; MATa; *his3*Δ1; *leu2*Δ0; *met15*Δ0; *ura3*Δ0; YIL162w::kanMX4; obtained from EUROSCARF, Oberursel, Germany) were generated by a modified lithium acetate-based method from Gietz and Woods (2002). First, yeast was struck on YPD plates and grown for 3 d at 30 °C. Afterwards, 5 mL of liquid YPD culture were inoculated with one colony from the YPD plate and incubated overnight at 30 °C in a shaker. Next day, this overnight culture was used to inoculate 100 mL of liquid YPD, which was then grown for 5 h at 30 °C in a shaker. Followingly, the culture was split into two 50 mL tubes and centrifuged at 700 g for 5 min to remove the medium. The cell pellets were washed once with 30 mL sterile ddH_2O each and centrifuged again. 1.5 µL of sterile TELiAc-buffer (11 mM Tris-HCl pH 7.5, 1.1 mM EDTA, 110 mM lithium acetate) were added to each pellet, the cells were resuspended and the solution was transferred into two 2 mL tubes. After centrifugation for 15 s at 18000 g, the supernatants were removed, 600 µL of TELiAc-buffer were added and the cells were combined in one tube after mixing.
The now chemically competent yeast cells were immediately used for transformation. For this, at least 100 ng of pSmash plasmids carrying inserts of choice were pipetted into 1.5 mL tubes and mixed with 10 µL of boiled salmon sperm carrier DNA (Invitrogen, Carlsbad, USA) before 50 µL of chemically competent yeast cells were added. After mixing, 500 µL of sterile PEG/LiAc-buffer (40 % PEG3350, 10 mM Tris-HCl pH 7.5, 1 mM EDTA, 100 mM lithium acetate) were added to each tube and the solutions were mixed by pipetting. Following a 30 min incubation at 30 °C

with gentle shaking every 10 min, 20 µL of DMSO were added and the solutions were again mixed by pipetting. Subsequently, the samples were incubated at 42 °C for 15 min with constant shaking and then centrifuged for 15 s at 18000 g to remove the supernatants. Finally, the cells were washed once in 1 mL sterile TE-buffer (10 mM Tris-HCl pH 7.5, 1 mM EDTA) before being resuspended in 50 µL TE-buffer. All samples were plated on separate SD/-L-plates containing 2 % glucose and incubated for 3 d at 30 °C. Afterwards, 3 growing colonies per construct were taken from a plate and resuspended in 100 µL sterile ddH_2O. From this, a dilution curve with six 1/5 dilution steps (1 (undiluted), 1/5, 1/25, 1/125, 1/625 and 1/3125) was created. 7.5 µL of each dilution step were plated on both SD/-L + 2 % glucose and SD/-L + 2 % raffinose + 2 µg/mL Antimycin A (Sigma-Aldrich, St. Louis, USA) plates and incubated for at least 3 d at 30 °C until yeast growth could be observed.
All plasmids used in this experiment can be found in Table S3.

Table 4.16: YPD medium.
Adjust pH to 6.0-6.3; *: only included in solid media; all components were from Formedium (Hunstanton, UK).

Amount	Component
1 % (w/v)	Yeast extract
2 % (w/v)	Peptone
2 % (w/v)	Glucose
2 % (w/v)	Agar*

Table 4.17: SD/-L medium.
Adjust pH to 6.0-6.3; all components were from Formedium (Hunstanton, UK); sterilized sugar solutions and antibiotics were added after autoclaving.

Amount	Component
6.7 g/L	Yeast nitrogen base without amino acids
670 mg/L	Complete Supplement Mixture without leucine
2 % (w/v)	Agar

4.11 Transient transformation of barley via particle bombardment

Transient transformation of barley epidermal cells was carried out using a protocol adapted from Schweizer et al. (1999). First, plasmids coding for genes-of-interest were mixed with 11 µL of a 27.5 mg/mL spherical gold nanoparticle solution (1 µm diameter; Bio-Rad, Hercules, USA). Usually, 1 µg of each plasmid was used per reaction; only for transformation markers, such as free fluorophores or GUS+, 0.5 µg plasmid DNA per reaction were used. The resulting volume was doubled by adding

the same amount of 2.5 M $CaCl_2$, followed by an addition of 3.33 µL of a 20 mg/mL protamine solution. After an incubation at room temperature for 30 min with gentle mixing every 10 min, the gold particles were pelleted by brief centrifugation. Following two washing steps with 400 µL of 100 % ethanol, the gold particles were resuspended in 6 µL of 100 % ethanol before being used in a particle delivery system (PDS-1000/HE^{TM}, Bio-Rad, Hercules, USA). For one transformation reaction, three primary leaves of barley were first detached and placed on 0.8 % agar plates with the adaxial side facing up, before being bombarded with the prepared gold-plasmid solution at 900 psi and 26 inHg. Transformed leaves were kept in growth chambers until analysis or inoculation. For all experiments except the *Bgh*-susceptibility assay, two technical replicates were created per plasmid combination. For *Bgh*-susceptibility assays, three technical replicates were generated.

4.12 Isolation and transformation of barley protoplasts

Wildtype barley protoplasts were isolated and transformed in the same manner as described in Weiß et al. (2022) for transgenic plants. After isolation, 1 mL of wildtype protoplasts (corresponding to 1 mil. cells) were mixed with 50 µg of pGY1-plasmids coding for GFP-tagged fusion proteins of 9o9, PLC and PIP (see Table S3). One day after transformation, protoplasts were transferred into tubes and pelleted via centrifugation for 3 min at 200 g. After removal of the supernatant, protoplasts were lysed by adding 50 µL of 4x SDS-loading dye (40 % (w/v) glycerol, 200 mM Tris-HCl pH 6.8, 20 % β-Mercaptoethanol, 8 % (w/v) SDS, 0.02 % (w/v) bromphenol blue; modified after Lämmli (1970)) and boiling for 20 min at 95 °C. To evidence protein stability, crude protein extracts were subjected to routine SDS-PAGE and αGFP Western blotting (see Section 4.18). For immunoprecipitation from barley protoplasts see Section 4.17.

4.13 Transient transformation of *N. benthamiana*

Agrobacterium tumefaciens-mediated transformation of wildtype *Nicotiana benthamiana* plants was performed with a protocol adapted from Yang et al. (2000). First, *A. tumefaciens* had to be transformed with binary plasmids. With two exceptions, all binary plasmids were pGWBs (see Table S3). To start, 50 µL of chemically-competent *A. tumefaciens* cells strain GV3101 (pMP90) were thawed on ice and combined with 5 µL of plasmid DNA. This solution was incubated on ice for 30 min, shock frozen in liquid N_2 and heat-shocked at 37 °C for 5 min. After a 5 min stabilization period on ice, 1 mL liquid LB-medium (see Section 4.6) was added and the sample was incubated for 3 h at 28 °C with constant shaking. The cells were pelleted by a 1 min at 18000 g centrifugation step, 1 mL of the supernatant was removed and the cells

were resuspended in the remaining medium before being plated on LB-agar plates containing 10 µg/mL Rifampicin, 30 µg/mL Gentamicin and 50 µg/mL Kanamycin. After incubation for 3 d at 28 °C, three growing colonies per construct were picked and struck again on LB-agar plates containing antibiotics to generate more bacterial material. From these plates, bacteria were scooped up with a pipette tip and used for the inoculation of 2.5 mL induction medium (see Table 4.21), which was then incubated overnight in a 28 °C shaker. Next day, the bacteria were pelleted using a 2 min at 3000 g centrifugation step and washed two times with 1 mL infiltration medium without acetosyringone (see Table 4.22) before being taken up in 1 mL infiltration medium with acetosyringone. The amount of bacteria in these samples was determined by measuring the optical density at 600 nm (OD_{600}) with a spectrophotometer (Nanodrop ND-1000, PEQLAB Biotechnologie, Erlangen, Germany). Followingly, the bacterial density of each sample was adjusted to an OD_{600} of 0.5. For co-expression of selected plasmids, corresponding bacterial solutions were mixed in a 1:1 ratio. All mixtures were combined with bacteria harboring a plasmid coding for the viral silencing inhibitor p19 to increase protein expression in *N. benthamiana* (Voinnet et al., 2003). After a 1 h incubation at room temperature, the bacterial solutions were infiltrated into the abaxial side of fully expanded leaves of six-week old *N. benthamiana* using 1 mL syringes without needles. The infiltrated areas were marked and the plants were placed in climate chambers operating under long-day conditions (day: 16 h light, 23 °C; night: 8 h dark, 21 °C; 55 % relative humidity). At 48 h post infiltration, transformed *N. benthamiana* leaves were used for CoIPs or microscopy.

Table 4.18: AB medium.
Adjust pH to 5.5 before autoclaving.

Amount	Component
3.9 g/L	MES
10 g/L	Glucose

Table 4.19: AB salt solution.

Amount	Component
20 g/L	NH_4Cl
6 g/L	$MgSO_4^-$ * 7 H_2O
3 g/L	KCl
0.2 g/L	$CaCl_2$
50 mg/L	$FeSO_4^-$ * 7 H_2O

Table 4.20: AB buffer solution.

Amount	Component
60 g/L	K_2HPO_4
20 g/L	NaH_2PO_4

Table 4.21: Induction medium.
Prepare only on the day of use.

Amount	Component
9.4 mL	AB medium
0.5 mL	AB salt solution
0.1 mL	AB buffer
30 µg/mL	Gentamicin
50 µg/mL	Kanamycin
100 µM	Acetosyringone

Table 4.22: Infiltration medium.
*: add only when needed.

Amount	Component
1 M	$MgSO_4$
0.5 M	MES pH 5.5
150 µM	Acetosyringone*

4.14 Confocal Laser Scanning Microscopy

Subcellular localisation experiments and fluorescence intensity measurements were performed with a Leica (Wetzlar, Germany) TCS SP5 confocal laser scanning microscope mounted on a DM6000 stage. Barley was transformed using biolistic transformation (see Section 4.11) with pGY1-plasmids (listed in Table S3), while *N. benthamiana* was transformed with binary plasmids using *A. tumefaciens* according to Section 4.13. Stably transgenic barley lines were generated as described in Section 4.2. Transiently transformed barley was analysed 24 h after transformation (hat), while *N. benthamiana* was imaged 48 h post infiltration. In case of *Bgh*-inoculated barley samples, transformed barley leaves were infected with 100-130 *Bgh* spores/mm^2 at 8 hat and imaged at 16 hpi.
Transformed barley or *N. benthamiana* cells were identified before analysis. All cells were captured with a HCX PL APO lambda blue 20.0x0.7 IMM UV objective (Leica, Wetzlar, Germany). CFP was excited with a 458 nm Argon laser line and detected between 463-485 nm; GFP was excited with a 488 nm Argon laser line and detected between 500-550 nm; mCitrine was excited with a 514 nm Argon laser line and

detected between 525-550 nm; mCherry was excited with a 561 nm DPSS diode laser and detected between 570-620 nm. Depending on the strength of the fluorescence signal, PMTs or HyDs (Leica, Wetzlar, Germany) were used for detection. When more than one fluorophore was imaged simultaneously, the sequential scan mode "between lines" was used to minimize fluorescence bleed-through. All fluorophores were scanned with a line average of 3. All images were captured as Z-stacks of single XY-optical sections with the Z-step size of each experiment indicated in figure legends. For fluorescence level measurements, the Z-stack step size was allowed to vary between cells in order to always capture each cell in 20 XY-optical sections. In general, every Z-stack started at the top of the cell and ended, when either the full width of the nucleus or cell was captured, whichever came later. For subcellular localisation experiments, laser excitation levels and detector gain were unique for each imaged cell, whereas for fluorescence level measurements these settings were kept equal in all replicates of one experiment.
Quantification of fluorescence levels was performed in Fiji (Schindelin et al., 2012). Imaged cells were first displayed as maximum intensity projections, followed by selecting regions of interest (ROIs) that contained only the transformed cells displayed in the Z-stacks. The mean pixel fluorescence intensities inside these ROIs were measured separately for each fluorophore as 8-bit grey scale values ranging from 0-255. All measurements were exported to Microsoft Excel 2016 (Microsoft, Redmond, USA), where the measured fluorescence levels of GFP were divided by those of mCherry (see Fig. 2.3) or vice versa (see Fig. 2.15) to normalize for the between-cells variation of fluorescence intensity levels. These ratios were plotted in GraphPad Prism V8.0 (GraphPad Software, San Diego, USA). Statistical analysis was performed in RStudio V1.2.5033 (`https://rstudio.com/`), which used R V3.6.3 (`https://www.R-project.org`). Statistical differences were determined using Wilcoxon rank-sum tests with continuity correction against an α of 0.05.
For λ-scanning, a single XY-section that showed the area of interest was selected and scanned with the Leica TCS SP5 running in xyλ-mode. The fluorescence emission spectrum in this XY-section was detected in 5 nm bins in a range from 500-760 nm (GFP) or 525-760 nm (mCitrine). Excitation was performed with 488 nm (GFP) or 514 nm (mCitrine) Argon laser lines and emission was captured with a HyD. ROIs inside the λ-scanned images were selected and measured in Leica LAS X V3.5.1 (Leica, Wetzlar, Germany). The normalized mean fluorescence intensities per wavelength were exported and plotted in GraphPad Prism V8.0 (GraphPad Software, San Diego, USA).
The recruitment assay of meGFP-RACB-CA-K167R and mCherry-RIC171 as well as the fluorescence intensity measurements of the different meGFP-RACB-K167R mutants were done according to Weiß et al. (2022).

4.15 FRET-FLIM measurements in *N. benthamiana*

FRET-FLIM measurements were carried out with an Olympus (Tokyo, Japan) FV3000 laser scanning microscope mounted on a motorized, inverted IX83 stand with a FCS/FLIM-FRET/rapidFLIM upgrade kit (PicoQuant, Berlin, Germany). For these experiments, transiently transformed *N. benthamiana* plants were used at 48 h post infiltration. This method was initially described for plasma membrane-associated plant receptor kinases overexpressed in *N. benthamiana* (Weidtkamp-Peters and Stahl, 2017), but could be adapted for cytosolic proteins when measurements were performed at the cell periphery of two directly adjacent epidermal cells. Hence, I measured FRET-FLIM in the lobes of abaxial *N. benthamiana* epidermal cells co-expressing meGFP- and mCherry-tagged proteins (see Table S3). To ensure co-expression of meGFP and mCherry and find suitable leaf areas, routine CLSM and light microscopy were performed before analysis. All cells were imaged with a UPLSAPO60XW 60x/NA 1.2/WD 0.28 water immersion objective (Olympus, Tokyo, Japan) with 4x zoom to fulfill the Nyquist-criterion.
To determine the lifetime of meGFP, time-correlated single-photon counting (TCSPC) was performed with the PicoQuant kit. Hereby, meGFP was excited with a pulsed 485 nm diode laser (LDH-D-C-485) and its emission was detected with two photon-counting PMA Hybrid 40 detectors operating two TCSPC modules (TimeHarp 260 PICO Dual, TimeHarp 260 NANO Dual). Laser pulse rate was 40 MHz, TCSPC resolution was set to 25 ps and at least 500 photons were collected per pixel. The image format was 512*512 pixels. Lifetime analysis was performed in the SymPhoTime 64 software V2.6 (PicoQuant, Berlin, Germany), using n-exponential reconvolution with two exponents (n=2) and a software-calculated internal response factor (cIRF). Regions of interest (ROIs) were used to select only those parts of the image that were in focus and showed fluorescence. Only measurements yielding χ^2-values between 1.0 and 2.0 and positive amplitudes were considered. The lifetime of meGFP was reported as intensity-weighted average lifetime τ and exported to GraphPad Prism V8.0 (GraphPad Software, San Diego, USA) for plotting. Statistical testing was conducted in RStudio V1.2.5033 (`https://rstudio.com/`) using R V3.6.3 (`https://www.R-project.org`). Statistical differences were assessed using Wilcoxon rank-sum tests with Bonferroni correction against an α of 0.05.

4.16 *Bgh* susceptibility assay

Barley epidermal cells were transiently transformed with plasmids for gene overexpression (pGY1, Schweizer et al. (1999)) or gene-silencing (pIPKTA30N, Douchkov et al. (2005)) as described in Section 4.11. pUbi-GUS+ was used as a transformation marker. At 24 hours after transformation for overexpression or 48 hat for silenc-

ing, transformed leaves were inoculated with 100-130 *Bgh* spores/mm^2. Staining and evaluation of susceptibility was performed as described in Weiß et al. (2022). Testing the *Bgh* susceptibility of transgenic GFP-tagged barley lines was performed as explained for the HA-tagged lines in Weiß et al. (2022). Lines were: BG654 E2 for eGFP-RACB-CA, BG655 E1 for eGFP-RACB-CA-ΔCSIL and BG656 E1 for eGFP. All lines were in generation T_1. Graphs were plotted in GraphPad Prism V8.0 (GraphPad Software, San Diego, USA). Statistical differences were assessed using Student's *t*-tests against an α of 0.05 in RStudio V1.2.5033 (`https://rstudio.com/`), which used R V3.6.3 (`https://www.R-project.org`). All plasmids can be found in Table S3. Gene specificity of the RNAi-silencing constructs was confirmed using the si-Fi software from Lück et al. (2019).

4.17 Immunoprecipitation

Immunoprecipitation (IP) was performed to either enrich and purify tagged proteins from crude extracts or to verify protein-protein interactions via targeted co-immunoprecipitation (CoIP) experiments. Therefore, GFP- and HA-tagged proteins were either transiently (co-) overexpressed in *N. benthamiana* (see Section 4.13) or barley protoplasts (see Section 4.12), or stably produced in transgenic barley lines. For protein extraction from transformed *N. benthamiana* leaves, 5 leaf discs of 1.2 mm diameter per sample were taken with a biopsy puncher, frozen in liquid N_2 and homogenized using a bead mill (TissueLyser II, QIAGEN, Hilden). 500 µL extraction buffer (10 % (w/v) glycerol, 25 mM Tris pH 7.5, 1 mM EDTA, 150 mM NaCl, 10 mM DTT, 1 mM PMSF, 0.5 % Nonidet P40 substitute, 1x protease inhibitor (P9599, Sigma-Aldrich, St. Louis, USA)) was added and the samples were tumbled end-over-end for 30 min at 4 °C, followed by a 10 min at 18000 g and 4°C centrifugation step to remove cell debris. For protein extraction from barley protoplasts, all protoplasts from one transformation reaction were pelleted using a 3 min at 200 g centrifugation step and the supernatant was removed. 400 µL extraction buffer was added and the samples were briefly vortexed before being incubated on ice for 10 min. For protein extraction from transgenic barley lines, one transgene-expressing barley leaf per construct was frozen in liquid nitrogen and homogenized using a mortar and pestle. 400 µL of extraction buffer was added and samples were tumbled end-over-end for 30 min at 4 °C, before being centrifuged for 10 min at 18000 g and 4 °C to remove cell debris. After protein extraction, the supernatants of all samples from *N. benthamiana* and barley were added to 10 µL/sample equilibrated GFP- or HA-specific magnetic beads and tumbled end-over-end for 1 h at 4 °C. For αGFP-IPs, the GFP-trap from Chromotek was used (gtma-10, Martinsried-Planegg, Germany), while αHA-IPs were performed with Pierce™ αHA magnetic beads (Thermo Fisher Scientific, Waltham, USA). Bead equilibration was performed 3x in

extraction buffer. For one equilibration or washing step (see below), the magnetic beads were first precipitated using a magnetic rack. Subsequently, the supernatant was removed and fresh 400 µL extraction or wash buffer was added. After protein extract-beads incubation, all samples were washed 5x in washing buffer (10 % (w/v) glycerol, 25 mM Tris pH 7.5, 1 mM EDTA, 150 mM NaCl, 1 mM PMSF, 1x protease inhibitor (P9599, Sigma-Aldrich, St. Louis, USA)). After the final washing step, the supernatants were fully removed and proteins were eluted by adding 50 µL/sample 4x SDS-loading dye (see Section 4.12) and boiled for 20 min at 95 °C. When additional samples apart from the eluted fractions were needed, 12.5 µL of 4x SDS-loading dye were mixed and boiled with 37.5 µL of samples taken after protein extraction ("Input"), incubation with the tag-specific beads ("Unbound") or the last washing step ("Wash"). All samples were analysed via SDS-PAGE and Western blotting (see Section 4.18). Experiments leading to the discovery of RACB-ubiquitination have been described in Weiß et al. (2022).

4.18 SDS-PAGE and Western blotting

SDS-polyacrylamide gelelectrophoresis (SDS-PAGE) and Western blotting were performed according to standard procedures. In general, all protein samples were resolved on 12 % polyacrylamide gels until the band with the lowest expected molecular weight had reached the end of the gel. Afterwards, the resolved proteins were blotted onto PVDF membranes using either semi-dry or wet-tank Western blotting techniques (devices for both were from Bio-Rad, Hercules, USA). If necessary, unspecific protein staining with Ponceau S was performed directly after blotting. For this, blots were incubated for 5 min in a Ponceau S staining solution (0.1 % (w/v) Ponceau S in 5 % acetic acid, Sigma-Aldrich, St. Louis, USA) for 5 min, then washed 3x with ddH_2O. For protein detection via antibodies, the membranes were first blocked for 1 h in a 5 % milk in PBS-T solution (137 mM NaCl, 2.7 mM KCl, 10 mM Na_2HPO_4, 1.8 mM KH_2PO_4, 0.05 % (v/v) Tween20, pH 7.4) at room temperature, before being incubated at 4 °C overnight in a shaker with the primary antibodies in a 5 % milk in PBS-T solution. Following three 5 min washing steps with PBS-T, the membranes were exposed to the secondary antibodies in 5 % milk in PBS-T for 1 h at room temperature. After another three 5 min washing steps with PBS-T, antibody-signals on membranes were detected with Pierce ECL Plus or SuperSignalWest DURA substrates (both Thermo Fisher Scientific, Waltham, USA). Capture of chemiluminescence was performed with a CCD camera (Fusion SL-4, Vilber, Collégien, France) or photosensitive X-ray films (Super RX-N, Fujifilm, Tokyo, Japan). All primary and secondary antibodies can be found in Table 4.23.

Table 4.23: Antibodies.
Primary antibodies with fitting secondary antibodies are listed as sets. n.n.: not needed, as the αHA-antibody was directly conjugated to horseradish peroxidase (HRP). AP: alkaline phosphatase. Companies: Santa Cruz Biotechnologies (Dallas, USA); Sigma-Aldrich (St. Louis, USA); Chromotek (Martinsried-Planegg, Germany); Cytiva (Marlborough, USA); NEB (Ipswich, USA).

Primary antibody	Dilution	Secondary antibody	Dilution
αGFP B-2 (Santa Cruz Biotechnologies)	1:1000	m-IgG$_\kappa$ BP-HRP (sc-516102, Santa Cruz Biotechnologies)	1:5000
αHA-HRP 3F10 (Sigma-Aldrich)	1:1000	n.n.	n.n.
αGST GE27-4577-01 (Cytiva)	1:2000	αgoat-AP (A4187, Sigma-Aldrich)	1:10000
αMBP E8032S (NEB)	1:2000	αmouse-AP (A3562, Sigma-Aldrich)	1:10000

4.19 Protein expression in *E. coli*

Protein expression in *E. coli* and purification were performed in collaboration with Dr. Mareike Heilmann (MLU Halle). *E. coli* strain Rosetta 2 were transformed with pGEX or pMAL plasmids harboring GST- or MBP-tagged fusion proteins (as described in Section 4.6; for plasmids see Table S3). For protein expression, one growing colony per construct was used to inoculate 30 mL 2YT-medium (see Table 4.24), which was then incubated overnight at 30 °C in a shaker. Next day, fresh 300 mL 2YT-medium were inoculated with 3 mL of overnight culture and grown in a shaker at 37 °C until an OD_{600} of 0.6-0.8 was reached. Bacterial growth was stopped via 30 min incubation on ice. Protein expression was induced by adding 0.1 M IPTG and cultures were placed at 18 °C in a shaker for 20-24 h. For harvesting, bacteria were fractioned into 50 mL aliquots and pelleted using centrifugation at 4 °C and 3000 g. All samples were frozen in liquid N_2 and stored at -80 °C until use.
For protein isolation, cells were resuspended in 3 mL GST-lysis buffer (50 mM Tris-HCl pH 7.4, 150 mM NaCl, 1x SigmaFast protease inhibitor cocktail without EDTA (Sigma-Aldrich, St. Louis, USA), 1 mM DTT, 2 mg/mL lysozyme) or MBP-lysis buffer (20 mM Tris-HCl pH 7.4, 200 mM NaCl, 1 mM EDTA, 1x SigmaFast protease inhibitor cocktail without EDTA (Sigma-Aldrich, St. Louis, USA), 1 mM DTT, 2 mg/mL lysozyme) and kept on ice for 30 min with occasional mixing. Cells were lysed via sonication (4000 J delivered in 2 s pulses) using a Vibra-Cell^{TM} 72442 with Bransonic B12 Ultrasonics Sonifier (Branson Ultrasonics, Brookfield, USA). Cell lysates were centrifuged for 15 min at 4 °C and 20000 g to separate soluble proteins from cell debris. The supernatants were either used directly (only lipid-blots with MBP-9o9, see Fig. 2.11) or subjected to affinity purification. For the latter, MBP-tagged proteins were enriched using amylose resin (NEB, Ipswich, USA),

while GST-fusion proteins were purified with Pierce^{TM} glutathion agarose resin (Thermo Fisher Scientific, Waltham, USA). Both resins were packed into Pierce^{TM} centrifugation columns (Thermo Fisher Scientific, Waltham, USA). Before adding the supernatants, packed columns were washed once with 3 mL ddH_2O and twice with either 3 mL GST-equilibration buffer (50 mM Tris-HCl pH 7.4, 150 mM NaCl, 1 mM DTT) or MBP-equilibration buffer (20 mM Tris-HCl pH 7.4, 200 mM NaCl, 1 mM EDTA, 1 mM DTT). Columns were centrifuged for 1 min at 400 g and 4 °C between each washing step. After adding the supernatants, columns were tumbled end-over-end for 1 h at room temperature. Subsequently, each column was washed 3x with 3 mL of its respective equilibration buffer. GST-tagged proteins were eluted with GST-elution buffer (50 mM glutathion, 50 mM Tris-HCl pH 7.4, 150 mM NaCl, 1 mM DTT), while MBP-fusion proteins were eluted with MBP-elution buffer (10 mM maltose, 20 mM Tris-HCl pH 7.4, 200 mM NaCl, 1 mM EDTA, 1 mM DTT). Eluted proteins were stored at -80 °C until use.

Table 4.24: 2YT-medium.
100 µg/mL carbenicillin was added post-sterilization.

Amount	Component
1.6 % (w/v)	Tryptone
0.5 % (w/v)	NaCl
1 % (w/v)	Yeast extract
0.2 % (w/v)	Glucose

4.20 Lipid-blot assays

To test protein interaction with lipids, lipid-blot experiments were performed. Before use, commercially available membranes with pre-spotted lipids (PIP Strips, Echelon Biosciences Inc., MoBiTec GmbH, Göttingen, Germany) were blocked for 30 min in a 3 % (w/v) non-fat milk solution in TBS (50 mM Tris-HCl pH 7.5, 150 mM NaCl). Afterwards, membranes were incubated overnight at 4 °C with 0.5 µg/mL purified proteins or 20 µL/mL crude protein extract (MBP-9o9 only, see Fig. 2.11) in 3 % non-fat milk in TBS with gentle shaking. Next day, membranes were washed 3x with TBS and fusion proteins were detected with antibodies specific for their respective tag (see Table 4.23). Membranes were incubated for 1 h at room temperature with the primary antibodies, followed by washing 3x with TBS. Followingly, membranes were incubated for 1 h at room temperature with fitting secondary antibodies and washed again 2x with TBS. Finally, membranes were washed once in AP-buffer (100 mM Tris-HCl pH 9.5, 100 mM NaCl, 5 mM $MgCl_2$). Detection was performed with 0.175 mg/mL 5-bromo-4-chloro-3-indolyl phosphate di-sodium salt (BCIP, Roth, Karlsruhe, Germany) and 0.338 mg/mL nitro blue tetrazolium chloride (NBT, Roth,

Karlsruhe, Germany) in AP-buffer. Reactions were stopped with ddH_2O when sufficient staining had been achieved.

4.21 RACB-CA interactor screening

For this experiment, transgenic barley lines in generation T_2 were used. Lines BG654 E2 and E12 were used for eGFP-RACB-CA, BG655 E1 and E10 for eGFP-RACB-CA-ΔCSIL and BG656 E1 and E6 for eGFP, respectively. For each construct, three biological replicates consisting of three technical replicates each were generated per condition (mock or *Bgh*-infected). For one technical replicate of the "infected" condition, 21 leaves belonging to one construct were placed on 0.8 % agar plates with the abaxial leaf side facing up. These plates were inoculated with 100-130 *Bgh* spores/mm^2 and placed under normal growth conditions for 24 h. For the "mock" condition, the same approach without inoculation was used. At 24 hpi, abaxial epidermal peels were pooled according to construct and condition and stored in liquid N_2 until homogenization. All samples were homogenized using a TissueLyser II (QIAGEN, Hilden, Germany). Proteins were extracted by adding 400 µL extraction buffer (see Section 4.17) and incubating samples for 30 min on ice with occasional mixing. Cell debris was pelleted by centrifugation at 18000 g at 4 °C for 10 min. Supernatants were then used for immunoprecipitation (IP) with 20 µL GFP-Trap magnetic agarose beads (gtma-10, Chromotek, Planegg, Germany) per sample. IPs were conducted according to standard methods (see Section 4.17). Briefly, beads were first equilibrated 3 times with 400 µL extraction buffer. After adding supernatants, samples were tumbled end-over-end for 1 h at 4 °C, then washed 5 times with washing buffer (see Section 4.17). Proteins were eluted in 100 µL of 2x NuPAGE LDS Sample Buffer (NP0008, Thermo Fisher Scientific, Waltham, USA) and boiled at 95 °C for 10 min. Samples were given to Dr. Julia Mergner (TUM) for analysis via mass spectrometry.

4.22 Mass spectrometry

All mass spectrometry experiments were conducted by Dr. Julia Mergner (TUM). The RACB-CA phosphosite-screenings and identification of the ubiquitination site were done as described in Weiß et al. (2022).
For identification of novel RACB-CA interactors, the following workflow was performed: Received samples were first reduced with 10 mM DTT for 1 h, before being alkylated with 55 mM chloroacetamide for 30 min at room temperature. All samples belonging to one biological replicate and treatment were loaded on the same gradient gel (4-12 % NuPAGE, Thermo Fisher Scientific, Waltham, USA) and run until roughly 1 cm was resolved, followed by in-gel digestion with trypsin

(Roche, Basel, Switzerland) in TEAB buffer according to a standard procedures. Digested peptides were analysed by liquid chromatography-coupled tandem mass spectrometry (LC-MS/MS) using a Dionex 3000 HPLC (Thermo Fisher Scientific, Waltham, USA) connected to an Orbitrap Q Exactive HF X mass spectrometer (Thermo Fisher Scientific, Waltham, USA). For liquid chromatography, a 75 µm * 2 cm trap column prepared with 5 µm particles of Reprosil Pur ODS-3 (Dr. Maisch GmbH, Ammerbuch, Germany) and a 75 µm * 40 cm analytical column packed with 3 µm particles of C18 Reprosil Gold 120 (Dr. Maisch GmbH, Ammerbuch, Germany) were used. Digested peptides were taken up in an aqueous solution of 0.1 % formic acid and loaded into the trap column. Peptide separation was achieved using a linear gradient of 4-32 % acetonitrile with 5 % DMSO and 0.1 % formic acid in water over 20 min, followed by a 10 min washing step. Flow rate was set to 300 nL/min at a temperature of 50 °C.
The mass spectrometer was run in "data-dependent" mode, in which it automatically switched between MS- and MS2-scans. Every full-scan mass spectrum in range of 360-1300 m/z was generated in "profile-mode" with a maximum injection time of 45 ms, an automatic gain control (AGC) target value of 3e6 and a resolution of 60000. High-resolution MS2-scans were generated for every top 12 precursor ions. To achieve this, a maximum injection time of 25 ms, an AGC target value of 2e5, a resolution of 15000, a higher-energy collisional dissociation fragmentation with 26 % normalized collision energy and a 1.3 m/z isolation width in centroid mode were used. The minimum AGC target value was adjusted to 2.2e3 with a dynamic exclusion of 20 s.
Identification and quantification of peptides was achieved using MaxQuant V1.5.8.3 operating with standard settings (Cox and Mann, 2008). Raw MS files were first searched against common contaminants and then compared to reference databases for barley (Morex V2, Mascher et al. (2017)) and *Bgh* (DH14, ID: UP000015441, Spanu et al. (2010)) to identify proteins. The sequences of the GFP-tagged proteins were included in this search. Trypsin/P was specified as the proteolytic enzyme, with a maximum of 2 missed cleavage sites allowed. The match-between-runs function was enabled, but limited to either mock-treated or *Bgh*-inoculated samples. Carbamidomethylation of cysteines was set as fixed modification. Variable modifications were: oxidation of methionines, N-terminal protein acetylation and phosphorylation of serine, threonine or tyrosine residues. All results were filtered according to 1 % false discovery rates in peptide spectrum matches, proteins and sites.
Results files from MaxQuant were imported into Perseus V1.5.5.3 (Tyanova et al., 2016) to perform statistical testing. Significantly enriched peptides between samples were identified using Student's two-tailed t-tests against an α of 0.05. Data was exported from Perseus into Microsoft Excel 2016 (Microsoft, Redmond, USA) to

screen for novel RACB-CA interaction partners. Criteria to be considered were: a unique presence or statistically significant enrichment in RACB-CA samples, the level of enrichment and presence of unique peptides.

4.23 Bioinformatic analyses

The conservation of the RACB-K167 ubiquitin acceptor site in all ROPs from barley, rice and *Arabidopsis* was analysed in Jalview V2.11.0 using a MUSCLE-alignment comparing the respective protein sequences (Edgar, 2004; Waterhouse et al., 2009). The resulting alignment was exported to Inkscape V1.2 (`https://inkscape.org/`) to graphically highlight the conserved lysine.

RACB's secondary structure motifs and G-protein domains were annotated as described in Figure S6 from Weiß et al. (2022). RACB's putative protein folds were generated using SWISS-MODEL (Waterhouse et al., 2018). As described in Weiß et al. (2022), GDP-bound RACB was modelled after GDP-bound *At*ROP4 (PDB entry: 2NTY.1, Thomas et al. (2007)), whereas GTP-RACB was modelled after GNP-*Hs*RAC1 (3TH5.1, Krauthammer et al. (2012)). Both models achieved acceptable scores (see Weiß et al. (2022)) and contained RACB's amino acids 1-178 and 7-178, respectively. The cartoon illustrations and surface structures highlighting the predicted GEF- and CRIB-binding interfaces together with the ubiquitin-acceptor site were generated in PyMOL V2.3.4 (Schrödinger, LLC, 2015). Amino acids participating in GEF- and CRIB-binding were taken from Abdul-Manan et al. (1999); Thomas et al. (2007) and Schaefer et al. (2011).

For the prediction of functional domains in 9o9, PLC and PIP, their amino acid sequences were fed into the NCBI CD-search algorithm (`https://www.ncbi.nlm.nih.gov/Structure/cdd/wrpsb.cgi`; Lu et al. (2020)) and blasted against the Uniprot database (The UniProt Consortium, 2020). Identified conserved domains and catalytic amino acids were highlighted in the sequences of PLC and PIP using Inkscape V1.2 (`https://inkscape.org/`).

The prediction of a signal peptide in 9o9 was conducted via SignalP Version 6.0 (Teufel et al., 2022).

Modelling the putative protein structure of 9o9 was performed via Alphafold V2.1.0 hosted in a Colab notebook (https://colab.research.google.com/github/deepmind/alphafold/blob/main/notebooks/AlphaFold.ipynb, Jumper et al. (2021)). The resulting protein structure was illustrated in PyMOL V2.3.4 (Schrödinger, LLC, 2015).

Identification of homologous proteins for 9o9, PLC and PIP in barley, rice, *Arabidopsis* or *Bgh* was performed by blasting the respective most recent proteomes (barley: Morex V3 (Mascher, 2021); rice: IRGSP 1.0 (Kawahara et al., 2013); *Arabidopsis*: Araport11 (Cheng et al., 2017); *Bgh*: race DH14 (Spanu et al., 2010)) with the amino acid sequences of the three proteins. Since blasting 9o9 revealed an unusually large

amount of potentially homologous proteins, only candidates fulfilling the following criteria were considered: they had to show an aligned sequence coverage higher than 30 %, an error value smaller than 0.05 and more than 30 % sequence identity with 9o9. Using SeaView V5.0.5 (Gouy et al., 2009), identified homologs were first compared to the sequences of 9o9, PLC and PIP via a MUSCLE-alignment running default parameters (Edgar, 2004) and then used to built phylogenetic maximum-likelihood (PhyML) trees. Tree-building parameters were: an LG-model, bootstrap with 100 replicates, model-given amino-acid equilibrium frequencies, no invariable sites, optimized across site rate variation, nearest-neighbour interchange for tree searching and five random starts. Resulting trees were exported and modelled in Inkscape V1.2 (`https://inkscape.org/`).

To identify expression patterns of *PLC* and *PIP* in different barley tissues, their matching transcripts in the barley reference transcript database (BaRTD, Mascher et al. (2017); Rapazote-Flores et al. (2019)) were identified via blasting their nucleotide sequences. Their tissue expression levels were exported and graphed in GraphPad Prism V8.0 (GraphPad Software, San Diego, USA).

A list of all genes used in this dissertation can found in Table S5.

References

Abd-El-Haliem, A. M., Vossen, J. H., van Zeijl, A., Dezhsetan, S., Testerink, C., Seidl, M. F., Beck, M., Strutt, J., Robatzek, S., and Joosten, M. H. A. J. 2016. Biochemical Characterization of the Tomato Phosphatidylinositol-specific Phospholipase C (PI-PLC) Family and its Role in Plant Immunity. *BBA - Molecular and Cell Biology of Lipids*, 1861(9):1365–1378.

Abdrabou, A. and Wang, Z. 2018. Posttranslational Modification and Subcellular Distribution of Rac1: an Update. *Cells*, 7(12):263.

Abdul-Manan, N., Aghazadeh, B., Liu, G. A., Majumdar, A., Ouerfelli, O., Siminovitch, K. A., and Rosen, M. K. 1999. Structure of Cdc42 in Complex with the GTPase-binding Domain of the 'Wiskott-Aldrich Syndrome' Protein. *Nature*, 399(6734):379–383.

Afzal, A. J., da Cunha, L., and Mackey, D. 2011. Separable Fragments and Membrane Tethering of Arabidopsis RIN4 Regulate Its Suppression of PAMP-Triggered Immunity. *The Plant Cell*, 23(10):3798–3811.

Agrios, G. N. 2005. Plant Diseases Caused By Fungi. In *Plant Pathology*, pages 385–614. Elsevier, Amsterdam Boston, Fifth edition.

Akamatsu, A., Wong, H. L., Fujiwara, M., Okuda, J., Nishide, K., Uno, K., Imai, K., Umemura, K., Kawasaki, T., Kawano, Y., and Shimamoto, K. 2013. An OsCEBiP/OsCERK1-OsRacGEF1-OsRac1 Module Is an Essential Early Component of Chitin-Induced Rice Immunity. *Cell Host & Microbe*, 13(4):465–476.

Aktories, K. 2011. Bacterial Protein Toxins that Modify Host Regulatory GTPases. *Nature Reviews Microbiology*, 9(7):487–498.

Albert, I., Böhm, H., Albert, M., Feiler, C. E., Imkampe, J., Wallmeroth, N., Brancato, C., Raaymakers, T. M., Oome, S., Zhang, H., Krol, E., Grefen, C., Gust, A. A., Chai, J., Hedrich, R., den Ackerveken, G. V., and Nürnberger, T. 2015. An RLP23–SOBIR1–BAK1 Complex Mediates NLP-triggered Immunity. *Nature Plants*, 1(10).

Amselem, J., Vigouroux, M., Oberhaensli, S., Brown, J. K. M., Bindschedler, L. V., Skamnioti, P., Wicker, T., Spanu, P. D., Quesneville, H., and Sacristán, S. 2015. Evolution of the EKA Family of Powdery Mildew Avirulence-effector Genes from the ORF 1 of a LINE retrotransposon. *BMC Genomics*, 16(1):917.

Anthony, R. G., Henriques, R., Helfer, A., Meszaros, T., Rios, G., Testerink, C., Munnik, T., Deák, M., Koncz, C., and Bögre, L. 2004. A Protein Kinase Target of

a PDK1 Signalling Pathway is Involved in Root Hair Growth in *Arabidopsis*. *The EMBO Journal*, 23(3):572–581.

Asai, S. and Shirasu, K. 2015. Plant Cells Under Siege: Plant Immune System Versus Pathogen Effectors. *Current Opinion in Plant Biology*, 28:1–8.

Axtell, M. J. and Staskawicz, B. J. 2003. Initiation of RPS2-Specified Disease Resistance in *Arabidopsis* Is Coupled to the AvrRpt2-Directed Elimination of RIN4. *Cell*, 112(3):369–377.

Basu, D., Le, J., Zakharova, T., Mallery, E. L., and Szymanski, D. B. 2008. A SPIKE1 Signaling Complex Controls Actin-dependent Cell Morphogenesis through the Heteromeric WAVE and ARP2/3 Complexes. *Proceedings of the National Academy of Sciences*, 105(10):4044–4049.

Berken, A. 2006. ROPs in the Spotlight of Plant Signal Transduction. *Cellular and Molecular Life Sciences*, 63(21):2446–2459.

Berken, A., Thomas, C., and Wittinghofer, A. 2005. A New Family of RhoGEFs Activates the ROP Molecular Switch in Plants. *Nature*, 436(7054):1176–1180.

Berken, A. and Wittinghofer, A. 2008. Structure and Function of Rho-type Molecular Switches in Plants. *Plant Physiology and Biochemistry*, 46(3):380–393.

Bi, G., Zhou, Z., Wang, W., Li, L., Rao, S., Wu, Y., Zhang, X., Menke, F. L. H., Chen, S., and Zhou, J.-M. 2018. Receptor-Like Cytoplasmic Kinases Directly Link Diverse Pattern Recognition Receptors to the Activation of Mitogen-Activated Protein Kinase Cascades in *Arabidopsis*. *The Plant Cell*, 30(7):1543–1561.

Bischoff, F., Vahlkamp, L., Molendijk, A., and Palme, K. 2000. Localization of *At*ROP4 and *At*ROP6 and Interaction with the Guanine Nucleotide Dissociation Inhibitor *At*RhoGDI1 from *Arabidopsis*. *Plant Molecular Biology*, 42(3):515–530.

Boller, T. and Felix, G. 2009. A Renaissance of Elicitors: Perception of Microbe-Associated Molecular Patterns and Danger Signals by Pattern-Recognition Receptors. *Annual Review of Plant Biology*, 60:379–406.

Bos, J. L., Rehmann, H., and Wittinghofer, A. 2007. GEFs and GAPs: Critical Elements in the Control of Small G-Proteins. *Cell*, 129(5):865–877.

Boulter, E. and Garcia-Mata, R. 2010. RhoGDI: A Rheostat for the Rho Switch. *Small GTPases*, 1(1):65–68.

Boutrot, F. and Zipfel, C. 2017. Function, Discovery, and Exploitation of Plant Pattern Recognition Receptors for Broad-Spectrum Disease Resistance. *Annual Review of Phytopathology*, 55(1):257–286.

Bozkurt, T. O., Schornack, S., Banfield, M. J., and Kamoun, S. 2012. Oomycetes, Effectors, and all that Jazz. *Current Opinion in Plant Biology*, 15(4):483–492.

Cai, Y., Deng, Y., Horenkamp, F., Reinisch, K. M., and Burd, C. G. 2014. Sac1-Vps74 Structure Reveals a Mechanism to Terminate Phosphoinositide Signaling in the Golgi Apparatus. *The Journal of Cell Biology*, 206(25113029):485–491.

Cao, Y., Liang, Y., Tanaka, K., Nguyen, C. T., Jedrzejczak, R. P., Joachimiak, A., and Stacey, G. 2014. The Kinase LYK5 is a Major Chitin Receptor in *Arabidopsis* and Forms a Chitin-Induced Complex with Related Kinase CERK1. *eLife*, 3.

Carol, R. J., Takeda, S., Linstead, P., Durrant, M. C., Kakesova, H., Derbyshire, P., Drea, S., Zarsky, V., and Dolan, L. 2005. A RhoGDP Dissociation Inhibitor Spatially Regulates Growth in Root Hair Cells. *Nature*, 438(7070):1013–1016.

Carver, T. L. W., Kunoh, H., Thomas, B. J., and Nicholson, R. L. 1999. Release and Visualization of the Extracellular Matrix of Conidia of *Blumeria graminis*. *Mycological Research*, 103(5):547–560.

Castillo-Lluva, S., Tan, C.-T., Daugaard, M., Sorensen, P. H. B., and Malliri, A. 2013. The Tumour Suppressor HACE1 Controls Cell Migration by Regulating Rac1 Degradation. *Oncogene*, 32(13):1735–1742.

Chanda, B., Xia, Y., Mandal, M. K., Yu, K., Sekine, K., Gao, Q.-m., Selote, D., Hu, Y., Stromberg, A., Navarre, D., Kachroo, A., and Kachroo, P. 2011. Glycerol-3-phosphate is a Critical Mobile Inducer of Systemic Immunity in Plants. *Nature Genetics*, 43(5):421–427.

Chang, F., Lemmon, C., Lietha, D., Eck, M., and Romer, L. 2011. Tyrosine Phosphorylation of Rac1: A Role in Regulation of Cell Spreading. *PLOS ONE*, 6(12):1–14.

Chen, L., Shiotani, K., Togashi, T., Miki, D., Aoyama, M., Wong, H. L., Kawasaki, T., and Shimamoto, K. 2010. Analysis of the Rac/Rop Small GTPase Family in Rice: Expression, Subcellular Localization and Role in Disease Resistance. *Plant and Cell Physiology*, 51(4):585–595.

Cheng, C.-Y., Krishnakumar, V., Chan, A. P., Thibaud-Nissen, F., Schobel, S., and Town, C. D. 2017. Araport11: A Complete Reannotation of the *Arabidopsis thaliana* Reference Genome. *The Plant Journal*, 89:789–804.

Chinchilla, D., Zipfel, C., Robatzek, S., Kemmerling, B., Nürnberger, T., Jones, J. D. G., Felix, G., and Boller, T. 2007. A Flagellin-Induced Complex of the Receptor FLS2 and BAK1 Initiates Plant Defence. *Nature*, 448(7152):497–500.

Choi, S., Prokchorchik, M., Lee, H., Gupta, R., Lee, Y., Chung, E.-H., Cho, B., Kim, M.-S., Kim, S. T., and Sohn, K. H. 2021. Direct Acetylation of a Conserved Threonine of RIN4 by the Bacterial Effector HopZ5 or AvrBsT Activates RPM1-dependent Immunity in *Arabidopsis*. *Molecular Plant*, 14(11):1951–1960.

Colin, L. A. and Jaillais, Y. 2020. Phospholipids Across Scales: Lipid Patterns and Plant Development. *Current Opinion in Plant Biology*, 53:1–9.

Cool, R. H., Schmidt, G., Lenzen, C. U., Prinz, H., Vogt, D., and Wittinghofer, A. 1999. The Ras Mutant D119N Is Both Dominant Negative and Activated. *Molecular and Cellular Biology*, 19(9):6297–6305.

Cox, J. and Mann, M. 2008. MaxQuant Enables High Peptide Identification Rates, Individualized ppb-range Mass Accuracies and Proteome-wide Protein Quantification. *Nature Biotechnology*, 26(12):1367–1372.

Cui, H., Tsuda, K., and Parker, J. E. 2015. Effector-Triggered Immunity: From Pathogen Perception to Robust Defense. *Annual Review of Plant Biology*, 66:487–511.

Dangl, J. L., Horvath, D. M., and Staskawicz, B. J. 2013. Pivoting the plant immune system from dissection to deployment. *Science*, 341(6147):746–751.

Day, B., Dahlbeck, D., Huang, J., Chisholm, S. T., Li, D., and Staskawicz, B. J. 2005. Molecular Basis for the RIN4 Negative Regulation of RPS2 Disease Resistance. *The Plant Cell*, 17(4):1292–1305.

Denninger, P., Reichelt, A., Schmidt, V. A. F., Mehlhorn, D. G., Asseck, L. Y., Stanley, C. E., Keinath, N. F., Evers, J.-F., Grefen, C., and Grossmann, G. 2019. Distinct RopGEFs Successively Drive Polarization and Outgrowth of Root Hairs. *Current Biology*, 29(11):1854–1865.e5.

Dodds, P. N. and Rathjen, J. P. 2010. Plant Immunity: Towards an Integrated View of Plant-Pathogen Interactions. *Nature Reviews Genetics*, 11(8):539–548.

Douchkov, D., Nowara, D., Zierold, U., and Schweizer, P. 2005. A High-Throughput Gene-Silencing System for the Functional Assessment of Defense-Related Genes in Barley Epidermal Cells. *Molecular Plant-Microbe Interactions*, 18(8):755–761.

Doumane, M., Lebecq, A., Colin, L., Fangain, A., Stevens, F. D., Bareille, J., Hamant, O., Belkhadir, Y., Munnik, T., Jaillais, Y., and Caillaud, M.-C. 2021. Inducible Depletion of PI(4,5)P_2 by the Synthetic iDePP System in *Arabidopsis*. *Nature Plants*, 7(5):587–597.

Dowler, S., Currie, R. A., Campbell, D. G., Deak, M., Kular, G., Downes, C. P., and Alessi, D. R. 2000. Identification of Pleckstrin-Homology-Domain-Containing Proteins with Novel Phosphoinositide-Binding Specificities. *Biochemical Journal*, 351(1):19–31.

Doyle, E. L., Stoddard, B. L., Voytas, D. F., and Bogdanove, A. J. 2013. TAL Effectors: Highly Adaptable Phytobacterial Virulence Factors and Readily Engineered DNA-targeting Proteins. *Trends in Cell Biology*, 23(8):390–398.

Dransart, E., Olofsson, B., and Cherfils, J. 2005. RhoGDIs Revisited: Novel Roles in Rho Regulation. *Traffic*, 6(11):957–966.

Dubois, G. A. and Jaillais, Y. 2021. Anionic Phospholipid Gradients: an Uncharacterized Frontier of the Plant Endomembrane Network. *Plant Physiology*, 185(3):577–592.

Eckardt, N. A. 2002. Plant Disease Susceptibility Genes? *The Plant Cell*, 14(9):1983–1986.

Edgar, R. C. 2004. MUSCLE: Multiple Sequence Alignment with High Accuracy and High Throughput. *Nucleic Acids Research*, 32(5):1792–1797.

Edwards, H. H. 2002. Development of Primary Germ Tubes by Conidia of *Blumeria graminis* f.sp. *hordei* on Leaf Epidermal Cells of *Hordeum vulgare*. *Canadian Journal of Botany*, 80(10):1121–1125.

Enders, T. A., Frick, E. M., and Strader, L. C. 2017. An *Arabidopsis* Kinase Cascade Influences Auxin-Responsive Cell Expansion. *The Plant Journal*, 92(1):68–81.

Engelhardt, S., Stam, R., and Hückelhoven, R. 2018. Good Riddance? Breaking Disease Susceptibility in the Era of New Breeding Technologies. *Agronomy*, 8(7):114.

Engelhardt, S., Trutzenberg, A., and Hückelhoven, R. 2020. Regulation and Functions of ROP GTPases in Plant-Microbe Interactions. *Cells*, 9(9):2016.

Engelhardt, S., Trutzenberg, A., Probst, K., Hofer, J., McCollum, C., Kopischke, M., and Hückelhoven, R. 2021. Barley RIC157 is Involved in RACB-mediated Susceptibility to Powdery Mildew. *bioRxiv*.

Engler, C., Kandzia, R., and Marillonnet, S. 2008. A One Pot, One Step, Precision Cloning Method with High Throughput Capability. *PLOS ONE*, 3(11):1–7.

Eshed, N. and Wahl, I. 1970. Host Ranges and Interrelations of *Erysiphe graminis hordei*, *E. graminis tritici*, and *E. graminis avenae*. *Phytopathology*, 60(4):628–634.

Eshed, N. and Wahl, I. 1975. Role of Wild Grasses in Epidemics of Powdery Mildew. *Phytopathology*, 65:57–63.

Essen, L.-O., Perisic, O., Cheung, R., Katan, M., and Williams, R. L. 1996. Crystal Structure of a Mammalian Phosphoinositide-specific Phospholipase Cδ. *Nature*, 380(6575):595–602.

Essen, L.-O., Perisic, O., Katan, M., Wu, Y., Roberts, M. F., and Williams, R. L. 1997. Structural Mapping of the Catalytic Mechanism for a Mammalian Phosphoinositide-Specific Phospholipase C. *Biochemistry*, 36(7):1704–1718.

Feiguelman, G., Fu, Y., and Yalovsky, S. 2018. ROP GTPases Structure-Function and Signaling Pathways. *Plant Physiology*, 176(1):57–79.

Felix, G., Duran, J. D., Volko, S., and Boller, T. 1999. Plants Have a Sensitive Perception System for the Most Conserved Domain of Bacterial Flagellin. *The Plant Journal*, 18(3):265–276.

Flannagan, R. S., Cosío, G., and Grinstein, S. 2009. Antimicrobial Mechanisms of Phagocytes and Bacterial Evasion Strategies. *Nature Reviews Microbiology*, 7(5):355–366.

Fodor-Dunai, C., Fricke, I., Potockỳ, M., Dorjgotov, D., Domoki, M., Jurca, M. E., Ötvös, K., Žárskỳ, V., Berken, A., and Fehér, A. 2011. The Phosphomimetic Mutation of an Evolutionarily Conserved Serine Residue Affects the Signaling Properties of Rho of Plants (ROPs). *The Plant Journal*, 66(4):669–679.

Fratini, M., Krishnamoorthy, P., Stenzel, I., Riechmann, M., Matzner, M., Bacia, K., Heilmann, M., and Heilmann, I. 2021. Plasma Membrane Nano-Organization Specifies Phosphoinositide Effects on Rho-GTPases and Actin Dynamics in Tobacco Pollen Tubes. *The Plant Cell*, 33(3):642–670.

Fu, Y. and Galán, J. E. 1999. A *Salmonella* Protein Antagonizes Rac1 and Cdc42 to Mediate Host-Cell Recovery after Bacterial Invasion. *Nature*, 401(6750):293–297.

Fu, Y., Gu, Y., Zheng, Z., Wasteneys, G., and Yang, Z. 2005. *Arabidopsis* Interdigitating Cell Growth Requires Two Antagonistic Pathways with Opposing Action on Cell Morphogenesis. *Cell*, 120(5):687–700.

Fu, Y., Xu, T., Zhu, L., Wen, M., and Yang, Z. 2009. A ROP GTPase Signaling Pathway Controls Cortical Microtubule Ordering and Cell Expansion in *Arabidopsis*. *Current Biology*, 19(21):1827–1832.

Furt, F., Simon-Plas, F., and Mongrand, S. 2010. Lipids of the Plant Plasma Membrane. In *The Plant Plasma Membrane*, pages 3–30. Springer Berlin Heidelberg.

Gao, Q., Wang, C., Xi, Y., Shao, Q., Li, L., and Luan, S. 2022. A Receptor-Channel Trio Conducts Ca^{2+}-Signalling for Pollen Tube Reception. *Nature*.

Georges, F., Das, S., Ray, H., Bock, C., Nokhrina, K., Kolla, V. A., and Keller, W. 2009. Over-expression of *Brassica napus* Phosphatidylinositol-phospholipase C2 in Canola Induces Significant Changes in Gene Expression and Phytohormone Distribution Patterns, Enhances Drought Tolerance and Promotes Early Flowering and Maturation. *Plant, Cell & Environment*, 32(12):1664–1681.

Gerth, K., Lin, F., Menzel, W., Krishnamoorthy, P., Stenzel, I., Heilmann, M., and Heilmann, I. 2016. Guilt by Association: A Phenotype-Based View of the Plant Phosphoinositide Network. *Annual Review of Plant Biology*, 68(1):349–374.

Gheysen, G. and Mitchum, M. G. 2011. How Nematodes Manipulate Plant Development Pathways for Infection. *Current Opinion in Plant Biology*, 14(4):415–421.

Gietz, R. D. and Woods, R. A. 2002. Transformation of Yeast by Lithium Acetate/Single-Stranded Carrier DNA/Polyethylene Glycol Method. In *Methods in Enzymology*, volume 350, pages 87–96. Elsevier.

Giraldo, M. C. and Valent, B. 2013. Filamentous Plant Pathogen Effectors in Action. *Nature Reviews Microbiology*, 11(11):800–814.

Glawe, D. A. 2008. The Powdery Mildews: A Review of the World's Most Familiar (Yet Poorly Known) Plant Pathogens. *Annual Review of Phytopathology*, 46(1):27–51.

Goellner, K., Loehrer, M., Langenbach, C., Conrath, U., Koch, E., and Schaffrath, U. 2010. *Phakopsora pachyrhizi*, the Causal Agent of Asian Soybean Rust. *Molecular Plant Pathology*, 11(2):169–177.

Goo, J. H., Park, A. R., Park, W. J., and Park, O. K. 1999. Selection of *Arabidopsis* Genes Encoding Secreted and Plasma Membrane Proteins. *Plant Molecular Biology*, 41(3):415–423.

Gouy, M., Guindon, S., and Gascuel, O. 2009. SeaView Version 4: A Multiplatform Graphical User Interface for Sequence Alignment and Phylogenetic Tree Building. *Molecular Biology and Evolution*, 27(2):221–224.

Green, J. R., Carver, T. L. W., and Gurr, S. J. 2002. The Formation and Function of Infection and Feeding Structures. *The Powdery Mildews: A Comprehensive Treatise*, pages 66–82.

Gu, Y., Fu, Y., Dowd, P., Li, S., Vernoud, V., Gilroy, S., and Yang, Z. 2005. A Rho Family GTPase Controls Actin Dynamics and Tip Growth via Two Counteracting Downstream Pathways in Pollen Tubes. *Journal of Cell Biology*, 169(1):127–138.

Gu, Y., Wang, Z., and Yang, Z. 2004. ROP/RAC GTPase: An Old New Master Regulator For Plant Signaling. *Current Opinion in Plant Biology*, 7(5):527–536.

Gómez-Gómez, L. and Boller, T. 2000. FLS2: An LRR Receptor–like Kinase Involved in the Perception of the Bacterial Elicitor Flagellin in *Arabidopsis*. *Molecular Cell*, 5(6):1003–1011.

Göhre, V., Spallek, T., Häweker, H., Mersmann, S., Mentzel, T., Boller, T., de Torres, M., Mansfield, J. W., and Robatzek, S. 2008. Plant Pattern-Recognition Receptor FLS2 Is Directed for Degradation by the Bacterial Ubiquitin Ligase AvrPtoB. *Current Biology*, 18(23):1824–1832.

Hacquard, S., Kracher, B., Maekawa, T., Vernaldi, S., Schulze-Lefert, P., and van Themaat, E. V. L. 2013. Mosaic Genome Structure of the Barley Powdery Mildew Pathogen and Conservation of Transcriptional Programs in Divergent Hosts. *Proceedings of the National Academy of Sciences*, 110(24):E2219–E2228.

Hardt, W.-D., Chen, L.-M., Schuebel, K. E., Bustelo, X. R., and Galán, J. E. 1998. *S. typhimurium* Encodes an Activator of Rho GTPases that Induces Membrane Ruffling and Nuclear Responses in Host Cells. *Cell*, 93(5):815–826.

Heilmann, I. 2016. Phosphoinositide Signaling in Plant Development. *Development*, 143(12):2044–2055.

Hensel, G., Kastner, C., Oleszczuk, S., Riechen, J., and Kumlehn, J. 2009. *Agrobacterium*-mediated Gene Transfer to Cereal Crop Plants: Current Protocols for Barley, Wheat, Triticale, and Maize. *International Journal of Plant Genomics*, 2009.

Hensgens, L. A. M., de Bakker, E. P. H. M., van Os-Ruygrok, E. P., Rueb, S., van de Mark, F., van der Maas, H. M., van der Veen, S., Kooman-Gersmann, M., Hart, L., and Schilperoort, R. A. 1993. Transient and Stable Expression of gusA Fusions with Rice Genes in Rice, Barley and Perennial Ryegrass. *Plant Molecular Biology*, 22(6):1101–1127.

Hirano, T., Konno, H., Takeda, S., Dolan, L., Kato, M., Aoyama, T., Higaki, T., Takigawa-Imamura, H., and Sato, M. H. 2018. PtdIns(3,5)P_2 Mediates Root Hair Shank Hardening in *Arabidopsis*. *Nature Plants*, 4(11):888–897.

Hirano, T., Munnik, T., and Sato, M. H. 2015. Phosphatidylinositol 3-phosphate 5-kinase, FAB1/PIKfyve Mediates Endosome Maturation to Establish Endosome-Cortical Microtubule Interaction in *Arabidopsis*. *Plant Physiology*, page 01368.2015.

Hirano, T., Munnik, T., and Sato, M. H. 2016. Inhibition of Phosphatidylinositol-3,5-bisphosphate Production has Pleiotropic Effects on Various Membrane Trafficking Routes in *Arabidopsis*. *Plant and Cell Physiology*, page pcw164.

Hirano, T., Stecker, K., Munnik, T., Xu, H., and Sato, M. H. 2017. Visualization of Phosphatidylinositol-3,5-Bisphosphate Dynamics by a Tandem ML1N-Based Fluorescent Protein Probe in *Arabidopsis*. *Plant and Cell Physiology*, 58(7):1185–1195.

Hoefle, C., Huesmann, C., Schultheiss, H., Börnke, F., Hensel, G., Kumlehn, J., and Hückelhoven, R. 2011. A Barley ROP GTPase ACTIVATING PROTEIN Associates with Microtubules and Regulates Entry of the Barley Powdery Mildew Fungus into Leaf Epidermal Cells. *The Plant Cell*, 23(6):2422–2439.

Hsu, F., Zhu, W., Brennan, L., Tao, L., Luo, Z.-Q., and Mao, Y. 2012. Structural Basis for Substrate Recognition by a Unique *Legionella* Phosphoinositide Phosphatase. *Proceedings of the National Academy of Sciences*, 109(34):13567–13572.

Hua, Z. and Vierstra, R. D. 2011. The Cullin-RING Ubiquitin-Protein Ligases. *Annual Review of Plant Biology*, 62:299–334.

Hückelhoven, R. 2005. Powdery Mildew Susceptibility and Biotrophic Infection Strategies. *FEMS Microbiology Letters*, 245(1):9–17.

Hückelhoven, R. and Panstruga, R. 2011. Cell Biology of the Plant-Powdery Mildew Interaction. *Current Opinion in Plant Biology*, 14(6):738–746.

Huesmann, C., Reiner, T., Hoefle, C., Preuss, J., Jurca, M. E., Domoki, M., Fehér, A., and Hückelhoven, R. 2012. Barley ROP Binding Kinase 1 Is Involved in Microtubule Organization and in Basal Penetration Resistance to the Barley Powdery Mildew Fungus. *Plant Physiology*, 159(1):311–320.

Hwang, J.-U., Vernoud, V., Szumlanski, A., Nielsen, E., and Yang, Z. 2008. A Tip-Localized RhoGAP Controls Cell Polarity by Globally Inhibiting Rho GTPase at the Cell Apex. *Current Biology*, 18(24):1907–1916.

Hwang, J.-U., Wu, G., Yan, A., Lee, Y.-J., Grierson, C. S., and Yang, Z. 2010. Pollen Tube Tip Growth Requires a Balance of Lateral Propagation and Global Inhibition of Rho-Family GTPase Activity. *Journal of Cell Science*, 123(3):340–350.

Hückelhoven, R., Eichmann, R., Weis, C., Hoefle, C., and Proels, R. K. 2013. Genetic Loss of Susceptibility: a Costly Route to Disease Resistance? *Plant Pathology*, 62(S1):56–62.

IPCC 2014. Climate Change 2014: Synthesis Report. Contribution of Working Groups I, II and III to the Fifth Assessment Report of the Intergovernmental Panel on Climate Change. *IPCC, Geneva, Switzerland*.

Ischebeck, T., Stenzel, I., Hempel, F., Jin, X., Mosblech, A., and Heilmann, I. 2011. Phosphatidylinositol-4,5-bisphosphate Influences *Nt*Rac5-mediated Cell Expansion in Pollen Tubes of *Nicotiana tabacum*. *The Plant Journal*, 65(3):453–468.

Jank, T., Bogdanović, X., Wirth, C., Haaf, E., Spoerner, M., Böhmer, K. E., Steinemann, M., Orth, J. H. C., Kalbitzer, H. R., Warscheid, B., Hunte, C., and Aktories, K. 2013. A Bacterial Toxin Catalyzing Tyrosine Glycosylation of Rho and Deamidation of Gq and Gi Proteins. *Nature Structural & Molecular Biology*, 20(11):1273–1280.

Jankovics, T., Komáromi, J., Fábián, A., Jäger, K., Vida, G., and Kiss, L. 2015. New Insights into the Life Cycle of the Wheat Powdery Mildew: Direct Observation of Ascosporic Infection in *Blumeria graminis* f.sp. *tritici*. *Phytopathology*, 105(6):797–804.

Jarosch, B., Kogel, K.-H., and Schaffrath, U. 1999. The Ambivalence of the Barley Mlo Locus: Mutations Conferring Resistance Against Powdery Mildew (*Blumeria graminis* f.sp. *hordei*) Enhance Susceptibility to the Rice Blast Fungus *Magnaporthe grisea*. *Molecular Plant-Microbe Interactions*, 12(6):508–514.

Jezyk, M. R., Snyder, J. T., Gershberg, S., Worthylake, D. K., Harden, T. K., and Sondek, J. 2006. Crystal Structure of Rac1 Bound to its Effector Phospholipase C-β2. *Nature Structural & Molecular Biology*, 13(12):1135–1140.

Jones, J. D. G. and Dangl, J. L. 2006. The plant immune system. *Nature*, 444(7117):323–329.

Jones, M. A., Shen, J.-J., Fu, Y., Li, H., Yang, Z., and Grierson, C. S. 2002. The Arabidopsis ROP2 GTPase Is a Positive Regulator of Both Root Hair Initiation and Tip Growth. *The Plant Cell*, 14(4):763–776.

Jørgensen, J. H. and Mortensen, K. 1977. Primary Infection by *Erysiphe graminis* f.sp. *hordei* of Barley Mutants with Resistance Genes in the Mlo Locus. *Phytopathology*, 67(5):678–685.

Jumper, J., Evans, R., Pritzel, A., Green, T., Figurnov, M., Ronneberger, O., Tunyasuvunakool, K., Bates, R., Žídek, A., Potapenko, A., Bridgland, A., Meyer, C., Kohl, S. A. A., Ballard, A. J., Cowie, A., Romera-Paredes, B., Nikolov, S., Jain, R., Adler, J., Back, T., Petersen, S., Reiman, D., Clancy, E., Zielinski, M., Steinegger, M., Pacholska, M., Berghammer, T., Bodenstein, S., Silver, D., Vinyals, O., Senior, A. W., Kavukcuoglu, K., Kohli, P., and Hassabis, D. 2021. Highly Accurate Protein Structure Prediction with AlphaFold. *Nature*, 596(7873):583–589.

Jung, H. W., Tschaplinski, T. J., Wang, L., Glazebrook, J., and Greenberg, J. T. 2009. Priming in Systemic Plant Immunity. *Science*, 324(5923):89–91.

Jurca, M. E., Bottka, S., and Fehér, A. 2008. Characterization of a Family of *Arabidopsis* Receptor-like Cytoplasmic Kinases (RLCK Class VI). *Plant Cell Reports*, 27(4):739–748.

Jørgensen, I. H. 1992. Discovery, Characterization and Exploitation of Mlo Powdery Mildew Resistance in Barley. *Euphytica*, 63(1):141–152.

Kaku, H., Nishizawa, Y., Ishii-Minami, N., Akimoto-Tomiyama, C., Dohmae, N., Takio, K., Minami, E., and Shibuya, N. 2006. Plant Cells Recognize Chitin Fragments for Defense Signaling through a Plasma Membrane Receptor. *Proceedings of the National Academy of Sciences*, 103(29):11086–11091.

Kaundal, A., Ramu, V. S., Oh, S., Lee, S., Pant, B., Lee, H.-K., Rojas, C. M., Senthil-Kumar, M., and Mysore, K. S. 2017. GENERAL CONTROL NONREPRESSIBLE 4 Degrades 14-3-3 and the RIN4 Complex to Regulate Stomatal Aperture with Implications on Nonhost Disease Resistance and Drought Tolerance. *The Plant Cell*, 29(9):2233–2248.

Kawahara, Y., de la Bastide, M., Hamilton, J. P., Kanamori, H., McCombie, W. R., Ouyang, S., Schwartz, D. C., Tanaka, T., Wu, J., Zhou, S., Childs, K. L., Davidson, R. M., Lin, H., Quesada-Ocampo, L., Vaillancourt, B., Sakai, H., Lee, S. S., Kim, J., Numa, H., Itoh, T., Buell, C. R., and Matsumoto, T. 2013. Improvement of the *Oryza sativa* Nipponbare Reference Genome using Next Generation Sequence and Optical Map Data. *Rice*, 6(1):4.

Kawano, Y., Akamatsu, A., Hayashi, K., Housen, Y., Okuda, J., Yao, A., Nakashima, A., Takahashi, H., Yoshida, H., Wong, H. L., Kawasaki, T., and Shimamoto, K. 2010. Activation of a Rac GTPase by the NLR Family Disease Resistance Protein Pit Plays a Critical Role in Rice Innate Immunity. *Cell Host & Microbe*, 7(5):362–375.

Kawano, Y., Kaneko-Kawano, T., and Shimamoto, K. 2014. Rho Family GTPase-Dependent Immunity in Plants and Animals. *Frontiers in Plant Science*, 5.

Kim, H.-S., Desveaux, D., Singer, A. U., Patel, P., Sondek, J., and Dangl, J. L. 2005a. The *Pseudomonas syringae* Effector AvrRpt2 Cleaves its C-terminally Acylated target, RIN4, from *Arabidopsis* Membranes to Block RPM1 Activation. *Proceedings of the National Academy of Sciences*, 102(18):6496–6501.

Kim, M. G., da Cunha, L., McFall, A. J., Belkhadir, Y., DebRoy, S., Dangl, J. L., and Mackey, D. 2005b. Two *Pseudomonas syringae* Type III Effectors Inhibit RIN4-Regulated Basal Defense in *Arabidopsis*. *Cell*, 121(5):749–759.

Klahre, U., Becker, C., Schmitt, A. C., and Kost, B. 2006. *Nt*RhoGDI2 Regulates Rac/Rop Signaling and Polar Cell Growth in Tobacco Pollen Tubes. *The Plant Journal*, 46(6):1018–1031.

Klahre, U. and Kost, B. 2006. Tobacco RhoGTPase ACTIVATING PROTEIN 1 Spatially Restricts Signaling of RAC/ROP to the Apex of Pollen Tubes. *The Plant Cell*, 18(11):3033–3046.

Koh, S., André, A., Edwards, H., Ehrhardt, D., and Somerville, S. 2005. *Arabidopsis thaliana* Subcellular Responses to Compatible *Erysiphe cichoracearum* Infections. *The Plant Journal*, 44(3):516–529.

Kost, B., Lemichez, E., Spielhofer, P., Hong, Y., Tolias, K., Carpenter, C., and Chua, N.-H. 1999. Rac Homologues and Compartmentalized Phosphatidylinositol-4,5-bisphosphate Act in a Common Pathway to Regulate Polar Pollen Tube Growth. *The Journal of Cell Biology*, 145(2):317–330.

Krauthammer, M., Kong, Y., Ha, B. H., Evans, P., Bacchiocchi, A., McCusker, J. P., Cheng, E., Davis, M. J., Goh, G., Choi, M., Ariyan, S., Narayan, D., Dutton-Regester, K., Capatana, A., Holman, E. C., Bosenberg, M., Sznol, M., Kluger, H. M., Brash, D. E., Stern, D. F., Materin, M. A., Lo, R. S., Mane, S., Ma, S., Kidd, K. K., Hayward, N. K., Lifton, R. P., Schlessinger, J., Boggon, T. J., and Halaban, R. 2012. Exome Sequencing Identifies Recurrent Somatic RAC1 Mutations in Melanoma. *Nature Genetics*, 44(9):1006–1014.

Krijger, J.-J., Horbach, R., Behr, M., Schweizer, P., Deising, H. B., and Wirsel, S. G. R. 2008. The Yeast Signal Sequence Trap Identifies Secreted Proteins of the Hemibiotrophic Corn Pathogen *Colletotrichum graminicola*. *Molecular Plant-Microbe Interactions*, 21(10):1325–1336.

Kulich, I., Vogler, F., Bleckmann, A., Cyprys, P., Lindemeier, M., Fuchs, I., Krassini, L., Schubert, T., Steinbrenner, J., Beynon, J., Falter-Braun, P., Längst, G., Dresselhaus, T., and Sprunck, S. 2020. ARMADILLO REPEAT ONLY Proteins Confine Rho GTPase Signalling to Polar Growth Sites. *Nature Plants*, 6(10):1275–1288.

Kumar, J., Hückelhoven, R., Beckhove, U., Nagarajan, S., and Kogel, K.-H. 2001. A Compromised Mlo Pathway Affects the Response of Barley to the Necrotrophic Fungus *Bipolaris sorokiniana* (Teleomorph: *Cochliobolus sativus*) and its Toxins. *Phytopathology*, 91(2):127–133.

Kunoh, H. 2002. Localized Induction of Accessibility and Inaccessibility by Powdery Mildew. *The Powdery Mildews: A Comprehensive Treatise*, pages 126–133.

Kusano, H., Testerink, C., Vermeer, J. E. M., Tsuge, T., Shimada, H., Oka, A., Munnik, T., and Aoyama, T. 2008. The *Arabidopsis* Phosphatidylinositol Phosphate 5-Kinase PIP5K3 Is a Key Regulator of Root Hair Tip Growth. *The Plant Cell*, 20(2):367–380.

Kusch, S. and Panstruga, R. 2017. mlo-Based Resistance: An Apparently Universal "Weapon" to Defeat Powdery Mildew Disease. *Molecular Plant-Microbe Interactions*, 30(3):179–189.

Kutateladze, T. G. 2010. Translation of the Phosphoinositide Code by PI Effectors. *Nature Chemical Biology*, 6(7):507–513.

Kwaaitaal, M., Nielsen, M. E., Böhlenius, H., and Thordal-Christensen, H. 2017. The Plant Membrane Surrounding Powdery Mildew Haustoria Shares Properties with the Endoplasmic Reticulum Membrane. *Journal of Experimental Botany*, 68(21-22):5731–5743.

Kwon, T., Kwon, D. Y., Chun, J., Kim, J. H., and Kang, S. S. 2000. Akt Protein Kinase Inhibits Rac1-GTP Binding through Phosphorylation at Serine 71 of Rac1*. *Journal of Biological Chemistry*, 275(1):423–428.

Langridge, P. 2018. *The Barley Genome*, pages 1–10. Springer-Verlag GmbH.

Lavy, M., Bloch, D., Hazak, O., Gutman, I., Poraty, L., Sorek, N., Sternberg, H., and Yalovsky, S. 2007. A Novel ROP/RAC Effector Links Cell Polarity, Root-meristem Maintenance, and Vesicle Trafficking. *Current Biology*, 17(11):947–952.

Lavy, M., Bracha-Drori, K., Sternberg, H., and Yalovsky, S. 2002. A Cell-specific, Prenylation-independent Mechanism Regulates Targeting of Type II RACs. *The Plant Cell*, 14(10):2431–2450.

Lavy, M. and Yalovsky, S. 2006. Association of Arabidopsis Type-II ROPs with the Plasma Membrane Requires a Conserved C-terminal Sequence Motif and a Proximal Polybasic Domain. *The Plant Journal*, 46(6):934–947.

Lawson, C. D. and Ridley, A. J. 2018. Rho GTPase Signaling Complexes in Cell Migration and Invasion. *Journal of Cell Biology*, 217(2):447–457.

Lenoir, G., D'Ambrosio, J. M., Dieudonné, T., and Čopič, A. 2021. Transport Pathways That Contribute to the Cellular Distribution of Phosphatidylserine. *Frontiers in Cell and Developmental Biology*, 9.

Lewis, J. D., Wan, J., Ford, R., Gong, Y., Fung, P., Nahal, H., Wang, P. W., Desveaux, D., and Guttman, D. S. 2012. Quantitative Interactor Screening with Next-Generation Sequencing (QIS-Seq) Identifies *Arabidopsis thaliana* MLO2 as a Target of the *Pseudomonas syringae* Type III Effector HopZ2. *BMC Genomics*, 13(1):8.

Li, H., Luo, N., Wang, W., Liu, Z., Chen, J., Zhao, L., Tan, L., Wang, C., Qin, Y., Li, C., et al. 2018. The REN4 Rheostat Dynamically Coordinates the Apical and Lateral Domains of *Arabidopsis* Pollen Tubes. *Nature Communications*, 9(1):1–15.

Li, S., Gu, Y., Yan, A., Lord, E., and Yang, Z.-B. 2008. RIP1 (ROP Interactive Partner 1)/ICR1 Marks Pollen Germination Sites and May Act in the ROP1 Pathway in the Control of Polarized Pollen Growth. *Molecular Plant*, 1(6):1021–1035.

Li, S., Wang, Q., Wang, Y., Chen, X., and Wang, Z. 2009. PLC-γ1 and Rac1 Coregulate EGF-Induced Cytoskeleton Remodeling and Cell Migration. *Molecular Endocrinology*, 23(6):901–913.

Lin, D., Cao, L., Zhou, Z., Zhu, L., Ehrhardt, D., Yang, Z., and Fu, Y. 2013. Rho GTPase Signaling Activates Microtubule Severing to Promote Microtubule Ordering in *Arabidopsis*. *Current Biology*, 23(4):290–297.

Lin, F., Krishnamoorthy, P., Schubert, V., Hause, G., Heilmann, M., and Heilmann, I. 2019. A Dual Role for Cell Plate-associated PI4Kβ in Endocytosis and Phragmoplast Dynamics During Plant Somatic Cytokinesis. *The EMBO Journal*, 38(4).

Liu, H.-T., Huang, W.-D., Pan, Q.-H., Weng, F.-H., Zhan, J.-C., Liu, Y., Wan, S.-B., and Liu, Y.-Y. 2006. Contributions of PIP_2-specific Phospholipase C and Free Salicylic Acid to Heat Acclimation-induced Thermotolerance in Pea Leaves. *Journal of Plant Physiology*, 163(4):405–416.

Liu, J., Elmore, J. M., Fuglsang, A. T., Palmgren, M. G., Staskawicz, B. J., and Coaker, G. 2009a. RIN4 Functions with Plasma Membrane H^+-ATPases to Regulate Stomatal Apertures during Pathogen Attack. *PLOS Biology*, 7(6):1–16.

Liu, J., Elmore, J. M., Lin, Z.-J. D., and Coaker, G. 2011. A Receptor-like Cytoplasmic Kinase Phosphorylates the Host Target RIN4, Leading to the Activation of a Plant Innate Immune Receptor. *Cell Host & Microbe*, 9(2):137–146.

Liu, Y., Boukhelifa, M., Tribble, E., and Bankaitis, V. A. 2009b. Functional Studies of the Mammalian Sac1 Phosphoinositide Phosphatase. *Advances in Enzyme Regulation*, 49(1):75–86.

Livak, K. J. and Schmittgen, T. D. 2001. Analysis of Relative Gene Expression Data Using Real-time Quantitative PCR and the $2^{-\Delta\Delta CT}$ Method. *Methods*, 25(4):402–408.

Lu, D., Lin, W., Gao, X., Wu, S., Cheng, C., Avila, J., Heese, A., Devarenne, T. P., He, P., and Shan, L. 2011. Direct Ubiquitination of Pattern Recognition Receptor FLS2 Attenuates Plant Innate Immunity. *Science*, 332(6036):1439–1442.

Lu, S., Wang, J., Chitsaz, F., Derbyshire, M. K., Geer, R. C., Gonzales, N. R., Gwadz, M., Hurwitz, D. I., Marchler, G. H., Song, J. S., Thanki, N., Yamashita, R. A., Yang, M., Zhang, D., Zheng, C., Lanczycki, C. J., and Marchler-Bauer, A. 2020. CDD/SPARCLE: the Conserved Domain Database in 2020. *Nucleic Acids Research*, 48:265–268.

Luna, E., Pastor, V., Robert, J., Flors, V., Mauch-Mani, B., and Ton, J. 2011. Callose Deposition: A Multifaceted Plant Defense Response. *Molecular Plant-Microbe Interactions*, 24(2):183–193.

Lybarger, L., Dempsey, D., Patterson, G. H., Piston, D. W., Kain, S. R., and Chervenak, R. 1998. Dual-color Flow Cytometric Detection of Fluorescent Proteins Using Single-laser (488-nm) Excitation. *Cytometry*, 31(3):147–152.

Lämmli, U. K. 1970. Cleavage of Structural Proteins during the Assembly of the Head of Bacteriophage T4. *Nature*, 227(5259):680–685.

Lück, S., Kreszies, T., Strickert, M., Schweizer, P., Kuhlmann, M., and Douchkov, D. 2019. siRNA-Finder (si-Fi) Software for RNAi-Target Design and Off-Target Prediction. *Frontiers in Plant Science*, 10.

Macho, A. P., Schwessinger, B., Ntoukakis, V., Brutus, A., Segonzac, C., Roy, S., Kadota, Y., Oh, M.-H., Sklenar, J., Derbyshire, P., Lozano-Durán, R., Malinovsky, F. G., Monaghan, J., Menke, F. L., Huber, S. C., He, S. Y., and Zipfel, C. 2014. A Bacterial Tyrosine Phosphatase Inhibits Plant Pattern Recognition Receptor Activation. *Science*, 343(6178):1509–1512.

Macho, A. P. and Zipfel, C. 2014. Plant PRRs and the Activation of Innate Immune Signaling. *Molecular Cell*, 54(2):263–272.

Macho, A. P. and Zipfel, C. 2015. Targeting of Plant Pattern Recognition Receptor-triggered Immunity by Bacterial Type-III Secretion System Effectors. *Current Opinion in Microbiology*, 23:14–22.

Mackey, D., Holt, B. F., Wiig, A., and Dangl, J. L. 2002. RIN4 Interacts with *Pseudomonas syringae* Type III Effector Molecules and Is Required for RPM1-Mediated Resistance in *Arabidopsis*. *Cell*, 108(6):743–754.

Makepeace, J. C., Oxley, S. J. P., Havis, N. D., Hackett, R., Burke, J. I., and Brown, J. K. M. 2007. Associations between Fungal and Abiotic Leaf Spotting and the Presence of Mlo Alleles in Barley. *Plant Pathology*, 56(6):934–942.

Malinovsky, F. G., Fangel, J. U., and Willats, W. G. T. 2014. The Role of the Cell Wall in Plant Immunity. *Frontiers in Plant Science*, 5.

Manoharan, K., Chae, H. S., Myoung, J., Cho, S. H., Shin, S. H., Cho, B. H., and Lee, W. S. 2000. Synthesis of Phosphatidylserine in Carrot Cells Cultured under Carbon-source Starvation. *Plant and Cell Physiology*, 41(10):1143–1148.

Mao, Y. and Tan, S. 2021. Functions and Mechanisms of SAC Phosphoinositide Phosphatases in Plants. *Frontiers in Plant Science*, 12.

Mascher, M. 2021. Pseudomolecules and Annotation of the Third Version of the Reference Genome Sequence Assembly of Barley cv. Morex [Morex V3].

Mascher, M., Gundlach, H., Himmelbach, A., Beier, S., Twardziok, S. O., Wicker, T., Radchuk, V., Dockter, C., Hedley, P. E., Russell, J., Bayer, M., Ramsay, L., Liu, H., Haberer, G., Zhang, X.-Q., Zhang, Q., Barrero, R. A., Li, L., Taudien, S., Groth, M., Felder, M., Hastie, A., Šimková, H., Staňková, H., Vrána, J., Chan, S., Muñoz-Amatriaín, M., Ounit, R., Wanamaker, S., Bolser, D., Colmsee, C., Schmutzer, T., Aliyeva-Schnorr, L., Grasso, S., Tanskanen, J., Chailyan, A., Sampath, D., Heavens, D., Clissold, L., Cao, S., Chapman, B., Dai, F., Han, Y., Li, H., Li, X., Lin, C., McCooke, J. K., Tan, C., Wang, P., Wang, S., Yin, S., Zhou, G., Poland, J. A., Bellgard, M. I., Borisjuk, L., Houben, A., Doležel, J., Ayling, S., Lonardi, S., Kersey, P., Langridge, P., Muehlbauer, G. J., Clark, M. D., Caccamo, M., Schulman, A. H., Mayer, K. F. X., Platzer, M., Close, T. J., Scholz, U., Hansson, M., Zhang, G., Braumann, I., Spannagl, M., Li, C., Waugh, R., and Stein, N. 2017. A Chromosome Conformation Capture Ordered Sequence of the Barley Genome. *Nature*, 544(7651):427–433.

Mauch-Mani, B., Baccelli, I., Luna, E., and Flors, V. 2017. Defense Priming: An Adaptive Part of Induced Resistance. *Annual Review of Plant Biology*, 68:485–512.

McCollum, C. 2021. *Investigation on Barley ROP INTERACTIVE PARTNER Proteins and Their Function in Barley Disease Susceptibility*. Dissertation, Technische Universität München, München.

McCollum, C., Engelhardt, S., Weiss, L., and Hückelhoven, R. 2020. ROP INTERACTIVE PARTNER b Interacts with RACB and Supports Fungal Penetration into Barley Epidermal Cells. *Plant Physiology*, 184(2):823–836.

Mergner, J., Frejno, M., List, M., Papacek, M., Chen, X., Chaudhary, A., Samaras, P., Richter, S., Shikata, H., Messerer, M., Lang, D., Altmann, S., Cyprys, P., Zolg, D. P., Mathieson, T., Bantscheff, M., Hazarika, R. R., Schmidt, T., Dawid, C., Dunkel, A., Hofmann, T., Sprunck, S., Falter-Braun, P., Johannes, F., Mayer, K. F. X., Jürgens, G., Wilhelm, M., Baumbach, J., Grill, E., Schneitz, K., Schwechheimer, C., and Kuster, B. 2020. Mass-spectrometry-based Draft of the *Arabidopsis* Proteome. *Nature*, 579(7799):409–414.

Miki, D., Itoh, R., and Shimamoto, K. 2005. RNA Silencing of Single and Multiple Members in a Gene Family of Rice. *Plant Physiology*, 138(4):1903–1913.

Mishina, T. E. and Zeier, J. 2007. Pathogen-associated Molecular Pattern Recognition rather than Development of Tissue Necrosis Contributes to Bacterial Induction of Systemic Acquired Resistance in *Arabidopsis*. *The Plant Journal*, 50(3):500–513.

Molendijk, A. J., Bischoff, F., Rajendrakumar, C. S. V., Friml, J., Braun, M., Gilroy, S., and Palme, K. 2001. *Arabidopsis thaliana* ROP GTPases are Localized to Tips of Root Hairs and Control Polar Growth. *The EMBO Journal*, 20(11):2779–2788.

Moriura, N., Matsuda, Y., Oichi, W., Nakashima, S., Hirai, T., Sameshima, T., Nonomura, T., Kakutani, K., Kusakari, S.-i., Higashi, K., et al. 2006. Consecutive Monitoring of Lifelong Production of Conidia by Individual Conidiophores of *Blumeria graminis* f.sp. *hordei* on Barley Leaves by Digital Microscopic Techniques with Electrostatic Micromanipulation. *Mycological Research*, 110(1):18–27.

Mueller-Roeber, B. and Pical, C. 2002. Inositol Phospholipid Metabolism in *Arabidopsis*. Characterized and Putative Isoforms of Inositol Phospholipid Kinase and Phosphoinositide-Specific Phospholipase C. *Plant Physiology*, 130(1):22–46.

Nakagawa, T., Kurose, T., Hino, T., Tanaka, K., Kawamukai, M., Niwa, Y., Toyooka, K., Matsuoka, K., Jinbo, T., and Kimura, T. 2007. Development of Series of Gateway Binary Vectors, pGWBs, for Realizing Efficient Construction of Fusion Genes for Plant Transformation. *Journal of Bioscience and Bioengineering*, 104(1):34–41.

Nandi, A., Welti, R., and Shah, J. 2004. The *Arabidopsis thaliana* Dihydroxyacetone Phosphate Reductase Gene SUPPRESSOR OF FATTY ACID DESATURASE DEFICIENCY 1 Is Required for Glycerolipid Metabolism and for the Activation of Systemic Acquired Resistance. *The Plant Cell*, 16(2):465–477.

Ngou, B. P. M., Ahn, H.-K., Ding, P., and Jones, J. D. G. 2021. Mutual Potentiation of Plant Immunity by Cell-surface and Intracellular Receptors. *Nature*, 592(7852):110–115.

Ngou, B. P. M., Ding, P., and Jones, J. D. G. 2022. Thirty Years of Resistance: Zig-zag through the Plant Immune System. *The Plant Cell*, 34(5):1447–1478.

Noack, L. C. and Jaillais, Y. 2017. Precision Targeting by Phosphoinositides: How PIs Direct Endomembrane Trafficking in Plants. *Current Opinion in Plant Biology*, 40:22–33.

Noack, L. C. and Jaillais, Y. 2020. Functions of Anionic Lipids in Plants. *Annual Review of Plant Biology*, 71:71–102.

Nottensteiner, M., Zechmann, B., McCollum, C., and Hückelhoven, R. 2018. A Barley Powdery Mildew Fungus Non-autonomous Retrotransposon Encodes a Peptide that Supports Penetration Success on barley. *Journal of Experimental Botany*, 69(15):3745–3758.

Novakova, P., Hirsch, S., Feraru, E., Tejos, R., van Wijk, R., Viaene, T., Heilmann, M., Lerche, J., Rycke, R. D., Feraru, M. I., Grones, P., Montagu, M. V., Heilmann, I., Munnik, T., and Friml, J. 2014. SAC Phosphoinositide Phosphatases at the Tonoplast Mediate Vacuolar Function in *Arabidopsis*. *Proceedings of the National Academy of Sciences*, 111(7):2818–2823.

Nühse, T. S., Bottrill, A. R., Jones, A. M. E., and Peck, S. C. 2007. Quantitative Phosphoproteomic Analysis of Plasma Membrane Proteins Reveals Regulatory Mechanisms of Plant Innate Immune Responses. *The Plant Journal*, 51(5):931–940.

Nürnberger, T., Brunner, F., Kemmerling, B., and Piater, L. 2004. Innate Immunity in Plants and Animals: Striking Similarities and Obvious Differences. *Immunological Reviews*, 198(1):249–266.

Nürnberger, T. and Lipka, V. 2005. Non-host Resistance in Plants: New Insights into an Old Phenomenon. *Molecular Plant Pathology*, 6(3):335–345.

Oberoi, T. K., Dogan, T., Hocking, J. C., Scholz, R.-P., Mooz, J., Anderson, C. L., Karreman, C., Meyer zu Heringdorf, D., Schmidt, G., Ruonala, M., Namikawa, K., Harms, G. S., Carpy, A., Macek, B., Köster, R. W., and Rajalingam, K. 2012. IAPs Regulate the Plasticity of Cell Migration by Directly Targeting Rac1 for Degradation. *The EMBO Journal*, 31(1):14–28.

Oerke, E.-C. 2006. Crop Losses To Pests. *The Journal of Agricultural Science*, 144(1):31–43.

Opalski, K. S., Schultheiss, H., Kogel, K.-H., and Hückelhoven, R. 2005. The Receptor-like MLO Protein and the RAC/ROP Family G-protein RACB Modulate Actin Reorganization in Barley Attacked by the Biotrophic Powdery Mildew Fungus *Blumeria graminis* f.sp. *hordei*. *The Plant Journal*, 41(2):291–303.

O'Connell, R. J. and Panstruga, R. 2006. Tête à Tête Inside a Plant Cell: Establishing Compatibility between Plants and Biotrophic Fungi and Oomycetes. *New Phytologist*, 171(4):699–718.

Park, S.-W., Kaimoyo, E., Kumar, D., Mosher, S., and Klessig, D. F. 2007. Methyl Salicylate Is a Critical Mobile Signal for Plant Systemic Acquired Resistance. *Science*, 318(5847):113–116.

Pathuri, I. P., Zellerhoff, N., Schaffrath, U., Hensel, G., Kumlehn, J., Kogel, K.-H., Eichmann, R., and Hückelhoven, R. 2008. Constitutively Activated Barley ROPs Modulate Epidermal Cell Size, Defense Reactions and Interactions with Fungal Leaf Pathogens. *Plant Cell Reports*, 27(12):1877–1887.

Pavan, S., Jacobsen, E., Visser, R. G. F., and Bai, Y. 2010. Loss of Susceptibility as a Novel Breeding Strategy for Durable and Broad-spectrum Resistance. *Molecular Breeding*, 25(1):1.

Pedersen, C., van Themaat, E. V. L., McGuffin, L. J., Abbott, J. C., Burgis, T. A., Barton, G., Bindschedler, L. V., Lu, X., Maekawa, T., Weßling, R., Cramer, R., Thordal-Christensen, H., Panstruga, R., and Spanu, P. D. 2012. Structure and Evolution of Barley Powdery Mildew Effector Candidates. *BMC Genomics*, 13(1):694.

Peng, J., Schwartz, D., Elias, J. E., Thoreen, C. C., Cheng, D., Marsischky, G., Roelofs, J., Finley, D., and Gygi, S. P. 2003. A Proteomics Approach to Understanding Protein Ubiquitination. *Nature Biotechnology*, 21(8):921–926.

Peng, Y., van Wersch, R., and Zhang, Y. 2018. Convergent and Divergent Signaling in PAMP-triggered Immunity and Effector-triggered Immunity. *Molecular Plant-Microbe Interactions*, 31(4):403–409.

Peterhansel, C., Freialdenhoven, A., Kurth, J., Kolsch, R., and Schulze-Lefert, P. 1997. Interaction Analyses of Genes Required for Resistance Responses to Powdery Mildew in Barley Reveal Distinct Pathways Leading to Leaf Cell Death. *The Plant Cell*, 9(8):1397–1409.

Petre, B. and Kamoun, S. 2014. How Do Filamentous Pathogens Deliver Effector Proteins into Plant Cells? *PLOS Biology*, 12(2):1–7.

Pieterse, C. M., Zamioudis, C., Berendsen, R. L., Weller, D. M., Van Wees, S. C., and Bakker, P. A. 2014. Induced Systemic Resistance by Beneficial Microbes. *Annual Review of Phytopathology*, 52:347–375.

Piffanelli, P., Ramsay, L., Waugh, R., Benabdelmouna, A., D'Hont, A., Hollricher, K., Jørgensen, J. H., Schulze-Lefert, P., and Panstruga, R. 2004. A Barley Cultivation-associated Polymorphism Conveys Resistance to Powdery Mildew. *Nature*, 430(7002):887–891.

Piffanelli, P., Zhou, F., Casais, C., Orme, J., Jarosch, B., Schaffrath, U., Collins, N. C., Panstruga, R., and Schulze-Lefert, P. 2002. The Barley MLO Modulator of Defense and Cell Death is Responsive to Biotic and Abiotic Stress Stimuli. *Plant Physiology*, 129(3):1076–1085.

Platre, M. P., Bayle, V., Armengot, L., Bareille, J., del Mar Marquès-Bueno, M., Creff, A., Maneta-Peyret, L., Fiche, J.-B., Nollmann, M., Miège, C., Moreau, P., Martinière, A., and Jaillais, Y. 2019. Developmental Control of Plant Rho GTPase Nano-organization by the Lipid Phosphatidylserine. *Science*, 364(6435):57–62.

Platre, M. P., Noack, L. C., Doumane, M., Bayle, V., Simon, M. L. A., Maneta-Peyret, L., Fouillen, L., Stanislas, T., Armengot, L., Pejchar, P., Caillaud, M.-C., Potocký, M., Čopič, A., Moreau, P., and Jaillais, Y. 2018. A Combinatorial Lipid Code Shapes the Electrostatic Landscape of Plant Endomembranes. *Developmental Cell*, 45(4):465–480.

Pliego, C., Nowara, D., Bonciani, G., Gheorghe, D. M., Xu, R., Surana, P., Whigham, E., Nettleton, D., Bogdanove, A. J., and Wise, R. P. 2013. Host-induced Gene Silencing in Barley Powdery Mildew Reveals a Class of Ribonuclease-like Effectors. *Molecular Plant-Microbe Interactions*, 26(6):633–642.

Pokotylo, I., Kravets, V., Martinec, J., and Ruelland, E. 2018. The Phosphatidic Acid Paradox: Too Many Actions for one Molecule Class? Lessons from Plants. *Progress in Lipid Research*, 71:43–53.

Potocký, M., Pleskot, R., Pejchar, P., Vitale, N., Kost, B., and Žárský, V. 2014. Live-cell Imaging of Phosphatidic Acid Dynamics in Pollen Tubes Visualized by Spo20p-derived Biosensor. *New Phytologist*, 203(2):483–494.

Qin, L., Zhou, Z., Li, Q., Zhai, C., Liu, L., Quilichini, T. D., Gao, P., Kessler, S. A., Jaillais, Y., Datla, R., Peng, G., Xiang, D., and Wei, Y. 2020. Specific Recruitment of Phosphoinositide Species to the Plant-Pathogen Interfacial Membrane Underlies *Arabidopsis* Susceptibility to Fungal Infection. *The Plant Cell*, 32(5):1665–1688.

Rademacher, E. and Offringa, R. 2012. Evolutionary Adaptations of Plant AGC Kinases: From Light Signaling to Cell Polarity Regulation. *Frontiers in Plant Science*, 3.

Rao, J. N., Liu, S. V., Zou, T., Liu, L., Xiao, L., Zhang, X., Bellavance, E., Yuan, J. X.-J., and Wang, J.-Y. 2008. Rac1 Promotes Intestinal Epithelial Restitution by Increasing Ca^{2+}-influx through Interaction with Phospholipase C-γ1 after Wounding. *American Journal of Physiology-Cell Physiology*, 295(6):C1499–C1509.

Rapacz, M., Stępień, A., and Skorupa, K. 2012. Internal Standards for Quantitative RT-PCR Studies of Gene Expression under Drought Treatment in Barley (*Hordeum vulgare* L.): The Effects of Developmental Stage and Leaf Age. *Acta Physiologiae Plantarum*, 34(5):1723–1733.

Rapazote-Flores, P., Bayer, M., Milne, L., Mayer, C.-D., Fuller, J., Guo, W., Hedley, P. E., Morris, J., Halpin, C., Kam, J., McKim, S. M., Zwirek, M., Casao, M. C., Barakate, A., Schreiber, M., Stephen, G., Zhang, R., Brown, J. W. S., Waugh, R., and Simpson, C. G. 2019. BaRTv1.0: An Improved Barley Reference Transcript Dataset to Determine Accurate Changes in the Barley Transcriptome using RNA-seq. *BMC Genomics*, 20(1):968.

Reiner, T., Hoefle, C., Huesmann, C., Ménesi, D., Fehér, A., and Hückelhoven, R. 2014. The *Arabidopsis* ROP-activated Receptor-like Cytoplasmic Kinase RLCK VI_A3 is Involved in Control of Basal Resistance to Powdery Mildew and Trichome Branching. *Plant Cell Reports*, 34(3):457–468.

Reiner, T., Hoefle, C., and Hückelhoven, R. 2015. A Barley SKP1-like Protein Controls Abundance of the Susceptibility Factor RACB and Influences the Interaction of Barley with the Barley Powdery Mildew Fungus. *Molecular Plant Pathology*, 17(2):184–195.

Rentel, M. C., Lecourieux, D., Ouaked, F., Usher, S. L., Petersen, L., Okamoto, H., Knight, H., Peck, S. C., Grierson, C. S., Hirt, H., and Knight, M. R. 2004. OXI1 Kinase is Necessary for Oxidative Burst-mediated Signalling in *Arabidopsis*. *Nature*, 427(6977):858–861.

Rhee, S. G. and Choi, K. D. 1992. Regulation of Inositol Phospholipid-specific Phospholipase C Isozymes. *The Journal of Biological Chemistry*, 267:12393–6.

Ridout, C. J., Skamnioti, P., Porritt, O., Sacristan, S., Jones, J. D. G., and Brown, J. K. 2006. Multiple Avirulence Paralogues in Cereal Powdery Mildew Fungi may Contribute to Parasite Fitness and Defeat of Plant Resistance. *The Plant Cell*, 18(9):2402–2414.

Rizo, J. and Südhof, T. C. 1998. C_2-domains, Structure and Function of a Universal Ca^{2+}-binding Domain. *Journal of Biological Chemistry*, 273(26):15879–15882.

Rodriguez, P. A. and Bos, J. I. B. 2013. Toward Understanding the Role of Aphid Effectors in Plant Infestation. *Molecular Plant-Microbe Interactions*, 26(1):25–30.

Saur, I. M., Bauer, S., Kracher, B., Lu, X., Franzeskakis, L., Müller, M. C., Sabelleck, B., Kümmel, F., Panstruga, R., Maekawa, T., and Schulze-Lefert, P. 2019. Multiple Pairs of Allelic MLA Immune Receptor-Powdery Mildew AVR(A) Effectors Argue for a Direct Recognition Mechanism. *eLife*, 8.

Schaefer, A., Höhner, K., Berken, A., and Wittinghofer, A. 2011. The Unique Plant RhoGAPs are Dimeric and Contain a CRIB Motif Required for Affinity and Specificity towards Cognate Small G-proteins. *Biopolymers*, 95(6):420–433.

Scheler, B., Schnepf, V., Galgenmüller, C., Ranf, S., and Hückelhoven, R. 2016. Barley Disease Susceptibility Factor RACB Acts in Epidermal Cell Polarity and Positioning of the Nucleus. *Journal of Experimental Botany*, 67(11):3263–3275.

Schindelin, J., Arganda-Carreras, I., Frise, E., Kaynig, V., Longair, M., Pietzsch, T., Preibisch, S., Rueden, C., Saalfeld, S., Schmid, B., Tinevez, J.-Y., White, D. J., Hartenstein, V., Eliceiri, K., Tomancak, P., and Cardona, A. 2012. Fiji: An Open-source Platform for Biological-image Analysis. *Nature Methods*, 9(7):676–682.

Schmidt, G., Sehr, P., Wilm, M., Selzer, J., Mann, M., and Aktories, K. 1997. Gln 63 of Rho is Deamidated by *Escherichia coli* Cytotoxic Necrotizing Factor 1. *Nature*, 387(6634):725–729.

Schnepf, V., Vlot, A. C., Kugler, K., and Hückelhoven, R. 2018. Barley Susceptibility Factor RACB Modulates Transcript Levels of Signalling Protein Genes in Compatible Interaction with *Blumeria graminis* f.sp. *hordei*. *Molecular Plant Pathology*, 19(2):393–404.

Schrödinger, LLC 2015. The PyMOL Molecular Graphics System, Version 1.8.

Schultheiss, H., Dechert, C., Kogel, K.-H., and Hückelhoven, R. 2002. A Small GTP-Binding Host Protein Is Required for Entry of Powdery Mildew Fungus into Epidermal Cells of Barley. *Plant Physiology*, 128(4):1447–1454.

Schultheiss, H., Dechert, C., Kogel, K.-H., and Hückelhoven, R. 2003. Functional Analysis of Barley RAC/ROP G-protein Family Members in Susceptibility to the Powdery Mildew Fungus. *The Plant Journal*, 36(5):589–601.

Schultheiss, H., Preuss, J., Pircher, T., Eichmann, R., and Hückelhoven, R. 2008. Barley RIC171 Interacts with RACB *in planta* and Supports Entry of the Powdery Mildew Fungus. *Cellular Microbiology*, 10(9):1815–1826.

Schweizer, P., Christoffel, A., and Dudler, R. 1999. Transient Expression of Members of the Germin-like Gene Family in Epidermal Cells of Wheat Confers Sisease Resistance. *The Plant Journal*, 20(5):541–552.

Sherwood, J. E. and Somerville, S. C. 1990. Sequence of the *Erysiphe graminis* f.sp. *hordei* Gene Encoding β-tubulin. *Nucleic Acids Research*, 18(4):1052.

Shimada, T. L., Betsuyaku, S., Inada, N., Ebine, K., Fujimoto, M., Uemura, T., Takano, Y., Fukuda, H., Nakano, A., and Ueda, T. 2019. Enrichment of Phosphatidylinositol 4,5-Bisphosphate in the Extra-Invasive Hyphal Membrane Promotes *Colletotrichum* Infection of *Arabidopsis thaliana*. *Plant and Cell Physiology*, 60(7):1514–1524.

Shimizu, T., Nakano, T., Takamizawa, D., Desaki, Y., Ishii-Minami, N., Nishizawa, Y., Minami, E., Okada, K., Yamane, H., Kaku, H., and Shibuya, N. 2010. Two LysM Receptor Molecules, CEBiP and OsCERK1, Cooperatively Regulate Chitin Elicitor Signaling in Rice. *The Plant Journal*, 64(2):204–214.

Simon, M. L. A., Platre, M. P., Assil, S., van Wijk, R., Chen, W. Y., Chory, J., Dreux, M., Munnik, T., and Jaillais, Y. 2014. A Multi-colour/multi-affinity Marker Set to Visualize Phosphoinositide Dynamics in *Arabidopsis*. *The Plant Journal*, 77(2):322–337.

Simon, M. L. A., Platre, M. P., Marquès-Bueno, M. M., Armengot, L., Stanislas, T., Bayle, V., Caillaud, M.-C., and Jaillais, Y. 2016. A PtdIns(4)P-driven Electrostatic Field Controls Cell Membrane Identity and Signalling in Plants. *Nature Plants*, 2(7).

Singh, A., Kanwar, Poonam andPandey, A., Tyagi, A. K., Sopory, S. K., Kapoor, S., and Pandey, G. K. 2013. Comprehensive Genomic Analysis and Expression Profiling of Phospholipase C Gene Family during Abiotic Stresses and Development in Rice. *PLOS ONE*, 8(4):1–14.

Skou, J.-P. 1982. Callose Formation Responsible for the Powdery Mildew Resistance in Barley with Genes in the Mlo Locus. *Journal of Phytopathology*, 104(1):90–95.

Skou, J.-P., Jørgensen, J. H., and Lilholt, U. 1984. Comparative Studies on Callose Formation in Powdery Mildew Compatible and Incompatible Barley. *Journal of Phytopathology*, 109(2):147–168.

Smokvarska, M., Jaillais, Y., and Martinière, A. 2021. Function of Membrane Domains in Rho-of-plant Signaling. *Plant Physiology*, 185(3):663–681.

Song, F. and Goodman, R. M. 2002. Molecular Cloning and Characterization of a Rice Phosphoinositide-specific Phospholipase C Gene, *Os*PI-PLC1, that is Activated in Systemic Acquired Resistance. *Physiological and Molecular Plant Pathology*, 61(1):31–40.

Sorek, N., Bloch, D., and Yalovsky, S. 2009. Protein Lipid Modifications in Signaling and Subcellular Targeting. *Current Opinion in Plant Biology*, 12(6):714–720.

Sorek, N., Gutman, O., Bar, E., Abu-Abied, M., Feng, X., Running, M. P., Lewinsohn, E., Ori, N., Sadot, E., Henis, Y. I., and Yalovsky, S. 2011. Differential Effects of Prenylation and *S*-Acylation on Type I and II ROPs Membrane Interaction and Function. *Plant Physiology*, 155(2):706–720.

Sorek, N., Poraty, L., Sternberg, H., Buriakovsky, E., Bar, E., Lewinsohn, E., and Yalovsky, S. 2017. Corrected and Republished from: Activation Status-coupled Transient *S*-acylation Determines Membrane Partitioning of a Plant Rho-related GTPase. *Molecular and Cellular Biology*, 37(23):e00333–17.

Spanu, P. D., Abbott, J. C., Amselem, J., Burgis, T. A., Soanes, D. M., Stüber, K., van Themaat, E. V. L., Brown, J. K. M., Butcher, S. A., Gurr, S. J., Lebrun, M.-H., Ridout, C. J., Schulze-Lefert, P., Talbot, N. J., Ahmadinejad, N., Ametz, C., Barton, G. R., Benjdia, M., Bidzinski, P., Bindschedler, L. V., Both, M., Brewer, M. T., Cadle-Davidson, L., Cadle-Davidson, M. M., Collemare, J., Cramer, R., Frenkel, O., Godfrey, D., Harriman, J., Hoede, C., King, B. C., Klages, S., Kleemann, J., Knoll, D., Koti, P. S., Kreplak, J., López-Ruiz, F. J., Lu, X., Maekawa, T., Mahanil, S., Micali, C., Milgroom, M. G., Montana, G., Noir, S., O'Connell, R. J., Oberhaensli, S., Parlange, F., Pedersen, C., Quesneville, H., Reinhardt, R., Rott, M., Sacristán, S., Schmidt, S. M., Schön, M., Skamnioti, P., Sommer, H., Stephens, A., Takahara, H., Thordal-Christensen, H., Vigouroux, M., Weßling, R., Wicker, T., and Panstruga, R. 2010. Genome Expansion and Gene Loss in Powdery Mildew Fungi Reveal Tradeoffs in Extreme Parasitism. *Science*, 330(6010):1543–1546.

Spoel, S. H. and Dong, X. 2012. How Do Plants Achieve Immunity? Defence Without Specialized Immune Cells. *Nature Reviews Immunology*, 12(2):89–100.

Stanislas, T., Hüser, A., Barbosa, I. C. R., Kiefer, C. S., Brackmann, K., Pietra, S., Gustavsson, A., Zourelidou, M., Schwechheimer, C., and Grebe, M. 2015. *Arabidopsis* D6PK is a Lipid Domain-dependent Mediator of Root Epidermal Planar Polarity. *Nature Plants*, 1(11).

Stolzenburg, M. C., Aist, J. R., and Israel, H. W. 1984. The Role of Papillae in Resistance to Powdery Mildew Conditioned by the Mlo Gene in Barley. I Correlative Evidence. *Physiological Plant Pathology*, 25(3):337–346.

Sun, J., Eklund, D. M., Montes-Rodriguez, A., and Kost, B. 2015. *In vivo* Rac/Rop Localization as well as Interaction with RhoGAP and RhoGDI in Tobacco Pollen Tubes: Analysis by Low-level Expression of Fluorescent Fusion Proteins and Bimolecular Fluorescence Complementation. *The Plant Journal*, 84(1):83–98.

Tamborski, J. and Krasileva, K. V. 2020. Evolution of Plant NLRs: From Natural History to Precise Modifications. *Annual Review of Plant Biology*, 71(1):355–378.

Tanaka, K. and Heil, M. 2021. Damage-Associated Molecular Patterns (DAMPs) in Plant Innate Immunity: Applying the Danger Model and Evolutionary Perspectives. *Annual Review of Phytopathology*, 59(1):53–75. PMID: 33900789.

Tasma, I. M., Brendel, V., Whitham, S. A., and Bhattacharyya, M. K. 2008. Expression and Evolution of the Phosphoinositide-specific Phospholipase C Gene Family in *Arabidopsis thaliana*. *Plant Physiology and Biochemistry*, 46(7):627–637.

Testerink, C., Dekker, H. L., Lim, Z.-Y., Johns, M. K., Holmes, A. B., de Koster, C. G., Ktistakis, N. T., and Munnik, T. 2004. Isolation and identification of phosphatidic acid targets from plants. *The Plant Journal*, 39(4):527–536.

Teufel, F., Almagro Armenteros, J. J., Johansen, A. R., Gíslason, M. H., Pihl, S. I., Tsirigos, K. D., Winther, O., Brunak, S., von Heijne, G., and Nielsen, H. 2022. SignalP 6.0 Predicts all Five Types of Signal Peptides using Protein Language Models. *Nature Biotechnology*.

The UniProt Consortium 2020. UniProt: the Universal Protein Knowledgebase in 2021. *Nucleic Acids Research*, 49(1):480–489.

Thomas, C., Fricke, I., Scrima, A., Berken, A., and Wittinghofer, A. 2007. Structural Evidence for a Common Intermediate in Small G Protein-GEF Reactions. *Molecular Cell*, 25(1):141–149.

Thomma, B. P. H. J., Nürnberger, T., and Joosten, M. H. A. J. 2011. Of PAMPs and Effectors: The Blurred PTI-ETI Dichotomy. *The Plant Cell*, 23(1):4–15.

Tong, J., Li, L., Ballermann, B., and Wang, Z. 2013. Phosphorylation of Rac1 T108 by Extracellular Signal-regulated Kinase in Response to Epidermal Growth Factor: a Novel Mechanism to Regulate Rac1 Function. *Molecular and Cellular Biology*, 33(22):4538–4551.

Torrino, S., Visvikis, O., Doye, A., Boyer, L., Stefani, C., Munro, P., Bertoglio, J., Gacon, G., Mettouchi, A., and Lemichez, E. 2011. The E3 Ubiquitin-Ligase HACE1 Catalyzes the Ubiquitylation of Active Rac1. *Developmental Cell*, 21(5):959–965.

Tripathy, M. K., Tyagi, W., Goswami, M., Kaul, T., Singla-Pareek, S. L., Deswal, R., Reddy, M. K., and Sopory, S. K. 2012. Characterization and Functional Validation of Tobacco PLC Δ for Abiotic Stress Tolerance. *Plant Molecular Biology Reporter*, 30(2):488–497.

Troch, V., Audenaert, K., Wyand, R. A., Haesaert, G., Höfte, M., and Brown, J. K. M. 2014. Formae Speciales of Cereal Powdery Mildew: Close or Distant Relatives? *Molecular Plant Pathology*, 15(3):304–314.

Trutzenberg, A., Engelhardt, S., Weiß, L., and Hückelhoven, R. 2022. Barley Guanine Nucleotide Exchange Factor *Hv*GEF14 is an Activator of the Susceptibility Factor *Hv*RACB and Supports Host Cell Entry by *Blumeria graminis* f.sp. *hordei*. *Molecular Plant Pathology*, n/a(n/a).

Tsien, R. Y. 1998. The Green Fluorescent Protein. *Annual Review of Biochemistry*, 67(1):509–544.

Tyanova, S., Temu, T., Sinitcyn, P., Carlson, A., Hein, M. Y., Geiger, T., Mann, M., and Cox, J. 2016. The Perseus Computational Platform for Comprehensive Analysis of (Prote) Omics Data. *Nature Methods*, 13(9):731–740.

United Nations, D. o. E. and Social Affairs, P. D. 2019. World Population Prospects 2019: Highlights. *ST/ESA/SER.A/423*.

van der Hoorn, R. A. L. and Kamoun, S. 2008. From Guard to Decoy: a New Model for Perception of Plant Pathogen Effectors. *The Plant Cell*, 20(8):2009–2017.

Van Leeuwen, W., Vermeer, J. E., Gadella Jr, T. W., and Munnik, T. 2007. Visualization of Phosphatidylinositol-4,5-bisphosphate in the Plasma Membrane of Suspension-cultured Tobacco BY-2 Cells and Whole *Arabidopsis* Seedlings. *The Plant Journal*, 52(6):1014–1026.

van Schie, C. C. N. and Takken, F. L. W. 2014. Susceptibility Genes 101: How To Be A Good Host. *Annual Review of Phytopathology*, 52:551–581.

Vergne, I., Chua, J., and Deretic, V. 2003. *Mycobacterium tuberculosis* Phagosome Maturation Arrest: Selective Targeting of PI3P-Dependent Membrane Trafficking. *Traffic*, 4(9):600–606.

Vermeer, J. E. M., van Leeuwen, W., Tobeña-Santamaria, R., Laxalt, A. M., Jones, D. R., Divecha, N., Gadella, T. W. J., and Munnik, T. 2006. Visualization of PtdIns3P Dynamics in Living Plant Cells. *The Plant Journal*, 47(5):687–700.

Vernooij, B., Friedrich, L., Morse, A., Reist, R., Kolditz-Jawhar, R., Ward, E., Uknes, S., Kessmann, H., and Ryals, J. 1994. Salicylic Acid Is Not the Translocated Signal Responsible for Inducing Systemic Acquired Resistance but Is Required in Signal Transduction. *The Plant Cell*, 6(7):959–965.

Vickers, C. E., Xue, G. P., and Gresshoff, P. M. 2003. A Synthetic Xylanase as a Novel Reporter in Plants. *Plant Cell Reports*, 22(2):135–140.

Voinnet, O., Rivas, S., Mestre, P., and Baulcombe, D. 2003. An Enhanced Transient Expression System in Plants Based on Suppression of Gene Silencing by the p19 Protein of Tomato Bushy Stunt Virus. *The Plant Journal*, 33(5):949–956.

Vossen, J. H., Abd-El-Haliem, A., Fradin, E. F., Van Den Berg, G. C. M., Ekengren, S. K., Meijer, H. J. G., Seifi, A., Bai, Y., Ten Have, A., Munnik, T., Thomma, B. P. H. J., and Joosten, M. H. A. J. 2010. Identification of Tomato Phosphatidylinositol-specific Phospholipase-C (PI-PLC) Family Members and the Role of PLC4 and PLC6 in HR and Disease Resistance. *The Plant Journal*, 62(2):224–239.

Wang, C.-R., Yang, A.-F., Yue, G.-D., Gao, Q., Yin, H.-Y., and Zhang, J.-R. 2008. Enhanced Expression of Phospholipase C 1 (*Zm*PLC1) Improves Drought Tolerance in Transgenic Maize. *Planta*, 227(5):1127–1140.

Wang, Q., Li, Y., Ishikawa, K., Kosami, K.-i., Uno, K., Nagawa, S., Tan, L., Du, J., Shimamoto, K., and Kawano, Y. 2018. Resistance Protein Pit Interacts with the GEF *Os*SPK1 to Activate *Os*Rac1 and Trigger Rice Immunity. *Proceedings of the National Academy of Sciences*, 115(49):E11551–E11560.

Wang, Y., Mousley, C. J., Lete, M. G., and Bankaitis, V. A. 2019. An Equal Opportunity Collaboration between Lipid Metabolism and Proteins in the Control of Membrane Trafficking in the trans-Golgi and Endosomal Systems. *Current Opinion in Cell Biology*, 59:58–72.

Waterhouse, A., Bertoni, M., Bienert, S., Studer, G., Tauriello, G., Gumienny, R., Heer, F. T., de Beer, T. A., Rempfer, C., Bordoli, L., Lepore, R., and Schwede, T. 2018. SWISS-MODEL: Homology Modelling of Protein Structures and Complexes. *Nucleic Acids Research*, 46(W1):W296–W303.

Waterhouse, A. M., Procter, J. B., Martin, D. M. A., Clamp, M., and Barton, G. J. 2009. Jalview Version 2 — a Multiple Sequence Alignment Editor and Analysis Workbench. *Bioinformatics*, 25(9):1189–1191.

Weidtkamp-Peters, S. and Stahl, Y. 2017. *Plant Receptor Kinases*, chapter The Use of FRET/FLIM to Study Proteins Interacting with Plant Receptor Kinases, pages 163–175. Springer New York, New York.

Weiß, L., Gaelings, L., Reiner, T., Mergner, J., Kuster, B., Fehér, A., Hensel, G., Gahrtz, M., Kumlehn, J., Engelhardt, S., and Hückelhoven, R. 2022. Posttranslational Modification of the RHO of Plants Protein RACB by Phosphorylation and Cross-Kingdom Conserved Ubiquitination. *PLOS ONE*, 17(3):1–30.

Wennerberg, K., Rossman, K. L., and Der, C. J. 2005. The Ras Superfamily at a Glance. *Journal of Cell Science*, 118(5):843–846.

Wicker, T., Oberhaensli, S., Parlange, F., Buchmann, J. P., Shatalina, M., Roffler, S., Ben-David, R., Doležel, J., Šimková, H., Schulze-Lefert, P., Spanu, P. D., Bruggmann, R., Amselem, J., Quesneville, H., van Themaat, E. V. L., Paape, T., Shimizu, K. K., and Keller, B. 2013. The Wheat Powdery Mildew Genome Shows the Unique Evolution of an Obligate Biotroph. *Nature Genetics*, 45(9):1092–1096.

Williams, R. L. 1999. Mammalian Phosphoinositide-specific Phospholipase C. *BBA - Molecular and Cell Biology of Lipids*, 1441(2):255–267.

Wilton, M., Subramaniam, R., Elmore, J., Felsensteiner, C., Coaker, G., and Desveaux, D. 2010. The Type III Effector $\text{HopF2}_{\text{Pto}}$ Targets *Arabidopsis* RIN4 Protein to Promote *Pseudomonas syringae* Virulence. *Proceedings of the National Academy of Sciences*, 107(5):2349–2354.

Winge, P., Brembu, T., Kristensen, R., and Bones, A. M. 2000. Genetic Structure and Evolution of RAC-GTPases in *Arabidopsis thaliana*. *Genetics*, 156(4):1959–1971.

Wolter, M., Hollricher, K., Salamini, F., and Schulze-Lefert, P. 1993. The *mlo* Resistance Alleles to Powdery Mildew Infection in Barley Trigger a Developmentally Controlled Defence Mimic Phenotype. *Molecular and General Genetics*, 239(1):122–128.

Wong, H. L., Pinontoan, R., Hayashi, K., Tabata, R., Yaeno, T., Hasegawa, K., Kojima, C., Yoshioka, H., Iba, K., Kawasaki, T., and Shimamoto, K. 2007. Regulation of Rice NADPH Oxidase by Binding of Rac GTPase to Its N-Terminal Extension. *The Plant Cell*, 19(12):4022–4034.

Wright, A. J., Thomas, B. J., and Carver, T. L. W. 2002. Early Adhesion of *Blumeria graminis* to Plant and Artificial Surfaces Demonstrated by Centrifugation. *Physiological and Molecular Plant Pathology*, 61(4):217–226.

Wu, G., Li, H., and Yang, Z. 2000. *Arabidopsis* RopGAPs are a Novel Family of Rho GTPase-activating Proteins that Require the Cdc42/Rac-interactive Binding Motif for ROP-specific GTPase Stimulation. *Plant Physiology*, 124(4):1625–1636.

Yalovsky, S. 2015. Protein Lipid Modifications and the Regulation of ROP GTPase Function. *Journal of Experimental Botany*, 66(6):1617–1624.

Yamaguchi, K., Imai, K., Akamatsu, A., Mihashi, M., Hayashi, N., Shimamoto, K., and Kawasaki, T. 2012. SWAP70 Functions as a Rac/ROP Guanine Nucleotide-exchange Factor in Rice. *The Plant Journal*, 70(3):389–397.

Yang, Y., Li, R., and Qi, M. 2000. *In vivo* Analysis of Plant Promoters and Transcription Factors by Agroinfiltration of Tobacco Leaves. *The Plant Journal*, 22(6):543–551.

Yang, Z. 2002. Small GTPases: Versatile Signaling Switches in Plants. *The Plant Cell*, 14(1):375–388.

Yu, X., Feng, B., He, P., and Shan, L. 2017. From Chaos to Harmony: Responses and Signaling upon Microbial Pattern Recognition. *Annual Review of Phytopathology*, 55:109–137.

Yuan, M., Jiang, Z., Bi, G., Nomura, K., Liu, M., Wang, Y., Cai, B., Zhou, J.-M., He, S. Y., and Xin, X.-F. 2021. Pattern-Recognition Receptors are Required for NLR-mediated Plant Immunity. *Nature*, 592(7852):105–109.

Zebell, S. G. and Dong, X. 2015. Cell-cycle Regulators and Cell Death in Immunity. *Cell Host & Microbe*, 18(4):402–407.

Zhang, Z., Henderson, C., Perfect, E., Carver, T. L. W., Thomas, B. J., Skamnioti, P., and Gurr, S. J. 2005. Of Genes and Genomes, Needles and Haystacks: *Blumeria graminis* and Functionality. *Molecular Plant Pathology*, 6(5):561–575.

Zhao, J., Mialki, R. K., Wei, J., Coon, T. A., Zou, C., Chen, B. B., Mallampalli, R. K., and Zhao, Y. 2013. SCF E3 ligase F-box Protein Complex SCF^{FBXL19} Regulates Cell Migration by Mediating Rac1 Ubiquitination and Degradation. *The FASEB Journal*, 27(7):2611–2619.

Zhao, Y., Yan, A., Feijó, J. A., Furutani, M., Takenawa, T., Hwang, I., Fu, Y., and Yang, Z. 2010. Phosphoinositides Regulate Clathrin-Dependent Endocytosis at the Tip of Pollen Tubes in *Arabidopsis* and Tobacco. *The Plant Cell*, 22(12):4031–4044.

Zhong, R. and Ye, Z.-H. 2003. The SAC Domain-Containing Protein Gene Family in *Arabidopsis*. *Plant Physiology*, 132(2):544–555.

Acknowledgements

Als Erstes möchte ich mich bei Prof. Dr. Ralph Hückelhoven für das Bereitstellen dieses überaus spannenden Promotionsthemas bedanken. Darüber hinaus möchte ich aber auch besonders für das Vertrauen Danke sagen, das mir entgegengebracht wurde, wenn ich mal wieder etwas Neues ausprobieren wollte. Weiterhin möchte ich mich für seinen fachlichen Input und seine Betreuung von sowohl mir, als auch meinem Promotionsthema bedanken.
Ich bedanke mich bei Prof. Dr. Brigitte Poppenberger-Sieberer und Prof. Dr. J. Philipp Benz für die freundliche Übernahme der Rollen der Zweitprüferin bzw. des Prüfungsvorsitzes.
Bei meinem Mentor Prof. Dr. Georg Kreimer möchte ich mich für die konstruktiven Gespräche während meiner Promotion bedanken.
Prof. Dr. Remco Stam und Dr. Martin Stegmann danke ich dafür, dass sie Teil meines Promotionskomitees waren, welches mich dabei unterstützt hat die erfolgsversprechenden Projekte zu erkennen und zu verfolgen.
Dr. Michaela Stegmann danke ich für ihre ausgezeichnete Einführung in die Welt der Konfokalmikroskopie.
Mein herzlicher Dank gilt Dr. Julia Mergner für die Durchführung zahlloser Massenspektrometrieversuche und ihre Unterstützung bei der Auswertung der schier endlosen Exceltabellen.
Bei Prof. Dr. Ingo Heilmann möchte ich mich für die freundliche Aufnahme an seinem Lehrstuhl während meines Forschungsaufenthaltes in Halle und die tolle Kollaboration bei den Lipidbindestudien bedanken. Weiterhin möchte ich besonders Dr. Mareike Heilmann und Dr. Irene Stenzel für die Erklärung und Durchführung von Versuchen im Rahmen der Kollaboration danken.
Bei einer Person kann ich mich gar nicht genug bedanken: Dr. Stefan Engelhardt. Ohne ihn und seine Hilfe was Angelegenheiten im Labor und außerhalb angeht würde es diese Arbeit nicht geben. Sein Fachwissen und seine Unterstützung sowohl bei der Planung, als auch bei der Durchführung von Versuchen bleibt für mich unschätzbar. Danke, Stefan.
Ein großer Dank gilt auch allen Phytos für meine unvergessliche Zeit hier am Lehrstuhl. Ganz besonders möchte ich Dr. Christopher McCollum, Lars Raasch, Sabine Eschrig und Tim Gerster für die unzähligen lustigen Momente und die gegenseitige Motivation danken. Ohne euch wäre es langweilig geworden.
Christoph Bartram, Lana Gaelings und Marina Hijano Moreno möchte ich für ihre tolle Mitarbeit in meinen Projekten im Rahmen von Praktika und Abschlussarbeiten danken.
Ganz besonders möchte ich mich bei den (technischen) Assistentinnen bedanken. Johanna, Vanessa, Lena, Luisa und Resi, ohne euch würde nichts im Labor funktion-

ieren. Vielen Dank für eure tatkräftige Unterstützung bei der Durchführung meiner Projekte!
Bei Claudia, Daniela und Traudl möchte ich mich herzlich für die Hilfe bei Verwaltungsangelegenheiten bedanken.
Dem SFB924 und der Graduiertenschule der TUM School of Life Sciences danke ich für die Bereitstellung finanzieller Mittel während meiner Promotion.
Mein herzlichstes Dankeschön geht an meine Familie und an meine Freunde. Ohne eure Unterstützung außerhalb des Labors hätte ich es nicht geschafft!
Zu guter Letzt geht mein Dank an meine wundervolle Frau Isi, dafür, dass sie immer an mich geglaubt und mich durch die Höhen und Tiefen meiner Promotion begleitet hat.

Supplementary Information

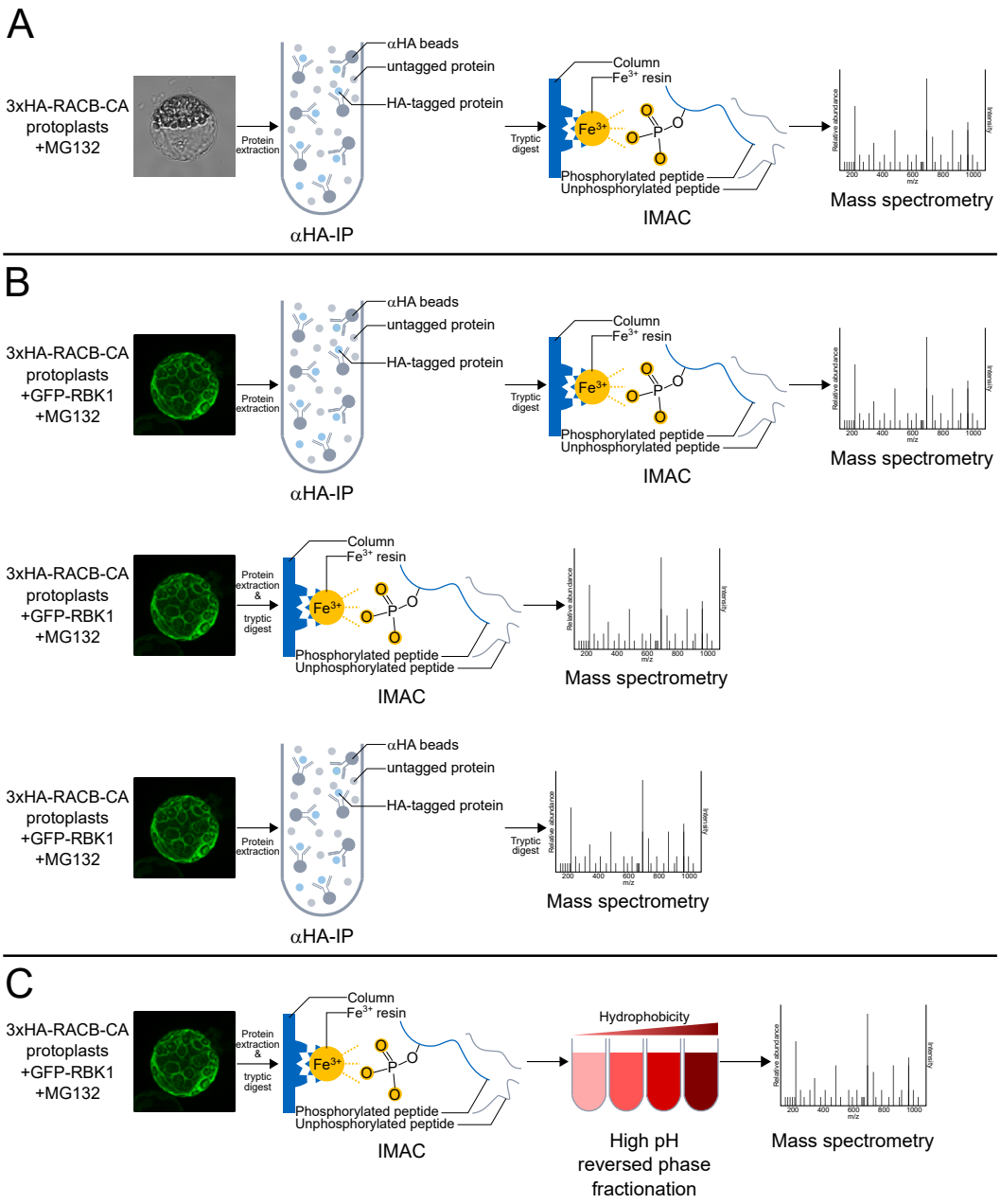

Figure S1: Schematic illustration of *in vivo* RACB-CA phosphosite screenings. In all screenings, mesophyll protoplasts were prepared from 3xHA-RACB-CA-overexpressing plants and treated with the proteasome inhibitor MG132. (**A**) In the first attempt, 3xHA-RACB-CA was enriched and purified via αHA-IP after protein extraction. Eluted proteins were digested using trypsin, and phosphopeptides were enriched via IMAC before identification via MS. (**B**) In the second experiment, 3xHA-RACB-CA-protoplasts were super-transformed with GFP-RBK1 before protein extraction and selective processing via αHA-IP and/or IMAC. Phosphorylated peptides were identified via MS. (**C**) In the third screening, GFP-RBK1-transformed 3xHA-RACB-CA-protoplasts were directly used for protein extraction, tryptic digest and IMAC. Resulting samples were further split according to their hydrophobicity via high pH reversed-phase fractionation before MS-analysis. Subfigures (**B**) and (**C**) were modified after Fig. S2 of Weiß et al. (2022).

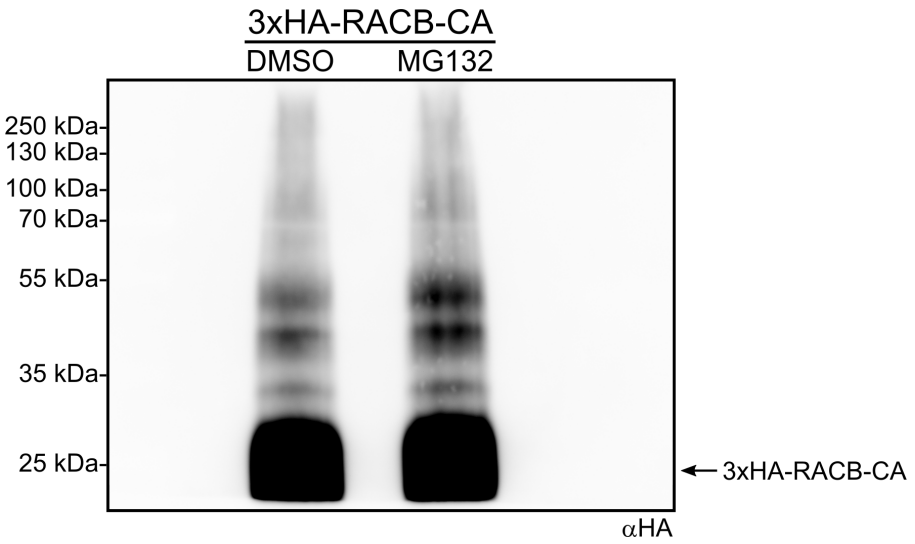

Figure S2: Ubiquitin-like laddering of 3xHA-RACB-CA is independent of MG132.
3xHA-RACB-CA and higher molecular weight bands could be observed independent of proteasome inhibition in an αHA Western blot. First leaves of transgenic barley plants overexpressing 3xHA-RACB-CA were floated on a solution either containing the proteasome inhibitor MG132 or its solvent DMSO. Extracted proteins were enriched via αHA-IP and analysed via SDS-PAGE and Western blot. This figure was modified after Fig. S4 of Weiß et al. (2022).

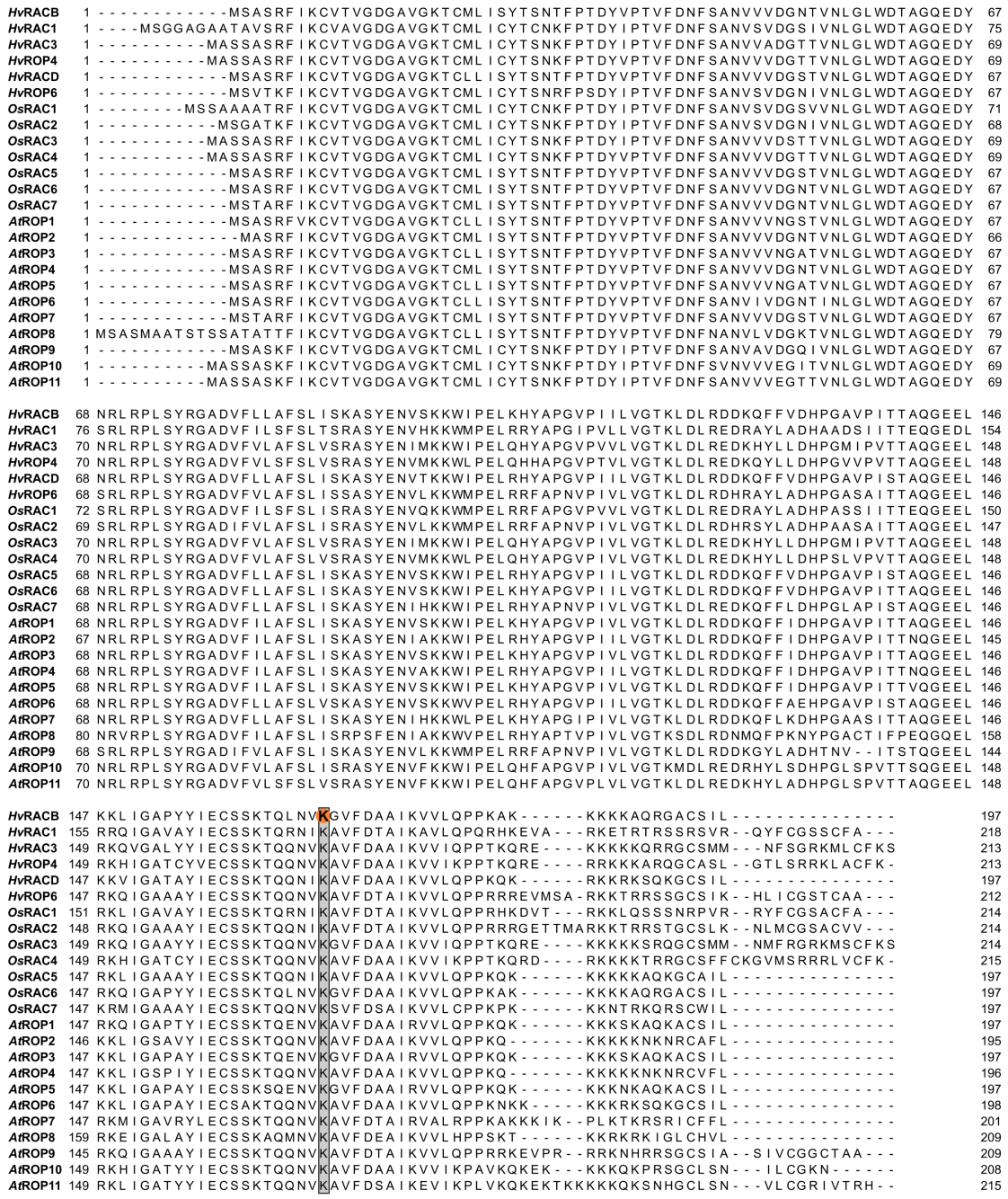

Figure S3: RACB-K167 is conserved in all ROPs of barley, rice and *Arabidopsis*. The ubiquitin acceptor site K167 in RACB (orange circle) is fully conserved in other barley, rice and *Arabidopsis* ROPs (grey box). Amino acid sequences of ROPs were compared using the MUSCLE alignment tool in Jalview (Edgar, 2004; Waterhouse et al., 2009). Data shown here was presented in a similar fashion in Figs. 5 and S5 in Weiß et al. (2022).

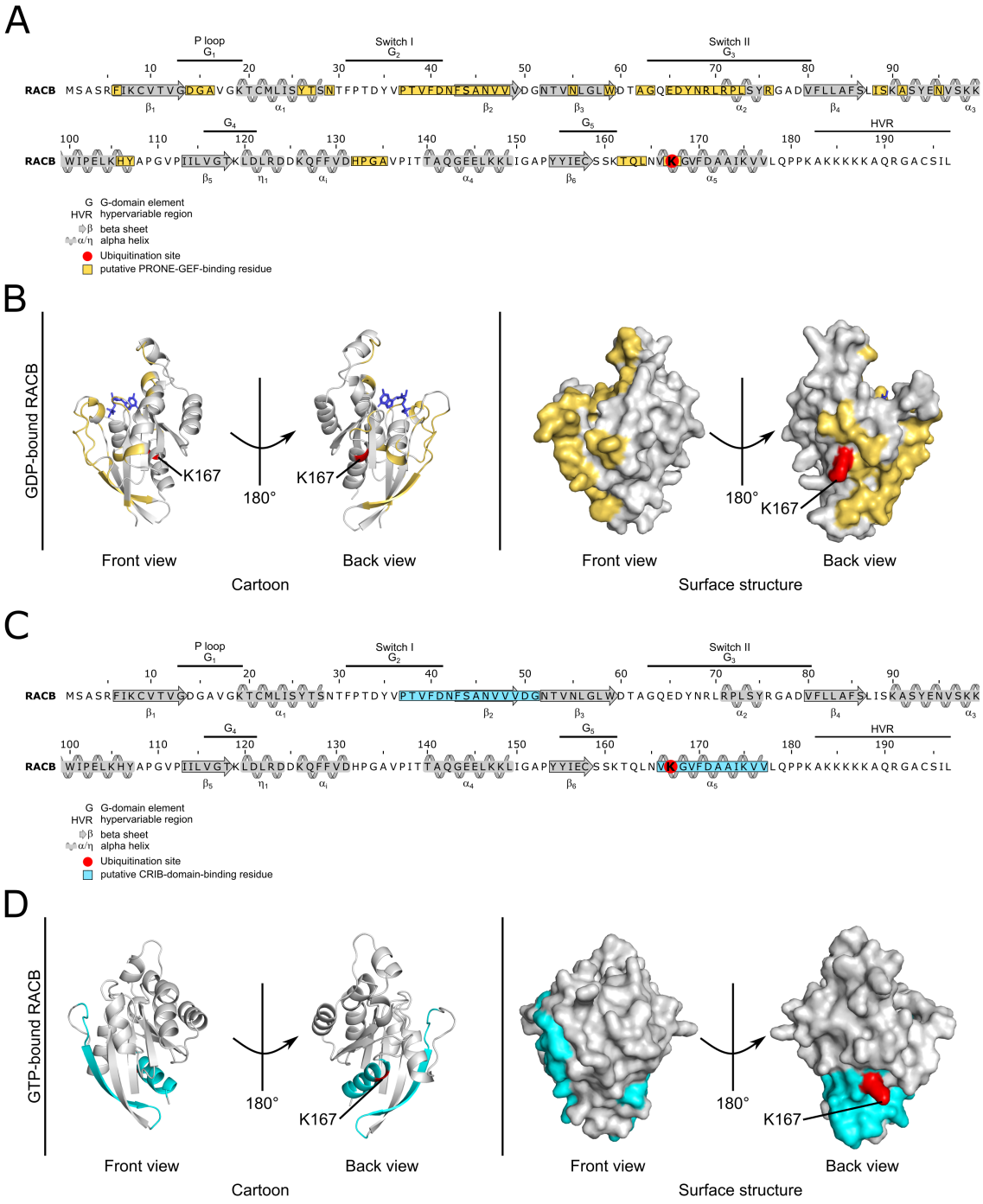

Figure S4: RACB-K167 is part of predicted GEF- and CRIB-binding interfaces. The predicted binding interfaces for PRONE-GEFs ((**A**), (**B**)) and CRIB-containing proteins ((**C**), (**D**)) are highlighted in the amino acid sequence ((**A**), (**C**)) or putative protein folds of GDP- ((**B**)) or GTP-bound ((**D**)) wildtype RACB. PRONE-GEF-binding sites were modelled on GDP-RACB, while CRIB-binding sites are displayed on GTP-RACB, since these RACB activity forms are most likely targeted by the respective proteins. The ubiquitination site K167 is a part of both interfaces (highlighted in red). GDP is shown in blue. PRONE-GEF- and CRIB-binding amino acids were taken from Thomas et al. (2007) and Abdul-Manan et al. (1999); Schaefer et al. (2011), respectively. Annotation of RACB's secondary structure motives and domains, as well as protein modelling are described in detail in Section 4.23. (**A**) and (**C**) of this figure were adapted from Fig. S6 of Weiß et al. (2022).

Table S1: Significantly enriched proteins in *Bgh*-infected eGFP-RACB-CA samples.
The enrichment factor denotes the fold increase in peptide abundance in *Bgh*-infected eGFP-RACB-CA samples compared to *Bgh*-infected eGFP samples. Gene identifiers belong to barley *cv.* Morex V2 (Mascher et al., 2017) or the *Bgh* DH14 proteome on UniProt (ID: UP000015441, Spanu et al. (2010)). Further characterized putative RACB-CA interactors are underlined. Statistical differences were assessed by two-tailed Student's *t*-tests. Exclusive: only detected in eGFP-RACB-CA samples.

p-value	Enrichment factor	Gene identifier	Annotation
0.000	exclusive	HORVU4Hr1G077220.4	Phosphoinositide phosphatase family protein
0.002	exclusive	HORVU1Hr1G075530.1	Cathepsin B-like cysteine proteinase
0.002	1.56	HORVU5Hr1G095550.1	Outward rectifying potassium channel
0.002	1.38	N1JGX9	Short chain dehydrogenase/ reductase/ methylenetetrahydrofolate reductase
0.004	2.74	HORVU3Hr1G049060.4	Vacuolar cation/proton exchanger 1a
0.004	exclusive	HORVU5Hr1G057050.29	Mitochondrial outer membrane protein porin 1
0.005	3.53	HORVU7Hr1G083670.3	Cytochrome P450 superfamily protein
0.007	1.31	HORVU2Hr1G029900.2	Protein kinase superfamily protein
0.007	64.45	N1JEY6	Putative effector protein
0.008	exclusive	HORVU3Hr1G108390.1	Orotidine 5-phosphate decarboxylase
0.009	1.62	HORVU7Hr1G052350.1	Myosin heavy chain-related
0.01	2.21	HORVU1Hr1G089680.3	Sugar transporter 1
0.011	1.66	HORVU5Hr1G078950.2	Mitochondrial dicarboxylate carrier
0.013	1.49	HORVU6Hr1G080480.1	Mitochondrial phosphate carrier protein
0.019	1.55	HORVU3Hr1G098670.1	Potassium transporter family protein
0.023	8.16	HORVU6Hr1G093230.2	Xyloglucan endotransglucosylase/ hydrolase family protein
0.024	2.72	HORVU4Hr1G077250.1	Eukaryotic translation initiation factor 3 subunit K
0.033	exclusive	HORVU6Hr1G076630.2	Thioesterase superfamily protein
0.034	exclusive	HORVU1Hr1G064700.2	Beta-hexosaminidase 3
0.037	1.29	HORVU2Hr1G124790.1	30S Ribosomal protein S11
0.037	1.31	HORVU6Hr1G070780.1	ADP, ATP carrier protein, mitochondrial
0.047	1.71	HORVU7Hr1G011290.1	54S ribosomal protein L4, mitochondrial
0.049	6.28	HORVU2Hr1G103890.12	Receptor kinase 2
0.05	1.98	HORVU2Hr1G028510.1	Ribosomal protein S4

Table S2: Significantly enriched proteins in mock-treated eGFP-RACB-CA samples.
The enrichment factor shows the fold increase in peptide abundance in mock-treated eGFP-RACB-CA samples compared to mock-treated eGFP samples. Gene identifiers are from barley *cv.* Morex V2 (Mascher et al., 2017) or the *Bgh* DH14 proteome on UniProt (ID: UP000015441, Spanu et al. (2010)). Further studied candidate RACB-CA interactors are underlined. Statistical significances were determined by two-tailed Student's *t*-tests. Exclusive: only detected in eGFP-RACB-CA samples.

p-value	Enrichment factor	Gene identifier	Annotation
0.004	1.84	HORVU2Hr1G010990.2	Aquaporin-like superfamily protein
0.007	1.44	HORVU2Hr1G013730.2	Phosphoinositide phospholipase C 6
0.008	1.55	HORVU4Hr1G076940.4	3-ketoacyl-CoA synthase 10
0.008	1.32	HORVU7Hr1G120030.4	Delta(24)-sterol reductase
0.016	1.97	HORVU4Hr1G001490.6	3-ketoacyl-CoA synthase 6
0.019	1.96	HORVU2Hr1G009890.1	Vacuolar protein-sorting-associated protein 33 homolog
0.02	1	HORVU4Hr1G007520.2	Coatomer, alpha subunit
0.021	3.1	HORVU7Hr1G109190.2	Hydroxyproline-rich glycoprotein family protein
0.023	2.22	HORVU7Hr1G083670.3	Cytochrome P450 superfamily protein
0.027	1.44	HORVU7Hr1G087190.1	V-type ATP synthase beta chain
0.029	1.46	HORVU3Hr1G059320.2	V-type proton ATPase subunit E
0.037	1.87	HORVU1Hr1G089680.3	Sugar transporter 1
0.038	1.45	HORVU2Hr1G038740.1	Aquaporin-like superfamily protein
0.038	1.80	HORVU2Hr1G096360.13	Aquaporin-like superfamily protein
0.041	1.17	HORVU5Hr1G069960.1	Purine permease 3
0.043	1.39	HORVU5Hr1G089400.1	Protein kinase superfamily protein
0.044	3.63	HORVU5Hr1G056470.1	Ras-related protein Rab-25

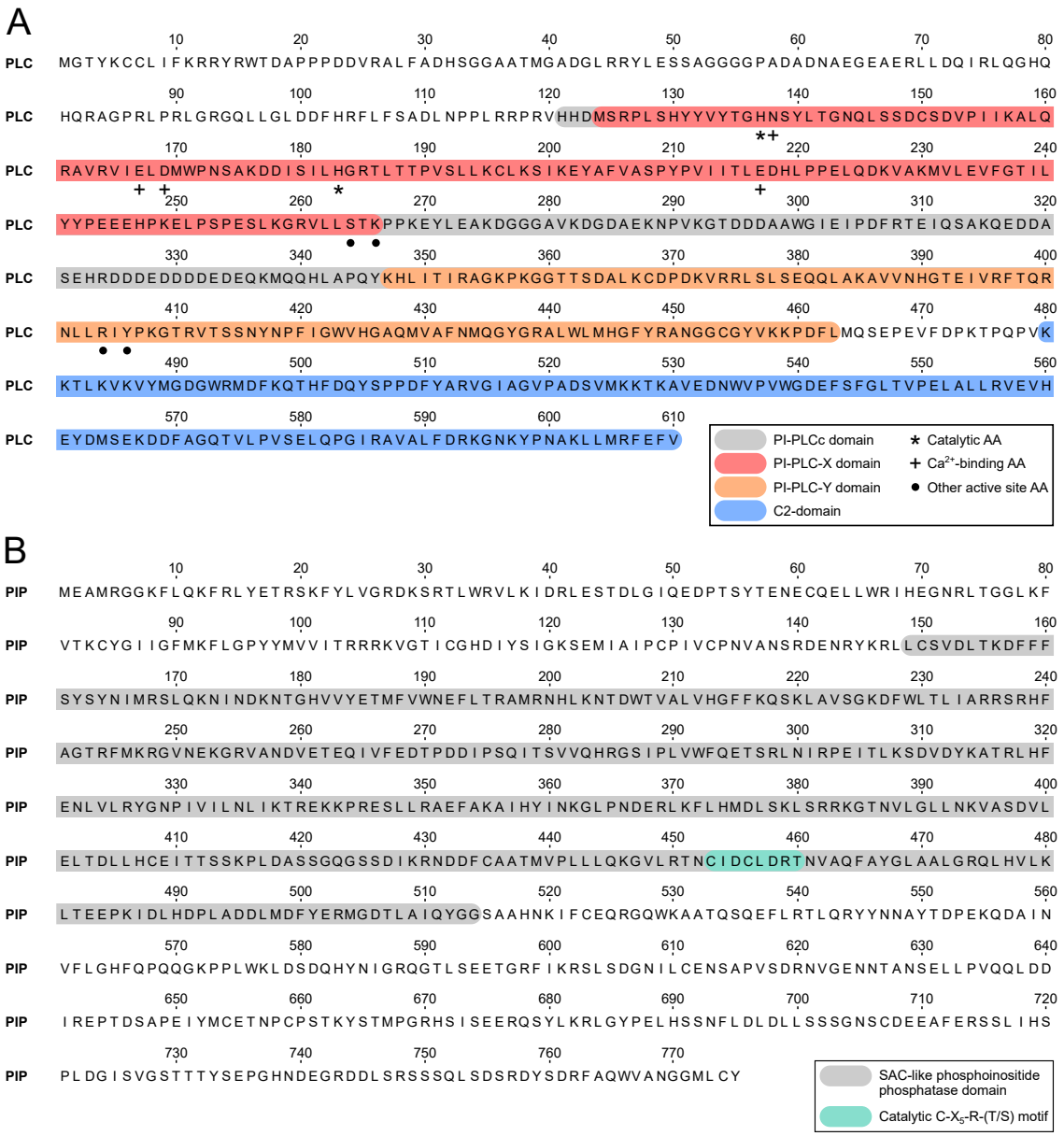

Figure S5: Annotation of conserved domains and residues in PLC and PIP. Conserved domains for PLC (**A**) and PIP (**B**) were identified using the NCBI conserved domain (CD)-search tool (Lu et al., 2020) or UniProt (The UniProt Consortium, 2020), respectively, and are highlighted in their amino acid sequences. PLC contains a name-giving PI-PLCc domain (grey), which is split into PI-PLC-X (red) and PI-PLC-Y (orange) domains, and a C2-domain (blue) (Rhee and Choi, 1992; Essen et al., 1997). Catalytic amino acids (asterisks), Ca^{2+}-binding residues (plus signs) and other structurally important active site amino acids (bullets) are indicated below the sequence (Essen et al., 1996, 1997; Williams, 1999; Jezyk et al., 2006). PIP possesses a SAC-like phosphoinositide phosphatase domain (grey), in which the catalytic motif (Liu et al., 2009b) is highlighted in cyan. AA: amino acid; X = any residue.

A

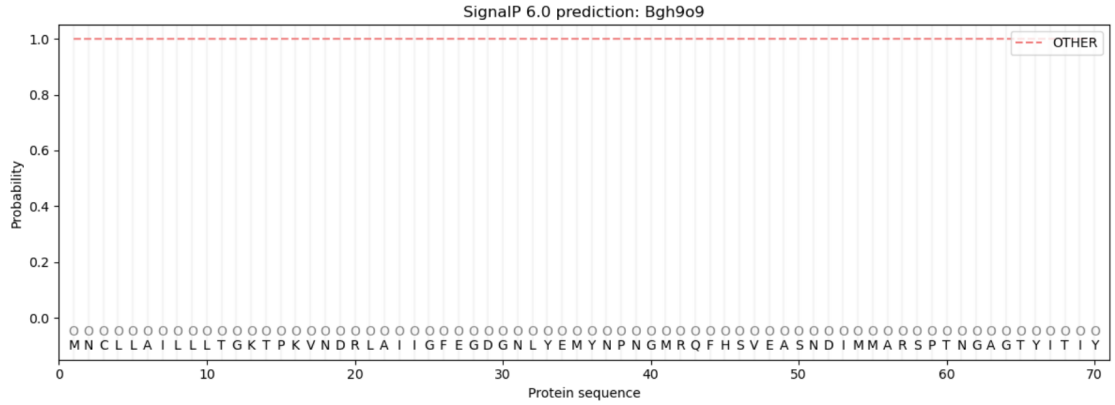
SignalP 6.0 prediction: Bgh9o9
OTHER
Probability
1.0
0.8
0.6
0.4
0.2
0.0
M N C L L A I L L L T G K T P K V N D R L A I I G F E G D G N L Y E M Y N P N G M R Q F H S V E A S N D I M M A R S P T N G A G T Y I T I Y
0
10
20
30
40
50
60
70
Protein sequence

B

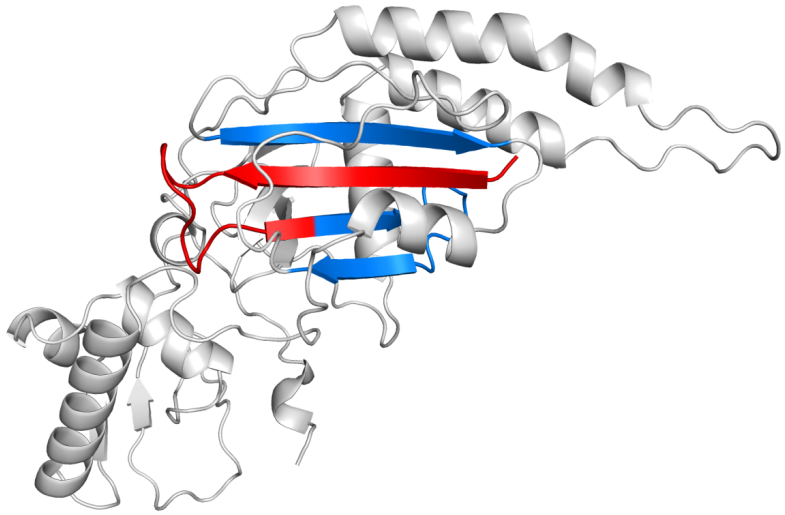

C

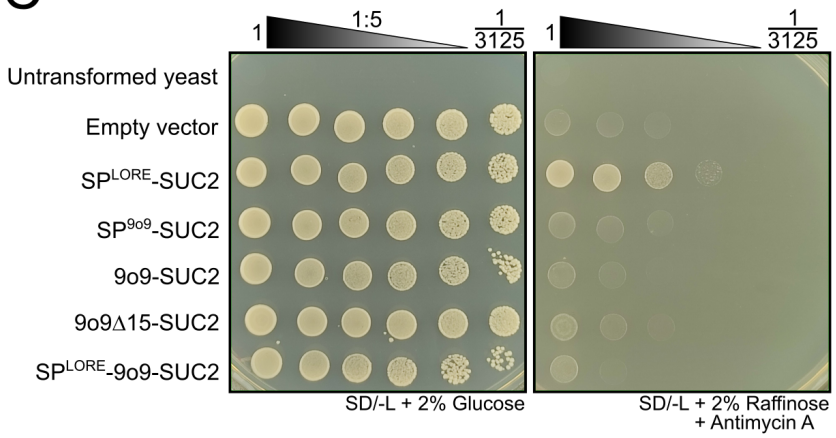
1
1:5
1/3125
1
1/3125
Untransformed yeast
Empty vector
SP^LORE-SUC2
SP^9o9-SUC2
9o9-SUC2
9o9Δ15-SUC2
SP^LORE-9o9-SUC2
SD/-L + 2% Glucose
SD/-L + 2% Raffinose
+ Antimycin A

Figure S6: Signal peptide analysis of 9o9.
(**A**) According to the signal peptide prediction tool SignalP (V6.0, Teufel et al. (2022), 9o9 does not contain a canonical signal sequence. (**B**) The first twenty-one amino acids of 9o9 (red) appear to be part of a four β-sheet motif (blue) in the predicted structure of 9o9. The putative protein fold of 9o9 was modelled with Alphafold (V2.1.0, Jumper et al. (2021)) and illustrated with PyMOL (V2.3.4, Schrödinger, LLC (2015)). (**C**) The ability of 9o9 to be secreted was analysed in the sucrose-auxotrophic invertase-deficient yeast strain Y02321. Full-length 9o9, its putative signal peptide (SP^{9o9}, amino acids 1-21), a signal peptide mutant (9o9-Δ15, lacking residues 2-15), a positive control (SP^{LORE} from the *Arabidopsis* RLK LORE (AT1G61380)) or a chimera (SP^{LORE} fused to full-length 9o9) were fused to the N-terminus of the yeast invertase SUC2, which complements yeast sucrose auxotrophy. The SUC2 enzyme used in this experiment lacked its N-terminal signal peptide, meaning it is only secreted, when its N-terminal fusion protein carries a secretion signal. The empty vector expressed unconjugated SUC2. Yeast growth on plates containing raffinose as the only sugar source confirmed presence of a signal peptide, glucose plates served as transformation control. Raffinose is a tri-saccharid of sucrose (D-glucose and D-fructose) and D-galactose, which can be hydrolyzed by invertase enzymes. Only SP^{LORE}-SUC2 fusions appeared to be secreted. Yeast was diluted in 1/5 dilution steps in a range from 1 (undiluted) to 1/3125. To increase stringency, Antimycin A was used as an inhibitor for oxidative respiration, which forced yeast to rely on fermentation (Krijger et al., 2008). SD/-L: standard-defined yeast medium containing all amino acids except leucine. This result could be confirmed in three independent biological replicates.

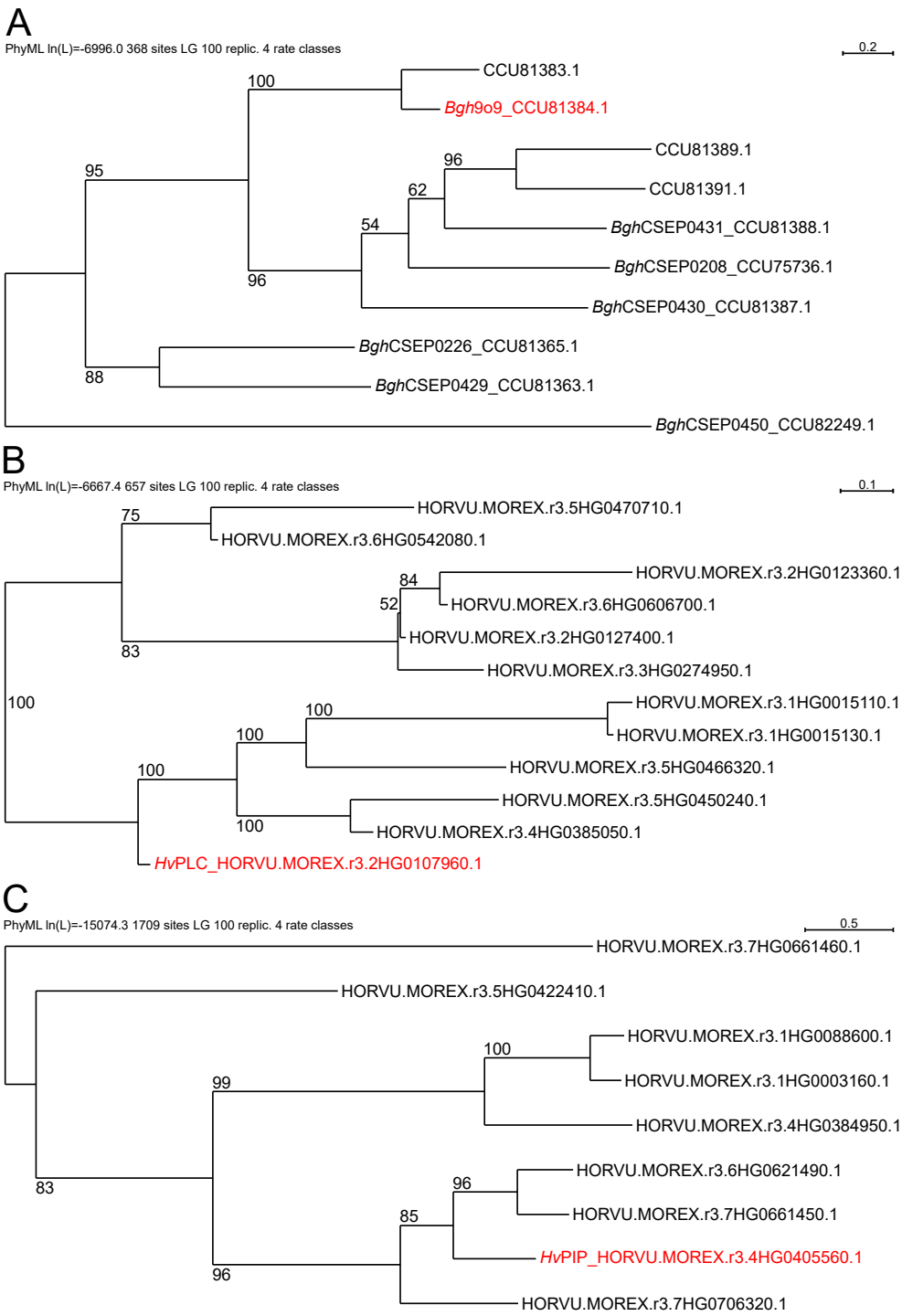

Figure S7: Homologs of 9o9, PLC and PIP in *Bgh* and barley.
Homologs of 9o9 in *Bgh* (**A**), or PLC (**B**) and PIP (**C**) in barley were identified by BLASTP searches against the respective proteomes (*Bgh* strain DH14, Spanu et al. (2010) or *cv.* Morex (V3), Mascher (2021)). 9o9, PLC and PIP are highlighted in red. Maximum-likelihood (PhyML) trees were built in SeaView (V5.0.5, Gouy et al. (2009)) after MUSCLE-alignment (Edgar, 2004). Bootstrap values of 100 iterations are shown. For more details about tree-building please see Section 4.23. Quality scores are depicted above each tree. Scale bar and branch length indicate the difference between sequences.

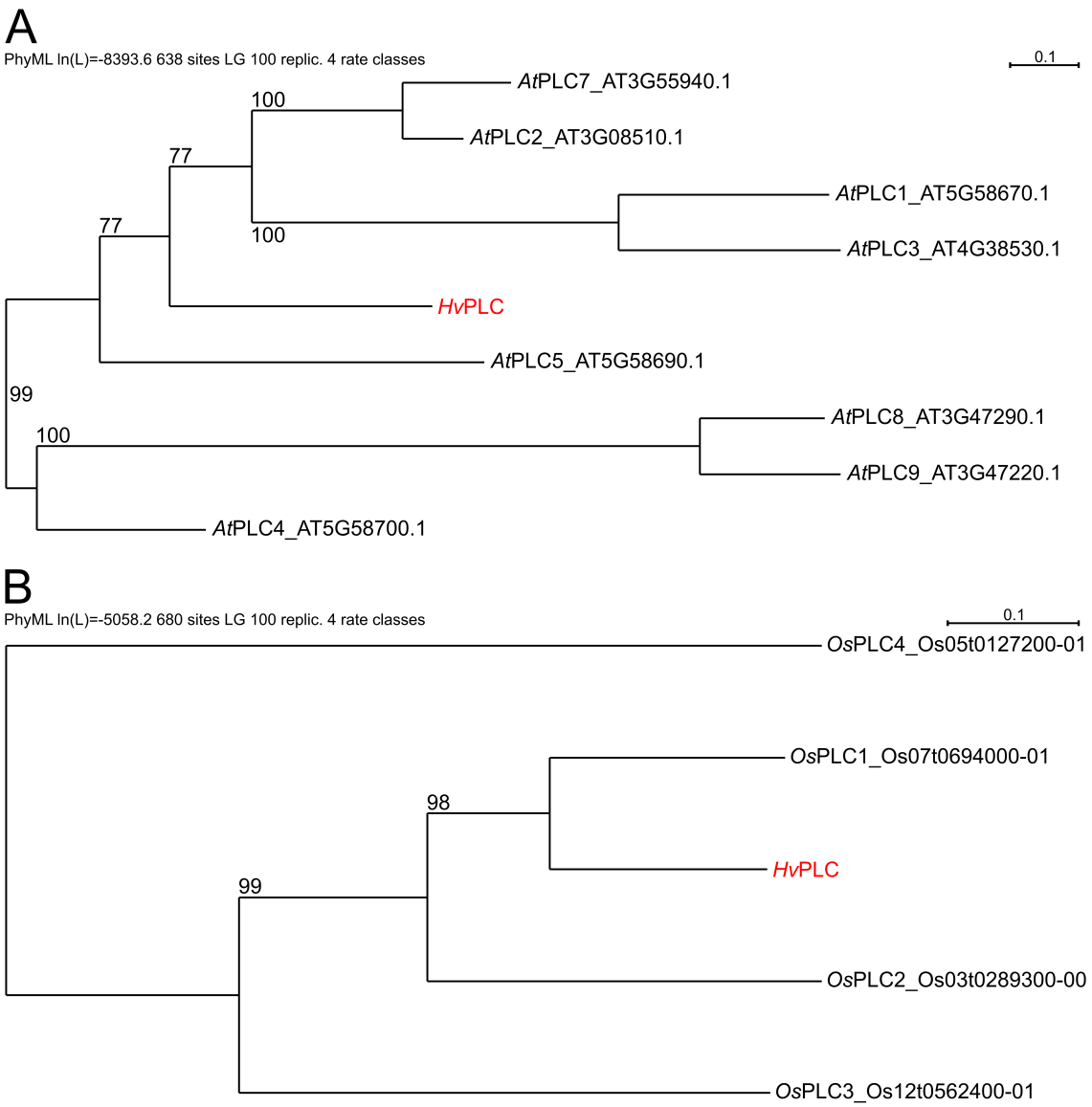

Figure S8: Homologs of PLC in *Arabidopsis thaliana* and rice.
Homologs of PLC (red) in *Arabidopsis thaliana* (*At*, (**A**) and rice (*Oryza sativa, Os*, **B**) were identified via BLASTP searches against the respective proteomes (Araport11, Cheng et al. (2017)) and IRGSP 1.0, Kawahara et al. (2013)). Maximum-likelihood (PhyML) trees were built in SeaView (V5.0.5, Gouy et al. (2009)) after MUSCLE-alignment (Edgar, 2004). Bootstrap values of 100 iterations are shown. For more details about tree-building please see Section 4.23. Quality scores are depicted above each tree. Scale bar and branch length indicate the difference between sequences. In Araport11, *At*PLC6 has no associated locus and sequence, hence it could not be included in this PhyML tree.

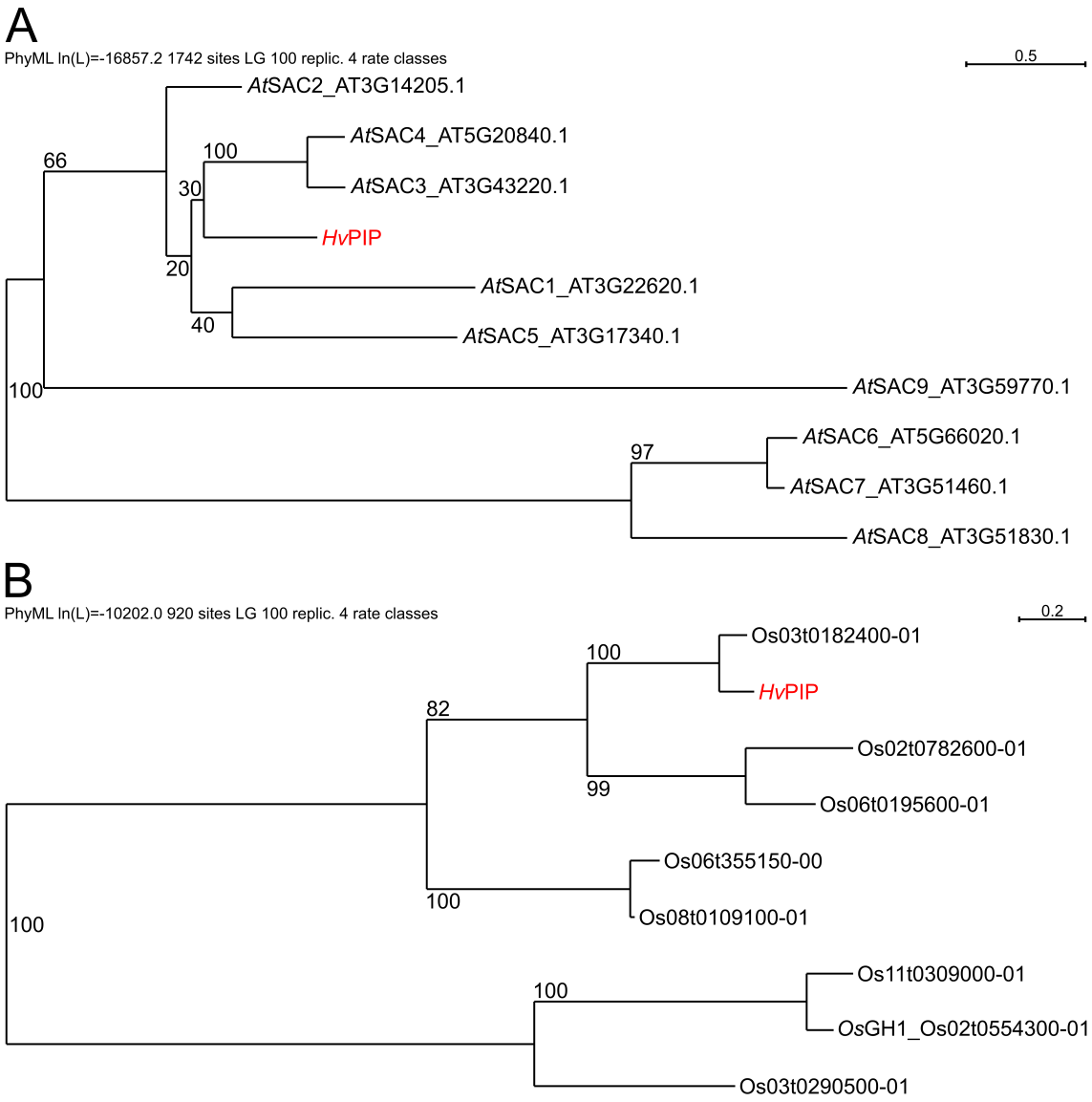

Figure S9: Homologs of PIP in *Arabidopsis thaliana* and rice.
Homologs of PIP (red) in *Arabidopsis thaliana* (*At*, (**A**)) and rice (*Oryza sativa, Os*, **B**) were identified via BLASTP searches against the respective proteomes (Araport11, Cheng et al. (2017)) and IRGSP 1.0, Kawahara et al. (2013)). Maximum-likelihood (PhyML) trees were built in SeaView (V5.0.5, Gouy et al. (2009)) after MUSCLE-alignment (Edgar, 2004). Bootstrap values of 100 iterations are shown. For more details about tree-building please see Section 4.23. Quality scores are depicted above each tree. Scale bar and branch length indicate the difference between sequences.

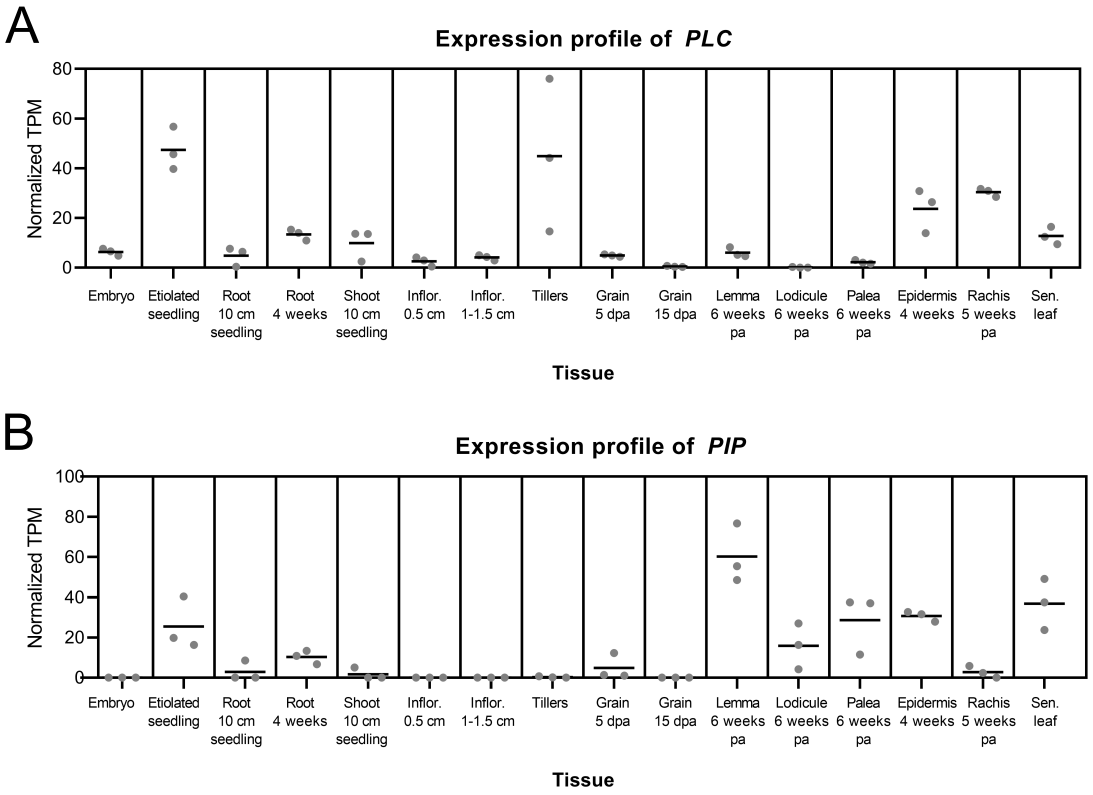

Figure S10: Gene expression of *PLC* and *PIP* across different developmental stages of barley.
The barley reference transcript database (BaRTD, `https://ics.hutton.ac.uk/barleyrtd/`, Mascher et al. (2017); Rapazote-Flores et al. (2019)) was used to investigate the gene expression profiles of *PLC* (**A**) and *PIP* (**B**) in sixteen different tissues of barley *cv.* Morex. *PLC* showed strongest expression (>40 average TPM) in etiolated seedlings and tillers, moderate expression (20-40 average TPM) in leaf epidermis and rachis, and low expression (<20 average TPM) in embryos, roots, shoots, inflorescences, early grains, lemmata, paleae, and senescing leaves. *PIP* was highest expressed in lemmata, moderately expressed in etiolated seedlings, lodicules, paleae, leaf epidermises and senescing leaves, and weakly expressed in roots, shoots, early grain and rachis. Average transcripts per million (TPM) from three biological replicates are shown (Mascher et al., 2017; Rapazote-Flores et al., 2019). BaRTD gene identifiers: PLC: BART1_0-u07950.001; PIP: BART1_0-u31129.001. Inflor.: inflorescence; Sen.: senescing; pa: post anthesis; dpa: days post anthesis.

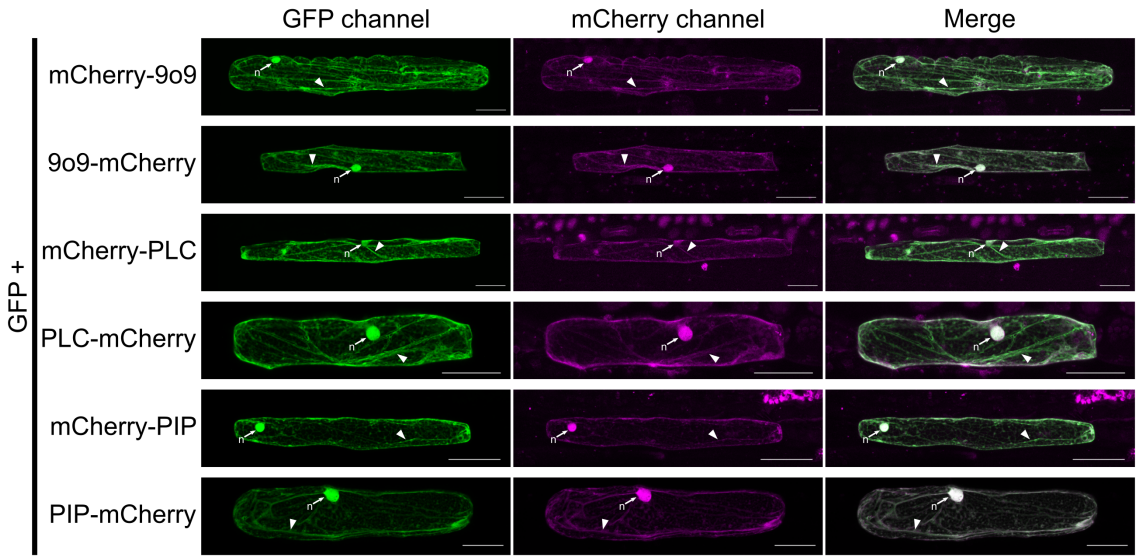

Figure S11: Subcellular localization of mCh-tagged 9o9, PLC and PIP in barley.
Barley epidermal cells were transiently transformed by particle bombardment with mCherry-tagged fusions proteins of 9o9, PLC and PIP. Free GFP was co-expressed in all samples as a marker for cytoplasmic and nuclear localization. All mCherry-tagged proteins exclusively showed cytoplasmic and nuclear localization and exhibited low levels of fluorescence. Nuclei (n, arrows) and prominent cytoplasmic strands (arrowheads) are highlighted. Cells were imaged by CLSM. Images show maximum intensity projections of Z-stacks containing at least 16 XY-optical sections captured in 1.5 µm Z-increments. Scale bar: 50 µm. Brightness of images was uniformly enhanced post-scanning for better visibility.

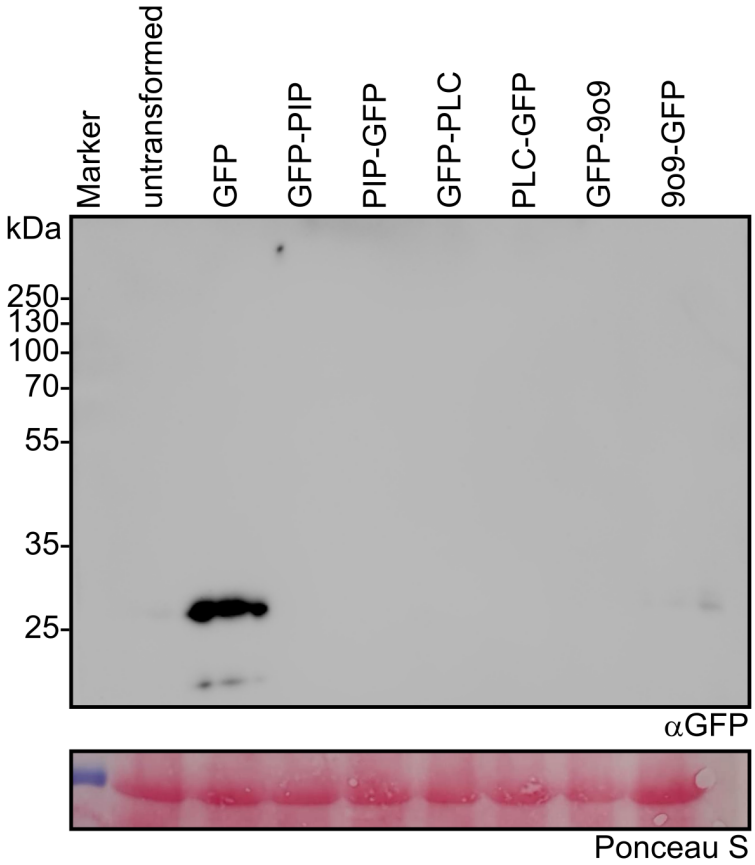

Figure S12: GFP-fusion constructs of 9o9, PLC and PIP are not stable in barley protoplasts.
Total protein was extracted from wildtype barley protoplasts transformed with GFP-fusion constructs of 9o9, PLC and PIP or free GFP. Protein stability was determined by αGFP-Western blotting. Only free GFP was expressed and stable in barley protoplasts. Ponceau S staining was used as a loading control. Untransformed protoplasts served as unspecific-binding control for the αGFP-antibody. Expected protein sizes: free GFP: 27 kDa; GFP-tagged 9o9: 63 kDa; GFP-tagged PLC: 96 kDa; GFP-tagged PIP: 116 kDa.

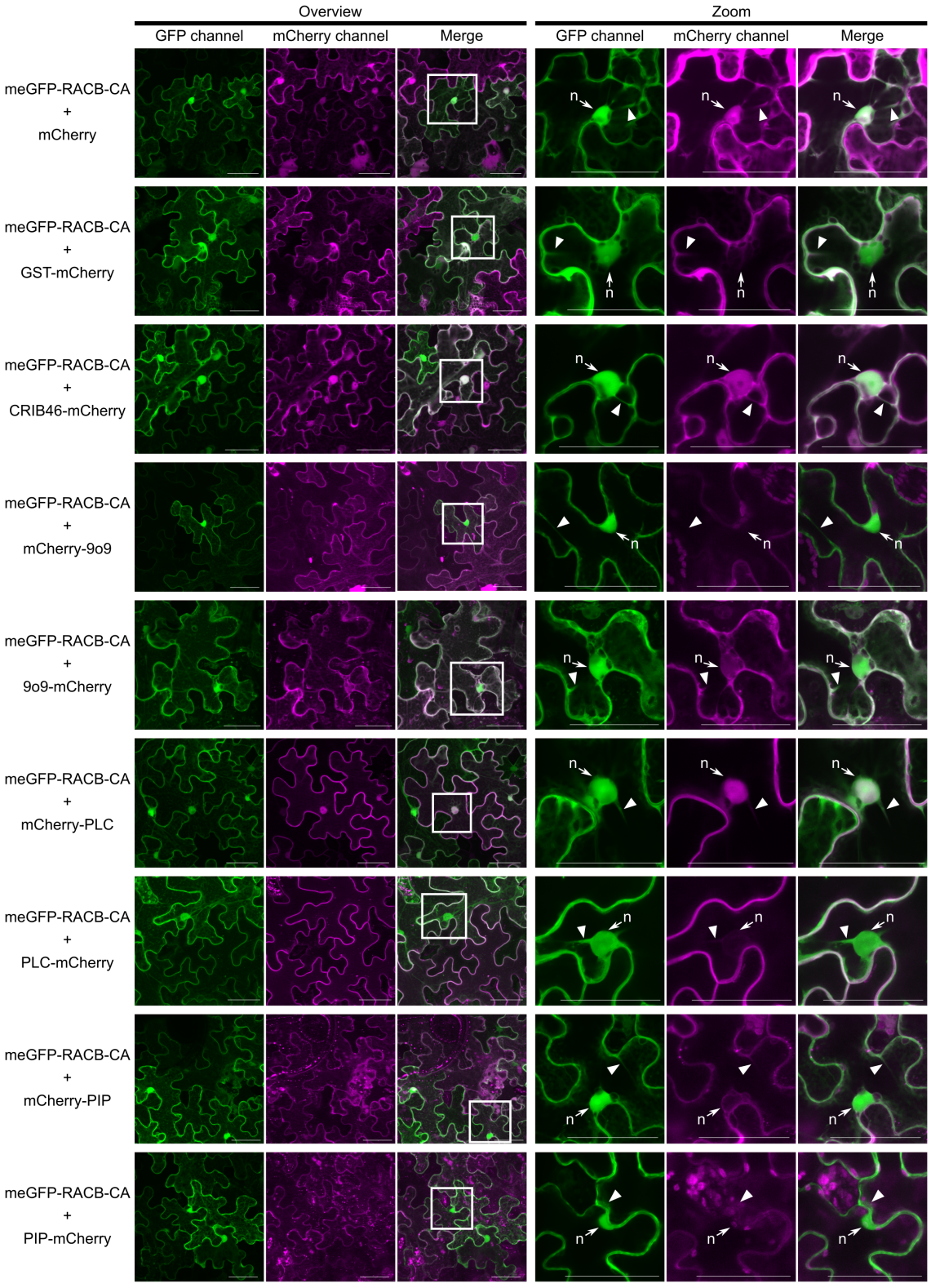
Overview
Zoom
GFP channel
mCherry channel
Merge
GFP channel
mCherry channel
Merge
meGFP-RACB-CA + mCherry
meGFP-RACB-CA + GST-mCherry
meGFP-RACB-CA + CRIB46-mCherry
meGFP-RACB-CA + mCherry-9o9
meGFP-RACB-CA + 9o9-mCherry
meGFP-RACB-CA + mCherry-PLC
meGFP-RACB-CA + PLC-mCherry
meGFP-RACB-CA + mCherry-PIP
meGFP-RACB-CA + PIP-mCherry
n

Figure S13: Localization of mCherry-tagged 9o9, PIP and PLC in presence of meGFP-RACB-CA in *N. benthamiana*.
Localization of 9o9, PLC and PIP does not change upon co-expression of meGFP-RACB-CA from observations described in Fig. 2.8. GST-mCherry was localized to the cytoplasm, whereas free mCherry and CRIB46-mCherry displayed cytoplasmic and nuclear fluorescence. Arrowheads point to cytoplasmic strands or accumulation of cytoplasmic material at the periphery, while arrows highlight nuclei (n). Images were acquired in *A. tumefaciens*-transformed *N. benthamiana* plants via CLSM. Maximum intensity projections of Z-stacks are shown. For overview images, a minimum of 10 XY-optical sections were acquired with a Z-step size of 1.5 µm, while the magnified images show Z-stacks of at least 11 XY-optical sections captured in 0.5 µm Z-steps. The white rectangle in the merge channel depicts the area that was re-scanned for the magnified images. Scale bar: 50 µm. Image brightness was uniformly enhanced post-imaging for better visibility.

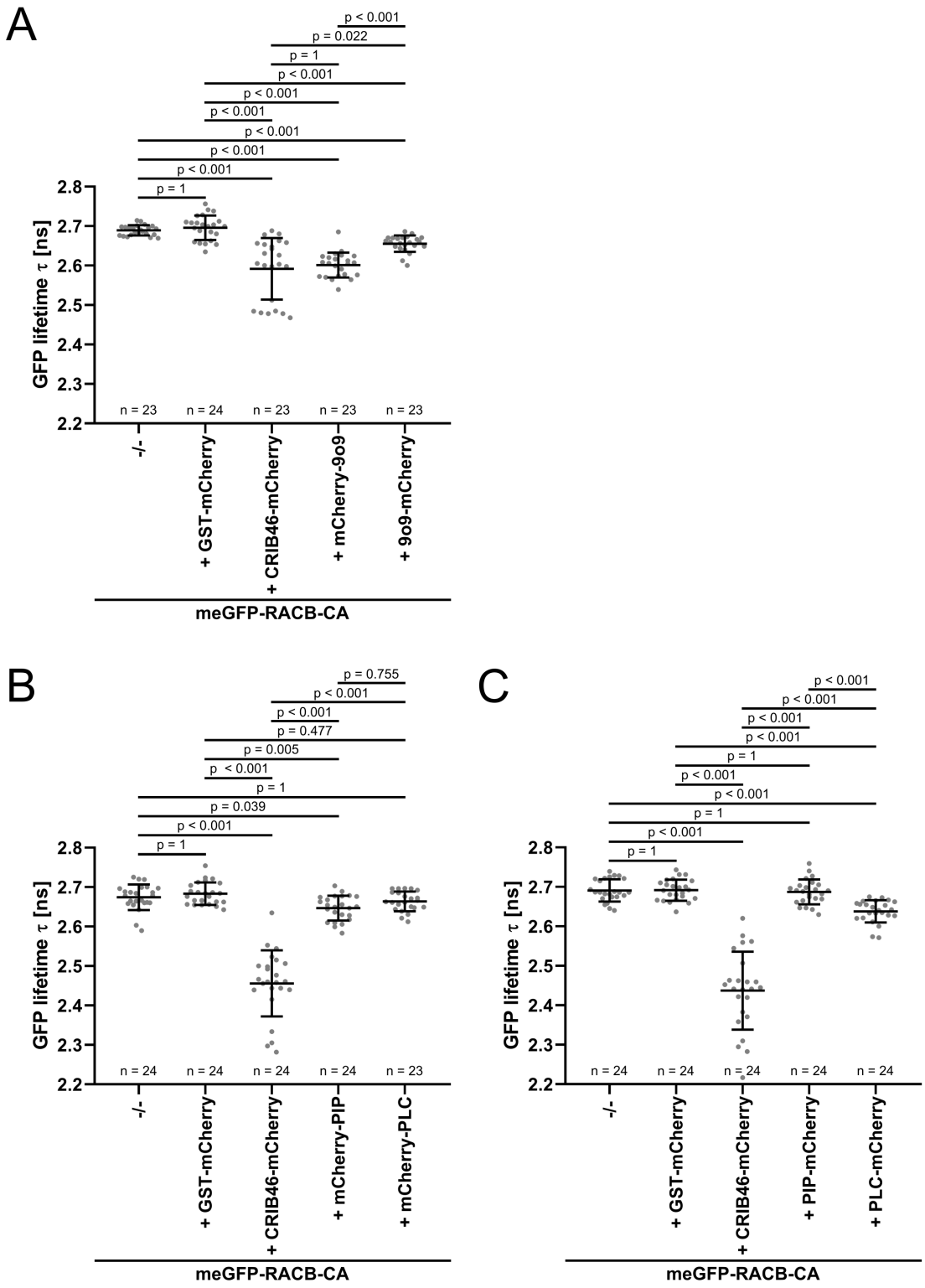

Figure S14: GFP-RACB-CA interacts with mCherry-tagged 9o9, PLC or PIP in FRET-FLIM experiments in *N. benthamiana*.
This figure shows all statistical comparisons of the FRET-FLIM experiment described in Fig. 2.10. Statistical differences were assessed by Wilcoxon-Rank-Sum tests with Bonferroni correction for multiple testing.

Table S3: Plasmids used in this dissertation.
n.a.: not available.

Plasmid	Cloning method	Source	Used for
Gateway entry vectors			
pDONR223-RACB-WT	n.a.	Hückelhoven lab	Cloning
pDONR223-RACB-WT-K167R	n.a.	Weiß et al. (2022)	Cloning
pDONR223-RACB-CA	n.a.	Hückelhoven lab	Cloning
pDONR223-RACB-CA-K167R	n.a.	Weiß et al. (2022)	Cloning
pDONR223-RACB-DN	n.a.	Hückelhoven lab	Cloning
pDONR223-RACB-DN-K167R	n.a.	Weiß et al. (2022)	Cloning
pDONR223-9o9	Gateway BP	This work	Cloning
pDONR223-9o9 (no stop codon)	Gateway BP	This work	Cloning
pDONR223-PLC_Zm	Gateway BP	This work	Cloning
pDONR223-PLC_Zm (no stop codon)	Gateway BP	This work	Cloning
pDONR223-PIP	Gateway BP	This work	Cloning
pDONR223-PIP (no stop codon)	Gateway BP	This work	Cloning
pDONR223-meGFP-10xGly-RACB-CA	GoldenGate (Esp3I), Gateway BP	(Trutzenberg et al., 2022)	Cloning
pDONR223-mCherry-10xGly-9o9	GoldenGate (Esp3I), Gateway BP	This work	Cloning
pDONR223-9o9-10xGly-mCherry	GoldenGate (Esp3I), Gateway BP	This work	Cloning
pDONR223-mCherry-10xGly-PLC_Zm	GoldenGate (Esp3I), Gateway BP	This work	Cloning
pDONR223-PLC_Zm-10xGly-mCherry	GoldenGate (Esp3I), Gateway BP	This work	Cloning
pDONR223-mCherry-10xGly-PIP	GoldenGate (Esp3I), Gateway BP	This work	Cloning
pDONR223-PIP-10xGly-mCherry	GoldenGate (Esp3I), Gateway BP	This work	Cloning
pDONR223-GST-10xGly-mCherry	GoldenGate (Esp3I), Gateway BP	(Trutzenberg et al., 2022)	Cloning
pDONR223-CRIB46-10xGly-mCherry	GoldenGate (Esp3I), Gateway BP	(Trutzenberg et al., 2022)	Cloning
pDONR223-mCitrine-2xML1N	Gateway BP	This work	Cloning
pDONR223-2xPHPLC	Gateway BP	This work	Cloning
pIPKTA38 (empty)	n.a.	Douchkov et al. (2005)	Cloning

Plasmids used in this dissertation. (*Continued.*)

Plasmid	Cloning method	Source	Used for
pIPKTA38-9o9	Classical (SalI + XbaI)	This work	Cloning
pIPKTA38-PLC	Classical (SalI + XbaI)	This work	Cloning
pIPKTA38-PIP	Classical (SalI + XbaI)	This work	Cloning
Silencing in planta			
pIPKTA30N (empty)	n.a.	Douchkov et al. (2005)	*Bgh* susceptibility assay
pIPKTA30N-9o9	Gateway LR	This work	*Bgh* susceptibility assay
pIPKTA30N-PLC	Gateway LR	This work	*Bgh* susceptibility assay
pIPKTA30N-PIP	Gateway LR	This work	*Bgh* susceptibility assay
Overexpression in planta			
p6i-2x35S-TE9-eGFP	n.a.	Hückelhoven lab	Generation of transgenic lines
p6i-2x35S-TE9-eGFP-RACB-CA	n.a.	Hückelhoven lab	Generation of transgenic lines
p6i-2x35S-TE9-eGFP-RACB-CA-ΔCSIL	n.a.	Hückelhoven lab	Generation of transgenic lines
p6i-2x35S-TE9-3xHA	n.a.	Hückelhoven lab	Generation of transgenic lines
p6i-2x35S-TE9-3xHA-RACB-CA	n.a.	Hückelhoven lab	Generation of transgenic lines
p6i-2x35S-TE9-3xHA-RACB-CA-ΔCSIL	n.a.	Hückelhoven lab	Generation of transgenic lines
pGY1-CFP	n.a.	Hückelhoven lab	Subcellular localization in barley
pGY1-GFP	n.a.	Hückelhoven lab	Subcellular localization in barley
pGY1-N-terminal-meGFP (empty)	n.a.	Hückelhoven lab	Cloning
pGY1-C-terminal-meGFP (empty)	n.a.	Hückelhoven lab	Cloning
pGY1-N-terminal-mCherry (empty)	n.a.	Hückelhoven lab	Subcellular localization in barley, cloning
pGY1-C-terminal-mCherry (empty)	n.a.	Hückelhoven lab	Cloning
pUbi-GUS+	Vickers et al. (2003)	Addgene No. 64402	*Bgh* susceptibility assay
pGY1-GFP-RBK1	n.a.	Hückelhoven lab	RACB-CA phosphosite screenings
pGY1-meGFP-RACB-WT	n.a.	Hückelhoven lab	Stability assessment in barley
pGY1-meGFP-RACB-WT-K167R	n.a.	Weiß et al. (2022)	Stability assessment in barley

Plasmids used in this dissertation. (*Continued.*)

Plasmid	Cloning method	Source	Used for
pGY1-meGFP-RACB-CA	n.a.	Hückelhoven lab	Stability assessment and recruitment assay in barley
pGY1-meGFP-RACB-CA-K167R	n.a.	Weiß et al. (2022)	Stability assessment and recruitment assay in barley
pGY1-meGFP-RACB-DN	n.a.	Hückelhoven lab	Stability assessment in barley
pGY1-meGFP-RACB-DN-K167R	n.a.	Weiß et al. (2022)	Stability assessment in barley
pGY1-mCherry-RIC171	n.a.	Hückelhoven lab	Recruitment assay in barley
pGY1-meGFP-2xPH^{FAPP1}	GoldenGate (Esp3I)	This work	Subcellular localization in barley
pGY1-mCitrine-2xML1N	Gateway LR	This work	Subcellular localization in barley
pGY1-meGFP-2xPH^{PLC}	Gateway LR	This work	Subcellular localization in barley
pGY1-mCherry-2xPH^{PLC}	Gateway LR	This work	Fluorescence quantification in barley
pGY1-meGFP-C2^{LACT}	GoldenGate (Esp3I)	This work	Subcellular localization in barley
pGY1-meGFP-9o9	Gateway LR	This work	Transformation of barley protoplasts
pGY1-9o9-meGFP	Gateway LR	This work	Transformation of barley protoplasts
pGY1-meGFP-PLC_Zm	Gateway LR	This work	Transformation of barley protoplasts
pGY1-PLC_Zm-meGFP	Gateway LR	This work	Transformation of barley protoplasts
pGY1-meGFP-PIP	Gateway LR	This work	Transformation of barley protoplasts
pGY1-PIP-meGFP	Gateway LR	This work	Transformation of barley protoplasts
pGY1-mCherry-9o9	Gateway LR	This work	Subcellular localization in barley
pGY1-9o9-mCherry	Gateway LR	This work	Subcellular localization in barley
pGY1-mCherry-PLC_Zm	Gateway LR	This work	Subcellular localization in barley
pGY1-PLC_Zm-mCherry	Gateway LR	This work	Subcellular localization in barley
pGY1-mCherry-PIP	Gateway LR	This work	Subcellular localization in barley
pGY1-PIP-mCherry	Gateway LR	This work	Subcellular localization in barley
pGY1-MAP-2xmCherry	GoldenGate (Esp3I)	This work	PI(4,5)P_2-depletion test
pGY1-MAP-mCherry-dOCRL	GoldenGate (Esp3I)	This work	PI(4,5)P_2-depletion test
pGY1-MAP-mCherry-dOCRL^{dead}	GoldenGate (Esp3I)	This work	PI(4,5)P_2-depletion test
pGY1 (empty)	n.a.	Schweizer et al. (1999)	*Bgh* susceptibility assay, cloning
pGY1 (empty) Gateway-compatible	n.a.	Hückelhoven lab	*Bgh* susceptibility assay, cloning
pGY1-RACB-CA	n.a.	Hückelhoven lab	*Bgh* susceptibility assay
pGY1-RACB-CA-K167R	Gateway LR	This work	*Bgh* susceptibility assay
pGY1-9o9	Classical (SmaI)	This work	*Bgh* susceptibility assay
pGY1-PLC_Zm	Gateway LR	This work	*Bgh* susceptibility assay
pGY1-PIP	Gateway LR	This work	*Bgh* susceptibility assay

Plasmids used in this dissertation. (*Continued.*)

Plasmid	Cloning method	Source	Used for
pGWB6-GFP (empty)	n.a.	Nakagawa et al. (2007)	Targeted CoIPs and subcellular localization in *N. benthamiana*, cloning
pGWB6-GFP-RACB-WT	Gateway LR	This work	Targeted CoIPs in *N. benthamiana*
pGWB6-GFP-RACB-CA	Gateway LR	This work	Targeted CoIPs in *N. benthamiana*
pGWB6-GFP-RACB-T20N	Gateway LR	This work	Targeted CoIPs in *N. benthamiana*
pGWB14-C-terminal-3xHA (empty)	n.a.	Nakagawa et al. (2007)	Cloning
pGWB15-N-terminal-3xHA (empty)	n.a.	Nakagawa et al. (2007)	Cloning
pGWB14-9o9-3xHA	Gateway LR	This work	Targeted CoIPs in *N. benthamiana*
pGWB15-3xHA-9o9	Gateway LR	This work	Targeted CoIPs in *N. benthamiana*
pGWB14-PLC_Zm-3xHA	Gateway LR	This work	Targeted CoIPs in *N. benthamiana*
pGWB16-3xHA-PLC_Zm	Gateway LR	This work	Targeted CoIPs in *N. benthamiana*
pGWB14-PIP-3xHA	Gateway LR	This work	Targeted CoIPs in *N. benthamiana*
pGWB15-3xHA-PIP	Gateway LR	This work	Targeted CoIPs in *N. benthamiana*
pGWB2 (empty)	n.a.	Nakagawa et al. (2007)	Cloning
pGWB2-meGFP-10xGly-RACB-CA	Gateway LR	(Trutzenberg et al., 2022)	FRET-FLIM and subcellular localization in *N. benthamiana*
pGWB2-mCherry-10xGly-9o9	Gateway LR	This work	FRET-FLIM and subcellular localization in *N. benthamiana*
pGWB2-9o9-10xGly-mCherry	Gateway LR	This work	FRET-FLIM and subcellular localization in *N. benthamiana*
pGWB2-mCherry-10xGly-PLC_Zm	Gateway LR	This work	FRET-FLIM and subcellular localization in *N. benthamiana*
pGWB2-PLC_Zm-10xGly-mCherry	Gateway LR	This work	FRET-FLIM and subcellular localization in *N. benthamiana*
pGWB2-mCherry-10xGly-PIP	Gateway LR	This work	FRET-FLIM and subcellular localization in *N. benthamiana*
pGWB2-PIP-10xGly-mCherry	Gateway LR	This work	FRET-FLIM and subcellular localization in *N. benthamiana*
pGWB2-GST-10xGly-mCherry	Gateway LR	(Trutzenberg et al., 2022)	FRET-FLIM and subcellular localization in *N. benthamiana*
pGWB2-CRIB46-10xGly-mCherry	Gateway LR	(Trutzenberg et al., 2022)	FRET-FLIM and subcellular localization in *N. benthamiana*
pGGPX-220-mCherry	n.a.	Ranf Lab	Subcellular localization in *N. benthamiana*
pBIN61-p19	n.a.	Voinnet et al. (2003)	Silencing inhibitor for *N. benthamiana* co-transformation
Overexpression in E. coli			
pGEX-6P-1 (free GST)	n.a.	GE-Healthcare	Protein expression in *E. coli*; cloning

Plasmids used in this dissertation. (*Continued.*)

Plasmid	Cloning method	Source	Used for
pMAL-c5X (free MBP)	n.a.	New England Biolabs	Protein expression in *E. coli*; cloning
pGEX-RACB-WT	Classical (SalI + NotI)	This work	Protein expression in *E. coli*
pGEX-RACB-5Q	PCR, blunt-end ligation	This work	Protein expression in *E. coli*
pGEX-AtROP6-WT	n.a.	Heilmann Lab	Protein expression in *E. coli*
pMAL-9o9	Classical (SalI + NotI)	This work	Protein expression in *E. coli*
pMAL-PLC_Zm	Classical (SalI + NotI)	This work	Protein expression in *E. coli*
pMAL-PIP	Classical (SalI + NotI)	This work	Protein expression in *E. coli*
Overexpression in yeast			
pSmash (empty)	n.a.	Goo et al. (1999)	Yeast secretion assay, cloning
pSmash-9o9	Classical (EcoRI + NotI)	This work	Yeast secretion assay
pSmash-9o9-d15	Classical (EcoRI + NotI)	This work	Yeast secretion assay
pSmash-SP(9o9)	GoldenGate (Esp3I)	This work	Yeast secretion assay
pSmash-SP(LORE)	GoldenGate (Esp3I)	This work	Yeast secretion assay
pSmash-SP(LORE)-9o9	GoldenGate (Esp3I), Classical (EcoRI + NotI)	This work	Yeast secretion assay

Table S4: Primers used in this dissertation.

All primers were from Eurofins Genomics (Ebersberg, Germany). F: forward primer; R: reverse primer; FP: fluorescent protein; can be either GFP or mCherry.

Primer	Primer sequence 5' to 3'	Template	Amplicon used for
Cloning primers			
SDM RACB-K167R F	GCTCGAAGACCCAACTAAATGTCAGGGGTGTATTTGAT	pDONR223-RACB-WT/CA/DN	pDONR223-RACB-WT/CA/DN-K167R
SDM RACB-K167R R	ATCAAATACACCCCTGACATTTAGTTGGGTCTTCGAGC	pDONR223-RACB-WT/CA/DN	pDONR223-RACB-WT/CA/DN-K167R
attB1 9o9 F	GGGGACAAGTTTGTACAAAAAAGCAGGCTTAATGAACTGTCTACTCGC	cDNA	pDONR223-9o9 (no stop)
attB2 9o9 R	GGGGACCACTTTGTACAAGAAAGCTGGGTTCTAGTAAGACTTTGAATACT	cDNA	pDONR223-9o9
attB2 9o9 no stop R	GGGGACCACTTTGTACAAGAAAGCTGGGTTGTAAGACTTTGAATACT	cDNA	pDONR223-9o9 no stop
attB1 PLC_Zm F	GGGGACAAGTTTGTACAAAAAAGCAGGCTTAATGGGTACTTATAAATGTTG	synthesized PLC_Zm	pDONR223-PLC_Zm no stop
attB2 PLC_Zm no stop R	GGGGACCACTTTGTACAAGAAAGCTGGGTCTACGAATTCAAACCGCATTAG	synthesized PLC_Zm	pDONR223-PLC_Zm no stop
attB1 PIP F	GGGGACAAGTTTGTACAAAAAAGCAGGCTTAATGGAGGCCATGAGAGG	cDNA	pDONR223-PIP (no stop)
attB2 PIP R	GGGGACCACTTTGTACAAGAAAGCTGGGTTTTAGTAGCAAAGCATGCCTC	cDNA	pDONR223-PIP
attB2 PIP no stop R	GGGGACCACTTTGTACAAGAAAGCTGGGTTGTAGCAAAGCATGCCTC	cDNA	pDONR223-PIP no stop
attB1-FP-10xGly-Esp3I F	GGGGACAAGTTTGTACAAAAAAGCAGGCTATGGTGAGCAAGGGCGAG	pGY1-N-ter.-meGFP/mCherry	FRET-FLIM constructs
attB1-FP-10xGly-Esp3I R	CGCCGCCGTCTCCCTCCTCCGCCGCCTCCTCCTCCTCCCCCTTTGTACAGCTCGTCCATGCC	pGY1-N-ter.-meGFP/mCherry	FRET-FLIM constructs
Esp3I-10xGly-FP-attB2 F	GCGGCGCGTCTCGGGGGAGGAGGAGGAGGCGGCGGAGGAGGGGTGAGCAAGGGCGAG	pGY1-N-ter.-meGFP/mCherry	FRET-FLIM constructs
Esp3I-10xGly-FP-attB2 R	GGGGACCACTTTGTACAAGAAAGCTGGGTCTATTTGTACAGCTCGTCCATGCC	pGY1-N-ter.-meGFP/mCherry	FRET-FLIM constructs
Esp3I-RACB-attB2 F	GCGGCGCGTCTCAGGAGGCATGAGCGCGTCCAGGTTC	pDONR223-RACB-CA	attB1-meGFP-10xGly-RACB-CA-attB2
Esp3I-RACB-attB2 R	GGGGACCACTTTGTACAAGAAAGCTGGGTCACCGCCTCCGGACTACAAGATGGAGCAAGCCCCCC	pDONR223-RACB-CA	attB1-meGFP-10xGly-RACB-CA-attB2
Esp3I-9o9-attB2 F	GCGGCGCGTCTCAGGAGGCATGAACTGTCTACTCGC	pDONR223-9o9	attB1-mCherry-10xGly-9o9-attB2
Esp3I-9o9-attB2 R	GGGGACCACTTTGTACAAGAAAGCTGGGTTCTAGTAAGACTTTGAATACT	pDONR223-9o9	attB1-mCherry-10xGly-9o9-attB2
attB1-9o9-Esp3I F	GGGGACAAGTTTGTACAAAAAAGCAGGCTTAATGAACTGTCTACTCGC	pDONR223-9o9	attB1-9o9-10xGly-mCherry-attB2
attB1-9o9-Esp3I R	GCGGCGCGTCTCTCCCCCGTAAGACTTTGAATACTTATC	pDONR223-9o9	attB1-9o9-10xGly-mCherry-attB2
Esp3I-PLC_Zm-attB2 F	GCGGCGCGTCTCAGGAGGCATGGGTACTTATAAATGTTG	pDONR223-PLC_Zm	attB1-mCherry-10xGly-PLC_Zm-attB2
Esp3I-PLC_Zm-attB2 R	GGGGACCACTTTGTACAAGAAAGCTGGGTTTTATACGAATTCAAACCGCATTAG	pDONR223-PLC_Zm	attB1-mCherry-10xGly-PLC_Zm-attB2
attB1-PLC_Zm-Esp3I F	GGGGACAAGTTTGTACAAAAAAGCAGGCTTAATGGGTACTTATAAATGTTG	pDONR223-PLC_Zm	attB1-PLC_Zm-10xGly-mCherry-attB2
attB1-PLC_Zm-Esp3I R	GCGGCGCGTCTCTCCCCCTACGAATTCAAACCGCATTAG	pDONR223-PLC_Zm	attB1-PLC_Zm-10xGly-mCherry-attB2
Esp3I-PIP-attB2 F	GCGGCGCGTCTCAGGAGGCATGGAGGCCATGAGAGG	pDONR223-PIP	attB1-mCherry-10xGly-PIP-attB2
Esp3I-PIP-attB2 R	GGGGACCACTTTGTACAAGAAAGCTGGGTTTTAGTAGCAAAGCATGCCTC	pDONR223-PIP	attB1-mCherry-10xGly-PIP-attB2
attB1-PIP-Esp3I F	GGGGACAAGTTTGTACAAAAAAGCAGGCTTAATGGAGGCCATGAGAGG	pDONR223-PIP	attB1-PIP-10xGly-mCherry-attB2
attB1-PIP-Esp3I R	GCGGCGCGTCTCTCCCCCGTAGCAAAGCATGCCTC	pDONR223-PIP	attB1-PIP-10xGly-mCherry-attB2

Primers used in this dissertation. (*Continued.*)

Primer	Primer sequence 5' to 3'	Template	Amplicon used for
attB1-GST-Esp3I F	GGGGACAAGTTTGTACAAAAAAGCAGGCTTATGTCCCCTATACTAGGTTATTGG	pGWB24, Nakagawa et al. (2007)	attB1-GST-10xGly-mCherry-attB2
attB1-GST-Esp3I R	GCGGCGCGTCTCTCCCCCTTTTGGAGGATGGTCGCCAC	pGWB24, Nakagawa et al. (2007)	attB1-GST-10xGly-mCherry-attB2
attB1-CRIB46-Esp3I F	GGGGACAAGTTTGTACAAAAAAGCAGGCTTAATGGCGAAGGAGCAGGAGAT	pGY1-mCherry-RIC171	attB1-CRIB46-10xGly-mCherry-attB2
attB1-CRIB46-Esp3I R	GCGGCGCGTCTCTCCCCCCGACGACCCCTCGATG	pGY1-mCherry-RIC171	attB1-CRIB46-10xGly-mCherry-attB2
attB1-mCit-2xML1N-attB2 F	GGGGACAAGTTTGTACAAAAAAGCAGGCTATGGTGAGCAAGGGCGAGG	Hirano et al. (2017)	pDONR223-mCitrine-2xML1N
attB1-mCit-2xML1N-attB2 R	ACCACTTTGTACAAGAAAGCTGGGT	Hirano et al. (2017)	pDONR223-mCitrine-2xML1N
attB1-2xPH^{PLC}-attB2	GGGGACAAGTTTGTACAAAAAAGCAGGCTTAATGGACTCGGGCCGGG	Simon et al. (2014)	pDONR223-2xPH^{PLC}
attB1-2xPH^{PLC}-attB2	GGGGACCACTTTGTACAAGAAAGCTGGGTCTACTGGATGTTGAGCTCCTTCAGG	Simon et al. (2014)	pDONR223-2xPH^{PLC}
9o9 RNAi XbaI F	GCGGCGTCTAGAAACTGTCTACTCGCCAT	pDONR223-9o9	pIPKTA38-9o9
9o9 RNAi SalI R	GTCGACGCGGCACTAGTAAGACTTTGAATACT	pDONR223-9o9	pIPKTA38-9o9
PLC RNAi XbaI F	GCGGCGTCTAGACATTTAGCTCCGCAGTATAAAC	cDNA	pIPKTA38-PLC
PLC RNAi SalI R	CGCCGCGTCGACCACACCGGCACCCAGTTGTC	cDNA	pIPKTA38-PLC
PIP RNAi XbaI F	GCGGCGTCTAGATGACACGAGCAATGCGGAAC	pDONR223-PIP	pIPKTA38-PIP
PIP RNAi SalI R	CGCCGCGTCGACGAAATCATCATTTCTTTTGATG	pDONR223-PIP	pIPKTA38-PIP
pGY1-Esp3I F	GCGGCGCGTCTCGAAATCACCAGTCTCTC	pGY1 (empty)	GoldenGate-compatible pGY1
pGY1-Esp3I R	GCGGCGCGTCTCCTGTCCTCTCCAAATG	pGY1 (empty)	GoldenGate-compatible pGY1
Esp3I-FP-10xGly-Esp3I F	GCGGCGCGTCTCGGACAGATGGTGAGCAAGGGC	pGY1-N-ter.-meGFP/mCherry	N-ter. FP fusions in pGY1
Esp3I-FP-10xGly-Esp3I R	CGCCGCCGTCTCCCTCCTCCGCCGCCTCCTCCTCCTCCCCCTTTGTACAGCT CGTCC	pGY1-N-ter.-meGFP/mCherry	N-ter. FP fusions in pGY1
Esp3I-FAPP1-1st-Esp3I F	GCGGCGCGTCTCAGGAGGCATGGAGGGGGTGTTGTAC	Simon et al. (2014)	pGY1-meGFP-10xGly-2xPH^{FAPP1}
Esp3I-FAPP1-1st-Esp3I R	CGCCGCCGTCTCGCCGCCTCCTCCCCCTTTAGTCCTTGTATCAGTCAAAC	Simon et al. (2014)	pGY1-meGFP-10xGly-2xPH^{FAPP1}
Esp3I-FAPP1-2nd-Esp3I F	GCGGCGCGTCTCGGCGGCATGGAGGGGGTGTTGTAC	Simon et al. (2014)	pGY1-meGFP-10xGly-2xPH^{FAPP1}
Esp3I-FAPP1-2nd-Esp3I R	CGCCGCCGTCTCGATTTCTATTTAGTCCTTGTATCAGTCAAAC	Simon et al. (2014)	pGY1-meGFP-10xGly-2xPH^{FAPP1}
Esp3I-C2^{LACT}-Esp3I F	GCGGCGCGTCTCAGGAGGCTGCACTGAACCCCTAG	Platre et al. (2018)	pGY1-meGFP-10xGly-C2^{LACT}
Esp3I-C2^{LACT}-Esp3I R	CGCCGCCGTCTCGATTTCTAACAGCCCAGCAG	Platre et al. (2018)	pGY1-meGFP-10xGly-C2^{LACT}
Esp3I-MAP-2xmCherry-Esp3I F	GCGGCGCGTCTCGGACAGGCAAGTTTGTACAAAAAAGCAGGCT	Doumane et al. (2021)	pGY1-MAP-2xmCherry
Esp3I-MAP-2xmCherry-Esp3I R	CGCCGCCGTCTCGATTTCCAACTATGTATAATAAAGTTGCCTA	Doumane et al. (2021)	pGY1-MAP-2xmCherry
Esp3I-MAP-mCherry-dOCRL-Esp3I F	GCGGCGCGTCTCGGACAGATGGGCTTACTCTGCAG	Doumane et al. (2021)	pGY1-MAP-mCherry-dOCRL(-dead)
Esp3I-MAP-mCherry-dOCRL-Esp3I R	CGCCGCCGTCTCGATTTCTTACTGTGGCTGATTATCG	Doumane et al. (2021)	pGY1-MAP-mCherry-dOCRL(-dead)
9o9 F	ATGAACTGTCTACTCGCCATTCTTTTG	cDNA	pGY1-9o9 (no overhang, blunt-end ligation)
9o9 R	CTAGTAAGACTTTGAATACTTATCCATCTC	cDNA	pGY1-9o9 (no overhang, blunt-end ligation)
RACB SalI F	GCGGCGGTCGACTTATGAGCGCGTCCAGG	pDONR223-RACB-WT	pGEX-RACB-WT
RACB NotI R	GCGGCGGCGGCCGCCTACAAGATGGAGCAAGCCC	pDONR223-RACB-WT	pGEX-RACB-WT
RACB-5Q F	CTGCTGCTGTGCCTTTGGTGGCTGC	pGEX-RACB-WT	pGEX-RACB-5Q

Primers used in this dissertation. (*Continued.*)

Primer	Primer sequence 5' to 3'	Template	Amplicon used for
RACB-5Q R	CAGCAGGCGCAGAGGGGGGCT	pGEX-RACB-WT	pGEX-RACB-5Q
9o9 NotI F	GCGGCGGCGGCCGCATGAACTGTCTACTCGCC	pDONR223-9o9	pMAL-9o9
9o9 SalI R	GCGGCGGTCGACCTAGTAAGACTTTGAATAC	pDONR223-9o9	pMAL-9o9
PLC_Zm NotI F	GCGGCGGCGGCCGCATGGGTACTTATAAATGTTG	pDONR223-PLC_Zm	pMAL-PLC_Zm
PLC_Zm SalI R	GCGGCGGTCGACTTATACGAATTCAAACCG	pDONR223-PLC_Zm	pMAL-PLC_Zm
PIP NotI F	GCGGCGGCGGCCGCATGGAGGCCATGAGAG	pDONR223-PIP	pMAL-PIP
PIP SalI R	GCGGCGGTCGACTTAGTAGCAAAGCATGCC	pDONR223-PIP	pMAL-PIP
9o9 EcoRI F	GCGGCGGAATTCATGAACTGTCTACTCGC	pDONR223-9o9	pSmash-9o9
9o9 Δ15 EcoRI F	GCGGCGGAATTCATGAAAGTAAATGATCGTCTAGC	pDONR223-9o9	pSmash-9o9-δ15
9o9 no stop NotI R	CGCCGCCGCGGCCGCGGTAAGACTTTGAATACTTATC	pDONR223-9o9	pSmash-9o9(-δ15)
SP(9o9) deletion 9o9 F	GCGGCGCGTCTCGCGCGGCCGCTTGG	pSmash-9o9	pSmash-SP(9o9)
SP(9o9) deletion 9o9 R	CGCCGCCGTCTCCTAGACGATCATTTACTTTTG	pSmash-9o9	pSmash-SP(9o9)
EcoRI-SP(LORE)-Esp3I F	GCGGCGGAATTCATGGGTATGGTTTTATTTG	Ranf lab	pSmash-SP(LORE)-9o9
EcoRI-SP(LORE)-Esp3I R	CGCCGCCGTCTCCTTTGCATAGCCACAAGTTG	Ranf lab	pSmash-SP(LORE)-9o9
Esp3I-9o9 no stop-NotI F	GCGGCGCGTCTCGCAAACTGTCTACTCGCC	pSmash-9o9	pSmash-SP(LORE)-9o9
Esp3I-9o9 no stop-NotI R	CGCCGCGCGGCCGCGGTAAGACTTTGAATACTTATC	pSmash-9o9	pSmash-SP(LORE)-9o9
SP(LORE) deletion 9o9 F	GCGGCGCGTCTCGTGCACGCGGCCGCTTGG	pSmash-SP(LORE)-9o9	pSmash-SP(LORE)
SP(LORE) deletion 9o9 R	CGCCGCCGTCTCCTGCATAGCCACAAGTTG	pSmash-SP(LORE)-9o9	pSmash-SP(LORE)
qRT-PCR primers			
qPCR UBC2 F	TCTCGTCCCTGAGATTGCCCACAT	cDNA	qRT-PCR
qPCR UBC2 R	TTTCTCGGGACAGCAACACAATCTTCT	cDNA	qRT-PCR
qPCR GAPDH F	GCCAGTTACTGTCTTTGGCGTC	cDNA	qRT-PCR
qPCR GAPDH R	GGCCTTGTCCTTGTCAGTGAAG	cDNA	qRT-PCR
qPCR Tub2 F	TTCTGGTGAGCATGGACTTG	cDNA	qRT-PCR
qPCR Tub2 R	CTGAATAGCTGGCCAAAAGG	cDNA	qRT-PCR
qPCR PIP F	ACCTGTGTCTGACCGTAATG	cDNA	qRT-PCR
qPCR PIP R	TCTGGTGCAGAATCAGTAGG	cDNA	qRT-PCR
qPCR PLC F	TGGTGACGCTGAGAAGAATC	cDNA	qRT-PCR
qPCR PLC R	GTCGTCCTCATCGTCATCTC	cDNA	qRT-PCR
qPCR 9o9 F	GTGGTGCTCAAGAGTAGCTT	cDNA	qRT-PCR
qPCR 9o9 R	TGTTTACTGGGCGCCATATT	cDNA	qRT-PCR

Table S5: List of genes used in this dissertation.

Genome identifier refers to the current annotation for barley (Morex V3, Mascher (2021)), rice (IRGSP 1.0, Kawahara et al. (2013)), *Arabidopsis* (Araport11, Cheng et al. (2017)) and *Bgh* (DH14, Spanu et al. (2010).

Name	Genome identifier	Genbank identifier
Barley genes		
*Hv*RAC1	HORVU.MOREX.r3.3HG0248920.1	CAD57743.1
*Hv*RACB	HORVU.MOREX.r3.6HG0549810.1	CAC83043.2
*Hv*RAC3	HORVU.MOREX.r3.6HG0615630.1	BAJ98596.1
*Hv*ROP4	HORVU.MOREX.r3.7HG0667150.1	CAD27896.1
*Hv*RACD	HORVU.MOREX.r3.6HG0634280.2	CAD27895.1
*Hv*ROP6	HORVU.MOREX.r3.1HG0077700.1	CAD27894.1
*Hv*PLC	HORVU.MOREX.r3.2HG0107960.1	BAK01542.1
*Hv*PIP	HORVU.MOREX.r3.4HG0405560.1	XP_044982841.1
*Hv*UBC2	HORVU.MOREX.r3.3HG0297350.1	XM_045121532.1
*Hv*GAPDH	HORVU.MOREX.r3.7HG0703580.1	XP_044962418.1
*Hv*RIC171	HORVU.MOREX.r3.2HG0198220.1	CAP62576.1
Rice genes		
*Os*RAC1	Os01t0229400-02	XP_015621645.1
*Os*RAC2	Os05t0513800-01	XP_015638759.1
*Os*RAC3	Os02t0742200-02	XP_015625155.1
*Os*RAC4	Os06t0234200-03	XP_015641323.1
*Os*RAC5	Os02t0834000-01	XP_015627011.1
*Os*RAC6	Os02t0120800-02	XP_015625732.1
*Os*RAC7	Os02t0312600-01	XP_015627590.1
*Os*PLC1	Os07t0694000-01	XP_015646464.1
*Os*PLC2	Os03t0289300-00	XP_015628700.2
*Os*PLC3	Os12t0562400-01	XP_015618103.1
*Os*PLC4	Os05t0127200-01	XP_015640813.1
*Os*GH1	Os02t0554300-01	XP_015626121.1
Os03t0182400-01	Os03t0182400-01	XP_015630614.1
Os06t0195600-01	Os06t0195600-01	XP_015643718.1
Os08t0109100-01	Os08t0109100-01	XP_015649890.1
Os06t0355150-00	Os06t0355150-00	KAB8102431.1
Os02t0782600-01	Os02t0782600-01	KAB8089206.1
Os11t0309000-03	Os11t0309000-03	XP_015615365.1
Os03t0290500-01	Os03t0290500-01	XP_015632624.1
Arabidopsis genes		
*At*ROP1	AT3G51300.1	NP_190698.1
*At*ROP2	AT1G20090.1	NP_173437.1
*At*ROP3	AT2G17800.1	NP_001077910.1
*At*ROP4	AT1G75840.1	NP_177712.1
*At*ROP5	AT4G35950.1	NP_195320.1
*At*ROP6	AT4G35020.1	NP_001190916.1
*At*ROP7	AT5G45970.1	NP_199409.1
*At*ROP8	AT2G44690.1	NP_566024.1
*At*ROP9	AT4G28950.1	NP_194624.1
*At*ROP10	AT3G48040.1	NP_566897.1
*At*ROP11	AT5G62880.1	NP_201093.1
*At*LORE	AT1G61380.1	NP_564775
*At*PLC1	AT5G58670.1	NP_568881.1
*At*PLC2	AT3G08510.1	NP_001030660.1
*At*PLC3	AT4G38530.1	NP_195565.2
*At*PLC4	AT5G58700.1	NP_001318832.1
*At*PLC5	AT5G58690.1	NP_001332556.1

List of genes used in this dissertation. (*Continued.*)

Name	Genome identifier	Genbank identifier
*At*PLC7	AT3G55940.1	NP_191153.1
*At*PLC8	AT3G47290.1	NP_190313.1
*At*PLC9	AT3G47220.1	NP_190306.2
*At*SAC1	AT1G22620.1	NP_173676.2
*At*SAC2	AT3G14205.1	NP_566481.1
*At*SAC3	AT3G43220.1	NP_189908.2
*At*SAC4	AT5G20840.1	NP_197584.2
*At*SAC5	AT1G17340.1	NP_173177.2
*At*SAC6	AT5G66020.1	NP_201403.2
*At*SAC7	AT3G51460.1	NP_190714.2
*At*SAC8	AT3G51830.1	NP_190751.2
*At*SAC9	AT3G59770.1	NP_001190138.1
Bgh genes		
*Bgh*9o9	BLGH_00506	CCU81384.1
*Bgh*β-TUB2	BLGH_02993	P16040.1